Title

Riemannian Geometry of Nonlinear Deformation

Author

Ameli, Siavash

Publication Date

2019

Peer reviewed|Thesis/dissertation

Riemannian Geometry of Nonlinear Deformation

by

Siavash Ameli

A dissertation submitted in partial satisfaction of the

requirements for the degree of

Doctor of Philosophy

in

Engineering - Mechanical Engineering

in the

Graduate Division

of the

University of California, Berkeley

Committee in charge:

Professor Shawn C. Shadden, Chair
Professor David J. Steigmann
Professor Panayiotis Papadopoulos
Professor Alan D. Weinstein

Fall 2019

Riemannian Geometry of Nonlinear Deformation

Abstract

Riemannian Geometry of Nonlinear Deformation

by

Siavash Ameli

Doctor of Philosophy in Engineering - Mechanical Engineering

University of California, Berkeley

Professor Shawn C. Shadden, Chair

The nonlinear (finite) deformation of flow is studied from the geometric point of view. First- and second-order covariant rates of deformation tensors are derived in the context of an arbitrary connection on frame bundles with torsion and Riemannian curvature. Also, the compatibility conditions of continua are extended to deformations on Einstein manifolds using a pullback Ricci curvature. We relate our compatibility conditions with existing formulations on Euclidean space.

A particular interest in studying nonlinear deformation here is to develop evolution equations for the principle rates and directions of finite deformation, which are quantities that are widely used to understand the flow topology. To this end, we present a spectral decomposition of two-point tensors on Riemannian manifolds. We derive evolution equations for the spectral decomposition, namely for the eigenvalues and eigenvectors of deformation tensors on Riemannian manifolds in terms of arbitrary covariant rates and using intrinsic Lie derivatives. We demonstrate the analogy between the spectral decomposition of deformation and attitude kinematics of moving frames. Geometric numerical integration of the evolution equations is explored through Lie group actions, namely the Lie algebra of quaternions. Our formulation extends attitude kinematics of deformation with Euler angles on 2-manifolds with the Riemannian metric. Numerical and analytic examples for both Euclidean space and Hamiltonian flows on Kählerian (symplectic) manifolds are given.

Accompanying our theoretical framework, a comprehensive high-performance computing platform for the Lagrangian analysis of flow is developed. The platform has been integrated into an online gateway with server-client architecture and available online as a community resource. Our platform is capable of processing up to billion-point grids and has been employed in real-time field experiments. We demonstrate practical applications of globe scale geophysical flows using comprehensive datasets.

To my mother, Bahar

Contents

List of Figures

List of Tables

List of Symbols

Sets, Manifolds

$\mathscr{I}$	Time interval, connected domain in $\mathbb{R}$,	9
$\mathscr{B}$	Material body, open set in $\mathbb{R}^n$,	9
$\mathscr{S}$	Configuration of body, an open set in $\mathbb{R}^n$,	9
$\mathscr{P}_{t_0}$	Referential configuration, $\boldsymbol{\varphi}_{t_0}(\mathscr{B})$,	9
$\mathscr{P}_t$	Spatial configuration, $\boldsymbol{\varphi}_t(\mathscr{B})$,	9
$\mathbb{CP}^1$	Complex projective line, Riemann sphere $\mathbb{S}^2 = \mathbb{C} \cup \{\infty\}$,	113

Bundles

$T_{\boldsymbol{x}}\mathscr{P}_t$	Tangent space at point $\boldsymbol{x}$,	11
$T\mathscr{P}_t$	Tangent bundle of manifold $\mathscr{P}_t$, i.e., $\bigsqcup_{\boldsymbol{x}\in\mathscr{P}_t} T_{\boldsymbol{x}}\mathscr{P}_t$,	11
$T^*\mathscr{P}_t$	Coangent bundle of manifold $\mathscr{P}_t$, dual of tangent bundle, $(T\mathscr{P}_t)^*$,	12
$\Gamma(E)$	Space of sections of fibre bundle E,	12
$S\mathscr{P}_t$	Sphere bundle of manifold $\mathscr{P}_t$,	20

Morphisms

$\mathrm{End}(E)$	Endomorphisms $E \otimes E^*$ mapping $E \to E$ over tensor bundle E,	33
$\mathrm{Aut}(E)$	Automorphisms $E \to E$, an invertible endomorpism,	14
$\mathrm{Sym}^2_+(E)$	Symmetric positive definite tensor bundles of E,	13
$\bigwedge^k E$	Alternating tensor bundles of $E^{\otimes k}$ on Grassmann's exterior algebra,	27
$\Omega^k(\mathscr{P}_t)$	Space of k-forms on $\mathscr{P}_t$, i.e., $\Gamma(\bigwedge^k(T^*\mathscr{P}_t))$,	44

$\mathrm{Isom}(\mathscr{P}_t, \mathbf{g})$	Isometry group on Rienammian manifold $(\mathscr{P}_t, \mathbf{g})$,	22
$\mathrm{Hom}(X, Y)$	Homeomorphisms between spaces X and Y,	26
$\mathrm{Symp}(\mathscr{P}_\mathrm{t}, \boldsymbol{\Omega})$	Symplectomorphisms on manifold $\mathscr{P}_t$ with symplectic structure $\boldsymbol{\Omega}$,	117
$\mathrm{Lie}(G)$	Lie algebra of Lie group G, that is $T_{\mathrm{id}}G$,	30

Tensors

tor	Torsion of connection on the vector bundle, the map $\Omega^2(\mathscr{P}_t) \to T\mathscr{P}_t$,	27
$\boldsymbol{\kappa}$	Contorsion tensor associated with the torsion tensor tor,	40
Hess	Hessian on vector bundle E, the map $\Gamma(T^*\mathscr{P}_t \otimes T^*\mathscr{P}_t) \to E$,	44
$\mathrm{Ric}_\mathbf{g}$	Ricci curvature of Riemannian manifold with metric $\mathbf{g}$,	45
$\mathrm{scal}_\mathbf{g}$	Scalar curvature of Riemannian manifold with metric $\mathbf{g}$,	46
K	Sectional curvature, also Gauss curvature,	45
$\mathrm{trace}_\mathbf{g}$	Trace of tensor with respect to metric tensor $\mathbf{g}$,	45
det	Determinant of a tensor or a flow,	31

Functors

$\boldsymbol{\phi}_*$, $\boldsymbol{\phi}^*$	Respectively, pushforward and pullback along homeomorphism $\boldsymbol{\phi}$,	10
$\boldsymbol{\phi}_{*^k}$	Pushforward only on the k^{th} argument of tensor,	33
∂_z, $\partial_{\bar{z}}$	Dolbeault operators on complex manifold,	115
$\boldsymbol{\partial}$	Covariant tangent vector,	11
$\boldsymbol{d}$	Exterior derivative $\Omega^k(\mathscr{P}_t) \to \Omega^{k+1}(\mathscr{P}_t)$,	12
$\boldsymbol{\iota}_X$	Inteior product $\Omega^k(\mathscr{P}_t) \to \Omega^{k-1}(\mathscr{P}_t)$,	31
D	Material time detivative, covariant derivative along velocity, $\partial/\partial t + \nabla_v$,	28
∇	Linear connection $\Gamma(E) \to \Gamma(\mathrm{Hom}(E, E))$ on tangent bundle E,	26
$\bar{\nabla}$	Levi-Civita connection,	39
$\nabla^\mathbf{g}$	Metric connection with respect to Riemannian metric $\mathbf{g}$,	39

∇^{triv}	Trivial connection,	76
$[X, Y]$	Jacobi-Lie braket, commutator of vector fields X and Y,	11
$\{X, Y\}$	Anticommutator of vector fields X and Y,	69
$\pounds_{\boldsymbol{\phi}}\mathbf{t}$	Autonommus Lie derivative of tensor $\mathbf{t}$ along the flow $\boldsymbol{\phi}$,	34
$\mathscr{L}_{\boldsymbol{\phi}}\mathbf{t}$	Non-autonommus Lie derivative of tensor $\mathbf{t}$, i.e., $\partial/\partial t + \pounds_{\boldsymbol{\phi}}$,	35
$\cdot_{\mathbf{g}}$	Inner product induced by metric tensor $\mathbf{g}$,	13
$\langle \cdot, \cdot \rangle$	Duality pairing between tangent and cotangent space,	13
$\mathscr{C}$	Contraction of tensor bundles, $X \times Y \to \mathbb{R}$,	44
$\flat$	Musical bundle canonical isomorphism $T\mathscr{P}_t \to T^*\mathscr{P}_t$,	14
$\sharp$	Musical bundle canonical isomorphism $T^*\mathscr{P}_t \to T\mathscr{P}_t$, inverse of $\flat$,	14
$*\boldsymbol{\omega}$	Hodge star operator as the isomorphism of $\Omega^k(\mathscr{P}_t) \to \Omega^{n-k}(\mathscr{P}_t)$,	92
$\oplus$	Direct sum,	19
$\otimes$	Tensor product,	12
$\odot$	Symmetric tensor product, also Hadamard matrix product,	114
$\wedge$	Skew-symmetric (exterior) tensor product,	31
$\owedge$	Kulkarni–Nomizu product,	46
$\circ$	Quaternionic product,	96

Classical Lie Groups

$\mathrm{GL}(n, \mathbb{R})$	General linear group of degree n over the field $\mathbb{R}$,	30
$\mathrm{SL}(n, \mathbb{R})$	Special linear group of degree n over the field $\mathbb{R}$,	32
$\mathrm{SO}(n, \mathbb{R})$	Special orthogonal group of degree n over the field $\mathbb{R}$,	62
$\mathrm{SU}(n, \mathbb{R})$	Special unitary group of degree n over the field $\mathbb{R}$,	96
$\mathfrak{gl}(n, \mathbb{R})$	Lie algebra of the group $\mathrm{GL}(n, \mathbb{R})$,	30
$\mathfrak{sl}(n, \mathbb{R})$	Lie algebra of the group $\mathrm{SL}(n, \mathbb{R})$,	32

$\mathfrak{so}(n,\mathbb{R})$	Lie algebra of the group $\mathrm{SO}(n,\mathbb{R})$,	68
$\mathfrak{su}(n,\mathbb{R})$	Lie algebra of the group $\mathrm{SU}(n,\mathbb{R})$,	97

Maps

$\boldsymbol{\varphi}_t$	Motion, Configuration at time t, diffeomorphism $\mathscr{B} \to \mathscr{S}$,	9
$\boldsymbol{\phi}_t$	Flow map, pathline, one-parameter diffemorphism $\boldsymbol{\varphi}_t \circ \boldsymbol{\varphi}_{t_0}^{-1}$,	10
$\boldsymbol{V}_t$	Material velocity at time t, referential map $\mathscr{P}_{t_0} \times \mathscr{I} \to T_{\boldsymbol{x}}\mathbb{R}^n$,	10
$\boldsymbol{v}_t$	Spatial velocity at time t, spatial map $\mathscr{P}_t \times \mathscr{I} \to T_{\boldsymbol{x}}\mathbb{R}^n$,	10
$\boldsymbol{A}_t$	Referential acceleratrion, referential map $\mathscr{P}_{t_0} \times \mathscr{I} \to T(T_{\boldsymbol{x}}\mathbb{R}^n)$,	10
$\boldsymbol{a}_t$	Spatial acceleratrion, spatial map $\mathscr{P}_t \times \mathscr{I} \to T(T_{\boldsymbol{x}}\mathbb{R}^n)$,	11
$\mathbf{F}$	Tangent map, deformation gradient, an isomorphism $T_{\boldsymbol{X}}\mathscr{P}_{t_0} \to T_{\boldsymbol{x}}\mathscr{P}_t$,	11
$\mathbf{F}^*$	Cotangent map, an isomorphism $T^*_{\boldsymbol{x}}\mathscr{P}_t \to T^*_{\boldsymbol{X}}\mathscr{P}_{t_0}$,	14
$\mathbf{F}^\intercal$	Transposition of $\mathbf{F}$, an isomorphism $T_{\boldsymbol{x}}\mathscr{P}_t \to T_{\boldsymbol{X}}\mathscr{P}_{t_0}$,	13
$\mathbf{C}$	Right deformation (Cauchy-Green) tensor, $T\mathscr{P}_{t_0} \to T\mathscr{P}_{t_0}$,	14
$\mathbf{b}$	Left deformation (Cauchy-Green) tensor, $T\mathscr{P}_t \to T\mathscr{P}_t$,	14
$\boldsymbol{\epsilon}$	Infinitesimal (Cauchy) strain tensor on $T\mathscr{P}_t$,	48
$\mathbf{H}$	Hencky (logarithmic) strain tensor, $T\mathscr{P}_{t_0} \to T\mathscr{P}_{t_0}$,	84
$\mathbf{l}$	Spatial rate of deformation gradient tensor, $T\mathscr{P}_t \to T\mathscr{P}_t$,	33
$\mathbf{k}$	Second spatial rate of deformation gradient tensor, $T\mathscr{P}_t \to T\mathscr{P}_t$,	52
$\mathbf{d}$	Spatial rate of deformation tensor, $T\mathscr{P}_t \to T\mathscr{P}_t$,	34
$\boldsymbol{\omega}$	Spin, $T\mathscr{P}_t \to T\mathscr{P}_t$,	34
$\mathbf{G}$	Riemannian metric tensor on referential manifold $\mathscr{P}_{t_0}$,	13
$\mathbf{g}$	Riemannian metric tensor on spatial manifold $\mathscr{P}_t$,	13
$\mathbf{h}$	Hermitian metric tensor on spatial manifold $\mathscr{P}_t$,	116
$\mathbf{J}$	Complex structure as a section in $\mathrm{End}(T\mathscr{P}_t)$,	115

$\boldsymbol{\Omega}$	Kähler symplectic form as a section in $\Omega^2(\mathscr{P}_t)$,	115
$\mathbf{R}$	Riemannian curvature, also rotation tensor in polar decomposition,	44
$\boldsymbol{\psi}$	Riemannian isometric ismomorphism $\mathrm{Isom}(\mathscr{P}_t, \mathbf{g})$,	22
$\boldsymbol{\Psi}$	Riemannian isometric isomorphism $\mathrm{Isom}(\mathscr{P}_{t_0}, \mathbf{G})$,	22
$\mathbf{U}$	Referential rotator, the tangent map $T\boldsymbol{\Psi} : T\hat{\mathscr{P}}_{t_0} \to T\mathscr{P}_{t_0}$,	61
$\mathbf{u}$	Spatial rotator, the tangent map $T\boldsymbol{\psi} : T\hat{\mathscr{P}}_t \to T\mathscr{P}_t$,	61
$\mathbf{W}$	Referential dynamic angular velocity tensor, $T\mathscr{P}_{t_0} \to T\mathscr{P}_{t_0}$,	64
$\mathbf{w}$	Spatial dynamic angular velocity tensor, $T\mathscr{P}_t \to T\mathscr{P}_t$,	64
$\mathbf{I}$	Trivial automorphism $T(\mathrm{id}_{\mathscr{P}_{t_0}})$ on $T\mathscr{P}_{t_0}$,	29
$\mathbf{i}$	Trivial automorphism $T(\mathrm{id}_{\mathscr{P}_t})$ on $T\mathscr{P}_t$,	36

Vectors, Covectors

$\boldsymbol{E}_A$	Basis vector $\partial/\partial X^A$ on the reference tangent space $T\mathscr{P}_{t_0}$,	11
$\boldsymbol{E}^{*A}$	Basis covector dX^A on the reference cotangent space $T^*\mathscr{P}_{t_0}$,	12
$\boldsymbol{e}_a$	Basis vector $\partial/\partial x^a$ on the spatial tangent space $T\mathscr{P}_t$,	11
$\boldsymbol{e}^{*a}$	Basis covector dx^a on the spatial cotangent space $T^*\mathscr{P}_t$,	12

Other variables

$\Gamma^A{}_{BC}$	Christoffel symbols of the second kind on the reference configuration,	48
$\gamma^a{}_{bc}$	Christoffel symbols of the second kind on the spatial configuration,	26
$\bar{\gamma}^a{}_{bc}$	Christoffel symbols of the Levi-Civita connection,	39
$\tau^a{}_{bc}$	Components of the torsion tensor tor,	27
J	Jacobian, also matrix of standard complex structure,	31
Λ_a	Eigenvalues of the right deformation tensor $\mathbf{C}$,	20
μ_a	Eigenvalues of the Henchy strain tensor $\mathbf{H}$,	84
H	Hamiltonian function,	117

Acknowledgments

I am grateful to my advisor, Shawn, who has extensively supported me. I am also thankful to the advisor of my advisor, Jerry Marsden, whom I never met, but has taught me through valuable publications he left behind for the world. This work was supported by the National Science Foundation, award numbers 1047963 and 1520825.

Chapter 1

Introduction

"Let no man ignorant of geometry enter here."

— Plato

1.1 Background and Motivation

The study of the kinematics of continua involves the characterization of deformation. A fundamental object in the local analysis of deformation is the *deformation gradient* tensor, which relates infinitesimal deviations in the undeformed (referential) configuration of a body with their evolution in the deformed (spatial) configuration. While the deformation gradient tensor encodes both stretching and rigid body motions, its polar decomposition is typically employed to separate these effects Truesdell and Noll [2004]. Alternative (left/right) polar decompositions lead to (left/right) *stretch tensors*, and the eigenvalues of either stretch tensor provide invariant quantities describing the modes of deformation of the material. The goal of the dissertation is to describe a framework for the *continuous* spectral decomposition of the stretch (or deformation) tensors for a body that is undergoing continuous deformation. While application to fluid mechanics provides primary motivation, the results are more broadly applicable.

In scenarios where a material body undergoes small-scale deformations, infinitesimal strain theory is applicable. In this case, the change between the referential and spatial coordinates is small, which implies that the Eulerian and Lagrangian descriptions become the same. Alternatively, in finite-strain theory, deformations between the referential and spatial configurations are large. In fluid mechanics, an instantaneous Eulerian description of the fluid is often used and is largely based on properties, or decompositions, of the *velocity gradient* tensor. In particular, this perspective characterizes the *time-rate* of the fluid motion, and this *differential-in-time* perspective implies *differential-in-space* deformations. Thus, the instantaneous Eulerian perspective used to describe fluid kinematics is analogous to the infinitesimal strain theory studied more broadly in continuum mechanics. On the other hand, the Lagrangian description of fluid kinematics considers the integrated motion of the fluid over time, in which case deformations

become large making this perspective analogous to finite strain theory in continuum mechanics. Namely, in the Lagrangian perspective, the evolution of the material is governed by the *flow map* and local deformation is characterized by the *tangent flow map*, otherwise known as the deformation gradient tensor mentioned above. These two perspectives (infinitesimal vs finite) on characterizing deformation are connected by the fact that the (finite) deformation gradient tensor can be obtained by integrating the (infinitesimal) velocity gradient tensor along pathlines in the flow. This computation is numerically challenging, however, for reasons described below.

In applications, the deformation gradient tensor, and in particular its spectral decomposition, is valuable in quantifying stretching and alignment in fluid flows [Tabor and Klapper, 1994]. For example, recent variational approaches to characterize Lagrangian coherent structures (LCS) by Haller [2011]; Oettinger, Blazevski, and Haller [2016] utilize singular values and eigenvectors of the deformation gradient tensor to define objects or material surfaces that organize flow topology. A simple example is the visualization of LCS by the spatial distribution of the finite-time Lyapunov exponent (FTLE) field, which is defined by the largest singular value of the deformation gradient tensor [Shadden, Lekien, and Marsden, 2005]. The deformation gradient for a fluid is often computed by finite-differencing pathline stencils, or as mentioned above by the integration of the velocity gradient tensor along pathlines Kasten, Petz, Hotz, Noack, and Hege [2009]; Allshouse and Peacock [2015]. In either case, singular values and eigenvectors can be obtained using a matrix spectral decomposition method of choice. However, computation of the deformation gradient itself can become numerically unstable as the eigenvectors become dominated by the strongest eigen-pair direction. This causes the matrix to become ill-conditioned and eventually it may become impossible to retrieve accurate spectral information of interest. If only the largest eigenpair is sought, the flow is 2D, or integration times are short, this problem is minimized. But as focus shifts to full eigen-pair information and complex 3D flows, this problem becomes relevant. Also, this ill-conditioning is a well-known difficulty and encountered especially when the Lyapunov spectra are computed for large deformations.

Because the singular values and eigenvectors of the deformation gradient tensor are the quantities directly used to characterize continuous deformation of continua, and because the computation of these quantities is numerically unstable, it is desirable to have a robust method to directly obtain these quantities. The eigenvalues and eigenvectors for *continuous* operators have been covered in seminal books of Rellich [1969] and Kato [1995], which discuss the existence of a continuous and differentiable spectral decomposition. And, on the other hand, the computation of a singular value decomposition (SVD) for a *constant* matrix has been well-established [Golub and Van Loan, 1996]. Combing these ideas, Bunse-Gerstner, Byers, Mehrmann, and Nichols [1991a] extended the theory of SVD to a matrix that depends smoothly on a parameter (e.g., time), and investigated the existence and uniqueness of an analytic SVD in this context, as well as numerical techniques for its computation. Subsequently,

Wright [1992] offered an alternative approach, which derived differential equations for the factors of a continuous SVD for a matrix depending smoothly on a parameter. The extension to the class of orthogonal decomposition of time-varying matrices has been investigated by Dieci and Eirola [1999] and they established strong conditions for such smooth decompositions to exist. The development of continuous evolution equations for spectral decompositions has been used in applications such as pseudo-rigid body dynamics [Holm, Schmah, and Stoica, 2009], stability and Lyapunov stability of dynamical systems [Goldhirsch, Sulem, and Orszag, 1987] and computing the full spectra of Lyapunov exponents of ergodic dynamical systems [Greene and Kim, 1987] and the exponential dichotomy spectra [Dieci and Elia, 2006]. Our approach herein extends the idea of deriving differential equations for a continuous SVD, but in the context of studying the continuous deformation of a continuum.

While most prior works have focused on SVD of a one-parameter *matrix*, the work herein extends these ideas to the broader context of *tensorial operators*. To do this, we use the *differential-geometric* view of the kinematics of deformation introduced in Hughes and Marsden [1977] and Marsden and Hughes [1983]. This viewpoint has motivated the reformulation of continuum mechanics using differential geometry [Epstein, 2010], such as for the characterization of stress [Kanso, Arroyo, Tong, Yavari, Marsden, and Desbrun, 2007; Simo and Marsden, 1984b,a] or the multiplicative decomposition of the deformation gradient [Sadik and Yavari, 2015]. The differential-geometric formulation enables us to use well-defined and coordinate-free mathematical objects that provide intrinsic relations among the associated tensors, which elucidates the structure and symmetries of the derived equations. Moreover, this enables us to identify an appropriate algebra to improve efficiency and accuracy of the SVD computations. A main result of the work herein is a singular-value decomposition theorem for the deformation gradient tensor that yields explicit differential equations for the eigenvalues and eigenvectors of the tensor. This is achieved in part by introducing a *tensorial decomposition* that results in the diagonalization of the deformation tensors. The development of direct evolution equations for the eigen-pairs of the deformation tensors has several advantages, including (1) solving the existing numerical problems of obtaining an accurate SVD for continuous deformation of continua, (2) the equations provide fundamental insight into the properties of covariant tensors describing fluid kinematics and (3) these quantities are more directly interpreted and used in flow characterizations.

1.2 Outline

The chapters and their dependencies are shown in the diagram below. Part I of the dissertation consists of Chapters 2 to 9, where we present the theory of this work. Part II consists of Chapters 10 to 12, where we provide examples and applications.

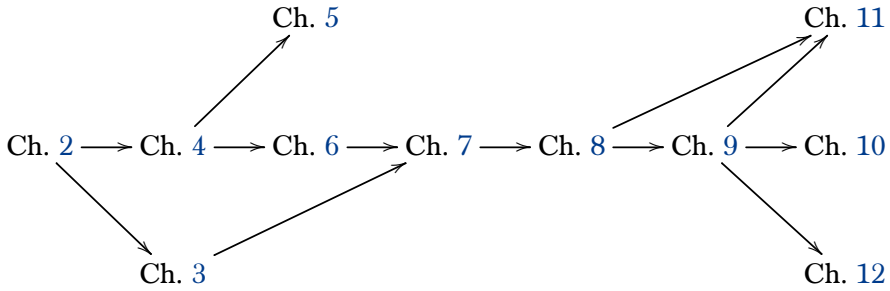

A summary of each chapter is as follows. The contributions in this dissertation are highlighted in each part.

Ch. 2 Here we review the basic notations and framework for describing the kinematics from the differential geometric view. In §2.2 we introduce the *flow map* and the *deformation gradient tensor* in §2.3 as the tangent of the flow map, and this tensor, along with referential and spatial metrics, are used to define the *left* and *right (Cauchy-Green) deformation tensors* in §2.4.

Ch. 3 Here we present three decompositions of deformation tensors. In §3.2 the polar decomposition is reviewed, by which we better understand the deformation gradient tensor. In §3.3 we define the spectral decomposition of deformation gradient tensor using Courant-Fisher-Weyl's minimax theorem. The eigenvalues and eigenvectors defined this way are consistent with those of deformation tensors. We will show that the eigenvalues of a map depend on the Riemannian metric used on both referential and spatial manifolds. Lastly, we propose a definition for the singular value decomposition (SVD) of a two-point tensor on Riemannian manifolds in §3.4. We revisit the singular value decomposition in Chapter 7.

Ch. 4 The goal here is to present the kinematics of tensors by deriving their first-order material time derivatives. The time rates are used in Chapters 6 and 7 for deriving evolution equations. To define the material time derivative we use the connection on the vector bundle of configuration manifold. We have used arbitrary connections with torsion. The material rates are essentially the pullback covariant derivatives along the flow. A brief introduction to a connection on a vector bundle is presented in §4.2. Our formulation with torsion necessitates the redefinition of a few existing variables in §4.5. The evolution equation of the deformation gradient is given in §4.3. Also, we review the rate of volume change, which will be useful later in Chapter 7 when we will revisit the Liouville theorem and isochoric flows. The first-order material rates of deformation are given in §4.7 and §4.9.

Ch. 5 The kinematics presented in Chapter 4 is the study of first-order variations of tensors on the vector bundle. In Chapter 5, we derive second-order variations of tensors. Our innovative derivations involve the Riemannian curvature of manifold explained in §5.2. An immediate application of Riemannian curvature is in the formulation of compatibility conditions necessary for the existence of a continuous deformation. In §5.3 we review the compatibility conditions of deformation and strain tensors for Riemann-flat space, and then we generalize them to other non-flat manifolds. In particular, we present novel compatibility conditions for deformation on Einstein manifolds, and model spaces of constant sectional curvature. The second material rates of deformation tensors are given in §5.4. In §5.5 we assume the flow is geodesic, which allows us to better interpret the role of curvature in the second-order evolution equations in terms of Jacobi fields. Chapter 5 is a point of departure that is not needed for the rest of the chapters.

Ch. 6 A later goal in chapter 7 is to derive evolution equations for the spectral decomposition of deformation, namely for eigenvalues and eigenvectors. This is achieved by isometric transformation on referential and spatial manifolds. In this chapter, we define general time-dependent isometric isomorphisms on manifolds, and we present the new evolution equations on the transformed manifolds. Our formulation is effectively analogous to the singular value decomposition of matrices, but for the tangent map between the tangent spaces of two Riemannian manifolds. The isometric isomorphisms on Riemannian manifolds are analogous to solid rotations in Euclidean space, hence similar concepts therein apply. For instance, associated with the group of *rotator tensors*, we can define the *spinor tensors* that represent the rate of rotation analogous to the angular velocity. We will show that only on the referential manifold, the spinors of the isometric isomorphisms are skew-symmetric tensors. In contrast, we found that the spinors on the spatial manifold are not necessarily skew-symmetric.

Ch. 7 Our goal in this chapter is to obtain the evolution equations for spectral decomposition of deformation tensors, that is, for their eigenvalues and eigenvectors. The motivation for the evolution equation of eigenvalues, in particular, is to perform the Lagrangian analysis of the flow. Ultimately, this enables us to identify coherent structures and the topological assessment of the flow patterns, which we explore later in Chapter 10 and Chapter 11. The novel formulation that we will present here is in the contexts of a general Riemannian manifold and arbitrary connection that may include torsion. In brief, our approach is to diagonalize the evolution equations that were given in Chapter 6. In the previous chapter, we have reformulated the evolution equations on a non-inertial frame by isometric isomorphisms, i.e., rotations of frames with spinors in referential and spatial configurations respectively. Here, we determine the spin tensors so that the deformation tensors are diagonalized on a given local frame. The diagonalized tensors are the spectral decomposition that we have seen Chapter 3.

Ch. 8 Here we assume the configuration manifold is the Euclidean space, and we make an analogy between our equations and the kinematics of moving frames, and the bipolar decomposition of pseudo-rigid bodies. Non-Euclidean formulations for 2-manifolds are given in Chapter 9. Here, we review the mathematical representation of rotation and some of their numerical integrations. An important representation of rotation in 3 dimensional space is by *unit quaternions* on $\mathbb{S}^3$. The attitude kinematics in terms of quaternions are presented in §8.5. In our numerical applications that will be given in later in Chapter 11 we have extensively utilized the numerical integration with quaternions as a Lie group integrator. In two-dimensional Euclidean space, the rotation is represented using Euler angles and given in §8.6.

Ch. 9 Here, our particular interests are two-dimensional manifolds, in which the rotation is represented by Euler angles in $\mathrm{SO}(2)$ Lie group. In contrast to Chapter 8, here we present non-Euclidean formulation on $\mathrm{SO}(2)$. In this chapter, we derive rate equations that are exclusively depended on Euler angles without the need of converting them to rotator matrices. These equations reduce computational costs since they shortcut several matrix multiplications. Throughout this chapter, it is assumed the connection on the vector bundle is trivial, so the metric tensor is not necessarily a parallel section. Additionally, we have explored the influence of the Riemannian metric on the deformation. For instance, we have found that the non-isothermal metric induces vorticity, besides the vorticity of the flow itself. This effect is explained by the skewness of the non-isothermal coordinates system. Lastly, we have defined the Euclidean equivalence of the rate of deformation and vorticity. When these new variables are employed, the evolution equations become as if they are written in Euclidean space.

Ch. 10 In this chapter, we demonstrate the developments in Chapters 7 and 9 by a numerical example of a symplectic flow of ideal vortices on the Riemann sphere $\mathbb{S}^2$. The Hamiltonian function of this flow has been given in the literature, but we re-derive the complexified Hamiltonian function on the Kähler manifold, where we can leverage three compatible geometric structures together, namely the Riemannian, complex and symplectic structures. A brief introduction to the Kählerian structures is presented to establish complex Hamiltonian of the flow. We will show numerical results for the set of six different vortex configurations that are in equilibrium. A goal throughout our development is to identify the Lagrangian coherent structures (LCS) of the fluid flows. To this end, we demonstrate the finite-time Lyapunov exponent (FTLE) field of the deformation for these six examples and observe that the ridges of the FTLE field distinguish the basins of individual vortices. Lastly, for the case of antipodal bipolar vortices, we present a novel analytical solution to the evolution equations of the spectral decomposition of deformation. Namely, we derive analytical equations of fields for eigenvalues

and eigenvectors of deformation for the flow of two vortices at north and south poles of the sphere.

Ch. 11 In this chapter, we provide numerical examples for Chapters 7 and 8. In particular, we compute FTLE for simple flows. The first three examples are the two-dimensional double-gyre model, the three-dimensional Arnold-Beltrami-Childress flow and the three-dimensional Stretching-Twisting-Folding flow. All these flows are presented in Euclidean space with the trivial metric, and the analytical equation for their velocity vector field is known. These flows can be used as a benchmark to test the accuracy of calculations. We leverage the incompressibility property of these flows (isochoric) to test the volume preservation of our theoretical framework, and we will show that, by orders of magnitudes, our formulations are significantly more accurate compared to other methods of computing FTLE. In the final example in this chapter, we use the turbulence dataset that an analytical equation of the flow is no longer known.

Ch. 12 Accompanying our theoretical framework, here we present software that we developed as a comprehensive computing platform for the Lagrangian analysis of practical oceanographic applications, which addresses the computational challenges and convenience of use for end-users. Lastly, we present a gallery of numerical computations of flow transport on oceanographic datasets by our software.

Ch. 13 This chapter concludes the dissertation.

Part I

Theory

Chapter 2

Deformation on Riemannian Manifolds

2.1 Introduction

This chapter briefly introduces the elements of the kinematics of continua from a Riemannian geometric perspective. Our notations on tensor algebra in this chapter are inherited from the pioneering work of Marsden and Hughes [1983], where the foundations of elasticity are reformulated in a geometric framework. In §2.2 we define the configurations spaces, the flow map, velocity, and acceleration. Furtherer details on the acceleration will be given later in Section 5.5. In §2.3 we introduce the tangent space and the deformation gradient tensor as the tangent map. In §2.4 we equip the manifolds with Riemannian metrics to measure the deformation.

2.2 Motion

Let a *material body* of fluid be an open set $\mathscr{B} \subset \mathbb{R}^n$. In what follows we tacitly consider $n = 2, 3$ for the dimension of Euclidean space. Let the *configuration* of body $\mathscr{B}$ be described by the diffeomorphism

$$\boldsymbol{\varphi} : \mathscr{B} \to \mathscr{S} \subset \mathbb{R}^n. \tag{2.2.1}$$

The *motion* of the body is defined by the map $t \mapsto \boldsymbol{\varphi}_t$ from time interval $\mathscr{I} \subset \mathbb{R}$ to the set of all configurations $\mathscr{S}$. At a reference time $t = t_0$ and current time t, the *referential* and *spatial configurations* are body images are denoted $\mathscr{P}_{t_0} := \boldsymbol{\varphi}_{t_0}(\mathscr{B})$ and $\mathscr{P}_t := \boldsymbol{\varphi}_t(\mathscr{B})$ respectively. Variables defined on $\mathscr{P}_{t_0}$ are referred to as ***material*** or ***referential*** variables. Similarly, variables associated with $\mathscr{P}_t$ are referred to as ***spatial*** variables. Herein we use upper case letters for referential variables on $\mathscr{P}_{t_0}$ and lower case letters for spatial variables on $\mathscr{P}_t$.[1]

[1] Upper case letters are also used for two-point tensors.

The ***flow map*** is the composition

$$\boldsymbol{\phi}(\boldsymbol{X}, t; t_0) \coloneqq \boldsymbol{\varphi}_t \circ \boldsymbol{\varphi}_{t_0}^{-1} \in C^1(\mathscr{P}_{t_0} \times \mathscr{I}; \mathscr{P}_t). \tag{2.2.2}$$

Unless stated, we usually fix t_0 and omit it from the notation. Flow map $\boldsymbol{\phi}_t$ is the action of the additive Lie group $(\mathbb{R}, +)$ on $\mathscr{P}_t$; For a fixed referential point $\boldsymbol{X} \in \mathscr{P}_{t_0}$, the orbit of one-parameter diffeomorphism $t \mapsto \boldsymbol{\phi}_t(\boldsymbol{X}) = \boldsymbol{\phi}(\boldsymbol{X}, t)$ defines a smooth *pathline* curve passing through the point $\boldsymbol{X}$. The pathline is the integral curve of the ***material velocity***

$$\boldsymbol{V}_t(\boldsymbol{X}) = \boldsymbol{V}(\boldsymbol{X}, t) \coloneqq \frac{\partial \boldsymbol{\phi}(\boldsymbol{X}, t)}{\partial t}, \tag{2.2.3}$$

which is the referential map $\boldsymbol{V}_t : \mathscr{P}_{t_0} \times \mathscr{I} \to T_{\boldsymbol{x}}\mathbb{R}^n$, where $T_{\boldsymbol{x}}$ denotes the tangent map at spatial point $\boldsymbol{x}$. Alternatively, the ***spatial velocity*** is the spatial map $\boldsymbol{v}_t : \mathscr{P}_t \times \mathscr{I} \to T_{\boldsymbol{x}}\mathbb{R}^n$ defined by

$$\boldsymbol{v}_t(\boldsymbol{x}) = \boldsymbol{v}(\boldsymbol{x}, t) \coloneqq \boldsymbol{\phi}_* \boldsymbol{V}_t = \boldsymbol{V}_t \circ \boldsymbol{\phi}_t^{-1}, \tag{2.2.4}$$

where $\boldsymbol{\phi}_*$ is the pushforward operation. The spatial velocity vector field $\boldsymbol{v}_t$ is a section of the tangent bundle $T\mathbb{R}^n = \mathbb{R}^n \times \mathbb{R}^n$. We assume $\boldsymbol{v}$ is a *complete vector field* so that a one-parameter group of diffeomorphism $\boldsymbol{\phi}_t$ generated by the flow along $\boldsymbol{v}_t$ exists for all times. The commutative diagram below summarizes the relation between velocity vector fields.

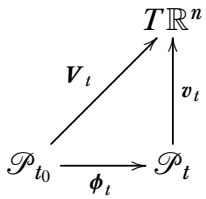

Because the spatial velocity vector field[2] $\boldsymbol{v}(\boldsymbol{x}, t)$ is typically the known quantity, we write the differential equation for a pathline using (2.2.4) as

$$\frac{D\boldsymbol{\phi}_t}{dt} \coloneqq \left.\frac{\partial \boldsymbol{\phi}(\boldsymbol{X}, t)}{\partial t}\right|_{\boldsymbol{X}} = \boldsymbol{v}_t \circ \boldsymbol{\phi}_t, \tag{2.2.5}$$

with initial condition $\boldsymbol{\phi}(\boldsymbol{X}, t_0) = \boldsymbol{X}$. We note that D/dt denotes the ***material time derivative***, for which material point $\boldsymbol{X} \in \mathscr{P}_{t_0}$ is fixed. A formal definition of material time derivative in terms of connection on manifold is given in §4.3. By integrating (2.2.5) the flow map $\boldsymbol{\phi}_t$ is obtained.

The second time rate of the flow map defines the acceleration of motion. The ***referential acceleration*** of motion $\boldsymbol{\phi}$ is the map $\boldsymbol{A} : \mathscr{P}_{t_0} \times \mathscr{I} \to T(T_{\boldsymbol{x}}\mathbb{R}^n)$ given by

$$\boldsymbol{A} \coloneqq \frac{\partial \boldsymbol{V}(\boldsymbol{X}, t)}{\partial t} = \frac{\partial^2 \boldsymbol{\phi}(\boldsymbol{X}, t)}{\partial t^2}, \tag{2.2.6}$$

[2]We denote the point vector and vector field with the same symbol.

where we have assumed $\boldsymbol{\phi}_t \in C^2(\mathscr{P}_{t_0} \times \mathscr{I}; \mathscr{P}_t)$. Similarly, the ***spatial acceleration*** vector of the motion is the map $\boldsymbol{a} : \mathscr{P}_t \times \mathscr{I} \to T(T_{\boldsymbol{x}}\mathbb{R}^n)$ defined by

$$\boldsymbol{a}_t(\boldsymbol{x}) = \boldsymbol{a}(\boldsymbol{x}, t) \coloneqq \boldsymbol{\phi}_* \boldsymbol{A}_t = \boldsymbol{A}_t \circ \boldsymbol{\phi}_t^{-1}. \tag{2.2.7}$$

The relation between referential and spatial acceleration is shown in the commutative diagram below.

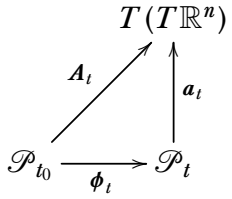

The spatial acceleration can be expressed by the material rate of spatial velocity as (see [Marsden and Hughes, 1983, Proposition 1.14])

$$\boldsymbol{a} = \frac{D\boldsymbol{v}}{dt} = \frac{\partial \boldsymbol{v}}{\partial t} + \nabla_{\boldsymbol{v}} \boldsymbol{v}, \tag{2.2.8}$$

where $\nabla_{\boldsymbol{v}} \boldsymbol{v}$ is the covariant derivative of velocity along the flow of $\boldsymbol{\phi}_t$.

2.3 Deformation Gradient Tensor

Suppose manifold $\mathscr{P}_t$ admits a differentiable structure. Let $T\mathscr{P}_{t_0}$ and $T\mathscr{P}_t$ denote the tangent bundles of the referential and spatial configuration spaces respectively. We characterize deformation through a linear isomorphism between tangent spaces $T_{\boldsymbol{X}}\mathscr{P}_{t_0}$ and $T_{\boldsymbol{x}}\mathscr{P}_t$ at referential and spatial points $\boldsymbol{X}$ and $\boldsymbol{x} = \boldsymbol{\phi}_t(\boldsymbol{X})$ respectively using the ***tangent map***

$$\mathbf{F} \coloneqq T\boldsymbol{\phi}_t : T_{\boldsymbol{X}}\mathscr{P}_{t_0} \to T_{\boldsymbol{x}}\mathscr{P}_t, \tag{2.3.1}$$

which is also known as the ***deformation gradient***. To represent $\mathbf{F}$ explicitly, we can parametrize manifolds $\mathscr{P}_{t_0}$ and $\mathscr{P}_t$ with respect to some coordinates. Let $\{X^A\}$ and $\{x^a\}$ denote local charts on coordinate patches of $\mathscr{P}_{t_0}$ and $\mathscr{P}_t$ respectively with indices[3] $A, a = 1, \ldots, n$. Moreover, let the set of *covariant vectors* (i.e., an equivalency class of one-parameter sub-manifolds) be identified by covariant derivatives

$$\left\{\boldsymbol{E}_A \coloneqq \frac{\boldsymbol{\partial}}{\boldsymbol{\partial} X^A}\right\}_A \quad \text{and} \quad \left\{\boldsymbol{e}_a \coloneqq \frac{\boldsymbol{\partial}}{\boldsymbol{\partial} x^a}\right\}_a,$$

denote bases for the tangent spaces $T_{\boldsymbol{X}}\mathscr{P}_{t_0}$ and $T_{\boldsymbol{x}}\mathscr{P}_t$ respectively. We assume the bases are *holonomic*, meaning that the Lie bracket in each basis vanish, i.e.,

$$[\boldsymbol{E}_A, \boldsymbol{E}_B] = \pounds_{\boldsymbol{E}_A} \boldsymbol{E}_B = \mathbf{0} \quad \text{and} \quad [\boldsymbol{e}_a, \boldsymbol{e}_b] = \pounds_{\boldsymbol{e}_a} \boldsymbol{e}_b = \mathbf{0}. \tag{2.3.2}$$

[3] Superscript indices indicate contravariant part of a tensor and subscript indices denote covariant part.

Similarly, the covectors (i.e., contravariant vectors) identified by the 1-forms

$$\left\{\boldsymbol{E}^{*A} := \frac{\boldsymbol{d}}{\boldsymbol{d}X^A}\right\}_A \quad \text{and} \quad \left\{\boldsymbol{e}^{*a} := \frac{\boldsymbol{d}}{\boldsymbol{d}x^a}\right\}_a,$$

denote dual bases of the cotangent spaces $T^*_{\boldsymbol{X}}\mathscr{P}_{t_0}$ and $T^*_{\boldsymbol{x}}\mathscr{P}_t$ respectively.[4,5] By using these bases, the deformation gradient can be represented as

$$\mathbf{F} = F^a{}_A \boldsymbol{e}_a \otimes \boldsymbol{E}^{*A}, \tag{2.3.3}$$

where $F^a{}_A$ are the coordinates of tensor $\mathbf{F}$ with respect to the chosen basis.[6,7] Here we can see that the deformation gradient is not a gradient vector, rather, it is a ***mixed two-point tensor*** contravariant (raised index) on $\mathscr{P}_{t_0}$ and covariant (lowered index) on $\mathscr{P}_t$.

The coordinates of $\mathbf{F}$ with respect to the specified bases are given by

$$F^a{}_A(\boldsymbol{X}) = \frac{\partial \phi^a_t}{\partial X^A}(\boldsymbol{X}), \tag{2.3.4}$$

which is evaluated at a referential point $\boldsymbol{X} \in \mathscr{P}_{t_0}$. The coordinates of $\mathbf{F}$ identify the ***Jacobian matrix*** of the flow map $\boldsymbol{\phi}_t$ with respect to the referential coordinate chart $\{X^A\}$, evaluated at referential point $\boldsymbol{X}$. Tensor $\mathbf{F}$ maps the referential tangent vector $\boldsymbol{Z} \in T_{\boldsymbol{X}}\mathscr{P}_{t_0}$ to the spatial tangent vector $\boldsymbol{z} \in T_{\boldsymbol{x}}\mathscr{P}_t$, namely it defines the pushforward of a vector field $\boldsymbol{Z}$,

$$\boldsymbol{z}(\boldsymbol{x}) := (\mathbf{F}\boldsymbol{Z})(\boldsymbol{\phi}^{-1}\boldsymbol{x}) = (T\boldsymbol{\phi}) \circ \boldsymbol{Z} \circ \boldsymbol{\phi}^{-1} =: \boldsymbol{\phi}_* \boldsymbol{Z}. \tag{2.3.5}$$

The commutative diagram below illustrates tangent map $\mathbf{F}$, where $\boldsymbol{Z} = \Gamma(T\mathscr{P}_{t_0})$ and $\boldsymbol{z} = \Gamma(T\mathscr{P}_t)$ represent sections of the fibre bundles for each space.

$$\begin{array}{ccc} T\mathscr{P}_{t_0} & \xrightarrow{\mathbf{F}} & T\mathscr{P}_t \\ \uparrow{\scriptstyle \boldsymbol{Z}} & & \uparrow{\scriptstyle \boldsymbol{z}} \\ \mathscr{P}_{t_0} & \xrightarrow[\boldsymbol{\phi}_t]{} & \mathscr{P}_t \end{array} \tag{2.3.6}$$

[4]Symbols $\boldsymbol{\partial}$ and $\boldsymbol{d}$ denote covariant and exterior derivatives respectively. Also, $\mathscr{L}_X Y$ is the Lie derivative of tensor field Y over the flow of X. The Jacobi-Lie bracket, or the commutator of fields X and Y is denoted by $[X, Y]$.

[5]The superscript $*$ on spaces or tensors denotes the corresponding dual. The symbol $*$ also denotes the pushforward (subscript) and pullback (superscript) operation.

[6]We use bold face such as $\mathbf{F}$ and $\mathbf{g}$ for second-order tensors and italic bold face such as $\boldsymbol{E}$ and $\boldsymbol{e}$ for first-order tensors.

[7]Staggering of indices on the coordinates of the two-point tensor indicates that the first column of indices relates to the referential manifold, and the second column of indices relates to the spatial manifold.

2.4 Measuring Deformation

Riemannian Manifold

The deformation gradient tensor $\mathbf{F}$ relates the evolution of tangent vectors from referential to spatial configurations. Here we provide a measure to quantify the deformation of tangent vectors. Since we have assumed the configuration spaces are submanifolds of Euclidean space, they are metrizable (Nagata-Smirnov's metrization Theorem, also see [Spivak, 1999, Appendix A] and [do Carmo, 1992, Proposition 2.10]). In order to quantify deformation we equip each manifold with a Riemannian metric, yielding Riemannian manifolds $(\mathscr{P}_{t_0}, \mathbf{G})$ and $(\mathscr{P}_t, \mathbf{g})$, where[8]

$$\mathbf{G} \in \Gamma\left(\mathrm{Sym}^2_+\left(T^*\mathscr{P}_{t_0}\right)\right), \qquad \mathbf{G} = G_{AB}\boldsymbol{E}^{*A} \otimes \boldsymbol{E}^{*B}, \tag{2.4.1a}$$

$$\mathbf{g} \in \Gamma\left(\mathrm{Sym}^2_+\left(T^*\mathscr{P}_t\right)\right), \qquad \mathbf{g} = g_{ab}\boldsymbol{e}^{*a} \otimes \boldsymbol{e}^{*b}, \tag{2.4.1b}$$

and Sym^2_+ is the space of symmetric positive-definite bilinear tensor bundles. The coordinates G_{AB} and g_{ab} are given by

$$G_{AB} = \mathbf{G}(\boldsymbol{E}_A, \boldsymbol{E}_B) = \boldsymbol{E}_A \cdot_{\mathbf{G}} \boldsymbol{E}_B,$$
$$g_{ab} = \mathbf{g}(\boldsymbol{e}_a, \boldsymbol{e}_b) = \boldsymbol{e}_a \cdot_{\mathbf{g}} \boldsymbol{e}_b,$$

where $\cdot_{\mathbf{G}}$ and $\cdot_{\mathbf{g}}$ are the inner products with metrics $\mathbf{G}$ and $\mathbf{g}$. The inner product induced by metric tensors between two referential tangent vectors $\boldsymbol{Z}_1 = Z_1^A\boldsymbol{E}_A$ and $\boldsymbol{Z}_2 = Z_2^B\boldsymbol{E}_B$ on $T_{\boldsymbol{X}}\mathscr{P}_{t_0}$ and between two spatial tangent vectors $\boldsymbol{z}_1 = z_1^a\boldsymbol{e}_a$ and $\boldsymbol{z}_2 = z_2^b\boldsymbol{e}_b$ on $T_{\boldsymbol{x}}\mathscr{P}_t$ are

$$\boldsymbol{Z}_1 \cdot_{\mathbf{G}} \boldsymbol{Z}_2 = \mathbf{G}(\boldsymbol{Z}_1, \boldsymbol{Z}_2) \coloneqq \langle \mathbf{G}\boldsymbol{Z}_1, \boldsymbol{Z}_2\rangle_{\boldsymbol{X}} = G_{AB}Z_1^AZ_2^B,$$
$$\boldsymbol{z}_1 \cdot_{\mathbf{g}} \boldsymbol{z}_2 = \mathbf{g}(\boldsymbol{z}_1, \boldsymbol{z}_2) \coloneqq \langle \mathbf{g}\boldsymbol{z}_1, \boldsymbol{z}_2\rangle_{\boldsymbol{x}} = g_{ab}z_1^az_2^b,$$

where $\langle ., . \rangle$ is the natural (canonical) duality paring between tangent and cotangent spaces over the field $\mathbb{R}$. The length and angles between above pair of tangent vectors on manifolds are measurable by the metric tensors.

Deformation Tensors

The metric tensors $\mathbf{G}$ and $\mathbf{g}$ together with deformation gradient tensor $\mathbf{F}$ quantify deformation of tangent vectors. The composition of above maps forms the *transposition* tensor $\mathbf{F}^\intercal : T_{\boldsymbol{x}}\mathscr{P}_t \to T_{\boldsymbol{X}}\mathscr{P}_{t_0}$ with respect to metrics $\mathbf{G}$ and $\mathbf{g}$ [Marsden and Hughes, 1983, p. 48] as

$$\mathbf{F}^\intercal = \mathbf{G}^{-1}\mathbf{F}^*\mathbf{g}, \tag{2.4.2}$$

[8] Γ denotes the space of smooth sections of a fibre bundle.

where $\mathbf{F}^* \coloneqq T^*\boldsymbol{\phi} : T^*\mathscr{P}_t \to T^*\mathscr{P}_{t_0}$ is the cotangent map, which is the adjoint of tensor $\mathbf{F}$ represented with $\mathbf{F}^* = F^a{}_A \boldsymbol{E}^{*A} \otimes \boldsymbol{e}_a$ (see commutative diagram 2.4.6). The transposition is defined to be compatible with metrics $\mathbf{G}$ and $\mathbf{g}$ such that

$$\mathbf{g}(z, \mathbf{F}Z) = \mathbf{G}(\mathbf{F}^\mathsf{T} z, Z),$$

for $Z \in T_X\mathscr{P}_{t_0}$ and $z \in T_x\mathscr{P}_t$.

The ***right (Cauchy-Green) deformation tensor*** is an automorphism $\mathrm{Aut}\left(T_X\mathscr{P}_{t_0}\right)$ defined as

$$\mathbf{C} \coloneqq \mathbf{F}^\mathsf{T}\mathbf{F}.$$

In similar fashion, the ***left (Cauchy-Green) deformation tensor*** is an automorphism[9] $\mathrm{Aut}\,(T_x\mathscr{P}_t)$ defined as

$$\mathbf{b} \coloneqq \mathbf{F}\mathbf{F}^\mathsf{T}.$$

In coordinates, the right and left deformation tensors can be written as

$$\mathbf{C} = C^A{}_B \boldsymbol{E}_A \otimes \boldsymbol{E}^{*B},$$
$$\mathbf{b} = b^a{}_b \boldsymbol{e}_a \otimes \boldsymbol{e}^{*b}.$$

We obtain $C^A{}_B = G^{AC} g_{ab} F^a{}_C F^b{}_B$, where G^{AC} is the inverse of G_{AC}.

Associated Deformation Tensors

By using the musical bundle isomorphisms $\flat\colon T\mathscr{P}_t \to T^*\mathscr{P}_t$ and $\sharp \coloneqq \flat^{-1}$ we define the ***associated deformation tensors***

$$\mathbf{C}^\flat = \mathbf{G}\mathbf{C}, \tag{2.4.3a}$$
$$\mathbf{b}^\sharp = \mathbf{b}\mathbf{g}^\sharp, \tag{2.4.3b}$$

where $\mathbf{g}^\sharp = \mathbf{g}^{-1}$.

Remark 2.4.1 (Symmetry of tensors versus matrices). The matrix representation of $\mathbf{C}^\flat = C_{AB}\boldsymbol{E}^{*A} \otimes \boldsymbol{E}^{*B}$ and $\mathbf{b}^\sharp = b^{ab}\boldsymbol{e}_a \otimes \boldsymbol{e}_b$ are symmetric, that is $C_{AB} = g_{ab}F^a{}_A F^b{}_B$ and $b^{ab} = G^{AB}F^a{}_A F^b{}_B$ are symmetric matrices. In contrast, the matrices $C^A{}_B$ and $b^a{}_b$ of the mixed covariant-contravariant deformation tensors $\mathbf{C}$ and $\mathbf{b}$ are *not* symmetric. Indeed, $\mathbf{C}$ and $\mathbf{b}$ are *symmetric* in the sense of transposition in (2.4.2) with respect to the metrics. For the

[9] An *automorphism* $\mathrm{Aut}(E)$ is an *isomorphic* endomorphism, $\mathrm{End}(E)$. Also, an *endomorphism* $\mathrm{End}(E)$ is a morphism form the set E to itself. On tensor bundle E, the endomorphism bundle $\mathrm{End}(E)$ is canonically isomorphic to the tensor product bundle $E \otimes E^*$, where E^* is the dual bundle of E.

deformation tensors $\mathbf{C}$ and $\mathbf{b}$ respectively, the transpositions induced by the metrics of their configuration spaces are

$$\mathbf{C}^\intercal = \mathbf{G}^{-1}\mathbf{C}^*\mathbf{G},$$
$$\mathbf{b}^\intercal = \mathbf{g}^{-1}\mathbf{b}^*\mathbf{g}.$$

By substituting the definitions of $\mathbf{C}$ and $\mathbf{b}$ in above, applying (2.4.2) together with $\mathbf{G}^* = \mathbf{G}$ and $\mathbf{g}^* = \mathbf{g}$, we can verify the symmetric properties $\mathbf{C}^\intercal = \mathbf{C}$ and $\mathbf{b}^\intercal = \mathbf{b}$. ▲

Remark 2.4.2 (Measuring deformation by associated tensors). We can use $\mathbf{C}^\flat$ to measure deformation of vectors on the referential configuration space, because the associated tensor is the map $T\mathscr{P}_{t_0} \to T^*\mathscr{P}_{t_0}$. This is the common interpretation of the right associated deformation tensor. Suppose that tangent vectors $\boldsymbol{Z}_1, \boldsymbol{Z}_2 \in T_{\boldsymbol{X}}\mathscr{P}_{t_0}$ are pullbacks of $\boldsymbol{z}_1, \boldsymbol{z}_2 \in T_{\boldsymbol{x}}\mathscr{P}_t$. That is $\boldsymbol{Z}_1 = \boldsymbol{\phi}^*\boldsymbol{z}_1$ and $\boldsymbol{Z}_2 = \boldsymbol{\phi}^*\boldsymbol{z}_2$. The lengths and angles of spatial (deformed) tangent vectors $\boldsymbol{z}_1$ and $\boldsymbol{z}_2$ are obtained by applying $\mathbf{C}^\flat$ to the referential (non-deformed) tangent vectors $\boldsymbol{Z}_1$ and $\boldsymbol{Z}_2$, with

$$\mathbf{C}^\flat(\boldsymbol{Z}_1, \boldsymbol{Z}_2) = \mathbf{g}(\boldsymbol{z}_1, \boldsymbol{z}_2) = \boldsymbol{z}_1 \cdot_{\mathbf{g}} \boldsymbol{z}_2. \tag{2.4.4}$$

▲

One can relate the associated deformation tensor with the pullback and pushforward of the metric tensors as (see [Marsden and Hughes, 1983, p. 57])

$$\mathbf{C}^\flat = \boldsymbol{\phi}^*\mathbf{g}, \tag{2.4.5a}$$
$$\mathbf{b}^\sharp = \boldsymbol{\phi}_*\mathbf{G}^\sharp, \tag{2.4.5b}$$

where $\mathbf{G}^\sharp = \mathbf{G}^{-1}$. The commutative diagram below summarizes relations expressed above. In particular, the relations $\mathbf{F}^\intercal = \mathbf{G}^{-1}\mathbf{F}^*\mathbf{g}$, $\mathbf{C}^\flat = \mathbf{G}\mathbf{C}$, $\mathbf{C}^\flat = \boldsymbol{\phi}^*\mathbf{g} = \mathbf{F}^*\mathbf{g}\mathbf{F}$, $\mathbf{C} = \mathbf{F}^\intercal\mathbf{F}$, $\mathbf{b} = \mathbf{F}\mathbf{F}^\intercal$, $\mathbf{b}^\sharp = \boldsymbol{\phi}_*\mathbf{G}^\sharp = \mathbf{F}\mathbf{G}^{-1}\mathbf{F}^*$ and $\mathbf{C}^\flat = \mathbf{F}^*\mathbf{g}\mathbf{F}$ can be inferred from the diagram.

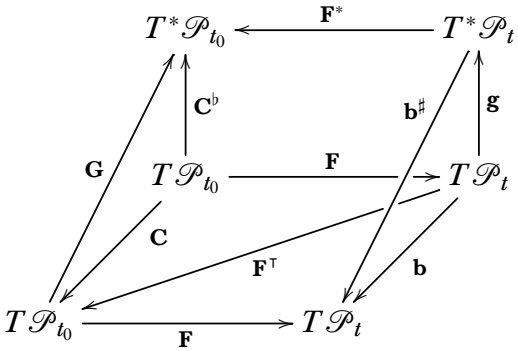

(2.4.6)

The vertical maps in the diagram relate configuration spaces to their corresponding dual spaces. The horizontal maps are pushforwards/pullbacks through the flow map in time. The

other maps extending out of the plane of the diagram indicate maps from configuration spaces to themselves (i.e., automorphisms, see Footnote 9). We will explain in the section 3.2, that these maps only stretch the space without any rotation or shift.

Chapter 3

Decompositions of Deformation

3.1 Introduction

In this chapter, we present three decompositions of the deformation tensors. In §3.2 we review the polar decomposition of the deformation gradient tensor $\mathbf{F}$. The polar decomposition represents the deformation gradient as the composition of a stretch map in referential configuration space, a parallel transport from referential to spatial configuration space, and rotation in spatial configuration space. Although the polar decomposition is not directly used in our formulations, it provides a better understanding of the tangent map and is closely related to the spectral decompositions that will substantially develop.

For an automorphism, i.e., an isomorphic map from a manifold to itself, the spectral decomposition is well understood. Examples are the right and left deformation tensors $\mathbf{C}$ and $\mathbf{b}$. However, to our knowledge, the spectral decomposition of maps between two different Riemannian spaces has received no attention. An example is the tangent map $\mathbf{F}$, as the isomorphism between the referential and spatial spaces. In §3.3 we define the spectral decomposition of $\mathbf{F}$ using Courant-Fisher-Weyl's minimax theorem. The eigenvalues defined this way are identical to the eigenvalues of deformation tensors $\mathbf{C}$ and $\mathbf{b}$. We will show that the eigenvalues of a map depend on the Riemannian metric used on both referential and spatial manifolds.

Lastly, we propose a definition for the singular value decomposition (SVD) in §3.4 for tangent map between two Riemannian manifolds. In our formulation, the matrices of left and right eigenvectors of the SVD are not unitary. Rather, they are orthogonal with respect to the metric tensors. The definition of SVD of $\mathbf{F}$ is consistent with the spectral decompositions of $\mathbf{C}$ and $\mathbf{b}$. That is, the singular values of $\mathbf{F}$ are the square root of the eigenvalues of $\mathbf{C}$ and $\mathbf{b}$, and the left and right eigenvectors of $\mathbf{F}$ are the same as the eigenvectors of $\mathbf{b}$ and $\mathbf{C}$ respectively. Additionally, the eigenvectors are intrinsic in the sense that they transform by covariant law under a change of coordinates.

3.2 Polar Decomposition

Since the right deformation tensor $\mathbf{C} : T\mathscr{P}_{t_0} \to T\mathscr{P}_{t_0}$ is a symmetric positive-definite linear transformation, there exists a unique symmetric positive-definite linear map $\mathbf{P} : T\mathscr{P}_{t_0} \to T\mathscr{P}_{t_0}$ such that $\mathbf{P} \coloneqq \mathbf{C}^{1/2}$. The tensor $\mathbf{P}$ is called the ***right stretch tensor***. Similarly, the ***left stretch tensor*** $\mathbf{p}$ exists such that it is the square root of the left deformation tensor, i.e., $\mathbf{p} \coloneqq \mathbf{b}^{1/2}$. Moreover, there exists an orthogonal tensor $\mathbf{R} : T\mathscr{P}_{t_0} \to T\mathscr{P}_t$ such that (see e.g., [Marsden and Ratiu, 1999, Prop. 9.2.1])

$$\mathbf{F} = \mathbf{RP} \quad \text{and} \quad \mathbf{F} = \mathbf{pR}.$$

These are the ***right*** and ***left polar decompositions*** of the deformation gradient tensor respectively.[1] The ***rotation tensor*** $\mathbf{R}$ is orthogonal, which implies $\mathbf{R}^\intercal\mathbf{R} = \mathbf{I}$ and $\mathbf{R}\mathbf{R}^\intercal = \mathbf{i}$. Here we have distinguished identity maps $\mathbf{I} : T\mathscr{P}_{t_0} \to T\mathscr{P}_{t_0}$ and $\mathbf{i} : T\mathscr{P}_t \to T\mathscr{P}_t$. The commutative diagram in Fig. 3.2.1 summarizes the polar decompositions of the deformation gradient tensor.

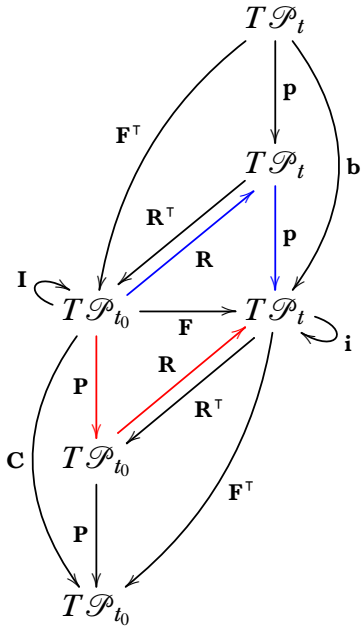

Figure 3.2.1: Left and right polar decompositions of the deformation gradient tensor are shown in red and blue respectively.

The symmetry and positive definiteness of stretch tensors ensure that they are diagonalizable and have a unique spectral decomposition. Let the set of orthonormal vectors $\{\hat{\boldsymbol{E}}_A\}$

[1] In continuum mechanics, the right and left stretch tensors are often denoted by $\mathbf{U}$ and $\mathbf{V}$. For notational consistency, we use $\mathbf{P}$ and $\mathbf{p}$ for the right and left stretch tensors, while $\mathbf{U}$ and $\mathbf{u}$ are used for singular value decomposition.

for $A = 1, \dots, n$ be eigenvectors of $\mathbf{C}$ or equivalently $\mathbf{P}$, and let the space $\hat{\mathscr{E}}_A$ be the invariant eigenspace spanned by eigenvector $\hat{\boldsymbol{E}}_A$. Similarly, let the set of orthonormal vectors $\{\hat{\boldsymbol{e}}_a\}$ for $a = 1, \dots, n$ be eigenvectors of $\mathbf{b}$, and let the space $\hat{\mathscr{E}}_a$ be the invariant eigenspace spanned by eigenvector $\hat{\boldsymbol{e}}_a$. By the spectral representation theorem [Conway, 1994, Theorem 5.1], the domain of symmetric operators $\mathbf{C}$ and $\mathbf{b}$ are decomposed into the direct sum of invariant eigenspaces that are mutually orthogonal. Hence,

$$T_X\mathscr{P}_{t_0} = \bigoplus_{A=1}^{n} \hat{\mathscr{E}}_A \quad \text{and} \quad T_x\mathscr{P}_t = \bigoplus_{a=1}^{n} \hat{\mathscr{E}}_a.$$

We observe that the tensor $\hat{\boldsymbol{E}}_A \otimes \hat{\boldsymbol{E}}^{*A}$ is a projection onto $\hat{\mathscr{E}}_A$ and the tensor $\hat{\boldsymbol{e}}_a \otimes \hat{\boldsymbol{e}}^{*a}$ is a projection onto $\hat{\mathscr{E}}_a$. So in eigenvector (principal) coordinates, the deformation and stretch tensors are diagonal and represented with

$$\mathbf{P} = P^A{}_B \boldsymbol{E}_A \otimes \boldsymbol{E}^{*B} = \Sigma^A \hat{\boldsymbol{E}}_A \otimes \hat{\boldsymbol{E}}^{*A}, \tag{3.2.1a}$$

$$\mathbf{C} = P^A{}_C P^C_B \boldsymbol{E}_A \otimes \boldsymbol{E}^{*B} = \Lambda^A \hat{\boldsymbol{E}}_A \otimes \hat{\boldsymbol{E}}^{*A}, \tag{3.2.1b}$$

$$\mathbf{p} = p^a{}_b \boldsymbol{e}_a \otimes \boldsymbol{e}^{*b} = \sigma^a \hat{\boldsymbol{e}}_a \otimes \hat{\boldsymbol{e}}^{*a}, \tag{3.2.1c}$$

$$\mathbf{b} = p^a{}_c p^c{}_b \boldsymbol{e}_a \otimes \boldsymbol{e}^{*b} = \lambda^a \hat{\boldsymbol{e}}_a \otimes \hat{\boldsymbol{e}}^{*a}, \tag{3.2.1d}$$

where the *stretch ratios* $\sigma^a = \Sigma^A \delta^a{}_A > 0$ for $A, a = 1, \dots, n$ are eigenvalues of either stretch tensors, and $\lambda^a = \Lambda^a \delta^a{}_A = (\sigma^a)^2$ are eigenvalues of the right deformation tensors. The vectors $\hat{\boldsymbol{E}}_A$ and $\hat{\boldsymbol{e}}_a$ are also called referential and spatial ***principal directions*** respectively.

The tensors in (3.2.1) are all one-point tensors since both bases are in the same space. In contrast, the rotation tensor is a two-point tensor having a basis from both referential and spatial configurations. In principal coordinates,

$$\mathbf{R} = R^a{}_A \boldsymbol{e}_a \otimes \boldsymbol{E}^{*A} = \hat{\boldsymbol{e}}_a \otimes \hat{\boldsymbol{E}}^{*A}. \tag{3.2.2}$$

Because $\mathbf{R}$ is orthogonal, it can be seen to generally represent *rotation* and *shift* from referential to spatial configuration spaces. The rotation part is an isometry on either referential or spatial configuration space. The shifting part is a parallel translation (also an isometry) from referential to spatial configuration space (see *shifter tensor* in [Marsden and Hughes, 1983, p. 57]). Altogether, $\mathbf{F}$ can be decomposed to either (1) a stretch in referential configuration followed by a rotation and shift to the spatial configuration, or (2) a rotation and shift from referential configuration followed by a stretch in spatial configuration. In Fig. 3.2.1 and equation (3.2.2) the rotation tensor plays two roles; it rotates in either space and then pushes the tangent vectors forward in time.

In this chapter, we define the eigenvalues of deformation in a Riemannian manifold from the geometric point of view and will show that they are indeed the same as the stretch ratios of stretch tensors. Also, we define the covariant singular value decomposition of deformation gradient tensor which is consistent with the spectral decomposition of deformation tensors.

3.3 Spectral Decomposition of Deformation on Riemannian Manifold

The associated tensors $\mathbf{C}^\flat$ and $\mathbf{b}^\flat$ intuitively give us a physical insight into the deformation since they are covariant in both indices, and they directly measure lengths and angles between two vectors, which is indeed the conception of deformation tensors. In contrast, mixed tensors $\mathbf{C}$ and $\mathbf{b}$ intuitively less related to measuring deformation. However, we will show that the eigenvalues are eigenvectors cannot be computed with the associated tensors $\mathbf{b}^\flat$ and $\mathbf{C}^\flat$. We will show that mixed covariant-contravariant tensors $\mathbf{C}$ and $\mathbf{b}$ are relevant instead. First, we should postulate a relevant definition for the eigenvalues and eigenvectors in a metric space.

In Euclidean space with trivial flat metric $g_{ab} = \delta_{ab}$, eigenvalues and eigenvectors are obtained with the spectral decomposition theorem of *matrices* C and b of the tensors $\mathbf{C} = \mathbf{C}^\flat$ and $\mathbf{b} = \mathbf{b}^\flat$ respectively. This rather algebraic approach does not convey properly into metric spaces, as one might use eigenvalues and eigenvectors of $\mathbf{C}^\flat$ and $\mathbf{b}^\flat$. In a space with non-trivial metric, an intrinsic definition of eigenvalues does not originate directly from the decomposition of matrix representations of tensors. Here we use the ***Courant-Fischer-Weyl's min-max theorem*** (variational theorem) [Kato, 1995, p. 60] to propose the eigenvalue problem in a geometric setting as follows.

Definition 3.3.1 (Spectral decomposition of tangent map on Riemannian Manifold). *Let $\boldsymbol{\phi} : \left(\mathscr{P}_{t_0}, \mathbf{G}\right) \to \left(\mathscr{P}_t, \mathbf{g}\right)$ be a diffeomorphism between two Riemannian manifolds. The **eigenvalues** $\Lambda_i \in \mathscr{C}(\mathscr{P}_{t_0})$ of deformation with the tangent map $T\boldsymbol{\phi} : T\mathscr{P}_{t_0} \to T\mathscr{P}_t$ are defined by*

$$\Lambda_i(\boldsymbol{X}, t) = \max_{\substack{S_i \subset T_{\boldsymbol{X}}\mathscr{P}_{t_0} \\ \dim(S_i) = i}} \min_{\boldsymbol{Z} \in S_i \setminus \{\mathbf{0}\}} \frac{\mathbf{g}(\boldsymbol{\phi}_* \boldsymbol{Z}, \boldsymbol{\phi}_* \boldsymbol{Z})}{\mathbf{G}(\boldsymbol{Z}, \boldsymbol{Z})}, \qquad i = 1, \cdots, n, \tag{3.3.1}$$

where, $S\mathscr{P}_{t_0}$ is the sphere bundle on $\mathscr{P}_{t_0}$. By using the inverse flow map we can equivalently define the eigenvalues

$$\lambda_i^{-1}(\boldsymbol{x}, t) = \max_{\substack{S_i \subset T_{\boldsymbol{x}}\mathscr{P}_t \\ \dim(S_i) = i}} \min_{\boldsymbol{z} \in S_i \setminus \{\mathbf{0}\}} \frac{\mathbf{G}(\boldsymbol{\phi}^* \boldsymbol{z}, \boldsymbol{\phi}^* \boldsymbol{z})}{\mathbf{g}(\boldsymbol{z}, \boldsymbol{z})}, \qquad i = 1, \cdots, n. \tag{3.3.2}$$

*The set of covariant vectors $\boldsymbol{Z}_i \in \Gamma\left(T\mathscr{P}_{t_0}\right)$ and $\boldsymbol{z}_i = \boldsymbol{\phi}_* \boldsymbol{Z}_i \in \Gamma\left(T\mathscr{P}_t\right)$ for $i = 1, \cdots, n$ that satisfies the above are termed the **right** and **left covariant eigenvectors** of the tangent map $T\boldsymbol{\phi}$ corresponding to the eigenvalues Λ_i.* ▲

The two definitions for eigenvalues Λ_i and λ_i of deformation are identical, which is verified in the following proposition.

Proposition 3.3.2 (Eigenvalue problem v.s. generalized eigenvalue problem). *In the definition 3.3.1,*

1. *Variational problem* (3.3.1) *leads to the generalized eigenvalue problem for tensor pairs* $(\mathbf{C}^\flat, \mathbf{G})$, *which is equivalent to the eigenvalue problem for tensor* $\mathbf{C}$ *with eigenvalues* Λ_i *and eigenvectors* $\boldsymbol{Z}$.

2. *Variational problem* (3.3.2) *leads to the generalized eigenvalue problem for tensor pairs* $(\mathbf{c}^\flat, \mathbf{g})$ *where* $\mathbf{c} \coloneqq \mathbf{b}^{-1}$, *which is equivalent to the eigenvalue problem for tensor* $\mathbf{b}$ *with eigenvalues* λ_i *and eigenvectors* $\boldsymbol{z}$.

3. *Both eigenvalue problems* (3.3.1) *and* (3.3.2) *are equivalent, i.e.,* $\Lambda_i = \lambda_i$ *and* $\boldsymbol{z}_i = \boldsymbol{\phi}_* \boldsymbol{Z}_i$ *for* $i = 1, \cdots, n$.

Proof. The first variation of the generalized Rayleigh quotient in the definition (3.3.1) can be represented with the critical point of the Lagrangian

$$L(\boldsymbol{Z}) = \mathbf{g}(\boldsymbol{\phi}_* \boldsymbol{Z}, \boldsymbol{\phi}_* \boldsymbol{Z}) - \Lambda \left(\mathbf{G}(\boldsymbol{Z}, \boldsymbol{Z}) - 1\right),$$

where, for now, $\Lambda \in \mathbb{R}$ is the Lagrange multiplier for the constraint $\boldsymbol{Z} \in S_{\boldsymbol{X}} \mathscr{P}_{t_0}$. Using (2.4.5a)

$$\mathbf{g}(\boldsymbol{\phi}_* \boldsymbol{Z}, \boldsymbol{\phi}_* \boldsymbol{Z}) = \left(\boldsymbol{\phi}^* \mathbf{g}\right)(\boldsymbol{Z}, \boldsymbol{Z}) = \mathbf{C}^\flat(\boldsymbol{Z}, \boldsymbol{Z}).$$

Hence $L(\boldsymbol{Z}) = \mathbf{C}^\flat(\boldsymbol{Z}, \boldsymbol{Z}) - \Lambda \left(\mathbf{G}(\boldsymbol{Z}, \boldsymbol{Z}) - 1\right)$. The directional derivative of the Lagrangian should vanish at a critical point. Let $\boldsymbol{Z}' \in T_{\boldsymbol{X}} \left(T_{\boldsymbol{X}} \mathscr{P}_{t_0}\right) \cong T_{\boldsymbol{X}} \mathscr{P}_{t_0}$, the directional derivative (or Lie derivative) of the scalar Lagrangian is

$$\mathscr{L}_{\boldsymbol{Z}'} L(\boldsymbol{Z}) = \left(2\mathbf{G}\left(\mathbf{C} - \Lambda \mathbf{I}\right)\right)(\boldsymbol{Z}, \boldsymbol{Z}') = 0, \qquad \forall \boldsymbol{Z}' \in T_{\boldsymbol{X}} \left(T_{\boldsymbol{X}} \mathscr{P}_{t_0}\right),$$

where $\mathbf{I} = \mathrm{id}_{T_{\boldsymbol{X}} \mathscr{P}_{t_0}}$. In the above derivation, we used the fact that the matrix representation of tensors $\mathbf{G}$ and $\mathbf{C}^\flat$ are symmetric (see remark 2.4.1). Also, the Lie derivative is coordinate-invariant and well-defined without assuming any additional structure on the manifold. By choosing a local chart on $\mathscr{P}_{t_0}$ around $\boldsymbol{X}$, the matrix representation of above yields $\det(C - \Lambda I) = 0$ which is the eigenvalue problem for the matrix C and concludes part (1).

Alternatively, one may start with Lagrangian

$$L(\boldsymbol{z}) = \mathbf{G}(\boldsymbol{\phi}^* \boldsymbol{z}, \boldsymbol{\phi}^* \boldsymbol{z}) - \lambda^{-1} \left(\mathbf{g}(\boldsymbol{z}, \boldsymbol{z}) - 1\right),$$

where Λ^{-1} is the Lagrange multiplier for the constraint $\boldsymbol{z} \in S_{\boldsymbol{x}} \mathscr{P}_t$. Similar to the above, we have

$$\mathbf{G}(\boldsymbol{\phi}^* \boldsymbol{z}, \boldsymbol{\phi}^* \boldsymbol{z}) = \left(\boldsymbol{\phi}_* \mathbf{G}\right)(\boldsymbol{z}, \boldsymbol{z}) = \mathbf{c}^\flat(\boldsymbol{z}, \boldsymbol{z}),$$

where $\mathbf{c} = \mathbf{b}^{-1}$. The Lagrangian becomes $L(\boldsymbol{z}) = \mathbf{c}^\flat(\boldsymbol{z}, \boldsymbol{z}) - \lambda^{-1} \left(\mathbf{g}(\boldsymbol{z}, \boldsymbol{z}) - 1\right)$ and its Lie derivative with respect to the variation $\boldsymbol{z}' \in T_{\boldsymbol{x}} \left(T_{\boldsymbol{x}} \mathscr{P}_t\right)$ and using $\mathbf{c}^\flat = \mathbf{g}\mathbf{b}^{-1}$ yields

$$\mathscr{L}_{\boldsymbol{z}'} L(\boldsymbol{z}) = \left(2\mathbf{g}\left(\mathbf{b}^{-1} - \lambda^{-1} \mathbf{i}\right)\right)(\boldsymbol{z}, \boldsymbol{z}') = 0, \qquad \forall \boldsymbol{z}' \in T_{\boldsymbol{x}} \left(T_{\boldsymbol{x}} \mathscr{P}_t\right),$$

where $\mathbf{i} = \mathrm{id}_{T_x\mathscr{P}_t}$. In the above derivation, we have used the fact that the matrices of tensors $\mathbf{g}$ and $\mathbf{c}^\flat$ are symmetric. By choosing a local chart on $\mathscr{P}_t$ around $\boldsymbol{x}$, the matrix representation of above yields an eigenvalue problem for the matrix b^{-1}, and concludes part (2).

Lastly, consider $\mathbf{F}^\intercal\mathbf{F}(z,z') - \Lambda\mathbf{I}(Z,Z') = \mathbf{0}$. Define $z = \boldsymbol{\phi}_* Z = \mathbf{F}Z$ and $z' = \boldsymbol{\phi}_* Z = \mathbf{F}Z$. Then one can write $\mathbf{F}^\intercal(z,z') - \Lambda\mathbf{F}^{-1}(z,z') = \mathbf{0}$; The pushforward of this equation using the left multiplication with $\mathbf{F}$ yields $\mathbf{b}(z,z') - \Lambda\mathbf{i}(z,z') = \mathbf{0}$. If the latter relation satisfies an eigenvalue problem for $\mathbf{b}$, then $\Lambda = \lambda$ and $z = \boldsymbol{\phi}_* Z$ should be the eigenvector, which concludes part (3). ■

Remark 3.3.3 (Well-posedness of spectral decomposition). The eigenvalues and eigenvectors depend on the choice of metric tensors $\mathbf{G}$ and $\mathbf{g}$ on the manifolds. However, the eigenvalues are invariant under ***Riemannian isometry groups*** $\mathrm{Isom}(\mathscr{P}_{t_0}, \mathbf{G})$ and $\mathrm{Isom}(\mathscr{P}_t, \mathbf{g})$ and the left/right eigenvector coordinates transform by the contravariant law. That is, under diffeomorphisms

$$\boldsymbol{\Psi} : (\hat{\mathscr{P}}_{t_0}, \hat{\mathbf{G}}) \to (\mathscr{P}_{t_0}, \mathbf{G}) \quad \text{and} \quad \boldsymbol{\psi} : (\hat{\mathscr{P}}_t, \hat{\mathbf{g}}) \to (\mathscr{P}_t, \mathbf{g}),$$

the spectral decomposition is invariant if

$$\hat{\mathbf{G}} = \boldsymbol{\Psi}^* \mathbf{G} \quad \text{and} \quad \hat{\mathbf{g}} = \boldsymbol{\psi}^* \mathbf{g}.$$

▲

Remark 3.3.4 (Orthogonality of eigenvectors with respect to metric). A basic fact from Linear algebra is that any pair of distinct eigenvalues of a symmetric matrix has orthogonal eigenvectors. The tensors $\mathbf{C}$ and $\mathbf{b}$ are symmetric in the sense of inner product with respect to their metrics, but the tensor themselves are not symmetric with respect to their arguments. For instance $\mathbf{C}(\boldsymbol{U}_1, \boldsymbol{U}_2) \neq \mathbf{C}(\boldsymbol{U}_2, \boldsymbol{U}_1)$. As a result, their matrix representations $C^A{}_B$ and $b^a{}_b$ are not symmetric matrices, which might suggest non-orthonormal eigenvectors. This can be resolved by considering the fact that the eigenvectors are orthonormal with respect to the metrics. To show this, let $\boldsymbol{U}_i$ and $\boldsymbol{U}_j$ be two right eigenvectors, then $\mathbf{C}^\flat(\boldsymbol{U}_i, \boldsymbol{U}_j) - \Lambda_i \mathbf{G}(\boldsymbol{U}_i, \boldsymbol{U}_j) = \mathbf{0}$. Since $\mathbf{C}^\flat$ is a symmetric tensor, by swapping indices i and j and subtracting the resulted equation from the original equations we obtain $\mathbf{G}(\boldsymbol{U}_i, \boldsymbol{U}_j) = \delta_{ij}$ provided that $\Lambda_i \neq \Lambda_j$. The same argument applies to left eigenvectors $\boldsymbol{u}_i$ and $\boldsymbol{u}_j$, implying the orthonormality condition $\mathbf{g}(\boldsymbol{u}_i, \boldsymbol{u}_j) = \delta_{ij}$. ▲

3.4 Singular Value Decomposition of Deformation Gradient

The singular value decomposition (SVD) packs the complete information on a linear operator. We seek a definition of decomposition of the matrix representation F of the linear map $\mathbf{F}$

such that (1) it accounts the metric structure of the Riemannian space and (2) it is consistent with the spectral decomposition of $\mathbf{F}^\intercal\mathbf{F}$ and $\mathbf{F}\mathbf{F}^\intercal$.

Define the matrices

$$\begin{aligned}\widetilde{F} &\coloneqq g^{\frac{1}{2}} F G^{-\frac{1}{2}},\\ \widetilde{C} &\coloneqq G^{\frac{1}{2}} C G^{-\frac{1}{2}},\\ \widetilde{b} &\coloneqq g^{\frac{1}{2}} b g^{-\frac{1}{2}}.\end{aligned}$$

Since metric tensors are symmetric and positive-definite, the square root matrices $g^{\pm\frac{1}{2}}$ and $G^{\pm\frac{1}{2}}$ are well-defined. Observe that

$$\widetilde{C} = \widetilde{F}^*\widetilde{F}, \quad \text{and} \quad \widetilde{b} = \widetilde{F}\widetilde{F}^*.$$

The above relations for the tilde matrices resemble the relations of deformation gradient matrix and Cauchy-Green matrices in Euclidean space. Hence, the properties that are known for these matrices in Euclidean space can be applied to $\widetilde{C}$ and $\widetilde{b}$. For instance, we readily know that $\widetilde{C}$ and $\widetilde{b}$ are symmetric and positive definite. We can also show that the matrices C and b are positive (semi-)definite, but not necessarily symmetric. These properties extend to the positiveness of tensors $\mathbf{C}$ and $\mathbf{b}$ as follows.

Proposition 3.4.1. *The eigenvalues of* $\mathbf{C}$ *and* $\mathbf{b}$ *are real and non-negative. Moreover, if* $\mathbf{F}$ *is an isomorphism, then, the eigenvalues of* $\mathbf{C}$ *and* $\mathbf{b}$ *are positive.*

Proof. Observe that $\widetilde{C}$ and C are conjugate with similarity transformation (as well as $\widetilde{b}$ and b), hence they share the same eigenspace. However, $\widetilde{C}$ and $\widetilde{b}$ are Gramian matrices of $\widetilde{F}$, so, they are positive-semidefinite with real non-negative eigenvalues. Moreover, if $\widetilde{F}$ or F is full rank, then C and b are positive-definite with real positive eigenvalues. ∎

The singular value decomposition of $\widetilde{F}$ and spectral decompositions of $\widetilde{C}$ and $\widetilde{b}$ are

$$\begin{aligned}\widetilde{F} &= \widetilde{u}\Sigma\widetilde{U}^*,\\ \widetilde{C} &= \widetilde{U}\Lambda\widetilde{U}^*,\\ \widetilde{b} &= \widetilde{u}\Lambda\widetilde{u}^*,\end{aligned}$$

where $\widetilde{u}, \widetilde{U} \in \mathrm{SO}(n)$ and the diagonal matrix Λ is the matrix of the eigenvalues of $\widetilde{C}$, and $\widetilde{b}$. Additionally, $\Sigma = \Lambda^{\frac{1}{2}}$ is the singular values of $\widetilde{F}$. Motivated by this, we define singular value decomposition of F.

Definition 3.4.2 (Singular value decomposition). *Let* $\mathbf{F} = T\boldsymbol{\phi}$ *denote the tangent map of the diffeomorphism* $\boldsymbol{\phi}$ *between two Riemannian manifolds* $\left(\mathscr{P}_{t_0}, \mathbf{G}\right)$ *and* $\left(\mathscr{P}_t, \mathbf{g}\right)$*. We define the* ***singular value decomposition*** *of the matrix* F *of the tensor* $\mathbf{F}$ *with respect to the Riemannian metrics by*

$$F = g^{-\frac{1}{2}}\widetilde{u}\Sigma\widetilde{U}^* G^{\frac{1}{2}}, \tag{3.4.1}$$

where $\widetilde{u}, \widetilde{U} \in \mathrm{SO}(n)$*, which* $\widetilde{U}^*\widetilde{U} = I$ *and* $\widetilde{u}^*\widetilde{u} = i$ *where* I *and* i *are identity matrices. Also,* Σ *is a diagonal matrix, and the diagonals* Σ_a*,* $a = 1, \cdots, n$ *are the* ***singular values****. The matrices of the* ***left and right eigenvectors*** *are* $u \coloneqq g^{-\frac{1}{2}}\widetilde{u}$ *and* $U \coloneqq G^{-\frac{1}{2}}\widetilde{U}$ *respectively.* ▲

Remark 3.4.3. One can re-write the above definition as

$$F = u\Sigma U^{-1}, \tag{3.4.2}$$

subject to weighted norm constraints with respect to the metrics by

$$\begin{aligned} G(U,U) &= U^* G U = I, \\ g(u,u) &= u^* g u = i. \end{aligned}$$

The above form is similar to the ***generalized singular value decomposition*** (GSVD) [Golub and Van Loan, 1996, p. 465, Theorem 8.7.4] with a difference that GSVD is defined with adjoint (transpose of matrix) of U as $F = u\Sigma U^*$, while the SVD defined in (3.4.2) uses the inverse of U. We also note that the eigenvectors (i.e., the columns of matrices U and u) in Definition 3.4.2 transform by covariant law and intrinsically well-defined for a two-point tensor. ▲

To compute the SVD for a given matrix F, first, construct $\widetilde{F} = g^{\frac{1}{2}} F G^{-\frac{1}{2}}$, then compute the conventional singular value decomposition of $\widetilde{F}$ as is done in the Euclidean space by $\widetilde{F} = \widetilde{u}\Sigma\widetilde{U}^*$. The diagonal matrix Σ is the matrix of singular values of F, and the matrices $u = g^{-\frac{1}{2}}$ and $U = G^{-\frac{1}{2}}\widetilde{U}$ are the matrices of the left and right eigenvectors of F. Similarly, to compute the spectral decomposition of C, first, construct $\widetilde{C} = G^{\frac{1}{2}} C G^{-\frac{1}{2}}$, then compute the conventional spectral decomposition of the symmetric matrix $\widetilde{C}$ as is done in the Euclidean space by $\widetilde{C} = \widetilde{U}\Lambda\widetilde{U}^*$. The columns of the matrix $U = G^{-\frac{1}{2}}\widetilde{U}$ are the right eigenvectors of C.

Chapter 4

Kinematics of Deformation

4.1 Introduction

The goal of this chapter is to derive first-order evolution equations for deformation tensors, in particular, the deformation gradient $\mathbf{F}$, and the left and right deformation tensors $\mathbf{b}$ and $\mathbf{C}$. We do so by obtaining their material time derivatives. The material rates are essentially the pullback covariant derivatives along the flow. A brief introduction to a connection on the vector bundle is presented in §4.2.

In literature, the kinematics of continua are often presented with torsion-free connections by default, such as the Levi-Civita connection. Despite the simplifications gained by this assumption, the underlying effect of the torsion of the connection is obscured. To this end, throughout our formulations we assume the connection is non-trivial and arbitrary, meaning it involves the *torsion tensor*. Our development with torsion necessitates the redefinition of some existing variables in kinematics. For instance, in §4.5 we redefine the Euler-Cauchy-Stokes decomposition of the rate of deformation tensor. The evolution equation of the deformation gradient is given in §4.3. Also, we review the rate of volume change, which will be useful later in Chapter 7 when we will revisit the Liouville theorem and isochoric flows.

Alternatively, the evolution equations can also be derived by Lie derivatives. In the same context, the *objective rates* in the mechanics of continua are also related to the Lie derivatives of second-order tensors. Our new formulation with arbitrary torsion generalizes objective rates of second-order tensors. In particular, in §4.6 we represent the Oldroyd and Cotter-Rivlin rates on general vector bundles.

Lastly, the first-order material rates of deformation are given in §4.7 and §4.9. In these formulations, the material rate of metric tensor appears. Because we use arbitrary connections, the metric tensor is no longer a parallel section with respect to the connection. In §4.8, we present the material rate of the metric tensor in terms of the *contorsion* of the connection.

4.2 Connection and Torsion on Tangent Bundle

Linear Connection

Let the ***linear Koszul connection*** on spatial tangent bundle with projection $\pi : T\mathscr{P}_t \to \mathscr{P}_t$ denoted by

$$\nabla : \Gamma\left(T\mathscr{P}_t\right) \to \Gamma\left(\mathrm{Hom}\left(T\mathscr{P}_t, T\mathscr{P}_t\right)\right).$$

In the spatial coordinate chart $\{x^a\}$, the connection is represented by ***Christoffel symbols of the second kind*** $\gamma^a{}_{bc}$ for $a, b, c = 1, \cdots, n$. The Christoffel symbols denote the coordinates of the covariant derivatives of the basis vectors [Spivak, 1999, p. 187], that is

$$\frac{\partial \boldsymbol{e}_a}{\partial x^b} = \nabla_{\boldsymbol{e}_b} \boldsymbol{e}_a = \gamma^c{}_{ba} \boldsymbol{e}_c.$$

Connection is not a tensor (a linear map), and the Christoffel symbols do not transform by covariant or contravariant laws.

Remark 4.2.1 (Types of connections). A linear connection can be defined in multiple ways depending on the assumptions to be held on the vector bundle. In the most common form, the ***linear Ehresmann connection*** defines the horizontal subspace by splitting the linear structure of the vector bundle [Epstein, 2010, §9.1]. The Koszul connection further allows defining the directional derivative that is discussed in §4.3. Since these two types of connections are related by bijection, in our development, we do not distinguish between them. ▲

Denote the covariant derivative of referential and spatial velocities $\boldsymbol{V}(\boldsymbol{X}, t) = V^a \boldsymbol{e}_a$ and $\boldsymbol{v}(\boldsymbol{x}, t) = v^a \boldsymbol{e}_a$ with $\nabla^{\boldsymbol{\phi}} \boldsymbol{V}$ and $\nabla \boldsymbol{v}$ respectively. Here,

$$\nabla^{\boldsymbol{\phi}} := \boldsymbol{\phi}^* \nabla : \Gamma\left(T\mathscr{P}_{t_0}\right) \to \Gamma\left(\mathrm{Hom}\left(T\mathscr{P}_t, T\mathscr{P}_t\right)\right),$$

denotes the ***pullback connection*** that is applied on the pullback bundle $\Gamma^{\boldsymbol{\phi}}\left(T\mathscr{P}_t\right)$. In referential and spatial coordinate charts $\{X^B\}$ and $\{x^b\}$, the coordinates of these covariant derivatives are given by

$$\nabla^{\boldsymbol{\phi}} \boldsymbol{V} = V^a{}_{|B} \boldsymbol{e}_a \otimes \boldsymbol{E}^{*B} := \left(\frac{\partial V^a}{\partial X^B} + \gamma^a{}_{bc} F^b{}_B V^c\right) \boldsymbol{e}_a \otimes \boldsymbol{E}^{*B}, \tag{4.2.1a}$$

$$\nabla \boldsymbol{v} = v^a{}_{|b} \boldsymbol{e}_a \otimes \boldsymbol{e}^{*b} := \left(\frac{\partial v^a}{\partial x^b} + \gamma^a{}_{bc} v^c\right) \boldsymbol{e}_a \otimes \boldsymbol{e}^{*b}. \tag{4.2.1b}$$

The subscripts $.|_B$ and $.|_b$ in (4.2.1) indicate the covariant derivative for the referential coordinate chart $\{X^B\}$ and the spatial coordinate chart $\{x^b\}$ respectively. We can express the covariant derivative of referential velocity with respect to referential coordinates, $V^a{}_{|B}$, as the pullback of the covariant derivative of spatial velocity with respect to spatial coordinates, $v^a{}_{|b}$, as follows:

Lemma 4.2.2 (Pullback connection of material velocity). *If* $\boldsymbol{\phi} \in C^1(\mathscr{P}_{t_0} \times \mathscr{I}; \mathscr{P}_t)$*, then*

$$\nabla^{\boldsymbol{\phi}} \boldsymbol{V} = (\nabla \boldsymbol{v})\mathbf{F}. \tag{4.2.2}$$

In the local charts $\{X^A\}$ *and* $\{x^a\}$ *that is* $V^a{}_{|B} = v^a{}_{|b} F^b{}_B$.

Proof. Suppose $\boldsymbol{x} = \boldsymbol{\phi}(\boldsymbol{X}, t)$. Recall from equations (2.2.3) and (2.2.5) that $\boldsymbol{V} = \boldsymbol{v} \circ \boldsymbol{\phi}$. With the chain rule we obtain

$$\nabla^{\boldsymbol{\phi}} \boldsymbol{V} = \nabla^{\boldsymbol{\phi}} (\boldsymbol{v} \circ \boldsymbol{\phi})_{\boldsymbol{X}} = (\nabla \boldsymbol{v})_{\boldsymbol{x}} \circ T_{\boldsymbol{X}} \boldsymbol{\phi} = (\nabla \boldsymbol{v})\, \mathbf{F}.$$

■

Torsion Tensor

A connection $\nabla_{z_1} z_2$ is not a tensor since it is not linear in its argument z_2. Nonetheless, the skew-symmetrization of connection is the tensor of torsion which is given as follows. The Cartan's ***torsion tensor*** of the connection ∇ is the homeomorphism

$$\mathrm{tor} \in \mathrm{Hom}\left(\bigwedge^2 \left(T^* \mathscr{P}_t \right), T\mathscr{P}_t \right),$$

where the symbol $\bigwedge$ denotes the space of alternating tensor bundles. Specifically, $\bigwedge^k (\mathscr{P}_t)$ is ***Grassmann (exterior) algebra*** of k-forms on $\mathscr{P}_t$ providing that $\mathscr{P}_t$ is Banach space [Abraham, Marsden, and Rațiu, 1988, §6.1.7]. In the local frame $\{\boldsymbol{x}^a\}$ the torsion is given by

$$\mathrm{tor} = \tau^a{}_{bc} \boldsymbol{e}_a \otimes \boldsymbol{e}^{*b} \otimes \boldsymbol{e}^{*c}. \tag{4.2.3}$$

On the *holonomic basis* of the tangent bundle (see (2.3.2)) the torsion coefficients are related to the Christoffel symbols by

$$\tau^a{}_{bc} := \gamma^a{}_{[bc]} = \gamma^a{}_{bc} - \gamma^a{}_{cb},$$

hence,

$$\mathrm{tor} = \gamma^a{}_{bc} \boldsymbol{e}_a \otimes \boldsymbol{e}^{*b} \wedge \boldsymbol{e}^{*c}. \tag{4.2.4}$$

The skew-symmetrization of connection is given by torsion as (see e.g., [Kobayashi and Nomizu, 1963, Ch. III, Theorem 5.1])

$$\mathrm{tor}(z_1, z_2) = \nabla_{z_1} z_2 - \nabla_{z_2} z_1 - [z_1, z_2]\,. \tag{4.2.5}$$

where $z_1, z_2 \in T\mathscr{P}_t$ are tangent vectors, and $[z_1, z_2]$ is the Lie bracket of vectors z_1 and z_2. A ***torsion-free*** connection with $\tau^a{}_{bc} = 0$ is referred to as ***symmetric connection***.

4.3 Material Rate of Deformation Gradient

Connection Along Homeomorphisms

Recall the connection ∇ on tangent bundle is a section of the tensor bundle $T\mathscr{P}_t \otimes T^*\mathscr{P}_t \otimes T^*\mathscr{P}_t$. Similarly, we define a connection induced by flow homeomorphism as follows. Fix a material point $\boldsymbol{X} \in \mathscr{P}_{t_0}$, and assume the flow $\boldsymbol{\phi}_t(\boldsymbol{X}) : \mathscr{I} \to \mathscr{P}_t$ is a one-parameter group of homeomorphism. The pullback connection $\boldsymbol{\phi}^*\nabla$ is the ***connection along the flow*** $\boldsymbol{\phi}_t$, which is a section of the pullback bundle $\boldsymbol{\phi}^*\left((T\mathscr{P}_t) \otimes T^*\mathscr{P}_t \otimes T^*\mathscr{P}_t\right)$ shown by the commutative diagram,

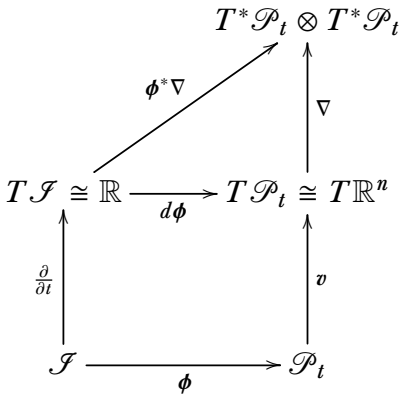

where $\cong$ denotes isomorphism. Also the tangent vectors $\partial/\partial t$, $\boldsymbol{v}$ and the maps ∇ and $\boldsymbol{\phi}^*\nabla$ are shown as sections. The pullback connection $\boldsymbol{\phi}^*\nabla$, often noted by $\nabla^{\boldsymbol{\phi}}$, is essentially the connection on the space $\mathscr{I}$ projected along the in the tangent direction $\partial/\partial t \in T\mathscr{I}$, and can be expressed by the connection ∇ projected in the direction of the pushforwarded vector $\boldsymbol{\phi}_*\left(\frac{\partial}{\partial t}\right) = d\boldsymbol{\phi}(\frac{\partial}{\partial t}) = \boldsymbol{v}$, given by

$$\boldsymbol{\phi}^*\nabla = \nabla^{\boldsymbol{\phi}}_{\frac{\partial}{\partial t}} = \nabla_{d\boldsymbol{\phi}(\frac{\partial}{\partial t})} = \nabla_{\boldsymbol{v}}.$$

The ***material time derivative*** (or material rate) of a tensor is the covariant time derivative along the flow and given by

$$\frac{D}{dt} \coloneqq \nabla_{\frac{\partial}{\partial t}} = \frac{\partial}{\partial t} + \nabla_{\boldsymbol{v}}. \tag{4.3.1}$$

Material Rate of Deformation Gradient by Torsion of Connection

In the following, we obtain the material time derivative of the deformation gradient tensor $\mathbf{F}$. In our development, we use arbitrary connection that may include torsion.

Proposition 4.3.1 (Material rate of deformation gradient). *If $\boldsymbol{\phi}_t \in C^1(\mathscr{P}_{t_0} \times \mathscr{I}; \mathscr{P}_t)$, then by using arbitrary linear connection ∇ on the spatial tangent bundle, the material rate of the*

deformation gradient tensor is given by

$$\frac{D\mathbf{F}}{dt} = \big(\nabla \boldsymbol{v} + \operatorname{tor}(\boldsymbol{v}, \cdot)\big)\mathbf{F}, \qquad \mathbf{F}(\boldsymbol{X}, t_0) = \mathbf{I}(\boldsymbol{X}), \tag{4.3.2}$$

where D/dt denotes the material time derivative, $\operatorname{tor}(\boldsymbol{v}, \cdot) = \tau^a{}_{cb} v^c \boldsymbol{e}_a \otimes \boldsymbol{e}^{*b}$ *is the contraction of spatial velocity with the first covariant index of torsion, and the identity* $\mathbf{I} \coloneqq T(\mathrm{id}_{\mathscr{P}_{t_0}}) = \delta^A_B \boldsymbol{E}_A \otimes \boldsymbol{E}^{*B}$ *is the trivial automorphism on* $T\mathscr{P}_{t_0}$.

Proof. Combining (2.3.3) with (2.3.4)

$$\mathbf{F}(\boldsymbol{X}, t) = \frac{\partial \boldsymbol{\phi}^a(t)}{\partial X^A} \boldsymbol{e}_a(\boldsymbol{x}) \otimes \boldsymbol{E}^{*A}(\boldsymbol{X}).$$

Since $\boldsymbol{x} = \boldsymbol{\phi}(\boldsymbol{X}, t)$ depends on time, so do bases $\boldsymbol{e}_a(\boldsymbol{x})$. The total (material) derivative with respect to t is

$$\begin{aligned}
\frac{D}{dt}\mathbf{F}(\boldsymbol{X}, t) &= \frac{\partial}{\partial X^A}\left(\frac{\partial \boldsymbol{\phi}^a(t)}{\partial t}\right) \boldsymbol{e}_a \otimes \boldsymbol{E}^{*A} + \frac{\partial \boldsymbol{\phi}^a}{\partial X^A}\frac{\partial x^b}{\partial t}\frac{\partial \boldsymbol{e}_a(\boldsymbol{x})}{\partial x^b} \otimes \boldsymbol{E}^{*A} \\
&= \frac{\partial V^a}{\partial X^A} \boldsymbol{e}_a \otimes \boldsymbol{E}^{*A} + F^a{}_A v^b \gamma^c{}_{ba} \boldsymbol{e}_c \otimes \boldsymbol{E}^{*A} \\
&= \left(\frac{\partial V^a}{\partial X^A} + \left(\gamma^a{}_{cb} - \gamma^a{}_{cb} + \gamma^a{}_{bc}\right) v^b F^c{}_A\right) \boldsymbol{e}_a \otimes \boldsymbol{E}^{*A} \\
&= \left(V^a{}_{|A} + \tau^a{}_{bc} v^b F^c{}_A\right) \boldsymbol{e}_a \otimes \boldsymbol{E}^{*A} \\
&= \left(v^a{}_{|c} + \tau^a{}_{bc} v^b\right) \boldsymbol{e}_a \otimes \boldsymbol{e}^{*c} F^c{}_A \boldsymbol{e}_c \otimes \boldsymbol{E}^{*A}.
\end{aligned}$$

Here we have used (2.2.3) and that $\partial \boldsymbol{e}_a / \partial x^b = \nabla_{\boldsymbol{e}_b} \boldsymbol{e}_a = \gamma^c{}_{ba} \boldsymbol{e}_c$. At the end, the Lemma 4.2.2 concludes (4.3.2). ∎

In local charts $\{X^A\}$ and $\{x^a\}$ we have

$$\frac{D\mathbf{F}}{dt} = \left(\frac{\partial F^a{}_A}{\partial t} + \gamma^a{}_{bc} v^b F^c{}_A\right) \boldsymbol{e}_a \otimes \boldsymbol{E}^{*A}. \tag{4.3.3}$$

Substituting above and (4.2.4) into tensorial relation (4.3.2) eliminates Christoffel symbols and simplifies to

$$\frac{\partial F^a{}_A}{\partial t} = \frac{\partial v^a}{\partial x^b} F^b{}_A, \tag{4.3.4}$$

which is independent of the choice of connection. Indeed, instead of the above direct derivation, we could use the Lie derivative of $\mathbf{F}$ that is independent of the connection on the vector bundle. We will explore the Lie derivative of $\mathbf{F}$ later in §4.6.

In general, the matrix differential equation 4.3.4 is solved by direct numerical integration. However, such computation usually becomes unstable for large deformations because the solution of these equations will be dominated by the strongest eigen-pair of the deformation gradient tensor. We can overcome this problem by considering evolution equations for the singular values and eigenvectors of the deformation gradient tensor directly. This can be achieved by diagonalizing our evolution equations (this is equivalently done by directly deriving evolution equations for the eigenvalues and eigenvectors of the deformation tensor).

Remark 4.3.2 (Lie Group and Lie Algebra of Deformation Gradient). In general, the configuration space of the matrix $F^a{}_A$ is the *general linear group* $\mathrm{GL}(n,\mathbb{R})$ where $\det(F) \neq 0$. However, the space of $\mathrm{GL}(n,\mathbb{R})$ is not connected [Marsden and Ratiu, 1999, Prop. 9.2.2]. Hence, for the continuous evolution of deformation, we consider the subgroup $F \in \mathrm{GL}^+(n,\mathbb{R})$, where

$$\mathrm{GL}^+(n,\mathbb{R}) = \{F \in \mathrm{GL}(n,\mathbb{R}) \mid \det(F) > 0\}\,.$$

The configuration space of the Lie group $\mathrm{GL}^+(n,\mathbb{R})$ is connected [Marsden and Ratiu, 1999, p. 285], hence, $\det(F)$ remains positive for $t \in \mathscr{I}$, corresponding to physical deformation of continua. Also, by setting $F = \mathrm{id}$ (the identity matrix) at $t = t_0$ in (4.3.4) it can be observed that the matrix of velocity gradient $\partial v^a/\partial x^b$ belongs to $\mathfrak{gl}(n,\mathbb{R})$, which is the Lie algebra of the general linear Lie group. That is,

$$\frac{\partial v}{\partial x} \in \mathfrak{gl}(n,\mathbb{R}) \coloneqq T_{\mathbf{I}}\mathrm{GL}^+(n,\mathbb{R}) = \mathrm{Lie}\left(\mathrm{GL}^+(n,\mathbb{R})\right),$$

where $\mathbf{I}$ is the identity tensor on referential configuration space. In other words, since $\dfrac{\partial v}{\partial x} = \dfrac{DF}{dt}F^{-1}$, the matrix $\partial v/\partial x$ is the *left-invariant field* on the corresponding Lie algebra under the group action of F. ▲

4.4 Isochoric Flows

The ***isochoric*** (volume-preserving) deformations are often of interest. Suppose $\mathbf{0} \neq \boldsymbol{\Theta}_{\mathbf{G}} \in \bigwedge^n(T^*\mathscr{P}_{t_0})$ and $\mathbf{0} \neq \boldsymbol{\theta}_{\mathbf{g}} \in \bigwedge^n(T^*\mathscr{P}_t)$ are ***volume forms*** on orientation preserving Riemannian n-manifolds $(\mathscr{P}_{t_0}, \mathbf{G})$ and $(\mathscr{P}_t, \mathbf{g})$ given by

$$\boldsymbol{\Theta}_{\mathbf{G}}(\boldsymbol{X}) = \sqrt{\det(\mathbf{G})}\bigwedge_{A=1}^{n}\boldsymbol{E}^{*A} = \sqrt{\det(\mathbf{G})}\,\left(dX^1 \wedge \cdots \wedge dX^n\right),$$

and

$$\boldsymbol{\theta}_{\mathbf{g}}(\boldsymbol{x}) = \sqrt{\det(\mathbf{g})}\bigwedge_{a=1}^{n}\boldsymbol{e}^{*a} = \sqrt{\det(\mathbf{g})}\,\left(dx^1 \wedge \cdots \wedge dx^n\right),$$

where $\wedge$ is the skew-symmetric tensor product on exterior algebra. Note the volume forms depend on the Riemannian metrics, and they can be defined by *Hodge star operator* as the Hodge dual of identity by $\boldsymbol{\Theta}_{\mathbf{G}} = *_{\mathbf{G}}(1)$ and $\boldsymbol{\theta}_{\mathbf{g}} = *_{\mathbf{g}}(1)$.

The volume preservation of the flow implies [Abraham and Marsden, 2008, Definition 2.5.16]

$$\boldsymbol{\Theta}_{\mathbf{G}} = \boldsymbol{\phi}^* \boldsymbol{\theta}_{\mathbf{g}}. \tag{4.4.1}$$

We provide two related views of volume-preserving flows in the forms of the determinant (or Jacobian) of the flow and the divergence of the velocity field that follows. Using the Lie derivative (see also §4.6) the rate of volume form $\boldsymbol{\theta}_{\mathbf{g}}$ is given by

$$\pounds_v \boldsymbol{\theta}_{\mathbf{g}} = \boldsymbol{\phi}_* \left.\frac{d}{dt}\right|_{t_0} \left(\boldsymbol{\phi}^* \boldsymbol{\theta}_{\mathbf{g}}\right) = \mathbf{0}.$$

On the other hand, by ***Cartan's magic formula*** the autonomous Lie derivative of the above relation can be expressed by

$$\pounds_v \boldsymbol{\theta}_{\mathbf{g}} = \boldsymbol{d}\left(\boldsymbol{\iota}_v \boldsymbol{\theta}_{\mathbf{g}}\right) + \boldsymbol{\iota}_v \left(\boldsymbol{d}\boldsymbol{\theta}_{\mathbf{g}}\right) = (\operatorname{div} v)\, \boldsymbol{\theta}_{\mathbf{g}}. \tag{4.4.2}$$

where $\boldsymbol{\iota}_v$ is the interior product[1], and $\boldsymbol{d}$ is the exterior derivative. Observe that $\boldsymbol{d}\boldsymbol{\theta}_{\mathbf{g}} = \mathbf{0}$ since the volume form is closed by Poincaré Lemma. Also, in the last equality of (4.4.2) the divergence theorem on Riemannian manifold is applied [Lee, 1997, p. 422], leading to the known identity $\boldsymbol{d}(\boldsymbol{\iota}_v \boldsymbol{\theta}_{\mathbf{g}}) = (\operatorname{div} v)\boldsymbol{\theta}_{\mathbf{g}}$. As a result, the isochoric flow indicates $\operatorname{div}(v) = 0$.

An alternative view of the volume preservation can be shown by the ***determinant*** of the flow $\boldsymbol{\phi}$ ([Abraham, Marsden, and Raţiu, 1988, Definition 6.2.2] or [Abraham and Marsden, 2008, Proposition 2.3.10]) defined by

$$\boldsymbol{\phi}^* \boldsymbol{\theta}_{\mathbf{g}} = \det(\boldsymbol{\phi}) \boldsymbol{\Theta}_{\mathbf{g}}.$$

Applying (4.4.1) implies $\det(\boldsymbol{\phi}) = 1$ for isochoric flows. In continuum mechanics contexts, the above formulation of the determinant is often expressed by the ***Jacobian***, $J \in C(\mathscr{P}_{t_0} \times \mathscr{T})$, of the deformation gradient

$$J(\boldsymbol{X}, t) := \det(\mathbf{F}) \frac{\sqrt{\det(\mathbf{g}(\boldsymbol{x}))}}{\sqrt{\det(\mathbf{G}(\boldsymbol{X}))}}. \tag{4.4.3}$$

Remark 4.4.1 (Jacobian on Riemannian manifold). On Riemannian manifold with non-trivial metric, $J \neq \det(\mathbf{F})$. In fact,

$$J = \det\left(\frac{\partial \phi^a}{\partial Z^A}\right) = \frac{\partial(\phi^1, \ldots, \phi^n)}{\partial(Z^1, \ldots, Z^n)},$$

[1] The *interior product* is defined by the contraction $\boldsymbol{\iota}_v \boldsymbol{\theta}_{\mathbf{g}}(z_1, z_2, \ldots, z_n) = \boldsymbol{\theta}_{\mathbf{g}}(v, z_2, \ldots, z_n)$. Often, the interior product is denoted by $v \lrcorner \boldsymbol{\theta}_{\mathbf{g}}$ [Lee, 1997, p. 358].

where Z^A are coordinates in ambient Euclidean space. Whereas

$$\det(\mathbf{F}) = \det\left(\frac{\partial \phi^a}{\partial X^A}\right) = \frac{\partial(\phi^1, \ldots, \phi^n)}{\partial(X^1, \ldots, X^n)}.$$

The proof of (4.4.3) can be found in [Marsden and Hughes, 1983, Proposition 5.3]. It is straightforward to show that

$$J^2 = \det(\mathbf{C}) = \det(\mathbf{b}), \tag{4.4.4}$$

Since $\mathbf{C} = \mathbf{G}^{-1}\mathbf{F}^*\mathbf{g}\mathbf{F}$ and $\mathbf{b} = \mathbf{F}\mathbf{G}^{-1}\mathbf{F}^*\mathbf{g}$ (see 2.4.6). ▲

The rate of J is given by the non-autonomous Lie derivative as (see [Marsden and Hughes, 1983, Ch. 1, Corollary 7.15])

$$\mathscr{L}_{\boldsymbol{\phi}} J = \frac{\partial J}{\partial t} = (\operatorname{div} \boldsymbol{v})\, J, \qquad J(t_0) = 1. \tag{4.4.5}$$

An isochoric flow implies $J(t) = 1$. Besides, if $\det(\mathbf{g}) = 1$, then F belongs to the *special linear group*, i.e., $F \in \mathrm{SL}(n, \mathbb{R})$ where $\det(F^a{}_A) = 1$ for all $t \in \mathscr{I}$ [Marsden and Hughes, 1983, §1.5, Prop. 5.6]. In such case, the matrix of velocity gradient belongs to the lie algebra of the special linear group, $\mathfrak{sl}(n, \mathbb{R})$, i.e.,

$$\frac{\partial v}{\partial x} \in \mathfrak{sl}(n, \mathbb{R}) := T_I \mathrm{SL}(n, \mathbb{R}),$$

where $\operatorname{trace}(\partial v/\partial x) = 0$. In above, I is the identity matrix.

4.5 Eulerian Description of Rate of Deformation

In continuum mechanics, the velocity gradient characterizes the Eulerian description of the rate of deformation. Furthermore, the velocity gradient is decomposed into symmetric and skew-symmetric tensors to distinguish the instantaneous rate of stretching and rotation, which is known as *Euler-Cauchy-Stokes decomposition Theorem* [Truesdell, 1992, p.118] or often regarded as the *Cauchy-Helmholtz Theorem* [Dimitrienko, 2011, p. 57, Theorem 2.20]. For flows defined on manifolds, the velocity gradient is replaced with the covariant derivative of spatial velocity $\mathbf{l} := \nabla \boldsymbol{v}$, the symmetric part gives the *rate of deformation* given by $d^\flat_{ab} := \frac{1}{2}\left(v_{a|b} + v_{b|a}\right)$ [Marsden and Hughes, 1983, p. 65] and the skew-symmetric part $\omega^\flat_{ab} := \frac{1}{2}\left(v_{a|b} - v_{b|a}\right)$ becomes the *Jaumann's spin tensor* [Marsden and Hughes, 1983, p.100].

The above descriptions were defined based on a torsion-free connection setting. Here we adapt these definitions for arbitrary connections.

Definition 4.5.1 (Material rate of deformation with arbitrary connection). *Inspired by equation* (4.3.2) *in Proposition 4.3.1, define the* ***spatial rate of deformation gradient tensor*** *with endomorphism* $\mathbf{l} \in \Gamma(\mathrm{End}(T\mathscr{P}_t))$ *by*

$$\mathbf{l} := \nabla \boldsymbol{v} + \mathrm{tor}(\boldsymbol{v}, \cdot). \tag{4.5.1}$$

In our notation in the above relation, $\mathrm{tor}(\boldsymbol{v}, \cdot)$ *means the vector* $\boldsymbol{v}$ *is contracted on the first argument of the tensor* tor. *In the local chart* $\{x^a\}$,

$$\mathbf{l}(\boldsymbol{x}, t) = \left(\frac{\partial v^a}{\partial x^b} + \gamma^a{}_{cb} v^c \right) \boldsymbol{e}_a \otimes \boldsymbol{e}^{*b}. \tag{4.5.2}$$

▲

The role of torsion of connection in $\mathbf{l}$ has been uncovered in the literature such as in [Romano, 2014, §3.2.2] and [Romano, Barretta, and Diaco, 2014, §11]. For symmetric connections, $\mathbf{l}$ is the covariant derivative of velocity, and in Euclidean space, it is known as the velocity gradient in continuum mechanics [Gurtin, Fried, and Anand, 2010, §9.3]. We avoid the conventional term since $\mathbf{l}$ is not a gradient, rather,

$$\mathbf{l} = \frac{D\mathbf{F}}{dt}\mathbf{F}^{-1} = \boldsymbol{\phi}_{*^2}\left(\frac{D\mathbf{F}}{dt}\right),$$

is the material rate of $\mathbf{F}$ viewed fully on the spatial manifold. Here, by $\boldsymbol{\phi}_{*^2}$ we indicate that the pushforward is on the second basis component of the two-point tensor[2].

To obtain the rate of deformation and spin, we use the transposition with respect to the spatial metric tensor similar to what is defined for the two-point tensor $\mathbf{F}$ (see [Marsden and Hughes, 1983, p.48, Proposition 3.4]).

Proposition 4.5.2 (Transposition on the spatial configuration manifold). *Let the tensor* $\mathbf{l} \in \Gamma(\mathrm{End}(T\mathscr{P}_t))$ *denote an endomorphism on* $T\mathscr{P}_t$ *equipped with metric* $\mathbf{g}$. *Then its transposition with respect to the metric is*

$$\mathbf{l}^\intercal = \mathbf{g}^{-1}\mathbf{l}^*\mathbf{g}, \tag{4.5.3}$$

where $\mathbf{l}^* \in \Gamma(\mathrm{End}(T^*\mathscr{P}_t))$ *is the adjoint of* $\mathbf{l}$.

Proof. Let $z_1, z_2 \in T_{\boldsymbol{x}}\mathscr{P}_t T$ be two tangent vectors. Then the transposition should satisfy $\mathbf{g}(z_1, \mathbf{l}z_2) = \mathbf{g}(\mathbf{l}^\intercal z_1, z_2)$. Using the symmetry of $\mathbf{g}$ we have $\mathbf{g}(z_1, \mathbf{l}z_2) = \mathbf{g}(\mathbf{l}z_2, z_1) = \big(\mathbf{gl}\big)^*(z_1, z_2)$ which concludes $\mathbf{gl}^\intercal = \mathbf{l}^*\mathbf{g}$. ■

Using the metric compatible transposition, we retrieve the Euler-Cauchy-Stokes Decomposition as follows;

[2] For general operations on two-point tensors see [Marsden and Hughes, 1983, p. 71].

Definition 4.5.3 (Euler-Cauchy-Stokes decomposition with torsion). *The rate of spatial deformation gradient tensor* $\mathbf{l}$ *can be decomposed into the symmetric* ***spatial rate of deformation*** *and the skew-symmetric* ***spin*** *tensors*

$$\mathbf{l} = \mathbf{d} + \boldsymbol{\omega}, \tag{4.5.4a}$$

where $\mathbf{d}$ *and* $\boldsymbol{\omega} \in \Gamma\left(\mathrm{End}\left(T\mathscr{P}_t\right)\right)$ *are*

$$\mathbf{d} \coloneqq \mathrm{sym}\left(\mathbf{l}\right) = \frac{1}{2}\left(\mathbf{l} + \mathbf{l}^{\intercal}\right) = \frac{1}{2}\left(\mathbf{l} + \mathbf{g}^{-1}\mathbf{l}^{*}\mathbf{g}\right), \tag{4.5.4b}$$

$$\boldsymbol{\omega} \coloneqq \mathrm{skew}\left(\mathbf{l}\right) = \frac{1}{2}\left(\mathbf{l} - \mathbf{l}^{\intercal}\right) = \frac{1}{2}\left(\mathbf{l} - \mathbf{g}^{-1}\mathbf{l}^{*}\mathbf{g}\right). \tag{4.5.4c}$$

▲

Remark 4.5.4 (Non-intrinsicness of Euler-Cauchy-Stokes decomposition). The tensor $\mathbf{l}$ is not *natural* in the sense that it depends on the choice of connection, but the arbitrariness of connection will not alter our subsequent derivations. In addition, the mixed tensors $\mathbf{d}$ and $\boldsymbol{\omega}$ depend on both connection ∇ on the tangent bundle and metric $\mathbf{g}$ on the cotangent bundle. In contrast, the associated tensors

$$\mathbf{d}^{\flat} = \frac{1}{2}\left(\mathbf{l}^{\flat} + \mathbf{l}^{\flat *}\right) \in \Gamma\left(T^{*}\mathscr{P}_t, T^{*}\mathscr{P}_t\right), \tag{4.5.5a}$$

and 2-form of vorticity

$$\boldsymbol{\omega}^{\flat} = \frac{1}{2}\left(\mathbf{l}^{\flat} - \mathbf{l}^{\flat *}\right) \in \Gamma\left(\bigwedge^{2}\left(T^{*}\mathscr{P}_t\right)\right), \tag{4.5.5b}$$

are metric-independent and only dependent on the connection. ▲

The matrices d^{a}_{b} and ω^{a}_{b} of mixed tensors are neither symmetric nor skew-symmetric, but the matrices d_{ab} and ω_{ab} of associated tensors are symmetric and skew-symmetric respectively.

4.6 Lie Derivatives and Objective Rates

A useful and intrinsic rate of tensors is the Lie derivative, which unlike the covariant derivative, does not require additional structures on the vector bundle. However, the Lie derivative requires the vector field of the flow defined in a neighborhood of a point on the manifold, in contrast, the material time derivative is point-wise, meaning it is defined without information from the neighborhood of the point of derivation. That is, the material (or covariant) rates are tensors.

We distinguish the autonomous and non-autonomous Lie derivative of tensors (see e.g., [Marsden and Hughes, 1983, Ch. 1, Definition 6.8], [Epstein, 2010, §5.6.6] or [Abraham, Marsden, and Rațiu, 1988, §5.4]). The ***autonomous Lie derivative*** along the homeomorphism $\boldsymbol{\phi}$ is

denoted by $\pounds_{\boldsymbol{\phi}}$, and can be defined by

$$\pounds_{\boldsymbol{\phi}}\mathbf{t} \coloneqq \frac{d}{dt}\left(\boldsymbol{\phi}_t^*\mathbf{t}(\boldsymbol{x}(t),t_0)\right)\Big|_{t=t_0}, \tag{4.6.1}$$

where $\mathbf{t}$ is an arbitrary tensor field defined along $\boldsymbol{\phi}$, and $\mathbf{t}(\boldsymbol{x}(t),t_0)$ implies t_0 is assumed to be fixed when taking the time derivative [Abraham, Marsden, and Raţiu, 1988, Theorem 5.4.1]. The autonomous Lie derivative commutes with pullback by

$$\boldsymbol{\phi}^*\left(\pounds_v\mathbf{t}\right) = \pounds_{\boldsymbol{\phi}^*v}\left(\boldsymbol{\phi}^*\mathbf{t}\right).$$

The ***non-autonomous Lie derivative*** $\mathscr{L}_{\boldsymbol{\phi}}$ along the homeomorphism $\boldsymbol{\phi}$ given by

$$\mathscr{L}_{\boldsymbol{\phi}}\mathbf{t} \coloneqq \frac{d}{dt}\left(\boldsymbol{\phi}_t^*\mathbf{t}(\boldsymbol{x}(t),t)\right)\Big|_{t=t_0},$$

where in the above time derivative is total in $\mathbf{t}(\boldsymbol{x}(t),t)$, meaning with respect to both time t, and implicitly with respect to time in $\boldsymbol{x}(t)$ [Abraham, Marsden, and Raţiu, 1988, Theorem 5.4.4]. It can be shown that

$$\mathscr{L}_{\boldsymbol{\phi}} = \frac{\partial}{\partial t} + \pounds_{\boldsymbol{\phi}}.$$

The autonomous Lie derivative in (4.6.1) measures the rate of change of $\mathbf{t}$ as evolves along $\boldsymbol{\phi}$ at a fixed time t, but it does not take into account the rate due to the change of time-dependent tensor field $\mathbf{t}(t)$ itself. In contrast, the non-autonomous Lie derivative measures the total rate of a tensor [Abraham, Marsden, and Raţiu, 1988, Theorem 5.4.4], i.e.,

$$\frac{d}{dt}\left(\boldsymbol{\phi}_t^*\mathbf{t}\right) = \boldsymbol{\phi}_t^*\left(\mathscr{L}_{\boldsymbol{\phi}}\mathbf{t}\right). \tag{4.6.2}$$

Using the definitions of the previous section, we present the evolution of $\mathbf{b}$ and $\mathbf{C}$ in terms of material time derivative. Since the Lie derivative is naturally defined on an abstract manifold, they are naturally used to derive the evolution equation of tensors. Then, we retrieve the evolution equation expressed in terms of the material time derivative. We first review the relation between the Lie derivative and the material time derivative using the arbitrary connection for a contravariant tensor.

Lemma 4.6.1 (Lie derivative of covariant and contravariant tensors). *Suppose the mixed second-order spatial tensor* $\mathbf{t} \in \Gamma\left(\mathrm{End}\left(T\mathscr{P}_t\right)\right)$ *is defined along the flow of diffeomorphism* $\boldsymbol{\phi}_t : \mathscr{P}_{t_0} \to \mathscr{P}_t$ *and its two-point tensor tangent map is* $\mathbf{F} : T\mathscr{P}_{t_0} \to T\mathscr{P}_t$. *Then*

1. *The non-autonomous Lie derivative of the contravariant tensor* $\mathbf{t}^\sharp \in \Gamma\left(T\mathscr{P}_t \otimes T\mathscr{P}_t\right)$ *along the flow* $\boldsymbol{\phi}_t$ *is*

$$\mathscr{L}_{\boldsymbol{\phi}}\mathbf{t}^\sharp = \frac{D\mathbf{t}^\sharp}{dt} - \mathbf{l}\mathbf{t}^\sharp - \mathbf{t}^\sharp\mathbf{l}^*, \tag{4.6.3a}$$

2. *The non-autonomous Lie derivative of the covariant tensor* $\mathbf{t}^\flat \in \Gamma\left(T\mathscr{P}_t \otimes T\mathscr{P}_t\right)$ *along the flow* $\boldsymbol{\phi}_t$ *is*

$$\mathscr{L}_{\boldsymbol{\phi}}\mathbf{t}^\flat = \frac{D\mathbf{t}^\flat}{dt} + \mathbf{t}^\flat\mathbf{l} + \mathbf{l}^*\mathbf{t}^\flat, \tag{4.6.3b}$$

where $\mathbf{l} \coloneqq \boldsymbol{\phi}_{*^2}\left(\dfrac{D(T\boldsymbol{\phi})}{dt}\right)$ *and the material time derivative is defined based on an arbitrary connection* ∇ *on* $T\mathscr{P}_t$.

Proof. Suppose $\mathbf{t}^\sharp = t^{ab}\boldsymbol{e}_a \otimes \boldsymbol{e}_b$. Using the tangent map $\mathbf{F} = T\boldsymbol{\phi}$ the pullback is

$$\boldsymbol{\phi}^*\mathbf{t}^\sharp = t^{ab}\left(\boldsymbol{\phi}^*\boldsymbol{e}_a\right) \otimes \left(\boldsymbol{\phi}^*\boldsymbol{e}_b\right) = \mathbf{F}^{-1}\mathbf{t}^\sharp\mathbf{F}^{-*}, \tag{4.6.4}$$

where $\mathbf{F}^{-*} = T^*\boldsymbol{\phi}^{-1}$ is the cotangent lift. Similarly, the pushforward of a referential tensor $\mathbf{T} = T^{AB}\boldsymbol{E}_A \otimes \boldsymbol{E}_B$ is

$$\boldsymbol{\phi}_*\mathbf{T} = T^{AB}\left(\boldsymbol{\phi}_*\boldsymbol{E}_A\right) \otimes \left(\boldsymbol{\phi}^*\boldsymbol{E}_B\right) = \mathbf{F}\mathbf{T}\mathbf{F}^*.$$

From the commutative property of Lie derivative and pullback in (4.6.2)

$$\mathscr{L}_{\boldsymbol{\phi}}\mathbf{t}^\sharp = \boldsymbol{\phi}_*\left(\left.\frac{d}{dt}\right|_{t=t_0}\left(\boldsymbol{\phi}^*\mathbf{t}^\sharp\right)\right) = \mathbf{F}\left(\frac{D}{dt}\left(\mathbf{F}^{-1}\mathbf{t}^\sharp\mathbf{F}^{-*}\right)\right)\mathbf{F}^*.$$

Taking the material time derivative of $\mathbf{F}\mathbf{F}^{-1} = \mathbf{i}$, where $\mathbf{i} = T\left(\mathrm{id}_{\mathscr{P}_t}\right)$ is the trivial automorphism on $T\mathscr{P}_t$, yields $(D\mathbf{F}^{-1}/dt) = -\mathbf{F}^{-1}\ (D\mathbf{F}/dt)\ \mathbf{F}^{-1}$ and its adjoint $D\mathbf{F}^{-*}/dt = -\mathbf{F}^{-*}\ (D\mathbf{F}/dt)^*\ \mathbf{F}^{-*}$. Substituting material time derivatives of $\mathbf{F}^{-1}$ and $\mathbf{F}^{-*}$ and using $\mathbf{l} = (D\mathbf{F}/dt)\ \mathbf{F}^{-1}$ from Proposition 4.3.1 yields (4.6.3a) of part (1).

Assume $\mathbf{t}^\flat = t_{ab}\boldsymbol{e}^{*a} \otimes \boldsymbol{e}^{*b}$, then

$$\boldsymbol{\phi}^*\mathbf{t}^\flat = t_{ab}\left(\boldsymbol{\phi}^*\boldsymbol{e}^{*a}\right) \otimes \left(\boldsymbol{\phi}^*\boldsymbol{e}^{*b}\right) = \mathbf{F}^*\mathbf{t}^\flat\mathbf{F}.$$

Similarly the pushforward of referential tensor $\mathbf{T} = T_{AB}\boldsymbol{E}^{*A} \otimes \boldsymbol{E}^{*B}$ is

$$\boldsymbol{\phi}_*\mathbf{T} = T_{AB}\left(\boldsymbol{\phi}_*\boldsymbol{E}^{*A}\right) \otimes \left(\boldsymbol{\phi}_*\boldsymbol{E}^{*B}\right) = \mathbf{F}^{-*}\mathbf{T}\mathbf{F}^{-1}.$$

Using the commutative property of Lie derivative and pullback in (4.6.2),

$$\mathscr{L}_{\boldsymbol{\phi}}\mathbf{t}^\flat = \boldsymbol{\phi}_*\left(\left.\frac{d}{dt}\right|_{t=t_0}\left(\boldsymbol{\phi}^*\mathbf{t}^\flat\right)\right) = \mathbf{F}^{-*}\left(\frac{D}{dt}\left(\mathbf{F}^*\mathbf{t}^\flat\mathbf{F}\right)\right)\mathbf{F}^{-1}.$$

Taking the material time derivatives and using $\mathbf{l} = \boldsymbol{\phi}_{*^2}\left(\dfrac{D\mathbf{F}}{dt}\right) = \dfrac{D\mathbf{F}}{dt}\mathbf{F}^{-1}$ concludes equation (4.6.3b) of part (2). ∎

Remark 4.6.2 (Objective rates). Suppose $\mathbf{t}$ is a covariant-contravariant spatial tensor of type $\binom{1}{1}$. The Lie derivative of the contravariant tensor $\mathbf{t}^\sharp$ of type $\binom{2}{0}$ in (4.6.3a) is known as ***Oldroyd objective rate*** [Marsden and Hughes, 1983, p. 99] and in terms of a torsion-free connection it is often written with

$$\overset{\triangledown}{\mathbf{t}}{}^\sharp = \dot{\mathbf{t}}^\sharp - (\nabla \boldsymbol{v})\, \mathbf{t}^\sharp - \mathbf{t}^\sharp\, (\nabla \boldsymbol{v})^* .$$

Similarly, the Lie derivative of the covariant tensor $\mathbf{t}^\flat$ of type $\binom{0}{2}$ in (4.6.3b) is known as ***Cotter-Rivlin objective rate*** and in terms of a torsion-free connection it is often written with

$$\overset{\triangle}{\mathbf{t}}{}^\flat = \dot{\mathbf{t}}^\flat + \mathbf{t}^\flat\, (\nabla \boldsymbol{v}) + (\nabla \boldsymbol{v})^*\, \mathbf{t}^\flat,$$

(see e.g., [Gurtin, Fried, and Anand, 2010, p.152] and [Holzapfel, 2000, §5.3]).

All objective rates of second-order tensors can be expressed with Lie derivatives [Marsden and Hughes, 1983, p. 99]. However, in that reference, the Lie derivatives have been expressed with torsion-free covariant derivative. Here, we extend the objective rate to incorporate the torsion of the connection. Recall from the Lemma 4.6.1 that the Lie derivatives in (4.6.3a) and (4.6.3b) in terms of a general connection ∇. Hence, the Oldroyd and Cotter-Rivlin objective rates are expressed with arbitrary connection respectively by

$$\overset{\triangledown}{\mathbf{t}}{}^\sharp = \dot{\mathbf{t}}^\sharp - \mathbf{l}\mathbf{t}^\sharp - \mathbf{t}^\sharp \mathbf{l}^*, \qquad \text{Oldroyd, with torsion,} \tag{4.6.5a}$$

$$\overset{\triangle}{\mathbf{t}}{}^\flat = \dot{\mathbf{t}}^\flat + \mathbf{t}^\flat \mathbf{l} + \mathbf{l}^* \mathbf{t}^\flat, \qquad \text{Cotter-Rivlin, with torsion.} \tag{4.6.5b}$$

The difference of the above objective rates with previous definitions is the replacement of $\nabla \boldsymbol{v}$ with $\mathbf{l}$, which incorporates the torsion of the frame bundle. ▲

In our developments, the Lie derivative of spatial deformation tensors appears frequently, which we present in the following. In particular, we will show the Lie derivative of tensors $\mathbf{F}$ and $\mathbf{b}$ are zero.

Lemma 4.6.3 (Lie derivative of deformation tensors). *Let the flow $\boldsymbol{\phi}_t \in C^1(\mathscr{P}_{t_0} \times \mathscr{I}; \mathscr{P}_t)$ be a one-parameter group diffeomorphism with tangent map $T\boldsymbol{\phi} = \mathbf{F}$. Then,*

1. *The non-autonomous Lie derivative of deformation gradient $\mathbf{F}$ vanishes, i.e.,*

$$\mathscr{L}_{\boldsymbol{\phi}} \mathbf{F} = \mathbf{0}. \tag{4.6.6a}$$

2. *The non-autonomous Lie derivative of $\mathbf{b}^\sharp = \mathbf{b}\mathbf{g}^{-1}$, i.e., the associated tensor of left deformation tensor, also vanishes, i.e.,*

$$\mathscr{L}_{\boldsymbol{\phi}} \mathbf{b}^\sharp = \mathbf{0}. \tag{4.6.6b}$$

3. The autonomous Lie derivative of $\mathbf{C}$ *vanishes, i.e.,*

$$\pounds_{\boldsymbol{\phi}}\mathbf{C} = \mathbf{0}. \tag{4.6.6c}$$

Proof. By definition, $\mathbf{F} = \boldsymbol{\phi}_*\mathbf{I}$ where $\mathbf{I} = \mathrm{Id}_{T\mathscr{P}_{t_0}}$ is the trivial automorphism. Thus, by (4.6.2), $\mathscr{L}_{\boldsymbol{\phi}}\mathbf{F} = \boldsymbol{\phi}_*(d\mathbf{I}/dt) = \mathbf{0}$ and concludes part (1). Recall from (2.4.3b) that $\mathbf{b}^\sharp = \mathbf{F}\mathbf{G}^{-1}\mathbf{F}^*$. Similar to (4.6.4), its pullback is $\boldsymbol{\phi}^*\mathbf{b}^\sharp = \mathbf{F}^{-1}\mathbf{b}^\sharp\mathbf{F}^{-*} = \mathbf{G}^{-1}$. Thus, by (4.6.2), $\mathscr{L}_{\boldsymbol{\phi}}\mathbf{b}^\sharp = \boldsymbol{\phi}_* d\mathbf{G}^{-1}/dt = \mathbf{0}$ since the referential metric $\mathbf{G} = \mathbf{G}(\boldsymbol{X})$ is time-independent, and concludes part 2. The tensor $\mathbf{C} = \mathbf{C}(\boldsymbol{X}, t)$ is purely referential and its autonomous Lie derivative is zero and concludes part (3). ■

From the part 3 of Lemma 4.6.3, it is obvious that the non-autonomous Lie derivative of $\mathbf{C}$ is

$$\mathscr{L}_{\boldsymbol{\phi}}\mathbf{C} = \frac{\partial \mathbf{C}}{\partial t} = \frac{D\mathbf{C}}{dt}.$$

Later in §4.9 we will derive an explicit expression for the material rate of $\mathbf{C}$.

4.7 Material Rate of the Left Deformation Tensor

Similar to the material rate of deformation gradient $\mathbf{F}$ that was presented in §4.3, here we derive the material rate of the left deformation tensor $\mathbf{b}$. We will show that the material rate can be explained using Lie derivative.

Proposition 4.7.1 (Material rate of the associated left deformation tensor). *For an arbitrary connection* ∇ *on the tangent bundle of the Riemannian manifold* $T\mathscr{P}_t$ *initially equipped with metric* $\mathbf{G}$*, the evolution of* $\mathbf{b}^\sharp(\boldsymbol{x}, t)$ *is given by*

$$\frac{D\mathbf{b}^\sharp}{dt} = \mathbf{l}\mathbf{b}^\sharp + \mathbf{b}^\sharp\mathbf{l}^*, \qquad \mathbf{b}^\sharp(\boldsymbol{X}, t_0) = \mathbf{G}^\sharp(\boldsymbol{X}). \tag{4.7.1}$$

Proof. From (2.4.5b) the pullback of $\mathbf{b}^\sharp$ is $\boldsymbol{\phi}^*\mathbf{b}^\sharp = \mathbf{G}^{-1}$, but $\mathbf{G}$ is time-independent, hence

$$\mathscr{L}_{\boldsymbol{\phi}}\mathbf{b}^\sharp = \boldsymbol{\phi}_* \left.\frac{d}{dt}\right|_{t=t_0} \left(\boldsymbol{\phi}^*\mathbf{b}^\sharp\right) = \boldsymbol{\phi}_* \left.\frac{d}{dt}\right|_{t=t_0} \mathbf{G}^{-1}(\boldsymbol{X}) = \mathbf{0}.$$

Using Lemma 4.6.1 for $\mathscr{L}_{\boldsymbol{\phi}}\mathbf{b}^\sharp = \mathbf{0}$ yields (4.7.1). Also, clearly at $t = t_0$, we have $\mathbf{b}^\sharp(\boldsymbol{X}, t_0) = \mathbf{G}^\sharp$. ■

Corollary 4.7.2 (Material rate of the left deformation tensor). *The evolution of left deformation tensor* $\mathbf{b}$ *on the Riemannian manifold* $(\mathscr{P}_t, \mathbf{g}, \nabla)$ *with an arbitrary connection is*

$$\frac{D\mathbf{b}}{dt} = \mathbf{l}\mathbf{b} + \mathbf{b}\mathbf{l}^\intercal + \mathbf{b}\mathbf{g}^{-1}\nabla_v\mathbf{g}, \qquad \mathbf{b}(\boldsymbol{X}, t_0) = \mathbf{i}, \tag{4.7.2}$$

where $\mathbf{i} := T(\mathrm{id}_{\mathscr{P}_t})$ *is the trivial automorphism on* $T\mathscr{P}_t$.

Proof. Substitute $\mathbf{b}^\sharp = \mathbf{b}\mathbf{g}^{-1}$ and also $D\left(\mathbf{g}^{-1}\right)/dt = -\mathbf{g}^{-1}\left(D\mathbf{g}/dt\right)\mathbf{g}^{-1}$ in Proposition 4.7.1. Also, $\partial\mathbf{g}(\boldsymbol{x})/\partial t = \mathbf{0}$ yields to $D\mathbf{g}/dt = \nabla_v\mathbf{g}$. Lastly by setting $\mathbf{l}^\mathsf{T}$ defined in (4.5.3) the result is immediate. ■

Remark 4.7.3 (Intrinsicness of the rate of the left deformation tensor). The above relation can be obtained directly from the intrinsic Lie derivative of Lemma 4.6.3 given by

$$\mathscr{L}_{\boldsymbol{\phi}}\mathbf{b}^\sharp = \mathbf{0},$$

Recall, the Lie derivative is independent of the connection. Accordingly, the statement of Corollary 4.7.2 is intrinsically independent of the connection. To see this, express the equation (4.7.2) in a local chart $\{x^a\}$ as

$$\begin{aligned}\frac{Db^a{}_b}{dt} &= \frac{\partial b^a{}_b}{\partial t} + \frac{\partial b^a{}_b}{\partial x^c}v^c \\ &= \frac{\partial v^a}{\partial x^c}b^c{}_b + b^a{}_c g^{cd}\frac{\partial v^e}{\partial x^d}g_{eb} + b^a{}_c g^{cd}\frac{\partial g_{db}}{\partial x^e}v^e.\end{aligned} \tag{4.7.3}$$

Remind the reader that the Lie derivative is canonical (or natural) whereas the covariant derivative requires an extra geometric structure on the manifold, and the connection allows us to represent the above rate with material time derivative. ▲

4.8 Contorsion and Parallel Transport of Riemannian Metric

We have seen in Corollary 4.7.2 that the material rate of deformation involves the term $\nabla_v\mathbf{g}$. In our later developments, the material rate of metric tensor also appears. For the choice of *metric connection* $\nabla^{\mathbf{g}}$, we have

$$\frac{D\mathbf{g}}{dt} = \nabla^{\mathbf{g}}_v\mathbf{g} = \mathbf{0}, \tag{4.8.1}$$

simplifying (4.7.2). We have assumed the metric of the space is time-invariant, i.e., $\partial\mathbf{g}/\partial t = \mathbf{0}$. The above relation is often known as the ***Ricci theorem*** [Sokolnikoff, 1951, §35]. The relation (4.8.1) implies that the metric $\mathbf{g}$ is a ***parallel section*** that lies in the horizontal subspace of the vector bundle $\mathrm{End}(T^*\mathscr{P}_t)$.

When the metric connection is also *symmetric*, it is known from the *Levi-Civita theorem* [do Carmo, 1992, Theorem 3.6] that the connection can be uniquely determined by the metric $\mathbf{g}$ as

$$\bar{\gamma}^a{}_{bc} = \frac{1}{2}g^{ak}\left(\frac{\partial g_{ck}}{\partial x^b} + \frac{\partial g_{bk}}{\partial x^c} - \frac{\partial g_{bc}}{\partial x^k}\right). \tag{4.8.2}$$

We denote the ***Levi-Civita connection*** described above by $\bar{\nabla}$ with coefficients $\bar{\gamma}^a{}_{bc}$.

For a general connection ∇, one can split the connection coefficients to

$$\gamma^{a}{}_{bc} = \bar{\gamma}^{a}{}_{bc} + \kappa^{a}{}_{bc},$$

(see [Kobayashi and Nomizu, 1963, p. 159]) where $\kappa^{a}{}_{bc}$ is the ***contorsion coefficients*** of the torsion tensor. Contorsion $\kappa^{a}{}_{bc}$ is defined with $\kappa^{a}{}_{bc} = g^{ad}\kappa_{dbc}$, where

$$\kappa_{abc} \coloneqq \tau_{abc} - \tau_{bca} + \tau_{cab}.$$

The contorsion tensor indicates the deviation of connection from a torsion-free connection. Recall from (4.8.1) that the metric tensor $\mathbf{g}$ is parallel with respect to the Levi-Civita connection $\bar{\nabla}$, that is,

$$\bar{\nabla}\mathbf{g} = \left(\frac{\partial g_{ab}}{\partial x^{k}} - \bar{\gamma}^{c}{}_{ka}g_{cb} - \bar{\gamma}^{c}{}_{kb}g_{ac}\right) \boldsymbol{e}^{*a} \otimes \boldsymbol{e}^{*b} \otimes \boldsymbol{e}^{*k} = \mathbf{0}.$$

Therefor, we can eliminate the contribution due to the torsion-free part of the connection and keep the contribution due to only the contorsion with

$$\begin{aligned}
\nabla_{v}\mathbf{g} &= \left(\frac{\partial g_{ab}}{\partial x^{k}} - \gamma^{c}{}_{ka}g_{cb} - \gamma^{c}{}_{kb}g_{ac}\right) v^{k}\boldsymbol{e}^{*a} \otimes \boldsymbol{e}^{*b} \\
&= -\left(g_{cb}\kappa^{c}{}_{ka} + g_{ac}\kappa^{c}{}_{kb}\right) v^{k}\boldsymbol{e}^{*a} \otimes \boldsymbol{e}^{*b} \\
&= -\left(\boldsymbol{\kappa}\mathbf{g} + \mathbf{g}\boldsymbol{\kappa}^{*}\right)(\boldsymbol{v}, \cdot)\,. \qquad (4.8.3)
\end{aligned}$$

In the above relation, by the notation $(\boldsymbol{v}, \cdot)$ we mean the contraction the vector $\boldsymbol{v}$ is applied to the first argument of the tensor $-\left(\boldsymbol{\kappa}\mathbf{g} + \mathbf{g}\boldsymbol{\kappa}^{*}\right)$. If we expand all covariant and material time derivatives in terms of the connection coefficients (or contorsion coefficients) in (4.7.2), all the connection coefficients should eliminate from the representation as given in the equation (4.7.3).

4.9 Material Rate of the Right Deformation Tensor

Recall that in §4.7 we have derived the material rate of the left deformation tensor $\mathbf{b}$. However, we have postponed the material rate of right deformation tensor $\mathbf{C}$ presented below, since its formulation involves the parallel transport of the Riemannian metric developed earlier. To obtain an equation for the material rate of $\mathbf{C}$ we first re-derive the Lie derivative for $\mathbf{g}$.

Proposition 4.9.1 (Lie derivative of the Riemannian metric). *The Lie derivative of the metric tensor along the flow $\boldsymbol{\phi}$ on the Riemannian manifold $(\mathscr{P}_t, \mathbf{g})$ is represented with the arbitrary connection ∇ with*

$$\mathscr{L}_{\boldsymbol{\phi}}\mathbf{g} = 2\mathbf{d}^{\flat} + \nabla_{v}\mathbf{g}. \qquad (4.9.1)$$

Proof. Using equation (4.6.3b) in Lemma 4.6.1, the non-autonomous Lie derivative of the covariant tensor $\mathbf{g} \in \Gamma\left((T^*\mathscr{P}_t) \otimes T^*\mathscr{P}_t\right)$ is

$$\mathscr{L}_{\boldsymbol{\phi}}\mathbf{g} = \frac{D\mathbf{g}}{dt} + \mathbf{g}\mathbf{l} + \mathbf{l}^*\mathbf{g}. \tag{4.9.2}$$

Since $\mathbf{g}(\boldsymbol{x})$ is not implicitly a function of time, $D\mathbf{g}/dt = \nabla_v \mathbf{g}$. Recall that $\mathbf{l}^\flat = \mathbf{g}\mathbf{l}$ and $\mathbf{l}^*\mathbf{g} = \left(\mathbf{g}\mathbf{l}\right)^* = \mathbf{l}^{\flat *}$. Using $\mathbf{d}^\flat = (\mathbf{l}^\flat + \mathbf{l}^{\flat *})/2$ concludes the proof. ■

Remark 4.9.2 (Metric connection and parallel transport). By using the metric connections $\nabla^{\mathbf{g}}$ where $\mathbf{g}$ becomes a parallel section in the vector bundle, i.e., $\nabla^{\mathbf{g}}\mathbf{g} = \mathbf{0}$, the proposition 4.9.1 simplifies to

$$\frac{1}{2}\mathscr{L}_{\boldsymbol{\phi}}\mathbf{g} = \mathbf{d}^\flat.$$

This relation is given in [Marsden and Hughes, 1983, p. 98, Corollary 6.12] where they have represented the Lie derivative in terms of Levi-Civita connection and is the unique metric torsion-free covariant derivative. ▲

Corollary 4.9.3 (Material rate of the right deformation tensor). *The evolution of right deformation tensor* $\mathbf{C}$ *for the flow on the Riemannian manifold* $\boldsymbol{\phi} : (\mathscr{P}_{t_0}, \mathbf{G}) \to (\mathscr{P}_t, \mathbf{g})$ *in term of its material time derivative using an arbitrary connection* ∇ *is*

$$\frac{D\mathbf{C}}{dt} = \mathbf{F}^\intercal \left(2\mathbf{d} + \mathbf{g}^{-1}\nabla_v \mathbf{g}\right)\mathbf{F}, \qquad \mathbf{C}(\boldsymbol{X}, t_0) = \mathbf{I}. \tag{4.9.3}$$

Proof. From the Lie derivative (see (4.6.2)) of the metric tensor we have

$$\left.\frac{d}{dt}\right|_{t=t_0} \left(\boldsymbol{\phi}^*\mathbf{g}\right) = \boldsymbol{\phi}^*\left(\mathscr{L}_{\boldsymbol{\phi}}\mathbf{g}\right).$$

Substituting $\mathbf{C}^\flat = \boldsymbol{\phi}^*\mathbf{g}$ from (2.4.5a) and using Proposition 4.9.1 gives

$$\frac{D\mathbf{C}^\flat}{dt} = \boldsymbol{\phi}^*\left(2\mathbf{d}^\flat + \mathbf{g}^{-1}\nabla_{\boldsymbol{\phi}}\mathbf{g}\right) = \mathbf{F}^*\left(2\mathbf{d}^\flat + \nabla_v \mathbf{g}\right)\mathbf{F}.$$

Remind the reader that $\mathbf{C}^\flat = \mathbf{G}\mathbf{C}$, also the referential metric $\mathbf{G}(\boldsymbol{X})$ is independent of time, so $D\mathbf{G}/dt = 0$, hence left multiplication by $\mathbf{G}^{-1}$ yields

$$\frac{D\mathbf{C}}{dt} = \left(\mathbf{G}^{-1}\mathbf{F}^*\mathbf{g}\right)\left(2\mathbf{g}^{-1}\mathbf{d}^\flat + \mathbf{g}^{-1}\nabla_v \mathbf{g}\right)\mathbf{F}.$$

Using (2.4.2) for $\mathbf{F}^\intercal$ and $\mathbf{d} = \mathbf{g}^{-1}\mathbf{d}^\flat$ yields (4.9.3). ■

Remark 4.9.4 (Intrinsicness of the rate of the right deformation tensor). When a metric connection $\nabla^{\mathbf{g}}$ is used, by parallel transport $\nabla^{\mathbf{g}}\mathbf{g} = \mathbf{0}$, simplifying the statement of Corollary 4.9.3. Indeed, (4.9.3) is intrinsic, i.e., independent of the choice of connection. To see this, observe that in local charts $\{X^A\}$ and $\{x^a\}$, the relation (4.9.3) is expressed by

$$\frac{DC^A{}_B}{dt} = \frac{\partial C^A{}_B}{\partial t} = G^{AC} F^a{}_C \left(g_{ab} \frac{\partial v^b}{\partial x^c} + \frac{\partial v^b}{\partial x^a} g_{bc} + \frac{\partial g_{ac}}{\partial x^b} v^b \right) F^c{}_B, \tag{4.9.4}$$

which is trivially independent of the connection. ▲

Chapter 5

Curvature

5.1 Introduction

The kinematics presented in Chapter 4 was the study of first-order variations of tensors on the vector bundle. In this chapter, we explore the second-order variations of tensors. Our development necessitates the definition of the second rate of deformation, which itself involves the acceleration of motion given in §2.2 and the Riemannian curvature of manifold explained in §5.2.

An immediate application of Riemannian curvature is in the formulation of compatibility conditions necessary for the existence of a continuous deformation. In §5.3, we review the compatibility conditions of the deformation and strain tensors for a Riemann-flat space, and then we generalize them to other non-flat manifolds. In particular, we present the compatibility conditions on Einstein manifolds and model spaces of constant sectional curvature. We revisit the known compatibility equations on the 3-dimensional Euclidean space and conclude that the reduction of the number of compatibility equations is mainly due to the absence of Weyl curvature.

We derive the second material rates of deformation tensors in §5.4. Also in §5.5, we assume the flow is trivialized by utilizing normal coordinate charts. This way, the flow is locally geodesic and allows us to better interpret the role of curvature in the second-order evolution equations.

Furthermore, we present an analogy between our formulation and Einstein's field equations in the vacuum. When the second-order evolution equations are applied to the evolution of tangent vectors, we make an analogy between our formulation and the Jacobi fields, which are the vector fields generated by the perturbations along geodesics.

5.2 Curvature Tensor

The ***curvature*** is the tensor $\mathbf{R} \in \Omega^2(\mathscr{P}_t) \otimes \Gamma(\mathrm{End}(T\mathscr{P}_t))$ and defined by[1,2]

$$\begin{aligned}\mathbf{R}(z_1, z_2)z_3 &:= \nabla_{z_1}\left(\nabla_{z_2} z_3\right) - \nabla_{z_2}\left(\nabla_{z_1} z_3\right) - \nabla_{[z_1,z_2]} z_3 \\ &= \left(\left[\nabla_{z_1}, \nabla_{z_2}\right] - \nabla_{[z_1,z_2]}\right) z_3,\end{aligned} \tag{5.2.1}$$

where z_1, z_2, and z_3 are tangent vectors. In the local chart $\{x^a\}$, the curvature tensor is expressed by[3]

$$\mathbf{R}(\boldsymbol{e}_c, \boldsymbol{e}_d)\boldsymbol{e}_b = R^a{}_{bcd}\boldsymbol{e}_a,$$

where the components $R^a{}_{bcd}$ are given by the Christoffel symbols as (see e.g., [Sokolnikoff, 1951, Equation 36.7])

$$R^a{}_{bcd} = \begin{vmatrix} \frac{\partial}{\partial x^c} & \frac{\partial}{\partial x^d} \\ \gamma^a{}_{cb} & \gamma^a{}_{db} \end{vmatrix} + \begin{vmatrix} \gamma^a{}_{ck} & \gamma^a{}_{dk} \\ \gamma^k{}_{cb} & \gamma^k{}_{db} \end{vmatrix}. \tag{5.2.2}$$

The tensor $\mathbf{R}$ is often known as *Riemann-Christoffel tensor of the second kind*. When a torsion-free connection is used, the curvature is identical to the skew-symmetric part of the Hessian tensor (see e.g., [Petersen, 2006, §3.1]),

$$\mathbf{R}(z_1, z_2)z_3 = \mathrm{Hess}(z_3)(z_1, z_2) - \mathrm{Hess}(z_3)(z_2, z_1),$$

where the Hessian tensor, $\mathrm{Hess} \in \Gamma(T^*\mathscr{P}_t \otimes T^*\mathscr{P}_t)$, is[4]

$$\mathrm{Hess}(z_3)(z_1, z_2) = \mathscr{C}\left(\nabla_{z_1}\left(\nabla z_3\right), z_2\right) = \mathscr{C}\left(\nabla\left(\nabla z_3\right), z_1, z_2\right),$$

and $\mathscr{C}$ denotes contraction[5].

The ***Riemannian curvature*** of the Riemannian manifold $(\mathscr{P}_t, \mathbf{g})$ is the curvature tensor defined based on a metric compatible connection. Recall from §4.8 that the Levi-Civita connection (i.e., a connection that is both metric compatible and torsion-free) is uniquely determined by the metric tensor. For this reason, the metric tensor also determines a Riemannian curvature tensor by substituting (4.8.2) into (5.2.2), yielding (see e.g., [Sokolnikoff, 1951, Equation 37.3])

$$R_{abcd} = \frac{1}{2}\left(\frac{\partial^2 g_{ad}}{\partial x^b \partial x^c} + \frac{\partial^2 g_{bc}}{\partial x^a \partial x^d} - \frac{\partial^2 g_{ac}}{\partial x^b \partial x^d} - \frac{\partial^2 g_{bd}}{\partial x^a \partial x^c}\right) + g_{kl}\left(\bar{\gamma}^k{}_{bc}\bar{\gamma}^l{}_{ad} - \bar{\gamma}^k{}_{bd}\bar{\gamma}^l{}_{ac}\right). \tag{5.2.3}$$

[1] Recall that $\Omega^k(\mathscr{P}_t) = \Gamma\left(\bigwedge^k(T^*\mathscr{P}_t)\right)$ is the space of k-forms on $\mathscr{P}_t$.

[2] Some authors define the curvature as the negative of (5.2.1) (see e.g., [do Carmo, 1992, Ch. 4, §2]), which the reader should be aware of.

[3] The order of arguments that appears in the component $R^a{}_{bcd}$ differ in various literature. For instance, Lee [1997, p. 118] defines $\mathbf{R}(\boldsymbol{e}_a, \boldsymbol{e}_b)\boldsymbol{e}_c = R_{abc}{}^d\boldsymbol{e}_d$.

[4] Often, the Hessian tensor $\mathrm{Hess}(z_3)(z_1, z_2)$ is denoted by $\nabla^2_{z_1,z_2} z_3$ (see e.g., [Lee, 1997, p. 54]).

[5] The *Contraction* is the smooth map denoted by $\mathscr{C} : X \times Y \to \mathbb{R}$ for two tensor bundles X and Y.

In the above, the terms involving $\bar{\gamma}$ depend purely on $\mathbf{g}$ as expected by (4.8.2). Also, the associated tensor $R_{abcd} = g_{ak}R^{k}{}_{bcd}$ is known as *Riemann-Christoffel tensor of the first kind*. This tensor is also denoted by

$$\mathbf{R}(z_1, z_2, z_3, z_4) = \mathbf{g}(\mathbf{R}(z_1, z_2)z_3, z_4).$$

The curvature tensor has the symmetric properties

$$\mathbf{R}(z_1, z_2, z_3, z_4) = -\mathbf{R}(z_2, z_1, z_3, z_4) = -\mathbf{R}(z_1, z_2, z_4, z_3) = \mathbf{R}(z_3, z_4, z_1, z_2). \tag{5.2.4}$$

Various quantities can be derived from the Riemannian curvature that are useful in studying curvature. The ***sectional curvature*** $K \in \Omega^2(\mathscr{P}_t)$ at the point $\boldsymbol{x}$ is defined by

$$K_{\boldsymbol{x}}(z_1 \wedge z_2) := \frac{\mathbf{R}(z_1, z_2, z_1, z_2)}{|z_1 \wedge z_2|^2},$$

where $z_1 \wedge z_2 \in \Omega^2_{\boldsymbol{x}}(\mathscr{P}_t)$ is a 2-blade (plane section) and $|z_1 \wedge z_2|$ is the area of the 2-blade. The Riemann curvature $\mathbf{R}$ can be uniquely determined by its sectional curvature K given for all 2-blades $z_1 \wedge z_2$ on the vector bundle [Chern, Chen, and Lam, 1999, Ch. 5, Theorem 3.1]. The ***Ricci curvature*** $\mathrm{Ric} \in \Gamma\left(\mathrm{Sym}^2(\mathrm{T}\mathscr{P}_t)\right)$ is the trace of $\mathbf{R}$ as[6]

$$\mathrm{Ric}(z_1, z_2) := \mathrm{trace}_{\mathbf{g}}\left(z \mapsto \mathbf{R}(z, z_1)z_2\right).$$

In the above relation, $\mathrm{trace}_{\mathbf{g}}(\mathbf{R})$ is the trace with respect to the metric $\mathbf{g}$, which is the contraction of $\mathbf{g}^{-1}\mathbf{R}$. In a local chart,

$$\mathrm{Ric}_{bd} = R^{a}{}_{bad} = g^{ac}R_{abcd},$$

and can be given explicitly by contracting (5.2.2) in terms of Levi-Civita connection as

$$\mathrm{Ric}_{ab} = \frac{\partial \bar{\gamma}^{k}{}_{ab}}{\partial x^k} - \frac{\partial \bar{\gamma}^{k}{}_{ka}}{\partial x^b} + \bar{\gamma}^{l}{}_{lk}\bar{\gamma}^{k}{}_{ba} - \bar{\gamma}^{l}{}_{bk}\bar{\gamma}^{k}{}_{la}. \tag{5.2.5a}$$

We recall from (4.8.2) that $\bar{\gamma}$ is determined by the metric. Using the identity

$$\bar{\gamma}^{k}{}_{ka} = \frac{\partial}{\partial x^a}\left(\ln\sqrt{\det(\mathbf{g})}\right),$$

an equivalent form of (5.2.5a) can be given by (see e.g., [Sokolnikoff, 1951, §38])

$$\mathrm{Ric}_{ab} = \frac{\partial \bar{\gamma}^{k}{}_{ab}}{\partial x^k} - \bar{\gamma}^{k}{}_{al}\bar{\gamma}^{l}{}_{kb} - \left(\frac{\partial^2}{\partial x^a \partial x^b} - \bar{\gamma}^{k}{}_{ab}\frac{\partial}{\partial x^k}\right)\left(\ln\sqrt{\det(\mathbf{g})}\right). \tag{5.2.5b}$$

[6] In literature, the Ricci curvature is defined differently up to a sign. For instance, in [Sokolnikoff, 1951, §38], $\mathrm{Ric}(z_1, z_2) = \mathrm{trace}_{\mathbf{g}}(z \mapsto \mathbf{R}(z_1, z)z_2)$, yielding $\mathrm{Ric}_{bc} = R^{a}{}_{bca}$.

The trace of Ricci curvature is known as the ***scalar curvature***, denoted by

$$\mathrm{scal} = \mathrm{trace}_{\mathbf{g}} \mathrm{Ric}\,.$$

In a local chart,

$$\mathrm{scal} := g^{bd}\,\mathrm{Ric}_{bd} = g^{bd} g^{ac} R_{abcd}.$$

It is useful to declare the traceless Ricci tensor,

$$\mathrm{Ric}^{\circ} := \mathrm{Ric} - \frac{\mathrm{scal}}{n}\mathbf{g}.$$

Since $\mathrm{trace}_{\mathbf{g}}\,\mathbf{g} = n$, it is easy to verify that $\mathrm{trace}_{\mathbf{g}}\,\mathrm{Ric}^{\circ} = 0$. A manifold with $\mathrm{Ric} = \mathbf{0}$ is called ***Ricci-flat***[7]. Similarly, a manifold satisfying $\mathrm{Ric}^{\circ} = \mathbf{0}$ is known as ***Einstein manifold***. Clearly, Riemann-flat implies Ricci-flat, and a Ricci-flat manifold is Einstein with $\mathrm{scal} = 0$, but the converse does not necessarily hold.

An n-manifold with $n \geq 3$ admits ***orthogonal decomposition of Riemannian curvature*** by (see e.g., [Gallot, Hulin, and Lafontaine, 2004, §3.K.1, Equation 3.127] or [Chow, Lu, and Ni, 2006, Ch.1, Equation 1.58])

$$\mathbf{R} = \frac{\mathrm{scal}}{2n(n-1)}\mathbf{g} \owedge \mathbf{g} + \frac{1}{n-2}\,\mathrm{Ric}^{\circ} \owedge \mathbf{g} + \mathbf{W}, \qquad n \geq 3, \tag{5.2.6a}$$

where $\owedge : \mathrm{Sym}^2(\mathscr{P}_t) \times \mathrm{Sym}^2(\mathscr{P}_t) \to \mathrm{Curv}(\mathscr{P}_t)$ is the ***Kulkarni-Nomizu product***. For two tensors $\mathbf{A}$ and $\mathbf{B}$ of rank $\binom{0}{2}$, the Kulkarni-Nomizu product is a tensor of rank $\binom{0}{4}$ and given by

$$\mathbf{A} \owedge \mathbf{B}(z_1, z_2, z_3, z_4) = \begin{vmatrix} \mathbf{A}(z_1, z_3) & \mathbf{A}(z_1, z_4) \\ \mathbf{B}(z_2, z_3) & \mathbf{B}(z_2, z_4) \end{vmatrix} + \begin{vmatrix} \mathbf{B}(z_1, z_3) & \mathbf{B}(z_1, z_4) \\ \mathbf{A}(z_2, z_3) & \mathbf{A}(z_2, z_4) \end{vmatrix}.$$

Also, $\mathbf{W}$ in (5.2.6a) is the ***Weyl curvature tensor***, which is the traceless part of the Riemann curvature and has the same symmetry as $\mathbf{R}$. The Weyl tensor is identically zero when $n < 4$. For a 2-manifold the traceless Ricci curvature is zero, so the only contributing term in above decomposition is the scalar curvature, i.e.,

$$\mathbf{R} = \frac{\mathrm{scal}}{4}\mathbf{g} \owedge \mathbf{g}, \qquad n = 2. \tag{5.2.6b}$$

In the orthogonal decomposition (5.2.6a), the Ricci part represents the rate of change of volume along geodesics. The scalar curvature, however, represents the deviation of volume from a geodesic ball due to deformation along geodesics. The Weyl tensor does not contribute to the curvature in dimensions $n = 2$ and 3 that we are most interested in.

[7] Non-trivial examples of Ricci-flat manifolds are hard to find [Besse, 1987, §0.23].

5.3 Compatibility Conditions of Continua

Compatibility conditions specify algebraic restrictions on the deformation tensors to guarantee the existence of a continuous displacement field. These conditions are related to the Riemannian curvature of the configuration spaces. We briefly review the compatibility conditions in Euclidean space, known as Saint-Venant conditions, and we generalize them to the other non-Euclidean manifolds. We will show the virtue of general compatibility conditions, even when represented in the Euclidean space.

Compatibility on Riemann-Flat Manifold

Suppose the configuration space $\mathcal{S}$ is a ***flat manifold*** where the Riemannian curvature tensor is identically zero. Such space is isometrically isomorphic to the Euclidean space $\mathbb{R}^n$. In (5.2.3) we have seen that $\mathbf{R}$ is essentially determined by the metric tensor $\mathbf{g}$. Thus, here, we denote the curvature by $\mathbf{R}_{(\mathscr{P}_t,\mathbf{g})}$. The Riemann-flatness, i.e., $\mathbf{R}_{(\mathscr{P}_t,\mathbf{g})} = \mathbf{0}$, implies a restriction on the metric $\mathbf{g}(\boldsymbol{x})$ on the spatial configuration space $\mathscr{P}_t$. The same condition can be concluded for the curvature of the referential configuration space, where the pullback curvature $\boldsymbol{\phi}^*\mathbf{R}$ should also identically vanish, i.e., $\boldsymbol{\phi}^*\mathbf{R} = \mathbf{0}$ (see e.g., [Marsden and Hughes, 1983, Ch. 1, Proposition 4.31] or [Dimitrienko, 2002, §10.6]). Recall from (2.4.5a) that $\boldsymbol{\phi}^*\mathbf{g} = \mathbf{C}^\flat$, which implies the isomorphism $(\mathscr{P}_{t_0}, \mathbf{C}^\flat) \to (\mathscr{P}_t, \mathbf{g})$ is a Riemannian isometry. This map is shown in the commutative diagram,

$$\begin{array}{ccc} \mathrm{Sym}^2\left(\Omega^2(\mathscr{P}_{t_0})\right) & \xrightarrow{\boldsymbol{\phi}} & \mathrm{Sym}^2\left(\Omega^2(\mathscr{P}_t)\right) \\ \uparrow{\scriptstyle \boldsymbol{\phi}^*\mathbf{R}} & & \uparrow{\scriptstyle \mathbf{R}} \\ (\mathscr{P}_{t_0}, \mathbf{C}^\flat) & \xrightarrow{\boldsymbol{\phi}} & (\mathscr{P}_t, \mathbf{g}) \end{array} \tag{5.3.1}$$

Thus, a Riemann-flat manifold admits

$$\boldsymbol{\phi}^*\mathbf{R}_{(\mathscr{P}_t,\mathbf{g})} = \mathbf{R}_{(\mathscr{P}_{t_0},\boldsymbol{\phi}^*\mathbf{g})} = \mathbf{R}_{(\mathscr{P}_{t_0},\mathbf{C}^\flat)} = \mathbf{0}.$$

Similar to (5.2.3), the above Riemannian curvature can be written by adopting $\mathbf{C}^\flat$ as a metric, i.e.,

$$\begin{aligned}\left(R_{(\mathscr{P}_{t_0},\mathbf{C}^\flat)}\right)_{ABCD} = \frac{1}{2}\left(\frac{\partial^2 C_{AD}}{\partial X^B \partial X^C} + \frac{\partial^2 C_{BC}}{\partial X^A \partial X^D} - \frac{\partial^2 C_{AC}}{\partial X^B \partial X^D} - \frac{\partial^2 C_{BD}}{\partial X^A \partial X^C}\right) \\ + C_{KL}\left(\hat{\Gamma}^K{}_{BC}\hat{\Gamma}^L{}_{AD} - \hat{\Gamma}^K{}_{BD}\hat{\Gamma}^L{}_{AC}\right),\end{aligned} \tag{5.3.2}$$

where $C_{AB} = G_{AK}C^{K}{}_{B}$. Also, $\hat{\Gamma}$ in the above denotes the Christoffel symbol of the Levi-Civita connection when $\mathbf{C}^\flat$ is used as the metric, i.e., (compare with (4.8.2)),

$$\hat{\Gamma}^{A}{}_{BC} = \frac{1}{2}C^{AK}\left(\frac{\partial C_{CK}}{\partial X^B} + \frac{\partial C_{BK}}{\partial X^C} - \frac{\partial C_{BC}}{\partial X^K}\right), \tag{5.3.3}$$

Also, the associated tensor in the above relation is $C^{AK} = C^{A}{}_{B}G^{BK}$. The Riemann-flatness of the manifold implies that the equation (5.3.2) should vanish, i.e.,

$$\left(R_{(\mathscr{P}_{t_0},\mathbf{C}^\flat)}\right)_{ABCD} = 0, \tag{5.3.4a}$$

The above relation is the compatibility condition on the tensor $\mathbf{C}$ [Sedov, 1966, p. 106, Equation 8.3]. It implies that an arbitrary symmetric positive-definite deformation tensor field $\mathbf{C}$ may not correspond to a continuous deformation unless it satisfies (5.3.4a). In three-dimensional space, the relation (5.3.4) presents 3^4 equations. By the symmetries of $\mathbf{R}$ and the Bianchi's first identity (see [Petersen, 2006, Ch 3, Proposition 4]) the number of equations reduces to only 6. (see also Remark 5.3.3). Due to the *Bianchi's second identity*, the six scalar equations are yet not entirely independent [Béda, Kozák, and Verhás, 1996, p. 31].

We note that the equation (5.3.4a) is the compatibility condition for the *finite* (nonlinear) deformation. A similar condition can be derived for an *infinitesimal* (linear) deformation. Let $\boldsymbol{\epsilon}$ be the infinitesimal strain tensor, which is the linear approximation of the finite deformation tensor $\mathbf{C}$ in the sense of Gâteaux derivative. By linearization of (5.3.2) and eliminating quadratic terms, we obtain

$$\frac{\partial^2 \epsilon_{ad}}{\partial x^b \partial x^c} + \frac{\partial^2 \epsilon_{bc}}{\partial x^a \partial x^d} - \frac{\partial^2 \epsilon_{ac}}{\partial x^b \partial x^d} - \frac{\partial^2 \epsilon_{bd}}{\partial x^a \partial x^c} = 0. \tag{5.3.4b}$$

The above relation is known as the ***Saint-Venant compatibility condition*** on the infinitesimal strain tensor [Sokolnikoff, 1951, Ch. 6, §106]. A trivial solution of the above set of equations is the affine functions since the compatibility differential equations are homogeneous and second order.

The compatibility condition can also be written for the rate of deformation tensor, $\mathbf{d}$. Recall from Proposition 4.9.1 that $\mathscr{L}_{\boldsymbol{\phi}}\mathbf{g} = 2\mathbf{d}^\flat + \bar{\nabla}_v\mathbf{g}$. But, we are working with a metric compatible connection, so $\bar{\nabla}\mathbf{g} = \mathbf{0}$. In the relation, (5.2.3) we replace the tensor $\mathbf{C}^\flat$ with $\mathbf{g}$, then we take the (Lie) time derivative of (5.2.3), apply $\mathscr{L}_{\boldsymbol{\phi}}\mathbf{g} = 2\mathbf{d}^\flat$, linearize the equation and eliminate quadratic terms to obtain

$$\frac{\partial^2 d_{ad}}{\partial x^b \partial x^c} + \frac{\partial^2 d_{bc}}{\partial x^a \partial x^d} - \frac{\partial^2 d_{ac}}{\partial x^b \partial x^d} - \frac{\partial^2 d_{bd}}{\partial x^a \partial x^c} = 0, \tag{5.3.4c}$$

where $d_{ab} = g_{ak}d^{k}{}_{b}$. The above relation is the compatibility condition for the rate of deformation tensor [Sedov, 1966, p. 107, Equation 8.7]. The above compatibility conditions can also be derived from the closely related *integrability conditions* [Talpaert, 2002, §3.2].

Compatibility condition on Einstein Manifold

The compatibility conditions can also be derived for non-Euclidean manifolds. Manifolds with ***constant sectional curvatures*** are of our interest since their universal covers specify model spaces for the elliptic, plane and hyperbolic manifolds (*Killing-Hopf Theorem* [do Carmo, 1992, Ch. 8, Theorem 4.1]). A constant sectional curvature $K_{\boldsymbol{x}}(z_1 \wedge z_2)$ is independent of both the point $\boldsymbol{x}$ on the manifold and the 2-blades $z_1 \wedge z_2$ on the vector bundle. The sectional curvatures $K = -1, 0, +1$ correspond to the model spaces $\mathbb{H}^n$, $\mathbb{R}^n$ and $\mathbb{S}^n$ respectively. The Riemannian curvature of manifolds with constant sectional curvature is

$$\mathbf{R} = \frac{K}{2}\mathbf{g} \owedge \mathbf{g}, \qquad K = \text{constant}. \tag{5.3.5}$$

By comparing the above relation with (5.2.6a), we see that a manifold of constant sectional curvature is essentially an Einstein manifold. Conversely, every three-dimensional Einstein manifold (where the Weyl curvature is zero) is a constant sectional manifold [Gallot, Hulin, and Lafontaine, 2004, p. 183], which can be simply verified by (5.2.6a). Other classes of manifolds are those of ***constant scalar curvature***. Every Einstein manifold has a constant scalar curvature. The significance of manifolds with constant scalar curvature is understood by the ***Yamabe problem*** (see e.g., [Gallot, Hulin, and Lafontaine, 2004, §3.M.1] or [Chow, Lu, and Ni, 2006, Appendix B, §4.1]), which states that on every closed manifold of positive scalar curvature, any given metric $\mathbf{g}$ can be multiplied by some smooth positive function to become a manifold of constant scalar curvature.

We start formulating compatibility conditions on the Einstein manifolds and then derive corollaries for manifolds of constant sectional curvature. In particular, we revisit the Riemann-flat manifold that was discussed earlier.

Proposition 5.3.1 (Compatibility condition on the Einstein manifolds). *Suppose the motion $\boldsymbol{\varphi} : \mathscr{B} \to \mathscr{S}$ of the body $\mathscr{B}$ is on the Einstein n-manifold $\mathscr{S}$. Let $\mathbf{C}$ be the right deformation tensor of the motion. Then, the motion continuously exists, i.e., $\boldsymbol{\varphi} \in C(\mathscr{B}; \mathscr{S})$, if $(\mathscr{P}_{t_0}, \mathbf{C}^\flat)$ is Einstein, i.e.,*

$$\mathrm{Ric}_{(\mathscr{P}_{t_0}, \mathbf{C}^\flat)} = \frac{\mathrm{scal}}{n}\mathbf{C}^\flat, \tag{5.3.6}$$

where $\mathrm{Ric}_{(\mathscr{P}_{t_0}, \mathbf{C}^\flat)}$ is the Ricci curvature when $\mathbf{C}^\flat$ is used as the metric and scal *is the scalar curvature of $\mathscr{S}$.*

Proof. By definition, an Einstein manifold satisfies $\mathrm{Ric}^\circ_{(\mathscr{P}_t, \mathbf{g})} = \mathbf{0}$ where subscript $\mathbf{g}$ indicates the metric used to form the curvature. The commutative diagram below relates the traceless Ricci curvatures of the referential and spatial configuration spaces by the Riemannian isometry

$\boldsymbol{\phi}^*\mathbf{g} = \mathbf{C}^\flat$ (see (2.4.5a)),

$$\begin{array}{ccc} \mathrm{Sym}^2\left(T\mathscr{P}_{t_0}\right) & \xrightarrow{\boldsymbol{\phi}} & \mathrm{Sym}^2\left(T\mathscr{P}_t\right) \\ \uparrow{\scriptstyle \boldsymbol{\phi}^*\,\mathrm{Ric}^\circ} & & \uparrow{\scriptstyle \mathrm{Ric}^\circ} \\ (\mathscr{P}_{t_0}, \mathbf{C}^\flat) & \xrightarrow{\boldsymbol{\phi}} & (\mathscr{P}_t, \mathbf{g}) \end{array} \tag{5.3.7}$$

Note that the pullback of a zero-section is also always a zero-section. Thus, $\boldsymbol{\phi}^*\,\mathrm{Ric}^\circ_{(\mathscr{P}_t,\mathbf{g})} = \mathbf{0}$ on the referential configuration space, i.e.,

$$\boldsymbol{\phi}^*\,\mathrm{Ric}^\circ_{(\mathscr{P}_t,\mathbf{g})} = \mathrm{Ric}_{(\mathscr{P}_{t_0},\boldsymbol{\phi}^*\mathbf{g})} - \frac{\boldsymbol{\phi}^*\,\mathrm{scal}}{n}\boldsymbol{\phi}^*\mathbf{g} = \mathbf{0}.$$

Also, an Einstein manifold has a constant scalar curvature, thus, $\boldsymbol{\phi}^*\,\mathrm{scal} = \mathrm{scal}$. Putting all together yields (5.3.6). ■

Corollary 5.3.2 (Compability condition on manifolds of constant sectional curvature). *Suppose the motion $\boldsymbol{\varphi} : \mathscr{B} \to \mathscr{S}$ of the body $\mathscr{B}$ is on the manifold of constant sectional curvature K with dimension $n < 4$. Then, the motion continuously exists if the right deformation tensor satisfies*

$$\frac{\partial \hat{\Gamma}^K{}_{AB}}{\partial X^K} - \hat{\Gamma}^K{}_{AL}\hat{\Gamma}^L{}_{KB} - \left(\frac{\partial^2}{\partial X^A \partial X^B} - \hat{\Gamma}^K{}_{AB}\frac{\partial}{\partial X^K}\right)\left(\ln\sqrt{\det(\mathbf{C}^\flat)}\right) = (n-1)KC_{AB}, \tag{5.3.8a}$$

where $\hat{\Gamma}$ is obtained from $\mathbf{C}^\flat$ by (5.3.3). Furthermore, the compatibility condition for the infinitesimal strain tensor $\boldsymbol{\epsilon}$ is

$$\frac{\partial}{\partial x^k}\left(\frac{\partial \epsilon_{bk}}{\partial x^a} + \frac{\partial \epsilon_{ak}}{\partial x^b} - \frac{\partial \epsilon_{ab}}{\partial x^k}\right) - \frac{\partial^2}{\partial x^a \partial x^b}\,\mathrm{trace}(\epsilon_{ab}) = 2(n-1)K\epsilon_{ab}. \tag{5.3.8b}$$

Similarly, the compatibility condition for the rate of deformation tensor $\mathbf{d}$ is

$$\frac{\partial}{\partial x^k}\left(\frac{\partial d_{bk}}{\partial x^a} + \frac{\partial d_{ak}}{\partial x^b} - \frac{\partial d_{ab}}{\partial x^k}\right) - \frac{\partial^2}{\partial x^a \partial x^b}\,\mathrm{trace}(d_{ab}) = 2(n-1)Kd_{ab}. \tag{5.3.8c}$$

Proof. A manifold of constant K is essentially Einstein, and the Proposition 5.3.1 applies. Additionally, for manifolds of dimension $n < 4$, the curvature can be completely characterized by Ricci tensor since the Weyl tensor vanishes (see the discussion in Remark 5.3.3). Thus, $\mathrm{Ric}^\circ_{(\mathscr{P}_{t_0},\mathbf{C}^\flat)} = \mathbf{0}$ establishes the compatibility condition that is both necessary and sufficient. We use (5.2.5b) to express Ricci curvature in terms of $\hat{\Gamma}$ where $\mathbf{C}^\flat$ is used as the metric. Also, the curvature of manifolds with constant K is given by (5.3.5). Comparing (5.3.5) with (5.2.6) shows $\mathrm{scal} = n(n-1)K$, and concludes (5.3.8a).

To obtain (5.3.8b), we linearize (5.3.8a) around a point $\boldsymbol{x} \in \mathscr{P}_t$ (or $\boldsymbol{X} \in \mathscr{P}_{t_0}$). Because the deformation is considered infinitesimal, here, we do not distinguish between referential

and spatial variables. For consistency, we use the lower case notation for variables. The linear approximation of the deformation tensor $\mathbf{C}$ is given by the infinitesimal strain tensor $\boldsymbol{\epsilon}$ as

$$\mathbf{C} = \mathbf{I} + \boldsymbol{\epsilon} + \mathcal{O}(|\boldsymbol{\epsilon}|^2),$$

where $\mathbf{I}$ is the trivial automorphism. The linear approximation of the associated deformation tensor is $\mathbf{C}^\flat$ is $C_{ab} = G_{ab} + \epsilon_{ab}$. By the normal neighborhood lemma [Lee, 1997, Lemma 5.10 and Proposition 5.11], we can simply choose a normal coordinate in a neighborhood of the point $\boldsymbol{x}$ where metrics are identified, i.e., $G_{ab} = g_{ab} = \delta_{ab}$. Linearizing (5.3.3) gives

$$\bar{\gamma}^k{}_{ab} = \frac{1}{2}\left(\frac{\partial \epsilon_{ka}}{\partial x^b} + \frac{\partial \epsilon_{kb}}{\partial x^a} - \frac{\partial \epsilon_{ab}}{\partial x^k}\right) + \mathcal{O}(|\boldsymbol{\epsilon}|^2),$$

where $\bar{\gamma} \sim \mathcal{O}(|\boldsymbol{\epsilon}|)$. It is clear that the term $\bar{\gamma}^k{}_{al}\bar{\gamma}^l{}_{kb} \sim \mathcal{O}(|\boldsymbol{\epsilon}|^2)$ drops out of the linearized equation. By the Jacobi formula for the derivative of determinants, we have the linear approximation

$$\ln\sqrt{\det(\mathbf{C}^\flat)} = \frac{1}{2}\ln\left(1 + \operatorname{trace}(\boldsymbol{\epsilon}) + \mathcal{O}(|\boldsymbol{\epsilon}|^2)\right) = \frac{1}{2}\operatorname{trace}(\boldsymbol{\epsilon}) + \mathcal{O}(|\boldsymbol{\epsilon}|^2),$$

where $\operatorname{trace}(\boldsymbol{\epsilon}) \sim \mathcal{O}(|\boldsymbol{\epsilon}|)$. After combining all the above, the remaining terms of order $\mathcal{O}(|\boldsymbol{\epsilon}|)$ yield (5.3.8b).

Lastly, (5.3.8c) is obtained by taking the Lie derivative of (5.3.8a) and applying Proposition 4.9.1, i.e., $\mathscr{L}_{\boldsymbol{\phi}}\mathbf{g} = 2\mathbf{d}^\flat$. Since the equation (5.3.8b) is already linearized, without further effort we realize that the relation (5.3.8c) is similar to (5.3.8b), except $\boldsymbol{\epsilon}$ is replaced by $\mathbf{d}^\flat$. ■

Remark 5.3.3 (Number of compatibility conditions on n-manifolds). Observe that the relations in (5.3.8) for $K = 0$ are identical to the *trace* of the compatibility conditions on Euclidean space given by (5.3.4). On a 3-manifold, each of the relations (5.3.4) represents the set of 3^4 coupled partial differential equations. Most of these equations are redundant, and they effectively reduce to only six equations[8]. In contrast, the relations (5.3.8) present 6 equations directly.

We emphasize that the reduction of 81 equations to 6 equations is *not* just due to the symmetries of $\mathbf{R}$. To show this by a counterexample, observe that the curvature tensor on an n-manifold has n^4 components. By accounting for three symmetry properties in (5.2.4), the number of non-repetitive components of $\mathbf{R}$ are still $n^4/2^3 + \mathcal{O}(n^3)$. Whereas, in $n = 3$, they reduce further to $n(n+1)/2 \sim \mathcal{O}(n^2)$ meaningful components, which is the size of non-repetitive components of the symmetric Ricci tensor.

Interestingly, such a drastic reduction of the set of compatibility equations occurs only in $n = 2$ and 3, regardless the manifold is Euclidean or otherwise. This is because, in addition to

[8]We remind the reader that due to the second Bianchi identity, these equations are yet not entirely independent.

the symmetries of the curvature tensor, the capacity of the 3-manifold plays an additional role in the reduction of equations which we will explain as follows. Recall that for a 3-manifold, the Weyl curvature $\mathbf{W}$ vanishes, simplifying curvature to

$$\mathbf{R} = \frac{\text{scal}}{12}\mathbf{g} \owedge \mathbf{g} + \left(\text{Ric} - \frac{\text{scal}}{3}\mathbf{g}\right) \owedge \mathbf{g}, \qquad n = 3.$$

So the whole structure of Riemannian curvature $\mathbf{R}$ can be effectively reconstructed from only the 6 components of symmetric Ricci curvature. In other words, a three-dimensional space does not have enough capacity to encompass all characteristics of curved space. In higher dimensions, however, the Ricci curvature cannot contain all information about the curvature alone, and the number of compatibility conditions expands to $\mathcal{O}(n^4)$ as the full curvature tensor should be used. ▲

Remark 5.3.4 (Compatibility conditions for isochoric flows). Recall from section 4.4 that for the isochoric flows, $\text{trace}(\mathbf{l}) = 0$. That is $\text{trace}_{\mathbf{g}}(\mathbf{d}^\flat) = 0$ which also means $\text{trace}_{\mathbf{g}}(\boldsymbol{\epsilon}) = 0$. Hence, the compatibility conditions on the Euclidean space ($K = 0$) of dimension $n < 4$ simplifies to the set of first-order differential equations,

$$\frac{\partial \epsilon_{bk}}{\partial x^a} + \frac{\partial \epsilon_{ak}}{\partial x^b} - \frac{\partial \epsilon_{ab}}{\partial x^k} = \alpha_{ab},$$

for some constants α_{ab} of the first integrals. ▲

5.4 Second Material Time Derivative of Deformation

Recall from Proposition 4.3.1 that we have derived the first material time derivative of deformation tensor as $D\mathbf{F}/dt = \mathbf{l}\mathbf{F}$ where $\mathbf{l}$ is the (first) rate of deformation. Similarly, we derive the second-order material time derivative, D^2/dt^2, of the tensors $\mathbf{F}$, $\mathbf{b}$, $\mathbf{b}^\sharp$, $\mathbf{C}$, and $\mathbf{C}^\flat$. The formulation of second material rates involves the gradient of acceleration. In Euclidean space, the relation

$$\frac{D^2\mathbf{F}}{dt^2} = (\nabla \boldsymbol{a})\,\mathbf{F}, \qquad \text{(Euclidean)} \tag{5.4.1}$$

is known, and can be found for instance in Gurtin, Fried, and Anand [2010, Equation 9.22]). We generalize (5.4.1) to the Riemannian manifolds. In our derivations, we assume the connection on the tangent bundle is arbitrary, and may include torsion. Additionally, here, the curvature tensor is not necessarily a Riemannian curvature unless the torsion tensor is set to zero.

Definition 5.4.1 (Second rate of the deformation gradient). *Assume the diffeomorphism $\boldsymbol{\phi}_t : C^2(\mathscr{I}; \mathscr{P}_t)$ is a flow on the manifold $\mathscr{P}_t$ with the curvature tensor $\mathbf{R}$. We define the **second spatial rate of deformation gradient** of the flow as the tensor $\mathbf{k} \in \Gamma(\text{End}(T\mathscr{P}_t))$, and given by*

$$\mathbf{k} := \nabla\mathbf{a} + \mathbf{R}(\boldsymbol{v}, \cdot)\boldsymbol{v} + \frac{D\,\text{tor}(\boldsymbol{v}, \cdot)}{dt} + \text{tor}(\boldsymbol{v}, \mathbf{l}), \tag{5.4.2}$$

where $\mathbf{a}$ *is the spatial acceleration,* $\mathbf{l}$ *is the (first) spatial rate of deformation tensor and* tor *is the torsion of the connection on the vector bundle. In components,* $\mathbf{R}(v,\cdot)v = R^a{}_{bcd}v^b v^d$ *and* $\operatorname{tor}(v,\cdot) = \tau^a{}_{bc}v^b$. ▲

In our notation above, $\mathbf{R}(v,\cdot)v = \mathscr{C}(v,\mathbf{R}v)$ where $\mathscr{C}$ denotes the contraction operator. We also remind the reader that $\operatorname{tor}(v,\cdot) = \mathscr{C}(v,\operatorname{tor})$, where the contraction is applied to the first index of the torsion tensor.

Observe that on a *flat Riemannian manifold* $\mathbf{R} = \mathbf{0}$, which simplifies $\mathbf{k}$. Additionally, if the covariant derivatives are expressed by torsion-free connection, i.e., tor $= \mathbf{0}$, the tensor $\mathbf{k}$ becomes the covariant derivative of acceleration, i.e., $\mathbf{k} = \nabla\mathbf{a}$. The contraction $\mathbf{k}(v) = \nabla_v \boldsymbol{a}$ in an autonomous velocity field is the ***jerk*** (or *jolt*) of the motion. When $\boldsymbol{a} = \mathbf{0}$, the tensor $\mathbf{k}$ is mainly influenced by the curvature, and will be explored on geodesic flows in §5.5.

The motivation for the definition of the second rate of deformation tensor $\mathbf{k}$ as the above will become evident in the Theorem 5.4.3 that follows. Beforehand, we need a lemma.

Lemma 5.4.2 (Material rate of the deformation tensor). *Let* $\mathbf{l} \in \Gamma(\operatorname{End}(T\mathscr{P}_t))$ *be the first-rate of the deformation tensor given in Definition 4.5.1, and expressed by an arbitrary connection* ∇ *on the vector bundle* $T\mathscr{P}_t$. *Then, the material rate of* $\mathbf{l}(\boldsymbol{x},t)$ *is given by*

$$\frac{D\mathbf{l}}{dt} = \mathbf{k} - \mathbf{l}^2. \tag{5.4.3}$$

Proof. Take the material time derivative of $\mathbf{l}$ by

$$\frac{D\mathbf{l}}{dt} = \frac{D(\nabla v)}{dt} + \frac{D\operatorname{tor}(v,\cdot)}{dt}. \tag{5.4.4}$$

In the above, the material time derivative of ∇v can further be given by (4.3.1) as

$$\frac{D(\nabla v)}{dt} = \frac{\partial}{\partial t}(\nabla v) + \nabla_v(\nabla v). \tag{5.4.5}$$

The time derivative $\partial/\partial t$ and covariant derivative ∇ commute. Hence, the first term on the right-hand side of the above relation can be written as $\partial(\nabla v)/\partial t = \nabla(\partial v/\partial t)$. The second term in the above relation is the Hessian, i.e.,

$$\nabla_v(\nabla v)(z) = \mathscr{C}(\nabla_v(\nabla v), z) = \operatorname{Hess}(v)(v,z).$$

Using the chain rule, the Hessian can be expressed by[9] (see e.g., [Petersen, 2006, p. 29])

$$\begin{aligned}\nabla_v(\nabla_z v) &= \operatorname{Hess}(v)(v,z) + \mathscr{C}(\nabla v, \nabla_v z)\\ &= \nabla_v(\nabla v)(z) + \nabla_{\nabla_v z} v,\end{aligned}$$

[9] Note that $\nabla_v(\nabla_z \boldsymbol{y}) \neq \nabla_v(\nabla \boldsymbol{y})(z)$ for a vector $\boldsymbol{y}$. The left term is the covariant derivative of the *vector* $\nabla_z \boldsymbol{y}$ in the direction of v, whereas the right term is the covariant derivative of the *second-order* tensor $\nabla \boldsymbol{y}$ along $\boldsymbol{x}$, and then contracted by z. Using the chain rule, it holds $\nabla_v(\nabla_z \boldsymbol{y}) = \mathscr{C}(z, \nabla_v(\nabla \boldsymbol{y})) + \mathscr{C}(\nabla_x z, \nabla \boldsymbol{y})$.

where the tangent vector z is introduced to track the argument of tensors and will be omitted later. Rearrangement yields

$$\nabla_v (\nabla v)(z) = \nabla_v (\nabla_z v) - \nabla_{\nabla_v z} v. \tag{5.4.6a}$$

By the definition of curvature in (5.2.1), the order of covariant derivatives in $\nabla_v (\nabla_z v)$ (the first term on the right side of the above relation) can be swapped by

$$\nabla_v (\nabla_z v) = \nabla_z (\nabla_v v) + \mathbf{R}(v, z)v + \nabla_{[v,z]} v. \tag{5.4.6b}$$

Recall from (4.2.5) that the Lie bracket in the above equation can be expressed by the torsion as

$$[v, z] = \nabla_v z - \nabla_z v - \operatorname{tor}(v, \cdot). \tag{5.4.6c}$$

Combining all three equations (5.4.6) leads to

$$\begin{aligned} \nabla_v (\nabla v)(z) &= \nabla_z (\nabla_v v) + \mathbf{R}(v, z)v - \nabla_{\nabla_z v + \operatorname{tor}(v,z)} v \\ &= \mathscr{C}(z, \nabla (\nabla_v v)) + \mathscr{C}(z, \mathbf{R}(v, \cdot)v) - \mathscr{C}(z, \nabla_{\nabla v + \operatorname{tor}(v,\cdot)} v). \end{aligned}$$

The second line above is justified by realizing that the argument z is linear in all right-hand side terms[10]. Henceforth, we can separate the argument z from the equation and write it as the contraction with the rest of the terms. Note that we were not able to do so on the equation (5.4.6a), since that equation is not linear in z. Omitting z from the above yields the tensor identity

$$\nabla_v (\nabla v) = \nabla (\nabla_v v) + \mathbf{R}(v, \cdot)v - \nabla_{\underbrace{\nabla v + \operatorname{tor}(v,\cdot)}_{\mathbf{l}}} v.$$

Moreover, in the third right term above, we realized that $\mathbf{l} = \nabla v + \operatorname{tor}(v, \cdot)$. Putting all together, the equation (5.4.5) becomes

$$\frac{D(\nabla v)}{dt} = \nabla \underbrace{\left(\frac{\partial v}{\partial t} + \nabla_v v \right)}_{\boldsymbol{a}} + \mathbf{R}(v, \cdot)v - \nabla_{\mathbf{l}} v.$$

Realize that the first right-hand side term inside the parenthesis is the spatial acceleration $\boldsymbol{a}$ given by (2.2.8). Finally, the material time derivative of $\mathbf{l}$ from (5.4.4) becomes

$$\frac{D\mathbf{l}}{dt} = \nabla \boldsymbol{a} + \mathbf{R}(v, \cdot)v + \frac{D \operatorname{tor}(v, \cdot)}{dt} - \underbrace{(\nabla_{\mathbf{l}} v + \operatorname{tor}(v, \mathbf{l}))}_{\mathbf{l}^2} + \operatorname{tor}(v, \mathbf{l}), \tag{5.4.7}$$

[10] Recall $\nabla_z y$ is linear in z. However, the connection is not linear in y, hence not a tensor.

where we have subtracted and added $\mathrm{tor}(\boldsymbol{v},\mathbf{l})$ in the last two terms of the right side in the above. Observe that the fourth and the fifth terms on the right inside form $\mathbf{l}^2 = \mathbf{l}(\mathbf{l})$, since

$$\mathbf{l}^2 = \mathscr{C}(\mathbf{l},\mathbf{l}) = \nabla_{\underbrace{\nabla \boldsymbol{v} + \mathrm{tor}(\boldsymbol{v},\cdot)}_{\mathbf{l}}} + \mathrm{tor}(\boldsymbol{v}, \underbrace{\nabla \boldsymbol{v} + \mathrm{tor}(\boldsymbol{v},\cdot)}_{\mathbf{l}}).$$

Substituting $\mathbf{l}^2$ in (5.4.7) concludes the proof. ∎

Theorem 5.4.3 (Second material rate of the deformation gradient). *If the flow $\boldsymbol{\phi}_t \in C^2(\mathscr{P}_{t_0} \times \mathscr{I}; \mathscr{P}_t)$, then the second material time derivative of the deformation gradient $\mathbf{F} = T\boldsymbol{\phi}_t$ using an arbitrary linear connection ∇ on the spatial tangent bundle is given by*

$$\frac{D^2\mathbf{F}}{dt^2} = \mathbf{k}\mathbf{F}, \qquad F(\boldsymbol{X}, t_0) = \mathbf{I}(\boldsymbol{X}), \tag{5.4.8}$$

where $\mathbf{I} := T(\mathrm{id}_{\mathscr{P}_{t_0}})$ is the trivial automorphism, and $\mathbf{k}$ is given by Definition 5.4.1. Moreover, in the local charts $\{X^A\}$ and $\{x^a\}$, the above relation is

$$\frac{\partial^2 F^a{}_A}{dt^2} = \left(\frac{\partial}{\partial x^d}\left(\mathscr{L}_{\boldsymbol{\phi}} v^a\right) + R^a{}_{bdc} v^b v^c\right) F^d{}_A, \tag{5.4.9}$$

with the non-autonomous Lie derivative of velocity given by $\mathscr{L}_{\boldsymbol{\phi}} v^a = \dfrac{\partial v^a}{\partial t} + v^b \dfrac{\partial v^a}{\partial x^b}$.

Proof. Take the material time derivative of relation $D\mathbf{F}/dt = \mathbf{l}\mathbf{F}$ from the Proposition 4.3.1 by,

$$\frac{D^2\mathbf{F}}{dt^2} = \frac{D\mathbf{l}}{dt}\mathbf{F} + \mathbf{l}\frac{D\mathbf{F}}{dt} = \left(\frac{D\mathbf{l}}{dt} + \mathbf{l}^2\right)\mathbf{F}.$$

Substituting $D\mathbf{l}/dt$ from Lemma 5.4.2 concludes (5.4.8). Without loss of generality, assume the connection is torsion-free, i.e., $\mathrm{tor} = \mathbf{0}$. Hence, the relation (5.4.8) in the local frame $\boldsymbol{e}_a \otimes \boldsymbol{E}^{*A}$ is

$$\frac{D^2 F^a{}_A}{dt^2} = \left(a^a{}_{|d} + R^a{}_{bdc} v^b v^c\right) F^d{}_A. \tag{5.4.10a}$$

With abuse of notation, $D^2F^a{}_A/dt^2$ in above denotes the component of the tensor $D^2\mathbf{F}/dt^2 = (D^2F^a{}_A/dt^2)\boldsymbol{e}_a \otimes \boldsymbol{E}^{*A}$. By taking the material derivation of (4.3.3) and a straightforward simplification we obtain

$$\begin{aligned}\frac{D^2 F^a{}_A}{dt^2} = \frac{\partial^2 F^a{}_A}{\partial t^2} \\ + \left(\frac{\partial v^b}{\partial t}\gamma^a{}_{bd} + \frac{\partial v^c}{\partial x^d}\gamma^a{}_{bc} v^d + \frac{\partial \gamma^a{}_{bd}}{\partial x^c} v^b v^c + \gamma^a{}_{bd}\frac{\partial v^b}{\partial x^c} v^c + \frac{\partial v^k}{\partial x^d}\gamma^a{}_{ck} v^c + \gamma^k{}_{bd}\gamma^a{}_{ck} v^b v^c\right) F^d{}_A.\end{aligned}$$

Also, $a^a{}_{|d}$ is the component of $\nabla \boldsymbol{a} = a^a{}_{|d}\boldsymbol{e}_a \otimes \boldsymbol{e}^{*d}$. Recall that the component of the acceleration $\boldsymbol{a} = a^a \boldsymbol{e}_a$ is given by

$$a^a = \frac{Dv^a}{dt} = \frac{\partial v^a}{\partial t} + \frac{\partial v^a}{\partial x^b} v^b + \gamma^a{}_{bc} v^b v^c.$$

Thus, by taking the covariant derivative of $\boldsymbol{a}$, the component $a^a{}_{|d}$ is obtained as

$$\begin{aligned} a^a{}_{|d} = \frac{\partial^2 v^a}{\partial t \partial x^d} + \frac{\partial^2 v^a}{\partial x^b \partial x^d} v^b + \frac{\partial v^a}{\partial x^b}\frac{\partial v^b}{\partial x^d} + \frac{\partial \gamma^a{}_{bc}}{\partial x^d} v^b v^c + \gamma^a{}_{bc}\frac{\partial v^b}{\partial x^d} v^c \\ + \gamma^a{}_{bc} v^b \frac{\partial v^c}{\partial x^d} + \frac{\partial v^b}{\partial t}\gamma^a{}_{db} + \frac{\partial v^c}{\partial x^b} v^b \gamma^a{}_{dc} + \gamma^k{}_{bc}\gamma^a{}_{dk} v^b v^c. \end{aligned} \tag{5.4.10b}$$

Putting together three equations (5.4.10) and considering the symmetry of Christoffel symbols, we get(remind the reader that we chose a torsion-free connection)

$$\frac{\partial^2 F^a{}_A}{\partial t^2} = \left(\frac{\partial}{\partial x^d} \underbrace{\left(\frac{\partial v^a}{\partial t} + v^b \frac{\partial v^a}{\partial v^b} \right)}_{\mathscr{L}_{\boldsymbol{\phi}} v^a} + \underbrace{\left(\frac{\partial \gamma^a{}_{dc}}{\partial x^b} - \frac{\partial \gamma^a{}_{bc}}{\partial x^d} + \gamma^a{}_{bk}\gamma^k{}_{dc} - \gamma^a{}_{dk}\gamma^k{}_{bc} \right)}_{R^a{}_{cbd}} v^b v^c \right) F^d{}_A.$$

Realizing the group of terms in the parentheses shown above is the Lie derivative and curvature (see (5.2.2)) concludes the proof. ■

The equation (5.4.9) is independent of the connection on the vector bundle, hence, it is intrinsic. Similar to the previous theorem, the second rate of left and right deformation tensors $\mathbf{b}$ and $\mathbf{C}$ and their associated tensors follow immediately. Again, we will assume the connection ∇ is arbitrary. We recall that if a metric connection is desired, one can simply set $\nabla_v \mathbf{g} = \mathbf{0}$ in the following developments.

Corollary 5.4.4 (Second material rate of the left deformation tensor). *Suppose the diffeomorphism $\boldsymbol{\phi} \in C^2(\mathscr{P}_{t_0} \times \mathscr{I}; \mathscr{P}_t)$ is the flow on a manifold with the curvature tensor $\mathbf{R}$. Then, the second material rate of the left deformation tensor, $\mathbf{b}$, is given by an arbitrary connection ∇ on the tangent bundle as*

$$\frac{D^2\mathbf{b}}{dt^2} = \left(\mathbf{k}\mathbf{b} + \mathbf{b}\mathbf{k}^\intercal\right) + 2\mathbf{l}\mathbf{b}\mathbf{l}^\intercal + 2\left(\mathbf{l}\mathbf{b} + \mathbf{b}\mathbf{l}^\intercal\right)\mathbf{g}^{-1}\nabla_v \mathbf{g} + \mathbf{b}\mathbf{g}^{-1}\nabla_v\left(\nabla_v \mathbf{g}\right). \tag{5.4.11a}$$

Also, the second rate of the associated tensor $\mathbf{b}^\sharp$ is

$$\frac{D^2\mathbf{b}^\sharp}{dt^2} = \mathbf{k}\mathbf{b}^\sharp + \mathbf{b}^\sharp\mathbf{k}^* + 2\mathbf{k}\mathbf{b}^\sharp\mathbf{k}^*. \tag{5.4.11b}$$

Proof. Recall that the material rate of metric tensor $\mathbf{g}(\boldsymbol{x})$ is $D\mathbf{g}/dt = \nabla_v \mathbf{g}$ and $D(\mathbf{g}^{-1})/dt = -\mathbf{g}^{-1}(\nabla_v \mathbf{g})\mathbf{g}^{-1}$. Similarly, its second derivative becomes $D(\nabla_v \mathbf{g})/dt = \nabla_v\left(\nabla_v \mathbf{g}\right)$. Also, in

Lemma 5.4.2 we have shown $D\mathbf{l}/dt = \mathbf{k} - \mathbf{l}^2$. The material rate of its transpose, $\mathbf{l}^\top$, is obtained from the Proposition 4.5.2 as

$$\begin{aligned}\frac{D(\mathbf{l}^\top)}{dt} = \frac{D}{dt}\left(\mathbf{g}^{-1}\mathbf{l}^*\mathbf{g}\right) &= \frac{D(\mathbf{g}^{-1})}{dt}\mathbf{l}^*\mathbf{g} + \mathbf{g}^{-1}\frac{D\mathbf{l}}{dt}\mathbf{g} + \mathbf{g}^{-1}\mathbf{l}^*\frac{D\mathbf{g}}{dt} \\ &= \mathbf{l}^\top(\mathbf{g}^{-1}\nabla_v\mathbf{g}) - (\mathbf{g}^{-1}\nabla_v\mathbf{g})\mathbf{l}^\top + \mathbf{k}^\top - (\mathbf{l}^\top)^2, \end{aligned} \tag{5.4.12}$$

where we have used $\mathbf{k}^\top = \mathbf{g}^{-1}\mathbf{k}^*\mathbf{g}$ and the adjoint tensor $D\mathbf{l}^*/dt = (D\mathbf{l}/dt)^* = \mathbf{k}^* - (\mathbf{l}^*)^2$. Take the material time derivative of $D\mathbf{b}/dt$ given by Corollary 4.7.2 as,

$$\frac{D^2\mathbf{b}}{dt^2} = \frac{D\mathbf{l}}{dt}\mathbf{b} + \mathbf{l}\frac{D\mathbf{b}}{dt} + \frac{D\mathbf{b}}{dt}\mathbf{l}^\top + \mathbf{b}\frac{D(\mathbf{l}^\top)}{dt} + \frac{D\mathbf{b}}{dt}\mathbf{g}^{-1}\nabla_v\mathbf{g} + \mathbf{b}\frac{D(\mathbf{g}^{-1})}{dt}\nabla_v\mathbf{g} + \mathbf{b}\mathbf{g}^{-1}\frac{D(\nabla_v\mathbf{g})}{dt},$$

and substitute all the above relations simplifies to (5.4.11a). Also, taking the second derivative of $\mathbf{b}^\sharp = \mathbf{F}\mathbf{G}^{-1}\mathbf{F}^*$ yields (5.4.11b). ■

Corollary 5.4.5 (Second material rate of the right deformation tensor). *Suppose the diffeomorphism $\boldsymbol{\phi} \in C^2(\mathscr{P}_{t_0}\times\mathscr{I};\mathscr{P}_t)$ is the flow map on a manifold with the curvature tensor $\mathbf{R}$. Then, the second material rate of the right deformation tensor, $\mathbf{C}$, is given by an arbitrary connection ∇ on the tangent bundle as*

$$\frac{D^2\mathbf{C}}{dt^2} = \mathbf{F}^\top\Big(\mathbf{k} + \mathbf{k}^\top + 2\mathbf{l}^\top\mathbf{l} + 2\mathbf{l}^\top(\mathbf{g}^{-1}\nabla_v\mathbf{g}) + 2(\mathbf{g}^{-1}\nabla_v\mathbf{g})\mathbf{l}\Big)\mathbf{F}. \tag{5.4.13a}$$

Also, the second derivative of the associated tensor $\mathbf{C}^\flat$ is

$$\frac{D^2\mathbf{C}^\flat}{dt^2} = \mathbf{F}^*\Big(\mathbf{k}^*\mathbf{g} + \mathbf{g}\mathbf{k} + 2\mathbf{l}^*\mathbf{g}\mathbf{l} + 2\mathbf{l}^*(\nabla_v\mathbf{g}) + 2(\nabla_v\mathbf{g})\mathbf{l}\Big)\mathbf{F}. \tag{5.4.13b}$$

Proof. The procedure is straightforward, and we omit the details. In brief, we take the material time derivative of $D\mathbf{C}/dt$ given by Corollary 4.9.3, substitute terms from the proof of Corollary 5.4.4 and simplify to obtain (5.4.13a). Also, taking the second derivative of $\mathbf{C}^\flat = \mathbf{F}^*\mathbf{g}\mathbf{F}$ yields (5.4.13b). ■

Remark 5.4.6 (Higher-order rates). In Euclidean space, relations (5.4.11b) and (5.4.13b) can be simply generalized to higher-order rates by means of ***Rivlin-Ericksen tensors*** (see e.g., [Truesdell and Noll, 2004, C.II §24] or [Truesdell, 1992, p. 123]). To do so, the Rivlin-Ericksen tensor $\mathbf{A}_m$ is defined by the recursion relation $\mathbf{A}_{m+1} := \dot{\mathbf{A}}_m + \mathbf{A}_m\mathbf{l} + \mathbf{l}^\top\mathbf{A}_m$, where $\mathbf{A}_1 = 2\mathbf{d}$. Then, the higher-order material rates are given by $D^m\mathbf{C}/dt^m = \mathbf{F}^\top\mathbf{A}_m\mathbf{F}$. On a non-flat manifold, however, such a generalization requires the utilization of higher-order tensors beyond the Riemannian curvature. ▲

5.5 Geodesic Flows and Jacobi Fields

Geodesic flows

A flow $\boldsymbol{\phi} \in C^2(\mathscr{P}_{t_0} \times \mathscr{I}; \mathscr{P}_t)$ is ***geodesic*** if its spatial acceleration identically vanishes along the flow, i.e.,

$$\boldsymbol{a}(\boldsymbol{\phi}_t(\boldsymbol{X}), t) = \frac{D\boldsymbol{v}}{dt} = \boldsymbol{0}, \quad \forall t \in \mathscr{I}. \tag{5.5.1}$$

In other words, the velocity $\boldsymbol{v}$ is parallel transported along the flow. For an autonomous vector field, the above geodesic condition reduces to $\nabla_{\boldsymbol{v}}\boldsymbol{v} = \boldsymbol{0}$.

Remark 5.5.1 (Non-intrinsicness of acceleration, and well-posedness of geodesic flows). Unlike the velocity vector $\boldsymbol{v}$, the acceleration vector $\boldsymbol{a}$ is not intrinsically defined on the manifold, meaning that it is not unique (see e.g., [do Carmo, 1992, Ch. 2, §1]). The non-uniqueness of the acceleration vector rely on the choice of linear projection applied to the derivative of velocity since the derivative of a tangent vector (such as $\boldsymbol{v}$) does not belong to the tangent bundle of the manifold. Such projection on the tangent bundle is embodied within the connection ∇ of the tangent bundle $T\mathscr{P}_t$.

However, the ***zero section*** of a vector bundle (here, $\mathbf{a} = \boldsymbol{0}$) is always well-defined and independent of the connection. Hence, geodesic flows are intrinsic, i.e., independent of the connection ∇. ▲

The material time derivative of (5.5.1) can be expressed in terms of the flow $\boldsymbol{\phi}$, yielding the *Euler-Lagrange* equations of the motion as

$$\frac{d^2\phi^a}{dt^2} + \frac{d\phi^b}{dt}\frac{d\phi^c}{dt}\gamma^a{}_{bc} = 0, \quad \text{with} \quad \begin{cases} \boldsymbol{\phi}(t_0) = \boldsymbol{X}, \\ \left.\dfrac{d\boldsymbol{\phi}}{dt}\right|_{t_0} = \boldsymbol{v}(\boldsymbol{X}, t_0). \end{cases}$$

The above set of equations is coupled second-order nonlinear ordinary differential equations. The existence and uniqueness of the *local* solution to the above differential equations is insured by the Picard-Lindelöf theorem of the regularity theory of ODEs. In contrast, the existence and uniqueness of the *global* solution (i.e., solution exists for all times) are less trivial. If a global solution exists, it is also unique and smooth [Petersen, 2006, Ch. 5, Lemma 7]. The compactness of the manifold $\mathscr{P}_t$ implies the geodesic solution is global [Petersen, 2006, Ch. 5, Lemma 8], which then $\mathscr{P}_t$ is known as *geodesically complete*. Conversely, a geodesically complete manifold implies compactness, which is known from the Hopf-Rinow theorem [do Carmo, 1992, Ch. 7, Theorem 2.8].

In correspondence with geometric mechanics, a force-free motion is geodesic, in which the body follows a straight trajectory in the view of the manifold. A tangible example is the motion of heavenly bodies in the presence of gravitational fields. The classical school of

thought regards such motion by the Newtonian's gravitational force. Whereas, by the *general theory of relativity* of Einstein [1915], the motion is viewed as force-free, but the body follows a geodesic trajectory in the curved 4-manifold of space-time, where the curvature is originated by the presence of the gravitational field.

Jacobi Fields and dexp Map

Our motivation to consider geodesic flows is to better interpret the second-order material rates derived in the previous section. In particular, the assumption $\boldsymbol{a} = \mathbf{0}$ simplifies equations, and the second rate of deformation is understood by the sole effect of curvature $\mathbf{R}$. For the sake of convenience, in this section, we use Levi-Civita connection. Using $\nabla \boldsymbol{a} = \mathbf{0}$ and tor $= \mathbf{0}$, the statement of Theorem 5.4.3 becomes

$$\frac{D^2\mathbf{F}}{dt^2} = \mathbf{R}(\boldsymbol{v}, \cdot)\boldsymbol{v}\mathbf{F}. \tag{5.5.2}$$

Let $\boldsymbol{J} \in T_{\boldsymbol{X}}\mathscr{P}_{t_0}$ be a referential tangent vector, with its pushforward $\boldsymbol{j} \in T_{\boldsymbol{\phi}_t(\boldsymbol{X})}\mathscr{P}_t$ given by $\boldsymbol{j} = \boldsymbol{\phi}_* \boldsymbol{J} = \mathbf{F}\boldsymbol{J}$. Equation (5.5.2) contracted by $\boldsymbol{J}$ becomes

$$\frac{D^2\boldsymbol{j}}{dt^2} = \mathbf{R}(\boldsymbol{v}, \boldsymbol{j})\boldsymbol{v}, \qquad \text{with} \quad \begin{cases} \boldsymbol{j}(t_0) = \boldsymbol{J}(\boldsymbol{X}), \\ \left.\frac{D\boldsymbol{j}}{dt}\right|_{t_0} = \dot{\boldsymbol{J}}(\boldsymbol{X}), \end{cases} \tag{5.5.3}$$

where $\dot{\boldsymbol{J}} \in T_{\boldsymbol{J}}\left(T_{\boldsymbol{X}}\mathscr{P}_{t_0}\right)$. The above relation is indeed the familiar ***Jacobi equation*** and the vector field $\boldsymbol{j}$ is the ***Jacobi field*** along geodesics $\boldsymbol{\phi}_t(\boldsymbol{X})$. Solutions of the above set of second-order ODEs exist uniquely as $2n$ independent vector fields $\boldsymbol{j}_a(t) \in T_{\boldsymbol{x}}(\mathscr{P}_t)$ and $\dot{\boldsymbol{j}}_a(t) \in T_{\boldsymbol{j}}\left(T_{\boldsymbol{x}}\mathscr{P}_t\right)$, $a = 1, \ldots, n$. Each of n independent solutions of $\boldsymbol{j}_a(t)$ and $\dot{\boldsymbol{j}}_a(t)$ respectively form a local frame on the tangent bundle and the second tangent bundle along the geodesic.

As an example, the vector field $\boldsymbol{j}(t) \coloneqq (\alpha_1 + \alpha_2 t)\boldsymbol{v}(t)$ is a Jacobi field parallel to the geodesic trajectory. It is possible to decompose a solution $\boldsymbol{j}(t) = \boldsymbol{j}_\perp(t) + \boldsymbol{j}_{||}(t)$, where $\boldsymbol{j}_\perp(t)$ always stay orthogonal to the geodesic (see [do Carmo, 1992, p. 118]).

From another point of view, the Jacobi fields can be interpreted as the perturbation vector field along geodesics. Using the normal neighborhood Lemma, a geodesic curve originating from a point $\boldsymbol{X}$ and in the direction of the velocity vector $\boldsymbol{v}$ is given by the exponential map $\exp : T_{\boldsymbol{X}}\mathscr{P}_{t_0} \to \mathscr{P}$ as

$$\boldsymbol{\phi}_t(\boldsymbol{X}) = \exp_{\boldsymbol{X}}(t\boldsymbol{v}).$$

The Jacobi fields are represented by the derivative of the exponential map, $d\exp : T\left(T_{\boldsymbol{X}}\mathscr{P}_{t_0}\right) \to T\mathscr{P}_t$ as (see [do Carmo, 1992, p. 114])

$$\boldsymbol{j}(t) = \left(d\exp_{\boldsymbol{X}}\right)_{t\boldsymbol{v}}\left(t\dot{\boldsymbol{J}}\right).$$

Chapter 6

Transformations under Isometric Isomorphisms

6.1 Introduction

A later goal in chapter 7 is to derive evolution equations for the spectral decomposition of deformation, namely for its eigenvalues and eigenvectors. To this end, we transform the referential and spatial coordinate charts such that the matrix of the deformation gradient tensor is diagonalized. This is achieved by the isometric transformation of local charts on both referential and spatial manifolds. In this chapter, we define general time-dependent isometric isomorphisms on referential and spatial manifolds, and we present the evolution equations on these transformed manifolds. Our formulation is effectively analogous to the singular value decomposition of matrices, but here they are given for the tangent map between the tangent spaces of two Riemannian manifolds.

The isometric isomorphisms on the Riemannian manifolds are analogous to solid rotations in Euclidean space, hence, similar concepts therein apply. For instance, associated with the group of *rotator tensors*, we can define the *spinor tensors* that represent the rate of rotation analogous to the angular velocity. In Euclidean space, spinors are skew-symmetric matrices on the Lie algebra of the rotation group. Recall that in tensorial form, the (skew) symmetry is understood for the transposition with respect to the Riemannian metrics. We will show that only on the referential manifold, the spinors of the isometric isomorphisms are skew-symmetric tensors. In contrast, we found the spinors on the spatial manifold are not necessarily skew-symmetric. Rather, the skew-symmetry is achieved when the Riemannian metric is *parallel* with respect to the connection on the tensor bundle.

6.2 Riemannian Isometry

Let the points $\hat{\boldsymbol{X}} \in \hat{\mathscr{P}}_{t_0}$ and $\hat{\boldsymbol{x}} \in \hat{\mathscr{P}}_t$ be the transformation of the points $\boldsymbol{X} \in \mathscr{P}_{t_0}$ and $\boldsymbol{x} \in \mathscr{P}_t$ respectively by the time-dependent maps

$$\boldsymbol{\Psi} : \left(\hat{\mathscr{P}}_{t_0}, \hat{\mathbf{G}}\right) \to \left(\mathscr{P}_{t_0}, \mathbf{G}\right), \qquad \boldsymbol{X} = \boldsymbol{\Psi}(\hat{\boldsymbol{X}}, t), \tag{6.2.1a}$$

$$\boldsymbol{\psi} : \left(\hat{\mathscr{P}}_t, \hat{\mathbf{g}}\right) \to \left(\mathscr{P}_t, \mathbf{g}\right), \qquad \boldsymbol{x} = \boldsymbol{\psi}(\hat{\boldsymbol{x}}, t). \tag{6.2.1b}$$

The transformed sets and variables are denoted by the hat $\hat{}$ symbol. We assume that the transformations are C^1 ***Riemannian isometric isomorphisms***[1], hence, due to the inverse function theorem they admit inverse.[2]

Define the tangent maps of isometries $\boldsymbol{\Psi}$ and $\boldsymbol{\psi}$ and their presentation in local chart $\{X^A\}$ and $\{x^a\}$ by

$$\mathbf{U} \coloneqq T\boldsymbol{\Psi} : T\hat{\mathscr{P}}_{t_0} \to T\mathscr{P}_{t_0}, \qquad \mathbf{U} = \left(\frac{\partial X^A}{\partial \hat{X}^B}\right) \boldsymbol{E}_A \otimes \hat{\boldsymbol{E}}^{*B}, \tag{6.2.2a}$$

$$\mathbf{u} \coloneqq T\boldsymbol{\psi} : T\hat{\mathscr{P}}_t \to T\mathscr{P}_t, \qquad \mathbf{u} = \left(\frac{\partial x^a}{\partial \hat{x}^b}\right) \boldsymbol{e}_a \otimes \hat{\boldsymbol{e}}^{*b}. \tag{6.2.2b}$$

Remark 6.2.1 (Tangent and cotangent maps of the transformations). The tangent map $\mathbf{U} = U^A{}_B \boldsymbol{E}_A \otimes \hat{\boldsymbol{E}}^{*B}$ has the inverse, the adjoint (cotangent map) and the adjoint inverse by

$$\begin{aligned}
&\mathbf{U}^{-1} = T\boldsymbol{\Psi}^{-1} : T\mathscr{P}_{t_0} \to T\hat{\mathscr{P}}_{t_0}, && \mathbf{U}^{-1} = (U^{-1})^A{}_B \hat{\boldsymbol{E}}_A \otimes \boldsymbol{E}^{*B},\\
&\mathbf{U}^* = T^*\boldsymbol{\Psi} : T^*\mathscr{P}_{t_0} \to T^*\hat{\mathscr{P}}_{t_0}, && \mathbf{U}^* = U^A{}_B \hat{\boldsymbol{E}}^{*B} \otimes \boldsymbol{E}_A,\\
&\mathbf{U}^{-*} = T^*\boldsymbol{\Psi}^{-1} : T^*\hat{\mathscr{P}}_{t_0} \to T^*\mathscr{P}_{t_0}, && \mathbf{U}^{-*} = (U^{-1})^A{}_B \boldsymbol{E}^{*B} \otimes \hat{\boldsymbol{E}}_A.
\end{aligned}$$

Recall that $T^*\boldsymbol{\Psi} = (T\boldsymbol{\Psi})^*$, which means the cotangent map $T^*\boldsymbol{\Psi}$ is the adjoint of the tangent map $T\boldsymbol{\Psi}$. The adjoint map is obtained by swapping the order of tensor bases. Also, $\mathbf{U}^{-*} \coloneqq (\mathbf{U}^*)^{-1}$ is the inverse of the adjoint tensor.

Similarly, the tangent map $\mathbf{u} = u^a{}_b \boldsymbol{e}_a \otimes \hat{\boldsymbol{e}}^{*b}$ has the inverse, the adjoint (cotangent map) and the adjoint inverse by

$$\begin{aligned}
&\mathbf{u}^{-1} = T\boldsymbol{\psi}^{-1} : T\mathscr{P}_t \to T\hat{\mathscr{P}}_t, && \mathbf{u}^{-1} = (u^{-1})^a{}_b \hat{\boldsymbol{e}}_a \otimes \boldsymbol{e}^{*b},\\
&\mathbf{u}^* = T^*\boldsymbol{\psi} : T^*\mathscr{P}_t \to T^*\hat{\mathscr{P}}_t, && \mathbf{u}^* = u^a{}_b \hat{\boldsymbol{e}}^{*b} \otimes \boldsymbol{e}_a,\\
&\mathbf{u}^{-*} = T^{-*}\boldsymbol{\psi} : T^*\hat{\mathscr{P}}_t \to T^*\mathscr{P}_t, && \mathbf{u}^{-*} = (u^{-1})^a{}_b \boldsymbol{e}^{*b} \otimes \hat{\boldsymbol{e}}_a.
\end{aligned}$$

▲

[1] We only need the *self*-isometries $\boldsymbol{\Psi} \in \mathrm{Isom}\left(\mathscr{P}_{t_0}, \mathbf{G}\right)$ and $\boldsymbol{\psi} \in \mathrm{Isom}\left(\mathscr{P}_t, \mathbf{g}\right)$. But for convenience, we distinguish between the two manifolds $\mathscr{P}_{t_0}$ and $\hat{\mathscr{P}}_{t_0}$, as well as $\mathscr{P}_t$ and $\hat{\mathscr{P}}_t$.

[2] Since for an isomorphism, the Jacobian determinant is non-zero, i.e., $|\partial\boldsymbol{\Psi}/\partial\hat{\boldsymbol{X}}| \neq 0$ and $|\partial\boldsymbol{\psi}/\partial\hat{\boldsymbol{x}}| \neq 0$.

Remark 6.2.2 (Transformation of the bases). By the maps $\boldsymbol{\Psi}$ and $\boldsymbol{\psi}$, the tangent vectors $\boldsymbol{e}_a$ and the cotangent covectors $\boldsymbol{E}^{*A}$ transform according to

$$\boldsymbol{E}^{*A} = \frac{\partial X^A}{\partial \hat{X}^B}\hat{\boldsymbol{E}}^{*B} = U^A{}_B\hat{\boldsymbol{E}}^{*B}, \qquad \text{(contravariant)} \tag{6.2.3a}$$

$$\boldsymbol{e}_a = \frac{\partial \hat{x}^b}{\partial x^a}\hat{\boldsymbol{e}}_b = (u^{-1})^b{}_a\hat{\boldsymbol{e}}_b. \qquad \text{(covariant)} \tag{6.2.3b}$$

▲

The *Riemannian isometry* of the maps $\boldsymbol{\Psi}$ and $\boldsymbol{\psi}$ implies that

$$\hat{\mathbf{G}}(\boldsymbol{X}, t) = \boldsymbol{\Psi}^*\mathbf{G}(\boldsymbol{X}) = \mathbf{U}^*\mathbf{G}\mathbf{U}, \tag{6.2.4a}$$

$$\hat{\mathbf{g}}(\boldsymbol{x}, t) = \boldsymbol{\psi}^*\mathbf{g}(\boldsymbol{x}) = \mathbf{u}^*\mathbf{g}\mathbf{u}, \tag{6.2.4b}$$

where $\mathbf{U}^* = T^*\boldsymbol{\psi}$ and $\mathbf{u}^* = T^*\boldsymbol{\psi}$ are the cotangent maps. The transpositions of the tensors $\mathbf{U}$ and $\mathbf{u}$ are

$$\mathbf{U}^\intercal = \hat{\mathbf{G}}^{-1}\mathbf{U}^*\mathbf{G}, \tag{6.2.5a}$$

$$\mathbf{u}^\intercal = \hat{\mathbf{g}}^{-1}\mathbf{u}^*\mathbf{g}. \tag{6.2.5b}$$

The above transpositions are compatible with the metrics. To observe this on the spatial manifold $\mathscr{P}_t$, consider the tangent vectors $\boldsymbol{z} \in T_{\boldsymbol{x}}\mathscr{P}_t$ and $\hat{\boldsymbol{z}} \in T_{\hat{\boldsymbol{x}}}\hat{\mathscr{P}}_t$ where $\boldsymbol{x} = \boldsymbol{\psi}(\hat{\boldsymbol{x}}, t)$ and $\boldsymbol{z} = \boldsymbol{\psi}_*\hat{\boldsymbol{z}} = \mathbf{u}\hat{\boldsymbol{z}}$. Then, it can be simply verified that the equation (6.2.5b) satisfies $\mathbf{g}_{\boldsymbol{x}}(\boldsymbol{z}, \mathbf{u}\hat{\boldsymbol{z}}) = \hat{\mathbf{g}}_{\hat{\boldsymbol{x}}}\left(\mathbf{u}^\intercal\boldsymbol{z}, \hat{\boldsymbol{z}}\right)$. The same argument can be made for $\mathbf{u}^\intercal$ in the equation (6.2.5a) on the referential manifold $\mathscr{P}_{t_0}$.

By combining the pullback metrics in (6.2.4) with the transpositions in (6.2.5) we obtain

$$\mathbf{U}^\intercal = \mathbf{U}^{-1}, \tag{6.2.6a}$$

$$\mathbf{u}^\intercal = \mathbf{u}^{-1}. \tag{6.2.6b}$$

The above relations imply that the matrices of isometry maps are *unitary* and belong to the *special orthogonal Lie group*, i.e., $U, u \in \mathrm{SO}(n)$, which is expected from *Myers–Steenrod's second theorem* for isometry maps [Myers and Steenrod, 1939]. We refer to the tangent maps $\mathbf{U}$ and $\mathbf{u}$ as *rotator tensors* on the tangent spaces of the referential and spatial manifolds respectively.

6.3 Transformation of Flow under Riemannian Isometry

At the moment, we assume the transformations $\boldsymbol{\Psi}$ and $\boldsymbol{\psi}$ are arbitrary isometric isomorphisms, but later we will obtain them specifically. Let $\hat{\boldsymbol{\phi}} \coloneqq \boldsymbol{\psi}^{-1} \circ \boldsymbol{\phi} \circ \boldsymbol{\Psi} : \hat{\mathscr{P}}_{t_0} \to \hat{\mathscr{P}}_t$ indicate the flow

between the two transformed manifolds. The commutative diagram

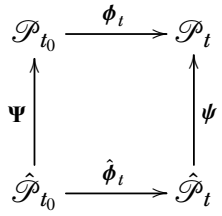

illustrates the transformation of the flow under isomorphisms. We denote the tangent map on the transformed manifolds by $\hat{\mathbf{F}} : T\hat{\mathscr{P}}_{t_0} \to T\hat{\mathscr{P}}_t$, and given by the composition

$$\hat{\mathbf{F}} \coloneqq \mathbf{u}^{\mathsf{T}}\mathbf{F}\mathbf{U}, \tag{6.3.1}$$

where we used $T\boldsymbol{\psi}^{-1} = \mathbf{u}^{-1} = \mathbf{u}^{\mathsf{T}}$.

The commutative diagram in Figure 6.3.1 incorporates the relations in 2.3.6 and 2.4.6, and extends (out of the page) these relations to the transformed spaces using the mappings defined in this section. In particular, we can observe the relations defining the *tensorial composition* (6.3.1).

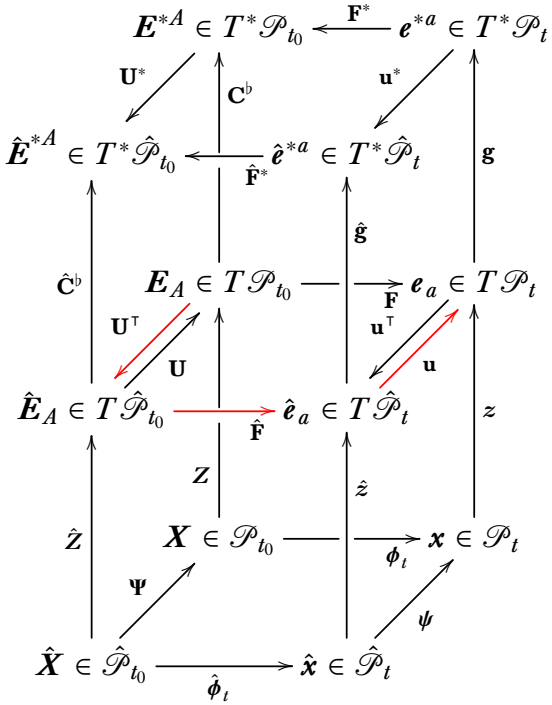

Figure 6.3.1: Commutative diagram for the tensorial decomposition of the deformation gradient tensor, i.e., $\mathbf{F} = \mathbf{u}\hat{\mathbf{F}}\mathbf{U}^{\mathsf{T}}$ (shown by the red arrows).

Definition 6.3.1 (Transformed Euler-Cauchy-Stokes decomposition). *The spatial isometry $\boldsymbol{\psi}$ induces the **transformed spatial rate of deformation tensor** with the endomorphism*

$$\hat{\mathbf{l}} \in \Gamma\left(\mathrm{End}\left(T\hat{\mathscr{P}}_t\right)\right), \qquad \hat{\mathbf{l}} \coloneqq \boldsymbol{\psi}^*\mathbf{l} = \mathbf{u}^\intercal \mathbf{l}\mathbf{u}. \tag{6.3.2a}$$

*Similarly, the **transformed spatial rate of deformation** and the **transformed spin** tensors are defined by*

$$\hat{\mathbf{d}} \in \Gamma\left(\mathrm{End}\left(T\mathscr{P}_t\right)\right), \qquad \hat{\mathbf{d}} \coloneqq \boldsymbol{\psi}^*\mathbf{d} = \mathbf{u}^\intercal \mathbf{d}\mathbf{u}, \tag{6.3.2b}$$

$$\hat{\boldsymbol{\omega}} \in \Gamma\left(\mathrm{End}\left(T\mathscr{P}_t\right)\right), \qquad \hat{\boldsymbol{\omega}} \coloneqq \boldsymbol{\psi}^*\boldsymbol{\omega} = \mathbf{u}^\intercal \boldsymbol{\omega}\mathbf{u}. \tag{6.3.2c}$$

The above definitions retrieve the Euler-Cauchy-Stokes decomposition $\hat{\mathbf{l}} = \hat{\mathbf{d}} + \hat{\boldsymbol{\omega}}$ on the transformed spatial manifold. The following diagram commutes.

$$\begin{array}{ccc} T\mathscr{P}_t & \xrightarrow{\mathbf{l},\mathbf{d},\boldsymbol{\omega}} & T\mathscr{P}_t \\ {\scriptstyle \mathbf{u}^\intercal=\mathbf{u}^{-1}}\downarrow\uparrow{\scriptstyle \mathbf{u}} & & {\scriptstyle \mathbf{u}^\intercal=\mathbf{u}^{-1}}\downarrow\uparrow{\scriptstyle \mathbf{u}} \\ T\hat{\mathscr{P}}_t & \xrightarrow[\hat{\mathbf{l}},\hat{\mathbf{d}},\hat{\boldsymbol{\omega}}]{} & T\hat{\mathscr{P}}_t \end{array}$$

▲

6.4 Angular Velocities of Isometric Isomorphisms

Since the transformations $\boldsymbol{\psi}$ and $\boldsymbol{\Psi}$ are time-dependent, we define the time rate of their tangent maps, i.e., the tensors $\mathbf{u}$ and $\mathbf{U}$.

Definition 6.4.1 (Angular velocity tensors). *We define the **referential dynamic angular velocity tensor** $\mathbf{W}$ and the **spatial angular velocity tensor** $\mathbf{w}$ respectively by*[3]

$$\mathbf{W} \in \Gamma\left(\mathrm{End}\left(T\mathscr{P}_{t_0}\right)\right), \qquad \mathbf{W} \coloneqq \boldsymbol{\Psi}_{*^2}\left(\frac{D\mathbf{U}}{dt}\right) = \frac{D\mathbf{U}}{dt}\mathbf{U}^\intercal, \tag{6.4.1a}$$

$$\mathbf{w} \in \Gamma\left(\mathrm{End}\left(T\mathscr{P}_t\right)\right), \qquad \mathbf{w} \coloneqq \boldsymbol{\psi}_{*^2}\left(\frac{D\mathbf{u}}{dt}\right) = \frac{D\mathbf{u}}{dt}\mathbf{u}^\intercal. \tag{6.4.1b}$$

Also, it will be useful to define the conjugate of the tensors $\mathbf{W}$ and $\mathbf{w}$ respectively by

$$\hat{\mathbf{W}} \in \Gamma\left(\mathrm{End}\left(T\hat{\mathscr{P}}_{t_0}\right)\right), \qquad \hat{\mathbf{W}} \coloneqq \boldsymbol{\Psi}^*\mathbf{W} = \mathbf{U}^\intercal\mathbf{W}\mathbf{U} = \mathbf{U}^\intercal\frac{D\mathbf{U}}{dt} = \boldsymbol{\Psi}^{*_1}\left(\frac{D\mathbf{U}}{dt}\right), \tag{6.4.1c}$$

$$\hat{\mathbf{w}} \in \Gamma\left(\mathrm{End}\left(T\hat{\mathscr{P}}_t\right)\right), \qquad \hat{\mathbf{w}} \coloneqq \boldsymbol{\psi}^*\mathbf{w} = \mathbf{u}^\intercal\mathbf{w}\mathbf{u} = \mathbf{u}^\intercal\frac{D\mathbf{u}}{dt} = \boldsymbol{\psi}^{*_1}\left(\frac{D\mathbf{u}}{dt}\right). \tag{6.4.1d}$$

▲

[3] We recall that $\boldsymbol{\Psi}^{*_i}$ and $\boldsymbol{\Psi}_{*^i}$ are the pullback and pushforward operations on the i-th component of the basis of a two-point tensor.

The relation between angular velocities and their pullbacks are summarized in the following commutative diagram.

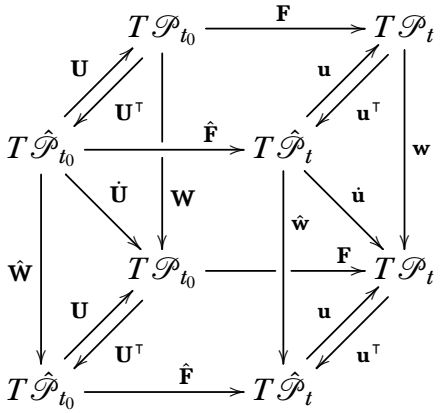

(6.4.2)

Also, note that the definition of $\mathbf{W}$ and $\mathbf{w}$ depend on the connection. For instance, from (6.4.1b) in the local chart $\{x^a\}$,

$$\mathbf{w} = \left(\left(\frac{\partial u^a_c}{\partial t} + \frac{\partial u^a_c}{\partial x^k} v^k \right) \left(u^{-1}\right)^c_b + \left(\gamma^a{}_{kb} - u^a_c \gamma^c{}_{kd} u^d_b \right) v^k \right) \boldsymbol{e}_a \otimes \boldsymbol{e}^{*b}.$$

In Euclidean space, the angular velocity tensors are skew-symmetric. However, on a general Riemannian manifold, the angular velocity tensors are not necessarily skew-symmetric with respect to the transposition with the metric tensors. One might falsely try to demonstrate the skew-symmetry of $\mathbf{w}$ by taking the material time derivative of $\mathbf{u}\mathbf{u}^\intercal = \hat{\mathbf{i}}$ to show that $\mathbf{w} = \dfrac{D\mathbf{u}}{dt}\mathbf{u}^\intercal = -\mathbf{u}\dfrac{D\left(\mathbf{u}^\intercal\right)}{dt}$. But, taking transposition of (6.4.1b) we obtain $\mathbf{w}^\intercal = \mathbf{u}\left(\dfrac{D\mathbf{u}}{dt}\right)^\intercal$. By comparing the two latter relations, the desired equation $\mathbf{w}^\intercal = -\mathbf{w}$ yields only if $\left(\dfrac{D\mathbf{u}}{dt}\right)^\intercal = \dfrac{D\left(\mathbf{u}^\intercal\right)}{dt}$ holds. However, the transposition and the material time derivative do not commute in general. In the following two propositions we explore the conditions for which $\mathbf{w}$ and $\mathbf{W}$ become skew-symmetric tensors.

Proposition 6.4.2 (Skewness of the spatial angular velocity tensor). *Let $\boldsymbol{\psi}\colon \left(\hat{\mathscr{P}}_t, \hat{\mathbf{g}}\right) \to \left(\mathscr{P}_t, \mathbf{g}\right)$ be a time-dependent Riemannian isometric isomorphism and suppose ∇ is an arbitrary connection on $\mathscr{P}_t$. Also, let $\mathbf{u} = T\boldsymbol{\psi}$ be the tangent map and $\mathbf{w}$ the angular velocity tensor defined in equation (6.4.1b). Then,*

$$\mathbf{w}^\intercal + \mathbf{w} = \mathbf{g}^{-1}\left(\boldsymbol{\psi}_*\left(\frac{\hat{D}\left(\boldsymbol{\psi}^*\mathbf{g}\right)}{dt}\right) - \frac{D\mathbf{g}}{dt}\right), \tag{6.4.3}$$

where the material time derivative $\hat{D}/dt$ is defined based on the pullback connection $\hat{\nabla} = \boldsymbol{\psi}^*\nabla$ on the transformed tangent bundle $T\hat{\mathscr{P}}_t$.

Proof. The above equation can be obtained by relating $\mathscr{L}_{(\boldsymbol{\psi}^{-1}\circ\boldsymbol{\phi})}\hat{\mathbf{g}}$ and $\mathscr{L}_{\boldsymbol{\phi}}\mathbf{g}$. We start with finding the Lie derivative of $\hat{\mathbf{g}} = \boldsymbol{\psi}^*\mathbf{g}$ along the flow of $\boldsymbol{\psi}^{-1}\circ\boldsymbol{\phi}$. The tangent map of this flow is $T\left(\boldsymbol{\psi}^{-1}\circ\boldsymbol{\phi}\right) = \mathbf{u}^{-1}\mathbf{F}$ as shown in the diagram,

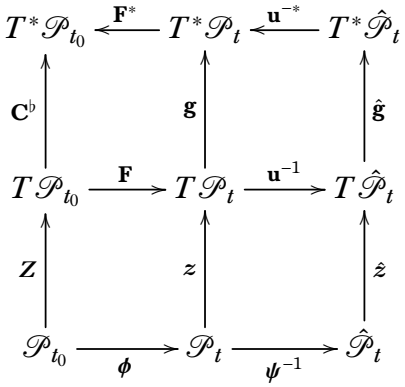

To use Lemma 4.6.1 for the flow $\boldsymbol{\psi}^{-1}\circ\boldsymbol{\phi}$, we find the spatial rate for $\mathbf{u}^{-1}\mathbf{F}$ on $T\hat{\mathscr{P}}_t$ with

$$\begin{aligned}(\boldsymbol{\psi}\circ\boldsymbol{\phi})_{*^2}\left(\frac{D\left(T\left(\boldsymbol{\psi}^{-1}\circ\boldsymbol{\phi}\right)\right)}{dt}\right) &= \frac{D\left(\mathbf{u}^{-1}\mathbf{F}\right)}{dt}\left(\mathbf{u}^{-1}\mathbf{F}\right)^{-1}\\ &= \mathbf{u}^{\mathsf{T}}\left(\frac{D\mathbf{F}}{dt}\mathbf{F}^{-1}\right)\mathbf{u} + \frac{D\left(\mathbf{u}^{\mathsf{T}}\right)}{dt}\mathbf{u}\\ &= \mathbf{u}^{\mathsf{T}}\mathbf{l}\mathbf{u} - \mathbf{u}^{\mathsf{T}}\frac{D\mathbf{u}}{dt}\\ &= \hat{\mathbf{l}} - \hat{\mathbf{w}}. \end{aligned} \tag{6.4.4}$$

In the above derivation, we have used $\dfrac{D\left(\mathbf{u}^{\mathsf{T}}\right)}{dt}\mathbf{u} = -\mathbf{u}^{\mathsf{T}}\dfrac{D\mathbf{u}}{dt}$ that can be obtained by taking the material time derivative of $\mathbf{u}^{\mathsf{T}}\mathbf{u} = \hat{\mathbf{u}}$. To calculate the Lie derivative of the covariant tensor $\hat{\mathbf{g}}$, we use equation (4.6.3b) of Lemma 4.6.1 for the flow $\boldsymbol{\psi}^{-1}\circ\boldsymbol{\phi}$ and the spatial rate $\hat{\mathbf{l}} - \hat{\mathbf{w}}$ by,

$$\mathscr{L}_{(\boldsymbol{\psi}^{-1}\circ\boldsymbol{\phi})}\hat{\mathbf{g}} = \frac{D\hat{\mathbf{g}}}{dt} + \hat{\mathbf{g}}\left(\hat{\mathbf{l}} - \hat{\mathbf{w}}\right) + \left(\hat{\mathbf{l}} - \hat{\mathbf{w}}\right)^*\hat{\mathbf{g}}.$$

On the other hand, the vector field of $\boldsymbol{\psi}^{-1}\circ\boldsymbol{\phi}$ on $\hat{\mathscr{P}}_t$ is the superposition of the two vector fields generated by the flows $\boldsymbol{\phi}$ and $\boldsymbol{\psi}^{-1}$. Hence,

$$\mathscr{L}_{(\boldsymbol{\psi}^{-1}\circ\boldsymbol{\phi})}\hat{\mathbf{g}} = \mathscr{L}_{\boldsymbol{\psi}^{-1}}\hat{\mathbf{g}} + \mathscr{L}_{\boldsymbol{\phi}}\hat{\mathbf{g}} = \mathscr{L}_{\boldsymbol{\psi}^{-1}}\hat{\mathbf{g}} + \boldsymbol{\psi}^*\mathscr{L}_{\boldsymbol{\phi}}\mathbf{g}. \tag{6.4.5}$$

In the last term in the above, we used the fact that the pullback $\boldsymbol{\psi}^*$ commutes with the Lie derivative $\mathscr{L}$. Recall that $\boldsymbol{\psi}^{-1}$ is an isometry which generates a *Killing vector field*, hence,

$\mathscr{L}_{\psi^{-1}}\hat{\mathbf{g}} = \mathbf{0}$ (see [Kobayashi and Nomizu, 1963, p. 237, Proposition 3.2]). Therefore, we have $\psi_*\mathscr{L}_{(\psi^{-1}\circ\phi)}\hat{\mathbf{g}} = \mathscr{L}_{\phi}\mathbf{g}$. Using $\mathbf{l} = \psi_*\hat{\mathbf{l}}$ and $\mathbf{w} = \psi_*\hat{\mathbf{w}}$, the pushforward of (6.4.5) is

$$\psi_*\left(\mathscr{L}_{(\psi^{-1}\circ\phi)}\hat{\mathbf{g}}\right) = \psi_*\left(\frac{D\mathbf{g}}{dt}\right) + \mathbf{g}\,(\mathbf{l}-\mathbf{w}) + (\mathbf{l}-\mathbf{w})\,\mathbf{g}. \tag{6.4.6}$$

Equating the Lie derivative of $\mathscr{L}_{\phi}\mathbf{g}$ given in the equation (4.9.2) of Proposition 4.9.1 with the pullback $\psi_*\left(\mathscr{L}_{(\psi^{-1}\circ\phi)}\hat{\mathbf{g}}\right)$ given above yields

$$\mathbf{w}^*\mathbf{g} + \mathbf{g}\mathbf{w} = \psi_*\left(\frac{\hat{D}\,(\psi^*\mathbf{g})}{dt}\right) - \frac{D\mathbf{g}}{dt}.$$

Left multiplication by $\mathbf{g}$ and using $\mathbf{w}^\intercal = \mathbf{g}^{-1}\mathbf{w}^*\mathbf{g}$ concludes (6.4.3). ■

Proposition 6.4.3 (Skewness of the referential angular velocity tensor). *Let* $\mathbf{\Psi}\colon \left(\hat{\mathscr{P}}_{t_0}, \hat{\mathbf{G}}\right) \to \left(\mathscr{P}_{t_0}, \mathbf{G}\right)$ *be a time-dependent isometric isomorphism and suppose* ∇ *is an arbitrary connection on* $\mathscr{P}_{t_0}$. *Also, let* $\mathbf{U} = T\mathbf{\Psi}$ *be the tangent map and* $\mathbf{W}$ *the angular velocity tensor defined in equation* (6.4.1a). *Then,*

$$\mathbf{W}^\intercal + \mathbf{W} = \mathbf{G}^{-1}\mathbf{\Psi}_*\left(\frac{\hat{D}\,(\mathbf{\Psi}^*\mathbf{G})}{dt}\right),$$

where the material time derivative $\hat{D}/dt$ *is based on the pullback connection* $\hat{\nabla} = \mathbf{\Psi}^*\nabla$ *on the transformed tangent bundle* $T\mathscr{P}_{t_0}$.

Proof. The isometry $\mathbf{\Psi}^{-1}$ generates a *Killing vector field*, hence, $\mathscr{L}_{\mathbf{\Psi}^{-1}}\hat{\mathbf{G}} = \mathbf{0}$. To calculate the Lie derivative of $\hat{\mathbf{G}}$ along $\mathbf{\Psi}^{-1}$, we use the rate of $T\mathbf{\Psi}^{-1} = \mathbf{U}^{-1}$ with $\dfrac{D\left(\mathbf{U}^{-1}\right)}{dt}\mathbf{U} = -\mathbf{U}^{-1}\dfrac{D\mathbf{U}}{dt} = -\hat{\mathbf{W}}$ in the equation (4.6.3b) in the Lemma 4.6.1 by,

$$\mathscr{L}_{\mathbf{\Psi}^{-1}}\hat{\mathbf{G}} = \frac{\hat{D}\hat{\mathbf{G}}}{dt} - \hat{\mathbf{G}}\hat{\mathbf{W}} - \hat{\mathbf{W}}^*\hat{\mathbf{G}} = \mathbf{0}.$$

Taking the pushforward $\mathbf{\Psi}_*$ of the above equation and using $\mathbf{G} = \mathbf{\Psi}_*\hat{\mathbf{G}}$ and $\mathbf{W} = \mathbf{\Psi}_*\hat{\mathbf{W}}$ leads to

$$\mathbf{\Psi}_*\left(\frac{\hat{D}\,(\mathbf{\Psi}^*\mathbf{G})}{dt}\right) = \mathbf{G}\mathbf{W} + \mathbf{W}^*\mathbf{G}.$$

Left multiplication with $\mathbf{G}^{-1}$ and using $\mathbf{W}^\intercal = \mathbf{G}^{-1}\mathbf{W}^*\mathbf{G}$ yields (6.4.3). ■

Remark 6.4.4. One might attempt to approach the above proof with $\mathscr{L}_{\mathbf{\Psi}}\mathbf{G} = \mathbf{0}$. Note that expressing this Lie derivative in terms of the connection leads to an equation with the material time derivative on the space $\hat{\mathscr{P}}_{t_0}$ instead, where $\hat{X}$ is assumed to be fixed, rather than the material time derivative on $\mathscr{P}_{t_0}$; which is not useful. We also note the analogy between Propositions 6.4.2 and 6.4.3, with the difference that $D\mathbf{G}/dt = \mathbf{0}$. ▲

Remark 6.4.5 (Skew symmetry of referential angular velocity). The isometries $\mathbf{U}$ and $\mathbf{u}$ are arbitrary, but they can be restricted by fixing the metrics $\hat{\mathbf{G}}$ and $\hat{\mathbf{g}}$. For instance, if we assume $D\hat{\mathbf{G}}/dt = \mathbf{0}$, such as when $\hat{\mathbf{G}} = \mathbf{I}$ (the identity tensor), then, $\mathbf{W}$ is skew-symmetric with respect to the metric $\mathbf{G}$. That is, $\mathbf{W}^\intercal + \mathbf{W} = \mathbf{0}$. Recall that the transposition is understood by the metric tensor i.e., $\mathbf{W}^\intercal = \mathbf{G}^{-1}\mathbf{W}^*\mathbf{G}$.

Similarly, the 2-form

$$\mathbf{W}^\flat = \mathbf{G}\mathbf{W} \in \Gamma\left(\bigwedge^2 \left(T^*\mathscr{P}_{t_0}\right)\right),$$

that is the *angular velocity* of the rotator $\mathbf{U}$, is skew-symmetric by $\left(\mathbf{W}^\flat\right)^* + \mathbf{W}^\flat = \mathbf{0}$ independent of the metric $\mathbf{G}$. That means its matrix representation is skew-symmetric in the sense that $W^\flat \in \mathfrak{so}(n) \coloneqq \mathrm{Lie}\,(\mathrm{SO}(n))$. ▲

Remark 6.4.6 (Skew-symmetry of spatial angular velocity). If $D\hat{\mathbf{g}}/dt = \mathbf{0}$, such as when we set $\mathbf{g} = \hat{\mathbf{i}}$, together with assuming that the connection ∇ is metric compatible, i.e., $D\mathbf{g}/dt = \mathbf{0}$, then, the tensor $\mathbf{w}$ becomes skew-symmetric with respect to the metric $\mathbf{g}$. That is, $\mathbf{w}^\intercal + \mathbf{w} = \mathbf{0}$. Recall that the transposition depends on the metric tensor i.e., $\mathbf{w}^\intercal = \mathbf{g}^{-1}\mathbf{w}^*\mathbf{g}$. Similarly,

$$\mathbf{w}^\flat = \mathbf{g}\mathbf{w} \in \Gamma\left(\bigwedge^2 \left(T^*\mathscr{P}_t\right)\right),$$

is the 2-from of angular velocity, and under the above assumptions on the metric $\hat{\mathbf{g}}$, the tensor $\mathbf{w}^\flat$ becomes skew-symmetric in the sense that $(\mathbf{w}^\flat)^* + \mathbf{w} = \mathbf{0}$. This implies the matrix $w^\flat \in \mathfrak{so}(n)$. ▲

The transformation $\boldsymbol{\psi}$ on the spatial configuration space introduces rotation with the rate $\mathbf{w}$. In the transformed coordinates, the rate of rotation is $\hat{\mathbf{w}}$. The difference of the spin due to the transformation and due to the rotation of the flow itself is noted by the relative spin defined below.

Definition 6.4.7 (Relative Spin). *We define the **relative spin** $\hat{\omega}'$ on the transformed tangent bundle as*

$$\hat{\omega}' \in \Gamma\left(\mathrm{End}(T\hat{\mathscr{P}}_t)\right), \quad \hat{\omega}' \coloneqq \hat{\omega} - \hat{\mathbf{w}}. \tag{6.4.7}$$

▲

The discrepancy of spin tensor $\hat{\omega}$ from the relative spin $\hat{\omega}'$ originates from the non-objectiveness of spin tensors. In contrast, the symmetric rate of deformation $\hat{\mathbf{d}}$ is frame-indifferent and transforms objectively. This statement is the manifestation of the ***Zaremba-Zorawski theorem*** [Truesdell, 1992, p. 146].

6.5 Evolution Equations on Transformed Manifolds

With the angular velocities and spin tensors, the evolution equations presented in Corollaries 4.9.3 and 4.7.2 are restated in the transformed manifolds as follows.

Theorem 6.5.1 (Material rate of left deformation tensor). *Let $\boldsymbol{\psi}\colon \left(\hat{\mathscr{P}}_t, \hat{\mathbf{g}}\right) \to \left(\mathscr{P}_t, \mathbf{g}\right)$ be an isometric isomorphism on the spatial manifold and let $\mathbf{u} \coloneqq T\boldsymbol{\psi}$ be its tangent map. Define the pullback of the left deformation tensor $\hat{\mathbf{b}} \coloneqq \boldsymbol{\psi}^*\mathbf{b} \in \operatorname{Aut}\left(T\hat{\mathscr{P}}_t\right)$. Then, the evolution of the left deformation tensor $\hat{\mathbf{b}}$ in the transformed manifold is*

$$\frac{D\hat{\mathbf{b}}}{dt} = \left[\hat{\omega}', \hat{\mathbf{b}}\right] + \left\{\hat{\mathbf{d}}, \hat{\mathbf{b}}\right\} + \hat{\mathbf{b}}\boldsymbol{\psi}^*\left(\mathbf{g}^{-1}\nabla_v\mathbf{g}\right), \qquad \hat{\mathbf{b}}(\boldsymbol{X}, t) = \hat{\mathbf{I}}. \tag{6.5.1}$$

where $\boldsymbol{\psi}^*\left(\mathbf{g}^{-1}\nabla_v\mathbf{g}\right) = \mathbf{u}^\intercal\left(\mathbf{g}^{-1}\nabla_v\mathbf{g}\right)\mathbf{u}$, and $\hat{\mathbf{I}}$ is the trivial automorphism on $T\hat{\mathscr{P}}_{t_0}$. The square brackets $[\cdot,\cdot]$ denote the Lie bracket (commutator)[4] and the brace $\{\cdot,\cdot\}$ denotes the anti-commutator[5].

Proof. We use the Corollary 4.7.2 for the composition map $\boldsymbol{\psi}^{-1}\circ\boldsymbol{\phi}$. Recall that $\mathbf{l} \coloneqq (D\mathbf{F}/dt)\,\mathbf{F}^{-1}$ is the spatial rate of $T\boldsymbol{\phi}$. Here, we replace $\mathbf{l}$ with the spatial rate of the tangent map composition $T\left(\boldsymbol{\psi}^{-1}\circ\boldsymbol{\phi}\right) = \mathbf{u}^\intercal\mathbf{F}$, which is already calculated in (6.4.4),

$$\frac{D\left(\mathbf{u}^\intercal\mathbf{F}\right)}{dt}\left(\mathbf{u}^\intercal\mathbf{F}\right)^{-1} = \hat{\mathbf{l}} - \hat{\mathbf{w}}.$$

Using Corollary 4.7.2 with the pullback quantities in the transformed manifold yields

$$\frac{D\hat{\mathbf{b}}}{dt} = \left(\hat{\mathbf{l}} - \hat{\mathbf{w}}\right)\hat{\mathbf{b}} + \hat{\mathbf{b}}\left(\hat{\mathbf{l}} - \hat{\mathbf{w}}\right)^\intercal + \hat{\mathbf{b}}\left(\hat{\mathbf{g}}^{-1}\frac{D\hat{\mathbf{g}}}{dt}\right).$$

Here, we used the material time derivative of $\hat{\mathbf{g}}(\boldsymbol{x}, t)$ since it is time-dependent. Decomposing $\hat{\mathbf{l}} = \hat{\mathbf{d}} + \hat{\omega}$ and substituting $\mathbf{w}^\intercal$ from Proposition 6.4.2 gives

$$\frac{D\hat{\mathbf{b}}}{dt} = \left(\hat{\mathbf{d}} + \hat{\omega} - \hat{\mathbf{w}}\right)\hat{\mathbf{b}} + \hat{\mathbf{b}}\left(\hat{\mathbf{d}} - \hat{\omega} + \hat{\mathbf{w}}\right) + \hat{\mathbf{b}}\boldsymbol{\psi}^*\left(\mathbf{g}^{-1}\frac{D\mathbf{g}}{dt}\right).$$

Since $\mathbf{g}$ is not explicitly a function of time, $D\mathbf{g}/dt = \nabla_v\mathbf{g}$. Using $\hat{\omega}' = \hat{\omega} - \hat{\mathbf{w}}$ from definition (6.4.7) and grouping into commutator and anti-commutator terms concludes (6.5.1). ∎

[4] The *Lie bracket* or *commutator* on two operators $\mathbf{A}$ and $\mathbf{B}$ is defined as the bilinear operator $[\mathbf{A},\mathbf{B}] \coloneqq \mathbf{AB} - \mathbf{BA}$.

[5] The *anti-commutator* on two operators $\mathbf{A}$ and $\mathbf{B}$ is defined as the bilinear operator $\{\mathbf{A},\mathbf{B}\} \coloneqq \mathbf{AB} + \mathbf{BA}$. Note, the symbol $\{,\}$ is often regarded as the *Lie-Poisson bracket*, but we use this symbol only for anti-commutator.

Remark 6.5.2 (Alternative proof of Theorem 6.5.1). The proof of Theorem 6.5.1 can also be approached with the Lie derivative of the composition map. Trivially, $\left(\boldsymbol{\psi}^{-1} \circ \boldsymbol{\phi}\right)^{*} \hat{\mathbf{b}} = \mathbf{I}$, which is illustrated by the commutative diagram,

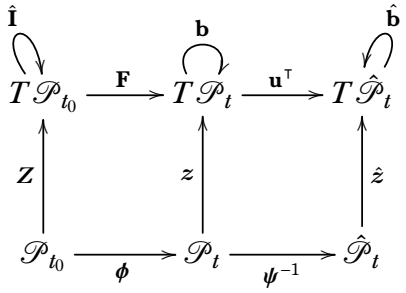

Thus, the Lie derivative on the composition map vanishes. By writing the Lie derivative for each map,

$$\mathscr{L}_{\left(\boldsymbol{\psi}^{-1}\circ\boldsymbol{\phi}\right)}\hat{\mathbf{b}} = \boldsymbol{\psi}_{*}^{-1}\mathscr{L}_{\boldsymbol{\phi}}\hat{\mathbf{b}} + \mathscr{L}_{\boldsymbol{\psi}^{-1}}\hat{\mathbf{b}} = \mathbf{0},$$

we observe that the extra term $\left[\hat{\mathbf{b}}, \hat{\mathbf{w}}\right]$ in 6.5.1 in Theorem 6.5.1 is originated from expressing the Lie derivative term $\mathscr{L}_{\boldsymbol{\psi}^{-1}}\hat{\mathbf{b}}$ in above with the rate $-\hat{\mathbf{w}}$ of the tangent map $\mathbf{u}^{\intercal}$ as $-\left(\hat{\mathbf{w}}\hat{\mathbf{b}} + \hat{\mathbf{b}}\hat{\mathbf{w}}^{\intercal}\right)$. ▲

Theorem 6.5.3 (Material rate of right deformation tensor). *Let* $\boldsymbol{\Psi}\colon \left(\hat{\mathscr{P}}_{t_0}, \hat{\mathbf{G}}\right) \to \left(\mathscr{P}_{t_0}, \mathbf{G}\right)$ *be an isometric isomorphism on the referential manifold and let* $\mathbf{U} := T\boldsymbol{\Psi}$ *be its tangent map. Define the pullback of the right deformation tensor* $\hat{\mathbf{C}} := \boldsymbol{\Psi}^{*}\mathbf{C} \in \operatorname{Aut}\left(T\hat{\mathscr{P}}_t\right)$. *Then, the evolution of the right deformation tensor* $\hat{\mathbf{C}}$ *in the transformed manifold is*

$$\frac{D\hat{\mathbf{C}}}{dt} = \left[\hat{\mathbf{C}}, \hat{\mathbf{W}}\right] + \hat{\mathbf{F}}^{\intercal}\left(2\hat{\mathbf{d}} + \boldsymbol{\psi}^{*}\left(\mathbf{g}^{-1}\nabla_{v}\mathbf{g}\right)\right)\hat{\mathbf{F}}, \qquad \hat{\mathbf{C}}\left(\boldsymbol{X}, t_0\right) = \hat{\mathbf{I}}, \tag{6.5.2}$$

where $\boldsymbol{\psi}^{*}\left(\mathbf{g}^{-1}\nabla_{v}\mathbf{g}\right) = \mathbf{u}^{\intercal}\left(\mathbf{g}^{-1}\nabla_{v}\mathbf{g}\right)\mathbf{u}$ *and* $\hat{\mathbf{I}}$ *is the trivial automorphism on* $T\hat{\mathscr{P}}_{t_0}$.

Proof. Taking the material time derivative of $\hat{\mathbf{C}} = \boldsymbol{\Psi}^{*}\mathbf{C} = \mathbf{U}^{\intercal}\mathbf{C}\mathbf{U}$ and writing expression in terms of $\hat{\mathbf{C}}$ obtains

$$\frac{D\hat{\mathbf{C}}}{dt} = \frac{D\left(\mathbf{U}^{\intercal}\right)}{dt}\mathbf{U}\hat{\mathbf{C}} + \mathbf{U}^{\intercal}\frac{D\mathbf{C}}{dt}\mathbf{U} + \hat{\mathbf{C}}\mathbf{U}^{\intercal}\frac{D\mathbf{U}}{dt}.$$

From (6.4.1c), $\mathbf{U}^{\intercal}\dfrac{D\mathbf{U}}{dt} = \hat{\mathbf{W}}$. Also, by taking the material time derivative of $\mathbf{U}^{\intercal}\mathbf{U} = \mathbf{I}$ we get $\dfrac{D\mathbf{U}^{\intercal}}{dt}\mathbf{U} = -\hat{\mathbf{W}}$. So,

$$\frac{D\hat{\mathbf{C}}}{dt} = \hat{\mathbf{C}}\hat{\mathbf{W}} - \hat{\mathbf{W}}\hat{\mathbf{C}} + \boldsymbol{\psi}^{*}\left(\frac{D\mathbf{C}}{dt}\right). \tag{6.5.3}$$

Also, $\left[\hat{\mathbf{C}}, \hat{\mathbf{W}}\right] = \hat{\mathbf{C}}\hat{\mathbf{W}} - \hat{\mathbf{W}}\hat{\mathbf{C}}$. Substituting $\dfrac{D\mathbf{C}}{dt}$ from Corollary 4.9.3 and applying the pullback $\boldsymbol{\psi}^{*}$ for each of tensors yields (6.5.2). ■

Remark 6.5.4 (Alternative proof of Theorem 6.5.3). The contribution of the Lie bracket term $\hat{\mathbf{C}}\hat{\mathbf{W}} - \hat{\mathbf{W}}\hat{\mathbf{C}} = [\hat{\mathbf{C}}, \hat{\mathbf{W}}]$ in equation (6.5.3) can also be justified by means of Lie derivative. As shown in the diagram,

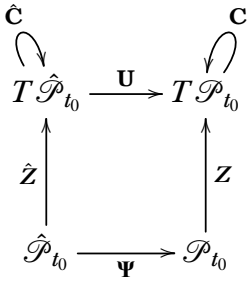

we have $\mathbf{C} = \left(\boldsymbol{\psi}^{-1}\right)^* \hat{\mathbf{C}}$ and $\boldsymbol{\psi}_*^{-1} = \boldsymbol{\psi}^*$, so

$$\mathscr{L}_{\boldsymbol{\psi}^{-1}} \hat{\mathbf{C}} = \boldsymbol{\psi}_*^{-1} \left(\frac{d}{dt}\bigg|_{t=t_0} \left(\boldsymbol{\psi}^{-1}\right)^* \hat{\mathbf{C}} \right) = \boldsymbol{\psi}^* \left(\frac{D\mathbf{C}}{dt} \right).$$

On the other hand, with the similar approach in Lemma 4.6.1 for $\hat{\mathbf{C}}^\sharp$ and using

$$\left(\boldsymbol{\Psi}^{-1}\right)_{*^2} \left(\frac{D\left(T\boldsymbol{\Psi}^{-1}\right)}{dt} \right) = -\hat{\mathbf{W}},$$

we obtain

$$\mathscr{L}_{\boldsymbol{\psi}^{-1}} \hat{\mathbf{C}}^\sharp = \frac{\hat{D}\hat{\mathbf{C}}^\sharp}{dt} + \hat{\mathbf{W}}\hat{\mathbf{C}}^\sharp + \hat{\mathbf{C}}^\sharp \hat{\mathbf{W}}^*. \tag{6.5.4}$$

Recall that $\hat{\mathbf{C}}^\sharp \hat{\mathbf{G}} = \hat{\mathbf{C}}$. Also,

$$\mathscr{L}_{\boldsymbol{\psi}^{-1}} \hat{\mathbf{G}} = \boldsymbol{\psi}^* \left(\frac{D\mathbf{G}}{dt} \right) = \mathbf{0},$$

since $\mathbf{G}$ is not a function of time. Hence, $\hat{\mathbf{G}}$ commutes with Lie derivative. Right-multiply (6.5.4) with $\hat{\mathbf{G}}$, commute the result with Lie derivative and use $\hat{\mathbf{W}}^\intercal = \hat{\mathbf{G}}^{-1}\hat{\mathbf{W}}^*\hat{\mathbf{G}}$ to obtain,

$$\left(\mathscr{L}_{\boldsymbol{\psi}^{-1}} \hat{\mathbf{C}}^\sharp\right) \hat{\mathbf{G}} = \mathscr{L}_{\boldsymbol{\psi}^{-1}} \hat{\mathbf{C}} = \left(\frac{\hat{D}\hat{\mathbf{C}}}{dt} - \hat{\mathbf{C}} \frac{\hat{D}\hat{\mathbf{G}}}{dt} \right) + \hat{\mathbf{W}}\hat{\mathbf{C}} + \hat{\mathbf{C}}\hat{\mathbf{W}}^\intercal.$$

Finally, the skew-symmetry of $\mathbf{W}$ in above yields (6.5.3). ▲

Chapter 7

Kinematics of Spectral Decomposition of Deformation

7.1 Introduction

Our goal in this chapter is to obtain the evolution equations for the spectral decomposition of deformation tensors, that is, for their eigenvalues and eigenvectors. The motivation for the evolution equation of eigenvalues, in particular, is to perform the Lagrangian analysis of the flow. Ultimately, this enables us to identify coherent structures and the topological assessment of the flow patterns, which we explore later in Chapters 10 to 12.

The rate equations for eigenvalues of deformation tensors are explored in many contexts in the kinematics of continua, which all has been formulated in Euclidean space with trivial metric. In the simplest form, Sowerby and Chu [1984] derived the rates of eigenvalues of Hencky strain tensor (a logarithmic strain tensor). Similar formulations can be found for instance in [Béda, Kozák, and Verhás, 1996, p. 69-70], [Dimitrienko, 2011, p. 76-77], and [Ogden, 1997, p. 129-130].

The evolution equations for eigenvalues are also derived independently in the context of dynamical systems. A particular motivation in that subject is the computation of ***Lyapunov exponents*** of chaotic dynamical systems from the flow map in the state space. The Lyapunov exponents are obtained from the singular value decomposition of the tangent map. The earliest form of the evolution equations of Lyapunov exponents is known to Greene and Kim [1987]. Geist, Parlitz, and Lauterborn [1990] compared several methods of computing Lyapunov exponents, including the method of the latter reference. Later, Bunse-Gerstner, Byers, Mehrmann, and Nichols [1991b] extended the computation of singular value decomposition of matrices that are a function of time, which is known as ***continuous singular value decomposition***. They also discussed the existence of solutions. Similarly, the differential equations for analytical singular value decomposition are given by Wright [1992]. In a more general setting, Dieci

and Eirola [1999] studied the smooth orthogonal decomposition of matrices of one parameter. They explored several aspects of the theory and computation of Lyapunov spectra, such as in Dieci and Vleck [2003]; Dieci and Elia [2006, 2008]; Dieci, Jolly, and Van Vleck [2010].

The novel formulation that we will present here incorporates in the presence of the Riemannian metric and arbitrary connection that may include torsion. In brief, our approach is to diagonalize the evolution equations that were given in Chapter 6. In the previous chapter, we have reformulated the evolution equations on a non-inertial frame by isometric isomorphisms, i.e., rotations of frames with the spinors $\mathbf{W}$ and $\mathbf{w}$ in the referential and spatial configurations respectively. Here, we determine the spin tensors $\mathbf{W}$ and $\mathbf{w}$ so that the deformation tensors $\mathbf{C}$ and $\mathbf{b}$ are diagonalized in a given local frame. The diagonalized tensors are the spectral decomposition that we have seen Chapter 3.

7.2 Diagonalization of Matrices of Deformation Tensors

At this point, the matrix-wise calculation of tensors for a choice of bases is convenient. We choose a referential and spatial basis $\boldsymbol{E}_A$ and $\boldsymbol{e}_a$ and proceed with the derivations with the *matrices* of tensors with respect to the chosen bases. We use the Roman (light) letters for the matrices of tensors, for instance, C denotes the matrix of the tensor $\mathbf{C}$ on the given basis, while $C^A{}_B$ is a component of the matrix C. In chapter 6, we have assumed the transformations $\boldsymbol{\psi}$ and $\boldsymbol{\Psi}$ are arbitrary, but henceforth, we assume these to be transformations that *diagonalize* coordinates representation $\hat{C}$ and $\hat{b}$ of the deformation tensors in the time varying frames $\hat{\boldsymbol{E}}_A$ and $\hat{\boldsymbol{e}}_a$. The coordinate representation of the tensors $\mathbf{F}$, $\mathbf{C}$, and $\mathbf{b}$ with respect to chosen frames $\boldsymbol{E}_A$ and $\boldsymbol{e}_a$ and also in the transformed frames $\hat{\boldsymbol{E}}_A$ and $\hat{\boldsymbol{e}}_a$ are

$$\begin{aligned}
\mathbf{F} &= F^a{}_A \boldsymbol{e}_a \otimes \boldsymbol{E}^{*A} &&= \hat{F}^a{}_A \hat{\boldsymbol{e}}_a \otimes \hat{\boldsymbol{E}}^{*A},\\
\mathbf{C} &= C^A{}_B \boldsymbol{E}_A \otimes \boldsymbol{E}^{*B} &&= \Lambda_A \hat{\boldsymbol{E}}_A \otimes \hat{\boldsymbol{E}}^{*A},\\
\mathbf{b} &= b^a{}_b \boldsymbol{e}_a \otimes \boldsymbol{e}^{*b} &&= \Lambda_a \hat{\boldsymbol{e}}_a \otimes \hat{\boldsymbol{e}}^{*a}.
\end{aligned}$$

In the above, we used $\Lambda \coloneqq \hat{C} = \hat{b}$ for diagonal matrix of eigenvalues of either $\mathbf{C}$ or $\mathbf{b}$. Also, with abuse of notation we indicate non-zero components of diagonal matrices (i.e., Λ) with a single index.

Let u and U denote the matrices of the tangent maps $\mathbf{u}$ and $\mathbf{U}$ of the isometries $\boldsymbol{\psi}$ and $\boldsymbol{\Psi}$ respectively. It is implied that $\boldsymbol{E}_A = U^B{}_A \hat{\boldsymbol{E}}_B$ and $\boldsymbol{e}_a = (u^{-1})^b{}_a \hat{\boldsymbol{e}}_b$ (see Remark 6.2.2). Clearly,

$$F(\boldsymbol{X}, t) = u(\boldsymbol{x}, t) \hat{F}(\boldsymbol{X}, t) U^{-1}(\boldsymbol{X}, t), \tag{7.2.1a}$$

$$C(\boldsymbol{X}, t) = U(\boldsymbol{X}, t) \Lambda(\boldsymbol{X}, t) U^{-1}(\boldsymbol{X}, t), \tag{7.2.1b}$$

$$b(\boldsymbol{x}, t) = u(\boldsymbol{x}, t) \Lambda(\boldsymbol{x}, t) u^{-1}(\boldsymbol{x}, t). \tag{7.2.1c}$$

In Euclidean space with the flat metric, it is trivial that $\hat{F}$ becomes diagonal whenever $\hat{C}$ and $\hat{b}$ are diagonal. When Λ, and consequently $\hat{F}$, are diagonal, the relation (7.2.1a) represents the *singular value decomposition* of the matrix F. Also, the relations (7.2.1b) and (7.2.1c) represent the *spectral decompositions* of C and b respectively. Both the spectral decompositions and the singular value decomposition in the above are consistent, in the sense that $\Lambda^{\frac{1}{2}} = \hat{F}$, and their left and right eigenvectors are identical. However, on a manifold with an arbitrary Riemannian metric, the above argument is not trivial. In the following, we will show that on an arbitrary metric space, the above decompositions still hold. In particular, we show that Λ and $\hat{F}$ are diagonalized *simultaneously*.

Proposition 7.2.1 (Simulataneous diagonalization of deformation matrices). *Suppose the matrices U and u diagonalize the matrices C and b simultaneously, i.e., to become the diagonal matrix Λ, by the matrix relations given in (7.2.1b) and (7.2.1c). The following statements hold for the other matrix relation, i.e., in (7.2.1a).*

1. *If the eigenvalues in the diagonals of Λ are distinct, then, $\hat{F}$ is always diagonal, but $\hat{F}$ is not invariant under an arbitrary scaling of the columns of U or u.*

2. *Moreover, if the eigenvalues Λ are distinct and the eigenvectors U and u have unit norm with respect to the metrics $\mathbf{G}$ and $\mathbf{g}$ respectively, then, $\hat{F} = \Sigma$ corresponds to the singular values of $\mathbf{F}$ where $\Sigma^2 = \Lambda$. The unit norm of eigenvectors is equivalent to assuming $\hat{\mathbf{G}} = \mathbf{I}$ and $\hat{\mathbf{g}} = \mathbf{i}$.*

Proof. Recall that $C = F^\intercal F$ and $b = FF^\intercal$ where $F^\intercal = G^{-1}F^* g$. The pushforward with u and U induces transformation on the metrics by $G = U^{-*}\hat{G}U^{-1}$ and $g = u^{-*}\hat{g}u^{-1}$, using the equations (6.2.4). The pullback of C and b using (7.2.1a), (7.2.1b), and (7.2.1c) respectively are

$$\hat{C} = \Lambda = \hat{F}^\intercal \hat{F}, \tag{7.2.2a}$$

$$\hat{b} = \Lambda = \hat{F}\hat{F}^\intercal, \tag{7.2.2b}$$

where $\hat{F}^\intercal = \hat{G}^{-1}\hat{F}^*\hat{g}$. By the left multiplication of (7.2.2a) with $\hat{F}$ and using (7.2.2b) we have $\hat{F}\hat{C} = \hat{F}\Lambda = \hat{F}\left(\hat{F}^\intercal \hat{F}\right) = \hat{b}\hat{F} = \Lambda\hat{F}$. So Λ and $\hat{F}$ commute, i.e., $\left[\Lambda, \hat{F}\right] = 0$. In components, $(\Lambda_a - \Lambda_b)\,\hat{F}^a{}_b = 0$. If $\Lambda_a \neq \Lambda_b$ when $a \neq b$, then, $\hat{F}^a{}_b = 0$, which concludes part (1).

The unit norm of eigenvectors in the columns of U and u is achieved by imposing

$$G(U,U) = U^* G U = \hat{G} = I,$$
$$g(u,u) = u^* g u = \hat{g} = i,$$

where $\hat{G} = I$ and $\hat{g} = i$ are set to the identity matrices. Thus, $\hat{F}^\intercal = \hat{F}^*$ and the two equations in (7.2.2a) become $\Lambda = \hat{F}^*\hat{F} = \hat{F}\hat{F}^*$. But, $\Lambda = \Sigma^2$ and $\hat{F}$ are diagonal, hence, $\hat{F} = \Sigma$ which is the matrix of the singular values and concludes part (2). ∎

Remark 7.2.2 (Existence of continuous singular value decomposition). A *continuous* spectral or singular value decomposition is the decomposition of a matrix that is a one-parameter family function, such as a function of time. It is known that the existence and uniqueness of a *continuous* singular value decomposition for a one-parameter matrix function is not trivial. That is, for a continuous (or even smooth) matrix function, the eigenvalues, singular values, and eigenvectors of the matrix might not be continuous or even exist for all ranges of the parameter of the matrix function.

For a symmetric matrix, such as $C(\boldsymbol{X}, t)$ and $b(\boldsymbol{X}, t)$ where t is the parameter and $\boldsymbol{X}$ is fixed, the continuity and differentiability of the eigenvalues and eigenvectors require the matrices to be a ***holomorphic*** along the real path $\boldsymbol{x} = \boldsymbol{x}(t)$ [Kato, 1995, §II, Theorems 6.1 and 6.8]. A holomorphic (or analytic) function is necessarily smooth, but the opposite can not be implied. There are C^∞ symmetric matrices where a continuous spectral decomposition does not even exist (e.g., [Kato, 1995, §II, Example 5.3]). Alternatively, for a non-symmetric matrix such as $F(\boldsymbol{X}, t)$, the holomorphy cannot ensure the existence of continuous eigenvectors (e.g., [Kato, 1995, §II, Example 5.9]).

In what follows, we assume the deformation tensor is *holomorphic*. This implies *existence*, but not necessarily *uniqueness*, of the singular value decomposition. That is, for matrices depending smoothly on a parameter (here time), the usual descending order of singular values is not guaranteed and the possibility of having negative singular values should be permitted [Bunse-Gerstner, Byers, Mehrmann, and Nichols, 1991a]. However, from the physical point of view, this condition does not happen in the deformation of continua since all singular values should remain positive. ▲

7.3 Diagonalization of Evolution Equations

In previous chapters, we have obtained two evolution equations for transformed left and right Cauchy-Green deformation tensors $\hat{\mathbf{b}}$ and $\hat{\mathbf{C}}$ in Theorems 6.5.1 and 6.5.3 respectively. Recall that the results in Corollaries 4.7.2 and 4.9.3 are independent of the choice of connection since they are originated from the Lie derivative of tensors along the flow map. Therefor, by writing rate equations in matrix form with respect to a basis, all Christoffel symbols should drop out.

In contrast, the rate of deformation gradient tensor $\mathbf{l}$ and the angular velocity tensors $\mathbf{W}$ and $\mathbf{w}$ depend on the connection, resulting in non-intrinsic matrices l, W, and w in the evolution equations in Theorems 6.5.1 and 6.5.3. To simplify calculations without loss of generality, we use the *trivial (or flat) connection* ∇^{triv} where all Christoffel symbols vanish, i.e.,

$\left(\gamma^{\text{triv}}\right)^{a}{}_{bc} = 0$. Henceforth, by the matrices

$$l = \frac{DF}{dt}F^{-1} = \frac{\partial v}{\partial x}, \tag{7.3.1a}$$

$$W = \frac{DU}{dt}U^{-1}, \tag{7.3.1b}$$

$$w = \frac{Du}{dt}u^{-1}, \tag{7.3.1c}$$

we imply the matrices of the tensors **l**, **W**, and **w** when the trivial connection is applied. One might consider l, W and w as the ***infinitesimal generators*** of F, U and u on their Lie groups.

Remark 7.3.1 (Existence of trivial connection). The trivial connections ∇^{triv} can only be defined on *trivial bundles*, requiring $\mathscr{P}_{t_0}$ and $\mathscr{P}_t$ be *parallelizable*. In other words, the manifold should admit a smooth global frame. Consequently, the tangent bundles are isomorphic to $\mathscr{P}_t \times \mathbb{R}^n$, ensuring that the trivial connection exists. However, we do not need to impose this requirement in our proceedings, since choosing the trivial connection is only a fictitious assumption to write the matrix form of equations directly from tensor equations conveniently, with a priori knowledge of independence with the choice of connection. ▲

Proposition 7.3.2 (Evolution equations of spectral decomposition I). *Let C and b denote the matrices of the right and left deformation tensors. Suppose the matrices $C(\boldsymbol{X}, t)$ and $b(\boldsymbol{x}, t)$ are holomorphic along the flow $\boldsymbol{\phi}$. Let U and u denote the matrices of isometries that diagonalize the deformation matrices by $C = U\Lambda U^{-1}$ and $b = u\Lambda u^{-1}$ where Λ is the diagonal matrix of eigenvalues. If the eigenvalues are distinct, then the material rate of Λ, u and U are given by*

$$\frac{DU}{dt} = U\hat{W}, \qquad U(\boldsymbol{X}, t_0) = U_0, \tag{7.3.2a}$$

$$\frac{Du}{dt} = u\hat{w}, \qquad u(\boldsymbol{X}, t_0) = U_0, \tag{7.3.2b}$$

$$\frac{D\Lambda}{dt} = \Lambda \odot \operatorname{diag}\left(2\hat{d} + \hat{f}\right), \qquad \Lambda(\boldsymbol{X}, t_0) = I, \tag{7.3.2c}$$

where $\odot$ denotes the Hadamard product [1]*, and $U_0 \in \mathrm{GL}(n)$ is any arbitrary full-rank matrix. The*

[1] Recall that the *Hadamard product* is an entry-wise product of matrices. Here in component, $\frac{D\Lambda_a}{dt} = \Lambda_a\left(2\hat{d}^a{}_a + \hat{h}^a{}_a\right)$.

matrices $\hat{W}$ and $\hat{w}$ are given by

$$\hat{W}^{A}_{\ B} = \begin{cases} \left(\dfrac{\hat{g}_{AA}}{\hat{g}_{BB}}\dfrac{\hat{G}_{BB}}{\hat{G}_{AA}}\right)^{\frac{1}{2}} \left(\dfrac{\Lambda_A^{\frac{1}{2}}\Lambda_B^{\frac{1}{2}}}{\Lambda_B - \Lambda_A}\right)\left(2\hat{d}^{A}_{\ B} + \hat{f}^{A}_{\ B}\right), & A \neq B, \\ \dfrac{1}{\hat{G}_{AA}}\left(\dfrac{1}{2}\dfrac{\hat{D}\hat{G}_{AA}}{dt} - \displaystyle\sum_{\substack{K=1 \\ K\neq A}}^{n} \hat{G}_{AK}\hat{W}^{K}_{\ A}\right), & A = B, \end{cases} \tag{7.3.3a}$$

and

$$\hat{w}^{a}_{\ b} = \begin{cases} \hat{\omega}^{a}_{\ b} + \left(\dfrac{\Lambda_b + \Lambda_a}{\Lambda_b - \Lambda_a}\right)\hat{d}^{a}_{\ b} + \left(\dfrac{\Lambda_a}{\Lambda_b - \Lambda_a}\right)\hat{f}^{a}_{\ b}, & a \neq b, \\ \dfrac{1}{\hat{g}_{aa}}\left(\dfrac{1}{2}\left(\dfrac{\hat{D}\hat{g}_{aa}}{dt} - \hat{f}^{\flat}_{aa}\right) - \displaystyle\sum_{\substack{k=1 \\ k\neq a}}^{n} \hat{g}_{ak}\hat{w}^{k}_{\ a}\right), & a = b. \end{cases} \tag{7.3.3b}$$

In the above relations, we defined the following pullback transformations

$$\hat{g} = u^* g u, \tag{7.3.4a}$$

$$\hat{G} = U^* G U, \tag{7.3.4b}$$

$$\hat{f} = u^{-1} f u, \qquad f = g^{-1} f^{\flat}, \qquad f^{\flat} := \frac{\partial g}{\partial x^k} v^k, \tag{7.3.4c}$$

$$\hat{d} = u^{-1} d u, \qquad d = g^{-1} d^{\flat}, \qquad d^{\flat} := \frac{1}{2}\left(l^{\flat} + l^{\flat *}\right), \tag{7.3.4d}$$

$$\hat{\omega} = u^{-1}\omega u, \qquad \omega = g^{-1}\omega^{\flat}, \qquad \omega^{\flat} := \frac{1}{2}\left(l^{\flat} - l^{\flat *}\right), \tag{7.3.4e}$$

$$l^{a}_{\ b} := \frac{\partial v^a}{\partial x^b}, \qquad l^{\flat} = g l, \tag{7.3.4f}$$

and the pullbacks are given by the orthonormal matrix $u^{\intercal} = u^{-1} = \hat{g}^{-1} u^* g$.[2]

Proof. In either Theorems 6.5.3 or 6.5.1, the matrix representation of the tensor

$$\boldsymbol{\psi}_*\left(\mathbf{g}^{-1}\nabla^{\text{triv}}_v \mathbf{g}\right) = \mathbf{u}^{\intercal}\left(\mathbf{g}^{-1}\nabla^{\text{triv}}_v \mathbf{g}\right)\mathbf{u},$$

(where the trivial connection ∇^{triv} is used) is $\hat{f} := u^{-1} f u$. The material rate of Λ from the material rate of $\hat{\mathbf{b}}$ in the Theorem 6.5.1 is

$$\frac{D\Lambda}{dt} = \left[\hat{\omega}', \Lambda\right] + \left\{\hat{d}, \Lambda\right\} + \Lambda\hat{f}. \tag{7.3.5}$$

[2] Unlike what our notation might suggest, the matrix f is not related to the (pullback) of deformation gradient F. Rather, f is the rate of metric.

where $\hat{\omega}'$ is defined in 6.4.7 using the angular velocity $\hat{w} = u^{-1}wu$ for the trivial connection. Since Λ is diagonal, the matrix $[\hat{\omega}', \Lambda]$ is off-diagonal, that is

$$\left[\hat{\omega}', \Lambda\right]^a_a = \hat{\omega}'^a{}_a \Lambda_a - \Lambda_a \hat{\omega}'^a{}_a = 0, \qquad i = 1, \cdots, n.$$

Hence, the diagonal elements of equation (7.3.5) are

$$\frac{D\Lambda_a}{dt} = 2\Lambda_a \hat{d}^a{}_a + \Lambda_a \hat{f}^a{}_a.$$

Writing the above with component-wise matrix product yields (7.3.2c). The off-diagonal elements of equation (7.3.5) are

$$0 = (\Lambda_b - \Lambda_a)\left(\hat{\omega}^a{}_b - w^a{}_b\right) + (\Lambda_b + \Lambda_a)\,\hat{d}^a{}_b + \Lambda_a \hat{f}^a{}_b, \qquad a \neq b = 1, \cdots, n.$$

Solving for $w^a{}_b$ by assuming $\Lambda_a \neq \Lambda_b$ yields (7.3.3b) for $a \neq b$.

The diagonal elements of w cannot be determined from (7.3.5) since they are eliminated from this equation. But, we can express them in terms of $\hat{g}$ with Proposition 6.4.2. First, we take the pullback $\boldsymbol{\psi}^*$ of equation (6.4.3), so it is represented by $\hat{\mathbf{w}}$. Recall that $\hat{\mathbf{w}}^\intercal = \hat{\mathbf{g}}^{-1}\hat{\mathbf{w}}^*\hat{\mathbf{g}}$, thus, by multiplying $\hat{\mathbf{g}}$ from the left side and writing the equation in the matrix form using the trivial connection we obtain

$$\hat{w}^*\hat{g} + \hat{g}\hat{w} = \frac{\hat{D}\hat{g}}{dt} - \hat{f}^\flat. \tag{7.3.6}$$

In deriving the above equation from (6.4.3), we used $\boldsymbol{\psi}^*\left(\frac{Dg}{dt}\right) = \mathbf{u}^*\left(\frac{Dg}{dt}\right)\mathbf{u}$ and then in the matrix form we have used $\frac{Dg}{dt} = \frac{\partial g}{\partial x^k}v^k = f^\flat$ followed by $u^* f^\flat u = \hat{f}^\flat$. The diagonal components of the matrix equation (7.3.6) are

$$\left(\hat{w}^a{}_a \hat{g}_{aa} + \sum_{\substack{k=1\\k\neq a}}^{n} \hat{w}^k{}_a \hat{g}_{ka}\right) + \left(\hat{g}_{aa}\hat{w}^a{}_a + \sum_{\substack{k=1\\k\neq a}}^{n} \hat{g}_{ak}\hat{w}^k{}_a\right) = \frac{\hat{D}\hat{g}_{aa}}{dt} - \hat{f}^\flat_{aa}, \qquad a = 1, \cdots, n.$$

We note that $\hat{g}_{ak} = \hat{g}_{ka}$, hence, by solving for $\hat{w}^a{}_a$ we obtain the second case of equation (7.3.3b).

Alternatively, we can use the material rate of Λ from the material rate of $\hat{\mathbf{C}}$ in Theorem 6.5.3. Since, $\Lambda = \hat{F}^\intercal \hat{F}$, by using $\hat{F}^\intercal = \Lambda \hat{F}^{-1}$, the matrix form of Theorem 6.5.3 becomes

$$\frac{D\Lambda}{dt} = \left[\Lambda, \hat{W}\right] + \Lambda \hat{F}^{-1}\left(2\hat{d} + \hat{f}\right)\hat{F}. \tag{7.3.7}$$

Note that $\left[\Lambda, \hat{W}\right]$ is an off-diagonal matrix, that is,

$$\left[\Lambda, \hat{W}\right]^A{}_A = \Lambda_A \hat{W}^A{}_A - \hat{W}^A{}_A \Lambda_A = 0.$$

The diagonal elements of this equation yield the same result for $\dfrac{D\Lambda_A}{dt}$ as derived above, but it is less straightforward. The off-diagonal elements of (7.3.7) are

$$0 = (\Lambda_A - \Lambda_B)\, \hat{W}^A{}_B + \Lambda_A \hat{F}_A^{-1} \left(2\hat{d}^A{}_B + \hat{f}^A{}_B\right) \hat{F}_B. \tag{7.3.8}$$

In the above, we used the fact that $\hat{F}$ is diagonal (see Proposition 7.2.1). In addition, $\Lambda = \hat{G}^{-1}\hat{F}^* \hat{g} \hat{F}$ (see equation (7.2.2a) from Proposition 7.2.1). Since $\hat{F}$ is diagonal, $\hat{G}\Lambda = \hat{F}\hat{g}\hat{F}$, so its diagonal components are $\hat{G}_{AA}\Lambda_A = \hat{F}_A^2 \hat{g}_{AA}$, allowing us to solve for $\hat{F}_A = \left(\hat{G}_{AA}/\hat{g}_{AA}\right)^{\frac{1}{2}} \Lambda_A^{\frac{1}{2}}$. Substituting $\hat{F}_A$ and $\hat{F}_B$ in (7.3.8) and solving for $W^A{}_B$ yields (7.3.3a) for $A \neq B$.

The diagonal elements of W cannot be determined from (7.3.7) since they are eliminated from this equation. But we can express them in terms of $\hat{G}$ with the Proposition 6.4.3. We take the pullback of equation (6.4.3), so it is represented by $\hat{\mathbf{W}}$. Recall that $\hat{\mathbf{W}} = \hat{\mathbf{G}}^{-1}\hat{\mathbf{W}}^*\hat{\mathbf{G}}$, so if we multiply the resulted equation by $\hat{\mathbf{G}}$ from the left side, its matrix representation is (recall the trivial connection is applied)

$$\hat{W}^* \hat{G} + \hat{G}\hat{W} = \frac{\hat{D}\hat{G}}{dt}.$$

The diagonals of the above matrix equation are

$$\left(\hat{W}^A{}_A \hat{G}_{AA} + \sum_{\substack{K=1 \\ K\neq A}}^{n} \hat{W}^K{}_A \hat{G}_{KA}\right) + \left(\hat{G}_{AA}\hat{W}^A{}_A + \sum_{\substack{K=1 \\ K\neq A}}^{n} \hat{G}_{AK}\hat{W}^K{}_A\right) = \frac{\hat{D}\hat{G}_{AA}}{dt}, \qquad A = 1, \cdots, n. \tag{7.3.9}$$

Recall that $\hat{G}_{AK} = \hat{G}_{KA}$. Solving for $W^A{}_A$ from above yields the second case of (7.3.3a). ■

Remark 7.3.3 (Symmetry of spinors). Recall from Remark 6.4.5 that the matrix $W^\flat$ is always skew-symmetric regardless of metric G. In contrast, by Remark 6.4.6, the matrix $w^\flat$ is not a skew-symmetric unless g is a parallel section. Also, both matrices W and w are not skew-symmetric (with respect to transposition) unless their metrics G and g are parallel. ▲

In the proof of Proposition 7.3.2, we have seen that the diagonals of $\hat{W}$ and $\hat{w}$ cannot be determined, instead, we have related them to the material rates of $\hat{G}$ and $\hat{g}$ using Propositions 6.4.2 and 6.4.3. We note that this is an artificial solution for $\hat{W}^A{}_A$ and $\hat{w}^a{}_a$ since the metrics $\hat{G} = U^* G U$ and $\hat{g} = u^* g u$ on the transformed spaces are not a priori defined if we do not know the transformations U and u.

We can find the physical meanings of the diagonal components ${W^A}_A$ and ${w^a}_a$ as follows. From equations (7.3.2a) and (7.3.2b) we have

$$W = U^{-1}\frac{DU}{dt} = \hat{G}^{-1}U^* G\frac{DU}{dt},$$
$$w = u^{-1}\frac{Du}{dt} = \hat{g}^{-1}u^* g\frac{Du}{dt}.$$

We can see that ${\hat{W}^A}_A$ and ${\hat{w}^a}_a$ are the rates of the norms of columns of U and u respectively (norms of eigenvectors). Since we did not impose any restriction on the length of the eigenvectors, the diagonals of W and w are undetermined. In the following theorem, we set $\hat{G}$ and $\hat{g}$ to impose unit norms on the eigenvectors and determine W and w completely.

Theorem 7.3.4 (Evolution equations of spectral decomposition II). *Let C and b denote the matrix representations of the right and left deformation tensors with respect to a local frame and assume $C(\boldsymbol{X}, t)$ and $b(\boldsymbol{x}, t)$ remain holomorphic along the flow. Let $C = U\Lambda U^{-1}$ and $b = u\Lambda u^{-1}$ denote the spectral decomposition of the positive-definite matrices C and b, where Λ is diagonal and the columns of U and u are the right and left eigenvectors of deformation which have unit norm with respect to the metrics G and g respectively. If the eigenvalues are distinct, then, the complete set of coupled ODEs for the evolution of $\Lambda(\boldsymbol{x}, t)$, $U(\boldsymbol{X}, t)$, and $u(\boldsymbol{x}, t)$ are given by*

$$\frac{D\boldsymbol{x}}{dt} = \boldsymbol{v}(\boldsymbol{x}, t), \qquad \boldsymbol{x}(\boldsymbol{X}, t_0) = \boldsymbol{X}, \tag{7.3.10a}$$
$$\frac{DU}{dt} = U\hat{W}, \qquad U(\boldsymbol{X}, t_0) = U_0, \tag{7.3.10b}$$
$$\frac{Du}{dt} = u\hat{w}, \qquad u(\boldsymbol{X}, t_0) = U_0, \tag{7.3.10c}$$
$$\frac{D\Lambda}{dt} = \Lambda \odot \operatorname{diag}(2\hat{d} + \hat{f}), \qquad \Lambda(\boldsymbol{X}, t_0) = I, \tag{7.3.10d}$$

where U_0 is an arbitrary full rank matrix that satisfies $U_0^* G U_0 = I$, and the skew-symmetric matrix $\hat{W}$ is

$${\hat{W}^A}_B = \begin{cases} \left(\dfrac{\Lambda_A^{\frac{1}{2}}\Lambda_B^{\frac{1}{2}}}{\Lambda_B - \Lambda_A}\right)\left(2{\hat{d}^A}_B + {\hat{f}^A}_B\right), & A < B, \\ 0, & A = B, \\ -{\hat{W}^B}_A, & A > B, \end{cases} \tag{7.3.11a}$$

and the matrix $\hat{w}$ (that is not necessarily skew-symmetric) is

$${\hat{w}^a}_b = {\hat{\omega}^a}_b + \begin{cases} \left(\dfrac{\Lambda_b + \Lambda_a}{\Lambda_b - \Lambda_a}\right){\hat{d}^a}_b + \left(\dfrac{\Lambda_a}{\Lambda_b - \Lambda_a}\right){\hat{f}^a}_b, & a \neq b, \\ -\dfrac{1}{2}\hat{f}^a{}_a, & a = b, \end{cases} \tag{7.3.11b}$$

In above relations, we used

$$\hat{f} = \hat{f}^\flat = u^* f^\flat u, \qquad f^\flat = \frac{\partial g}{\partial x^k} v^k, \tag{7.3.12a}$$

$$\hat{d} = \hat{d}^\flat = u^* d^\flat u, \qquad d^\flat = \frac{1}{2}\left(l^\flat + l^{\flat *}\right), \tag{7.3.12b}$$

$$\hat{\omega} = \hat{\omega}^\flat = u^* \omega^\flat u, \qquad \omega^\flat = \frac{1}{2}\left(l^\flat - l^{\flat *}\right), \tag{7.3.12c}$$

and the associated velocity gradient is $l^\flat = gl$ *where* $l^a{}_b = \dfrac{\partial v^a}{\partial x^b}$. *Here,* $\hat{f}$ *and* $\hat{d}$ *are symmetric and* $\hat{\omega}$ *is skew-symmetric matrix.*

Proof. To constrain the eigenvectors with the unit norm with respect to the metric tensors, we set

$$G(U,U) = U^* G U = \hat{G} = \hat{I},$$
$$g(u,u) = u^* g u = \hat{g} = \hat{\imath}.$$

Therefor, the initial condition U_0 should satisfy $U_0^* G U_0 = I$. Applying $\hat{G}_{AB} = \delta_{AB}$ as well as $\hat{g}_{ab} = \delta_{ab}$ in relations (7.3.3b) and (7.3.3a) in the Proposition 7.3.2 simplifies to equations (7.3.11a) and (7.3.11b) respectively. Lastly, $\hat{g} = \hat{\imath}$ simplifies $u^{-1} = u^\intercal = \hat{g}^{-1} u^* g = u^* g$, so $\hat{d} = u^{-1} d u = u^* g d u = u^* d^\flat u$. The same can be applied to $\hat{\omega} = u^* \omega^\flat u$ as well as $\hat{f} = u^{-1} f u = \left(u^* g\right)\left(g^{-1} f^\flat\right) u = u^* k^\flat u$. ■

The set of ordinary differential equations of the above theorem can be used in practice. In the following remarks, we brief some considerations for the numerical implementations of the differential equations.

Remark 7.3.5 (Initial conditions). At $t = t_0$, the deformation gradient tensor $\mathbf{F}$ is the two-point identity tensor. Hence, $\mathbf{\Lambda}$ is unique and equal to the referential identity map. However, the initial conditions for referential and spatial rotators $\mathbf{U}$ and $\mathbf{u}$ are not unique; their initial conditions may start with an arbitrary unitary tensor as long as $U^a{}_b = u^a{}_b$. In particular, the identity matrix can be used as an initial condition for these matrices. ▲

Remark 7.3.6 (Isothermal metric). The symmetry of $\hat{d}$ (and respectively skew-symmetry of $\hat{\omega}$) does not imply the symmetry of d (respectively the skew-symmetry of ω). As we have mentioned earlier, d and ω are respectively symmetric and skew-symmetric with respect to the transposition with the metric. However, if g is an ***isothermal metric***, i.e., $g_{ab}(\boldsymbol{x}) = \rho(\boldsymbol{x})\delta_{ab}$ where $\rho \in C^\infty(\mathscr{P}_t)$, then, $l^\intercal = g^{-1} l^* g = l^*$, which leads to the symmetry and skew-symmetry of d and ω respectively. ▲

Remark 7.3.7 (Order of ODEs in Theorem 7.3.4). The set of coupled ordinary differential equations in Theorem 7.3.4 consists of the positions $\boldsymbol{x}$, the eigenvalue tensor $\boldsymbol{\Lambda}$, and the right and left transformations $\mathbf{U}$ and $\mathbf{u}$. The n scalar equations for the position $\boldsymbol{x}$ in (7.3.10a) are decoupled from the other equations. Also, the matrices of $\mathbf{U}$ and $\mathbf{u}$ each consists of n^2 components. But, since $\mathbf{U}, \mathbf{u} \in SO(n)$, they have $n(n-1)/2$ independent degrees of freedom. This can be verified by observing that the tensors $\hat{\mathbf{W}}, \hat{\mathbf{w}} \in \mathfrak{so}(n)$ are skew-symmetric and have $n(n-1)/2$ meaningful components. Also, the diagonal tensor $\boldsymbol{\Lambda}$ has n eigenvalues on its diagonals. Overall the set of three unknown tensors $\mathbf{U}$, $\mathbf{u}$ and $\boldsymbol{\Lambda}$ have n^2 degrees of freedom. Thus, the set of ODEs with $2n(n+1)$ equations is of the order $n(n+1)$. ▲

Remark 7.3.8 (Symmetry and dimensionality reduction of ODEs). Note that the matrices $f^\flat$ and $d^\flat$ are symmetric, and $\omega^\flat$ is skew-symmetric. Recall in Proposition 7.3.2 that matrices f, d, ω, W and w do not have (skew) symmetry. In contrast to Proposition 7.3.2, in Theorem 7.3.4 we assumed $\hat{g}$ is identity, hence, the matrices f, d and $\hat{d}$ become symmetric and ω and W become skew-symmetric. Nonetheless, the matrix w is not skew-symmetric unless $\hat{f} = 0$, which occurs only if the metric $g(\boldsymbol{x}(t))$ is *constant along the streamlines* of the flow. We can leverage the skew symmetry of W (and w if it is) to reduce the dimensionality of evolution equations for U (and u). We will discuss the dimensionality reduction of deformation equations in chapters 8 and 9. ▲

Remark 7.3.9 (Intrinsicness of Proposition 7.3.2 and Theorem 7.3.4). For convenience, in both Proposition 7.3.2 and Theorem 7.3.4 we have trivialized the connection, which greatly simplifies the derivations. If another connection is used, the matrices d, f, ω, w, W will change accordingly. Also, material time derivatives $\dot{\Lambda}$, $\dot{u}$ and $\dot{U}$ will be changed. However, the equations are independent of the connection. That is, when an arbitrary connection is used and write all tensors and material rates in terms of the Christoffel symbols, the Christoffel symbols cancel out from the sides of the equations. An advantage of using the trivial connection at first place is that the material time rates of the matrices $\dot{\Lambda}$, $\dot{u}$ and $\dot{U}$ are also their Lie derivative. ▲

Remark 7.3.10 (Numerical advantage of Theorem 7.3.4 over Proposition 4.3.1). The deformation gradient $\mathbf{F}$ can be numerically integrated over time either directly by Proposition 4.3.1 or indirectly by the continuous singular value decomposition in Theorem 7.3.4. Using the formulation in Theorem 7.3.4 we can separate evolution equations of $\mathbf{F}$ into diagonal and off-diagonal equations. This enables us to solve for the singular values and left and right eigenvectors on the fly without directly integrating the deformation gradient tensor. At any time along integration, the deformation gradient tensor can be recovered from $\mathbf{F} = \mathbf{u}\boldsymbol{\Lambda}^{1/2}\mathbf{U}^\intercal$. Such alternative numerical integration is compared with the direct integration method in Fig. 7.3.1.

The continuous singular value decomposition is computationally more robust since direct integration with Proposition 4.3.1 may become ill-conditioned as the left eigenvectors of tensor $\mathbf{F}$ collapse to the dominant eigenvector due to numerical errors. In contrast, because of preservation of the orthogonality of the left and right eigenvectors (the columns of matrices u and U) in Theorem 7.3.4, its numerical solution is stable.

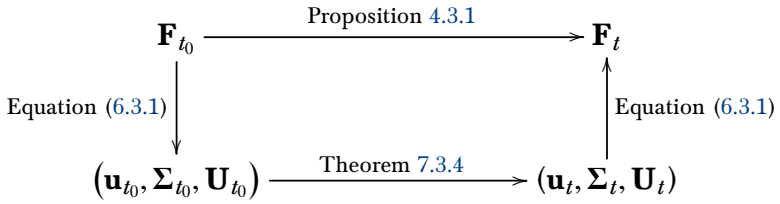

Figure 7.3.1: Evolving deformation gradient tensor using continuous singular value decomposition

▲

Remark 7.3.11 (Avoidance of crossing of eigenvalues). According to relations (7.3.11a) and (7.3.11b), the spinors $\hat{\mathbf{W}}$ and $\hat{\mathbf{w}}$ are undefined when two eigenvalues are identical. Such a case occurs particularly at initial time $t = t_0$ when all eigenvalues are initialized identically since $F(t_0) = I$ requires $\Lambda_A(t_0) = 1$ for $A = 1, \dots, n$. Consequently, the equations (7.3.10b) and (7.3.10c) for left and right eigenvectors u and U become singular. Thus, Theorem 7.3.4 can only be used when the eigenvalues always remain distinct without crossing, i.e.,

$$\Lambda_A(t) \lneq \Lambda_B(t), \quad A < B, \quad t > t_0,$$

In practice, a complete crossing of eigenvalues rarely happens due to the phenomenon of ***avoided crossing***, in which two eigenvalues approach closely and diverge, thus the order of eigenvalues preserved without crossing [Lax, 2007, Ch. 9, §5]. This phenomenon is originally discovered in Quantum mechanics by von Neumann and Wigner [1929], and later explored by Zener [1932] in the context of the non-adiabatic crossing of energy levels. The difficulty of integrating a system with avoided crossing is the violation of an *adiabatic transition*, where a jump of $\mathcal{O}(1)$ in dynamics occurs within a small time-interval of $\mathcal{O}(\delta)$ with $\delta \ll 1$ [Hairer, Lubich, and Wanner, 2002, p. 535].

Both of crossing of eigenvalues and the avoided crossing within a non-adiabatic transitions cause stall of the numerical integration. We believe the numerical treatment for an avoided crossing of eigenvalues requires the diagonalization of higher-order evolution equations that were given in §5.4. In practice, a naive resolution to this issue is to switch the numerical integration to the direct method of Proposition 4.3.1 for a small time-interval $[t, t + \delta]$ whenever eigenvalues are close within tolerance at some time t. Once the eigenvalues diverge above a tolerance, the numerical scheme can switch back to the continuous singular value decomposition by Theorem 7.3.4. ▲

7.4 Rate of Volume Change and Liouville Theorem

We revisit the isochoric flow that was discussed earlier in §4.4. Here, we measure the rate of change of the volume in the view of the eigenvalues of the deformation. Here, we use the ***Hencky strain tensor*** [Holzapfel, 2000, p. 88] defined by

$$\mathbf{H} := \ln(\mathbf{C}^{\frac{1}{2}}) = \lim_{m\to 0} \frac{1}{2m}\left(\mathbf{C}^m - \mathbf{I}\right), \tag{7.4.1}$$

which is used for the logarithmic strain measure [Gurtin and Spear, 1983]. A geometric point of view of the logarithmic stretches has been developed by Neff, Eidel, and Martin [2016] on Riemannian spaces and the rate of logarithmic strain has been studied by Xiao, Bruhns, and Meyers [1997] in the Euclidean setting. Here, we readily can derive the evolution of the logarithmic strain in Riemannian spaces. If $\mu_a := \frac{1}{2}\ln\Lambda_a$ denote the eigenvalues of $\mathbf{H}$, it is immediate from (7.3.10d) that

$$\frac{D\mu_a}{dt} = \frac{1}{2\Lambda_a}\frac{D\Lambda_a}{dt} = \hat{d}^a{}_a + \frac{1}{2}\hat{f}^a{}_a, \qquad \mu_a(\boldsymbol{X},t) = 0, \qquad a = 1,\cdots,n, \tag{7.4.2}$$

which is the rate for logarithmic stretch rate. This measure of strain is closely related to finite-time Lyapunov exponent (FTLE) and is of interest in the context of non-autonomous dynamical systems and identifying regions with coherent structures in the fluid flow [Shadden, Lekien, and Marsden, 2005].

For an isochoric flow, we have seen in §4.4 that $\operatorname{div}(\boldsymbol{v}) = 0$ and the Jacobian $J = \det(\boldsymbol{\phi}) = 1$. It is straightforward to relate this property to the eigenvalues of deformation. Recall from Remark 4.4.1 that $\det(C) = \det(b) = J^2$. Therefor for an isochoric flow,

$$J^2 = \prod_{i=1}^{n} \Lambda_i = 1.$$

Alternatively, we can approach the above conclusion from the Theorem 7.3.4, and given below. We will show our derivation is indeed the extension of the Liouville theorem to metric spaces.

Corollary 7.4.1 (Liouville theorem on Riemannian manifold). *Let μ denote the diagonal matrix of the eigenvalues of Hencky strain tensor $\mathbf{H} \in \Gamma\left(\operatorname{Aut}\left(T\mathscr{P}_{t_0}\right)\right)$ for the flow $\boldsymbol{\phi}\colon \left(\mathscr{P}_{t_0}, \mathbf{G}\right) \to \left(\mathscr{P}_t, \mathbf{g}\right)$ on the Riemannian manifold with spatial velocity $\boldsymbol{v}$. Then,*

$$\frac{D}{dt}\left(\sum_{a=1}^{n}\mu_a\right) = \operatorname{div}(\boldsymbol{v}). \tag{7.4.3}$$

For isochoric flows, it holds $\sum_{a=1}^{n}\mu_a = 0$.

Proof. The trace of equation (7.4.2) is

$$\frac{D}{dt}\left(\sum_{a=1}^{n}\mu_a\right) = \operatorname{trace}\left(\hat{d}+\frac{1}{2}\hat{f}\right) = \operatorname{trace}\left(d+\frac{1}{2}f\right). \tag{7.4.4}$$

The last equality is obtained by realizing that the trace is invariant under similarity transformations $\hat{d} = u^{-1}du$ and $\hat{f} = u^{-1}ku$, so $\operatorname{trace}\left(\hat{d}+\frac{1}{2}\hat{f}\right) = \operatorname{trace}\left(d+\frac{1}{2}f\right)$. Recall that we use the trivial connection for l from (7.3.1a), also $d = \left(l+l^{\intercal}\right)/2$. Consider that $l^{\intercal}$ and l are similar matrices since $l^{\intercal} = g^{-1}l^{*}g$. We obtain the trace of d as

$$\operatorname{trace}(d) = \frac{1}{2}\Big(\operatorname{trace}(l) + \operatorname{trace}\left(g^{-1}l^{*}g\right)\Big) = \operatorname{trace}(l) = \frac{\partial v^k}{\partial x^k}. \tag{7.4.5}$$

On the other hand, to find the trace of f, we apply the Jacobi's formula for the derivative of determinant (see the proof in [Sokolnikoff, 1951, p. 81]) as,

$$\frac{\partial \det(g)}{\partial x^k} = \det(g)\,g^{ab}\frac{\partial g_{ab}}{\partial x^k}.$$

Using the identity above, we obtain the trace of f by

$$\begin{aligned}\operatorname{trace}(f) &= \operatorname{trace}\left(g^{-1}\frac{\partial g}{\partial x^k}v^k\right)\\ &= \frac{1}{\det(g)}\frac{\partial\left(\det(g)\right)}{\partial x^k}v^k\\ &= \frac{2}{\sqrt{\det(g)}}\frac{\partial\sqrt{\det(g)}}{\partial x^k}v^k.\end{aligned} \tag{7.4.6}$$

The last line above can be easily obtained if we write the second line as $\dfrac{\partial\left(\ln\left(\det(g)\right)\right)}{\partial x^k}v^k$. Putting together the relations (7.4.5) and (7.4.6) into equation (7.4.4) yields

$$\begin{aligned}\frac{D}{dt}\left(\sum_{a=1}^{n}\mu_a\right) &= \frac{1}{\sqrt{\det(g)}}\left(\frac{\partial v^k}{\partial x^k}\sqrt{\det(g)} + \frac{\partial\sqrt{\det(g)}}{\partial x^k}v^k\right)\\ &= \frac{1}{\sqrt{\det(g)}}\frac{\partial\left(\sqrt{\det(g)}v^k\right)}{\partial x^k}\\ &= \operatorname{div}(v)\,.\end{aligned}$$

The second line above is the expression of the divergence on the Riemannian manifold using the metric tensor [Marsden and Hughes, 1983, p. 78, Definition 4.27]. Also, clearly for isochoric flow $\operatorname{div}(v) = 0$, hence the initial condition $\mu(\boldsymbol{X}, t_0) = I$ implies $\sum_{a=1}^{n}\mu_a = 0$ for all $t \in \mathscr{I}$. ■

Remark 7.4.2. Corollary 7.4.1 holds even in the case of crossing eigenvalues, even though Theorem 7.3.4 is not valid to obtain the eigenvalues. ▲

Remark 7.4.3. The statement of Corollary 7.4.1 can also be written as

$$\frac{D}{dt}\left(\prod_{a=1}^{n}\Lambda_a\right) = 2\,(\operatorname{div} \boldsymbol{v})\prod_{a=1}^{n}\Lambda_a, \tag{7.4.7}$$

or in terms of Jacobian as $DJ/dt = (\operatorname{div} \boldsymbol{v})\, J$. We have encountered a similar equation in terms of the Lie derivative of J in (4.4.5). Here, since we have trivialized the connection, the material time derivative and the Lie derivative have identical matrix representations. In Euclidean space where $\mathbf{g}$ and $\mathbf{G}$ are identified, by (4.4.3) we have $J = \det(\mathbf{F})$, and (7.4.7) becomes

$$\mathscr{L}_{\boldsymbol{\phi}}\,(\det(\mathbf{F})) = (\operatorname{div} \boldsymbol{v})\det(\mathbf{F}), \qquad \text{(in Euclidean space)},$$

which is known as the ***Abel-Liouville-Jacobi-Ostrogradskii identity*** in dynamical systems [Hairer, Lubich, and Wanner, 2002, p. 228]. ▲

7.5 Iso-spectral Flows and Isometry

We conclude this chapter by studying iso-spectral flows, which simplifies our previous derivations to better interpret the evolution equations. In iso-spectral flows, the eigenvalues are invariant under the flow i.e.,

$$\frac{D\Lambda_a}{dt} = 0, \qquad a = 1, \cdots, n.$$

We will show that the evolution of the left deformation tensors of such flows is governed by the Lax differential equation and produce isometries.

Theorem 7.5.1 (Killing vector field generates iso-spectral flow). *Let the diffeomorphism $\boldsymbol{\phi}\colon \left(\mathscr{P}_{t_0}, \mathbf{G}\right) \to \left(\mathscr{P}_t, \mathbf{g}\right)$ be a flow on a Riemannian manifold with the complete velocity vector field $\boldsymbol{v}$. Then the followings are equivalent,*

1. *The flow $\boldsymbol{\phi}$ is iso-spectral, i.e., $\dfrac{D\Lambda}{dt} = 0$.*
2. *The spatial velocity $\boldsymbol{v}$ is a **Killing vector field**, i.e., $\mathscr{L}_{\boldsymbol{v}}\mathbf{g} = \mathbf{0}$.*
3. *The flow $\boldsymbol{\phi} : (\mathscr{P}_{t_0}, \mathbf{G}) \to (\mathscr{P}_t, \mathbf{g})$ is a Riemannian isometry.*
4. *The referential spinor is identically zero, i.e., $\mathbf{W} = \mathbf{0}$.*

5. *The right deformation tensor is a parallel on the vector bundle, i.e.,* $\dfrac{D\mathbf{C}}{dt} = \mathbf{0}$.

6. *The tangent map is purely rotational, i.e.,* $\mathbf{F} \in \mathrm{SO}(n)$.

7. *The left deformation tensor is the Lax pair of* $\mathbf{l}$*, i.e.,* $\mathbf{b}$ *satisfies the* ***Lax equation****,*

$$\frac{D\mathbf{b}}{dt} = [\mathbf{l}, \mathbf{b}]\,. \tag{7.5.1}$$

Proof. If $\dfrac{D\Lambda}{dt} = 0$, then from equation (7.3.5) we have

$$\left(\hat{d} + \hat{\omega} - \hat{w}\right)\Lambda + \Lambda\left(\hat{d} - \hat{\omega} + \hat{w}\right) + \Lambda\hat{f} = 0. \tag{7.5.2}$$

Since Λ is constant with the initial condition $\Lambda(t_0) = I$, the above relation simplifies to $2\hat{d} + \hat{f} = 0$. We pull back the latter equation with $d = u\hat{d}u^{-1}$ and $f = u\hat{f}u^{-1}$, and write (7.5.2) as $2d + f = 0$. This relation should be satisfied on any local frame, which leads to the tensorial form $2\mathbf{d} + \mathbf{f} = \mathbf{0}$ where $\mathbf{f} = \nabla^{\mathrm{triv}}_v \mathbf{g}$ and ∇^{triv} is the trivial connection. Recall from Proposition 4.9.1 that,

$$\mathscr{L}_{\boldsymbol{\phi}}\mathbf{g} = 2\mathbf{d}^\flat + \mathbf{g}^{-1}\nabla^{\mathrm{triv}}_v \mathbf{g} = \mathbf{g}^{-1}\left(2\mathbf{d} + \mathbf{f}\right) = \mathbf{0}.$$

In the above, we used the trivial connection for consistency with Theorem 7.3.4 where a trivial connection is assumed to define variables such as d and f. Recall that both the above Lie derivative and the statement of Theorem 7.3.4 is intrinsic regardless of the connection. Using any other connection yields the same conclusion, even though the matrices d and f would be different. By the above relation, (1) implies (2). Also, (3) follows from [Marsden and Hughes, 1983, p. 99, Definition 6.15]. Substituting the relation $2\mathbf{d} + \mathbf{f} = \mathbf{0}$ in (7.3.11a) yields $\mathbf{W} = \mathbf{0}$, which implies (4). The same relation applied to Corollary 4.9.3 yields $D\mathbf{C}/dt = \mathbf{0}$, which concludes 5. Recall from §3.2 that $\mathbf{C} = \mathbf{P}^2$ where $\mathbf{P}$ is the stretch tensor. So $D\mathbf{P}/dt = \mathbf{0}$, implying that $\mathbf{P}(t) = \mathbf{P}(t_0) = \mathbf{I}$ is the identity map. By the polar decomposition, $\mathbf{F} = \mathbf{PR} = \mathbf{R}$ where $\mathbf{R}$ is the rotation tensor and orthogonal. So (6) is concluded.

Lastly, by the relation $\mathbf{f} = \mathbf{g}^{-1}\nabla^{\mathrm{triv}}_v \mathbf{g} = -2\mathbf{d} = -(\mathbf{l} + \mathbf{l}^\intercal)$, the Corollary 4.7.2 yields,

$$\frac{D\mathbf{b}}{dt} = \mathbf{lb} + \mathbf{bl}^\intercal + \mathbf{bf} = \mathbf{lb} - \mathbf{bl},$$

which concludes equation (7.5.1). We remind the reader that the above relation is intrinsic, regardless of the choice of connection, but for consistency with the Theorem 7.3.4 have used the trivial connection. It is straightforward to show the converse, where (7) implies (1). ■

Remark 7.5.2 (Symmetric Lax equation). The class of equations of the form in (7.5.1) are called ***Lax equations*** and the matrices of tensors $\mathbf{l}$ and $\mathbf{b}$ are called ***Lax pairs***[3]. Lax equation is known to convey the iso-spectral property (see e.g., [Hairer, Lubich, and Wanner, 2002, §IV.3.2 and §X.1.5]). From the Euler-Cauchy-Stokes decomposition $\mathbf{l} = \mathbf{d} + \boldsymbol{\omega}$ and the property $2\mathbf{d} + \mathbf{f} = \mathbf{0}$ of the iso-spectral flows, one might write (7.5.1) as

$$\frac{D\mathbf{b}}{dt} = \left[\boldsymbol{\omega} - \frac{\mathbf{f}}{2}, \mathbf{b}\right].$$

Hence, iso-spectral deformation is governed only by the spin of the flow, $\boldsymbol{\omega}$, and the change of metric along the streamlines, $\mathbf{f}$. It is known that the Lax equation is symmetric (i.e., $\mathbf{b}$ remains symmetric) if the Lax counterpart of $\mathbf{b}$ is skew-symmetric. In Euclidean space where $\mathbf{g}$ is identified, we have $\mathbf{f} = \mathbf{0}$, also $\boldsymbol{\omega}$ becomes skew-symmetric, leading to a symmetric iso-spectral flow (see e.g., [Diele and Sgura, 1999, §2.2]). For a non-trivial $\mathbf{g}$, the tensor $\mathbf{b}$ (and $\boldsymbol{\omega}$) is yet (skew-) symmetric but with respect to the transposition induced by $\mathbf{g}$. Hence, we refer to equation (7.5.1) as *symmetric iso-spectral flow.* ▲

An iso-spectral flow is produced by the Killing vector field. By a given metric, the Killing vector field is generated by solving the differential equation

$$2d^a{}_b = v^a{}_{|b} + v^b{}_{|a} = 0,$$

where the covariant derivative used in the above relation is the Levi-Civita connection (i.e., $\mathbf{f} = \mathbf{0}$). In Euclidean space, a Killing vector field is simply the translation and rotation of the special Euclidean group $\mathrm{SE}(n)$ that is produced by the motion of a solid body. For non-Euclidean manifolds, a non-trivial Killing vector field might not exist. For instance, manifolds of negative Ricci curvature, i.e., $\mathrm{Ric} < 0$, do not have a trivial Killing vector field [Petersen, 2006, Bochner Theorem, p. 191]. Also, on manifolds with $\mathrm{Ric} \leq 0$, the Killing vector field is parallel. Interestingly, every Killing vector field is a Jacobi field (see §5.5) along geodesics [Jost, 2011, Corollary 5.2.1].

[3]The Lax form was introduced by Lax [1968] in the *Korteweg-de Vries partial differential equations*, which can be regarded as an infinite-dimensional dynamical system. Later, Flaschka [1974] introduced the Lax form in the *Toda lattice*, which is a finite-dimensional dynamical system (see also [Moser and Zehnder, 2005, p. 216-219]).

Chapter 8

Kinematics on Lie Algebra

8.1 Introduction

The set of evolution equations for the rotator tensors $\mathbf{u}$ and $\mathbf{U}$ in Theorem 7.3.4 is the attitude kinematics of the eigenvector frames. In this chapter, we assume the configuration manifold is the Euclidean space, and we make an analogy between our equations and the kinematics of moving frames, and the bipolar decomposition of pseudo-rigid bodies. Non-Euclidean formulations for 2-manifolds are given in Chapter 9.

In this chapter, we review the mathematical representation of rotation and their numerical integrations. Rotation in Euclidean space is represented by the special orthogonal group $\mathrm{SO}(n)$. Corresponding to the Lie group is the Lie algebra $\mathrm{so}(n)$ of skew-symmetric spinors. The representation of rotation on the Lie algebra is optimal in the sense that a minimal number of variables are used to parameterize the state of rotation. A trivialization map projects the Lie group to the corresponding Lie algebra and briefly discussed in §8.3.

The projections by trivialization maps are not unique and the lead to the various parameterizations of rotation, such as Cayley-Klein and Euler-Rodrigues parameterization, and exponential map. The latter is of special interest, and we briefly explain in §8.4. Another important representation of rotation in 3-dimensional space is by *unit quaternions* on $\mathbb{S}^3$. The attitude kinematics in terms of quaternions are presented in §8.5. In our numerical applications that will be given in later in Chapter 11, we have extensively utilized the numerical integration with quaternions as a Lie group integrator. In two-dimensional Euclidean space, rotation is represented using Euler angles and given in §8.6. For arbitrary dimension n, the Lie algebra of rotation can be represented by the *Clifford algebra* [Hestenes and Sobczyk, 1984] but we will not discuss here.

Several numerical integration schemes have been developed to incorporate the group action on manifolds. These methods are known as *geometric* or *Lie group integrators*. Further details can be found in McLachlan and Quispel [2006] and Hairer [2001].

8.2 An Analogy with Attitude Kinematics

Orthogonal Moving Frames of Eigenvectors

The set of evolution equations in Theorem 7.3.4 can be interpreted in the following way. Let the spatial orthonormal vectors $\boldsymbol{u}_b(\boldsymbol{x},t) = u^a{}_b(\boldsymbol{x},t)\boldsymbol{e}_a(\boldsymbol{x})$ with $b = 1,\dots,n$ and the referential orthonormal vectors $\boldsymbol{U}_B(\boldsymbol{X},t) = U^A{}_B(\boldsymbol{X},t)\boldsymbol{E}_A(\boldsymbol{X})$ with $B = 1,\dots,n$ indicate the left and right eigenvectors of the deformation gradient tensor $\mathbf{F}$. The components $u^a{}_b$ and $U^A{}_B$ of eigenvectors are the columns of left and right transformation matrices in the singular value decomposition given in (7.2.1a). We can view each set of eigenvectors as composing a frame in each configuration space as shown in Fig. 8.2.1 (here shown for dimension $n = 3$). Recall that the evolution of each frame is described by (7.3.10b) and (7.3.10c). The evolution equations for $\mathbf{u}$ and $\mathbf{U}$ can be interpreted as a rotation of orthonormal moving frames shown in figure 8.2.1, such that the left orthonormal frame $\boldsymbol{u}_b$ is rotating and translating by the flow-map along the pathline on the point $\boldsymbol{x}$, while the right orthonormal frame $\boldsymbol{U}_B$ is fixed at the initial point $[X]$ and only rotates. Thus, these differential equations effectively describe two ***attitude kinematics*** in each of the configuration space.

This analogy has also been explored in the ***bipolar decomposition*** of ***pseudo-rigid body kinematics*** Cohen and Muncaster [1988], which considers the motion of a simple object that undergoes small elastic deformation. Historically, this subject was motivated by the *Dirichlet's ellipsoidal problem* in astrophysics, where the equilibrium of a homogeneous rotating mass and under its gravitation is questioned [Chandrasekhar, 1969, Ch. 4]. In the bipolar decomposition, the configuration of a pseudo (or affine) rigid body is characterized by an orientation preserving linear map in $\mathrm{GL}^+(\mathrm{n},\mathbb{R})$, which, via an SVD procedure, is decomposed as a product of (1) a member of $\mathrm{SO}(n)$ that rotates the referential coordinate frame, (2) a member of $\mathrm{Diag}^+(n,\mathbb{R})$ that stretches the object, and (3) a member of $\mathrm{SO}(n)$ that rotates the spatial coordinate frame (see also [Holm, Schmah, and Stoica, 2009, §10]).

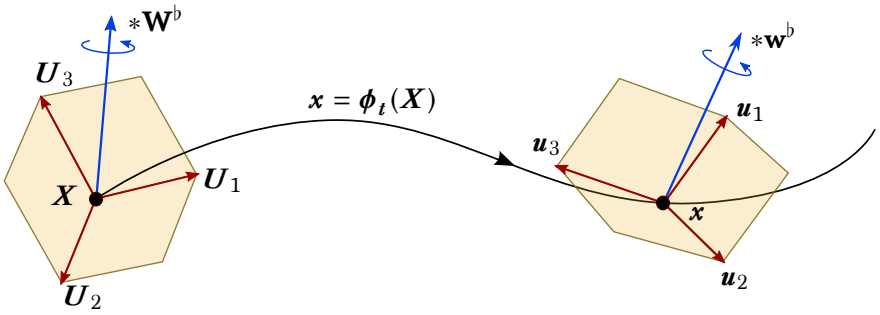

Figure 8.2.1: Orthogonal moving frames corresponding to the left and right eigenvectors.

The continuous singular value decomposition allows us to extract out the rotations due to the left and right moving frames so that the pure deformation in the rotating coordinate

frames can be integrated from equation (7.3.10d) along the pathline. Figure 8.2.2 illustrates the spatial image of the diagonal map $\mathbf{\Sigma} \coloneqq \mathbf{\Lambda}^{1/2}$ on the unit ball in the reference configuration space.

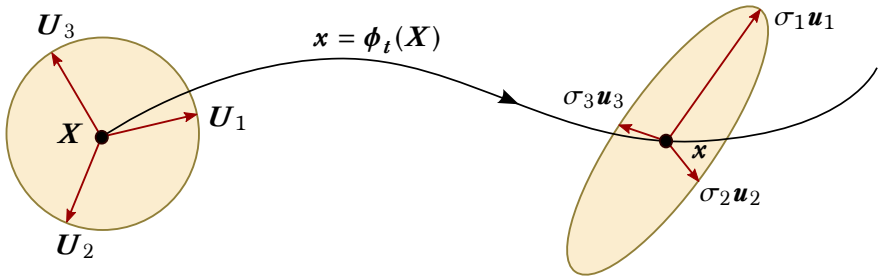

Figure 8.2.2: The continuous diagonal map $\mathbf{\Sigma}(\boldsymbol{X}, t)$, maps the unit sphere on the reference configuration to its image, an ellipsoid, on the spatial configuration space.

Inertial and Dynamic Moving Frames

The evolution equations (7.3.10b) and (7.3.10c) are represented in the *rotating* (or *dynamic*) *frame* of each of the configuration spaces. Alternatively, these equations can be represented in *inertial frames*, which are independent of the rotation of the frame itself.[1] We will show that such conversion from dynamic to inertial frames enables us to express the evolution equations on the Lie algebra in a more convenient form (see §8.3). We refer to the angular velocity tensors $\hat{\mathbf{W}}$ and $\hat{\mathbf{w}}$ as ***dynamic spinors***, and the angular velocity tensors $\mathbf{W}$ and $\mathbf{w}$ as ***inertial spinors***. Recall from 6.4.1 that,

$$\mathbf{W} \coloneqq \frac{D\mathbf{U}}{dt}\mathbf{U}^{\mathsf{T}}, \quad \text{and} \quad \mathbf{w} \coloneqq \frac{D\mathbf{u}}{dt}\mathbf{u}^{\mathsf{T}}.$$

Also, the relations between dynamic and inertial spinors are

$$\hat{\mathbf{W}} = \mathbf{U}\mathbf{W}\mathbf{U}^{\mathsf{T}}, \quad \text{and} \quad \hat{\mathbf{w}} = \mathbf{u}\mathbf{w}\mathbf{u}^{\mathsf{T}}.$$

Hence, the dynamic spinors are conjugate to the inertial spinors under the spatial and referential transformations $\mathbf{u}$ and $\mathbf{U}$ respectively. Recall that these relations are illustrated in commutative diagram (6.4.2). The evolution of rotators $\mathbf{u}$ and $\mathbf{U}$ using either inertial or dynamic spinors are

$$\dot{\mathbf{U}}(\boldsymbol{X}, t) = \mathbf{U}(\boldsymbol{X}, t)\hat{\mathbf{W}}(\boldsymbol{X}, t) = \mathbf{W}(\boldsymbol{X}, t)\mathbf{U}(\boldsymbol{X}, t), \qquad \mathbf{U}(t_0) = \mathbf{I}, \tag{8.2.1a}$$

$$\dot{\mathbf{u}}(\boldsymbol{x}, t) = \mathbf{u}(\boldsymbol{x}, t)\hat{\mathbf{w}}(\boldsymbol{x}, t) = \mathbf{w}(\boldsymbol{x}, t)\mathbf{u}(\boldsymbol{x}, t), \qquad \mathbf{u}(t_0) = \mathbf{i}. \tag{8.2.1b}$$

[1] In rigid body kinematics, these two frames are referred to as the *body frame* and the *spatial frame* [Holm, Schmah, and Stoica, 2009, §1.5]. However, to avoid overlap with our terminology (i.e., *spatial* configuration), we have used *dynamic* and *inertial* to respectively denote the *body* and *spatial* frames. Both of these frames can be applied to rotations in either referential or spatial configurations.

From the computational point of view, either of dynamic or inertial formulations may be effectively used to numerically integrate the differential equations.

The terminology of inertial and dynamic spinors is inspired by their pseudo-vectors in attitude kinematics, which can be defined by the *Hodge dual* of spinors. In three-dimensional space, for instance, the Hodge star operator is the isomorphism

$$* : \bigwedge^2 (T^*\mathscr{P}) \to \bigwedge^1 (T^*\mathscr{P}),$$

which maps the 2-form spinors to their Hodge duals as 1-form pseudo-vectors. We denote pseudo-vectors with an arrow symbol $\vec{\cdot}$ above the variable. The referential and spatial pseudo-vectors

$$\vec{\boldsymbol{W}} := *\mathbf{W}^\flat, \quad \text{and} \quad \vec{\boldsymbol{w}} := *\mathbf{w}^\flat,$$

are called ***inertial angular velocities*** in attitude kinematics and are the axes of rotations for the right and left moving frames respectively as shown in Fig. 8.2.1. In contrast, the pseudo-vectors

$$\vec{\hat{\boldsymbol{W}}} := *\hat{\mathbf{W}}^\flat, \quad \text{and} \quad \vec{\hat{\boldsymbol{w}}} := *\hat{\mathbf{w}}^\flat,$$

are ***dynamic angular velocities*** and they represent the axis of rotation for co-frames.

Remark 8.2.1 (Hodge dual on covariant-contravariant spinors). Since the spinors $\mathbf{W}$, $\hat{\mathbf{W}}$, $\mathbf{w}$, and $\hat{\mathbf{w}}$ are covariant-contravariant tensors of type $\binom{1}{1}$, the Hodge star operator cannot be directly applied. For obtaining pseudo-vectors from spinors, the associated tensors (i.e., $\mathbf{W}^\flat$, $\hat{\mathbf{W}}^\flat$, $\mathbf{w}^\flat$ and $\hat{\mathbf{w}}^\flat$) are formed by lowering index action $\flat$, resulting in a covariant tensor. Then, the Hodge star operator can be applied [Abraham, Marsden, and Raţiu, 1988, §6.1.11]. ▲

8.3 Evolution on the Lie Algebra

The numerical integration of equations in (8.2.1) requires that both rotators $\mathbf{U}$ and $\mathbf{u}$ remain unitary, that is, $\mathbf{U}, \mathbf{u} \in \mathrm{SO}(n)$ for all t. However, not all integration schemes (e.g., Runge-Kutta) preserve orthogonality. Moreover, due to the orthogonal symmetry, the rotators can be represented in a lower-dimensional space to be integrated more efficiently. This section aims to exploit the symmetry in evolution equations on the Lie group and represent them on their Lie algebra.

The Lie algebra $\mathfrak{so}(n) = T_{\mathbf{I}}\mathrm{SO}(n)$ is the tangent space of the special orthogonal Lie group $\mathrm{SO}(n)$ at the identity tensor $\mathbf{I}$, and consists of skew-symmetric tensors.[2] *Trivialization* maps

[2] The fractur font denotes a Lie algebra for a variable with the same name.

associate the Lie algebra to Lie group or vice versa. We represent the evolution equations for the rotating frames using the Lie algebra representation.

Let the skew-symmetric tensors $\mathfrak{U}, \mathfrak{u} \in \mathfrak{so}(n)$ be tensors in the Lie algebra corresponding to the tensors $\mathbf{U}, \mathbf{u}$ in the Lie group $\mathrm{SO}(n)$. We have distinguished the trivialization map, τ, for the referential rotator $\tau : \mathfrak{U} \mapsto \mathbf{U}$ and the spatial rotator $\tau : \mathfrak{u} \mapsto \mathbf{u}$, but in matrix form, both maps are the same. In the following, we use tensors and their matrices interchangeably.

Let the discrete maps

$$K_t^{t+\Delta t} : \mathbf{U}(t) \mapsto \mathbf{U}(t+\Delta t), \quad \text{and} \quad k_t^{t+\Delta t} : \mathbf{u}(t) \mapsto \mathbf{u}(t+\Delta t),$$

denote the numerical integrators on the Lie group. By the composition of pushforwards and pullbacks of the trivialization maps, we can construct equivalent discrete maps on the Lie algebra as

$$\mathfrak{K}_t^{t+\Delta t} : \mathfrak{U}(t) \mapsto \mathfrak{U}(t+\Delta t), \qquad K_t^{t+\Delta t} := \tau \circ \mathfrak{K}_t^{t+\Delta t} \circ \tau^{-1}, \tag{8.3.1a}$$

$$\mathfrak{k}_t^{t+\Delta t} : \mathfrak{u}(t) \mapsto \mathfrak{u}(t+\Delta t), \qquad k_t^{t+\Delta t} := \tau \circ \mathfrak{k}_t^{t+\Delta t} \circ \tau^{-1}. \tag{8.3.1b}$$

The conjugacy of the maps $\mathfrak{K}$ and $\mathfrak{k}$ with the maps K and k are shown in the commutative diagrams

$$\begin{array}{ccc} \mathbf{U}(t) \in \mathrm{SO}(n) & \xrightarrow{K_t^{t+\Delta t}} & \mathbf{U}(t+\Delta t) \in \mathrm{SO}(n) \\ \Big\downarrow{\scriptstyle T^{-1}} & & \Big\uparrow{\scriptstyle T} \\ \mathfrak{U}(t) \in \mathfrak{so}(n) & \xrightarrow{\mathfrak{K}_t^{t+\Delta t}} & \mathfrak{U}(t+\Delta t) \in \mathfrak{so}(n) \end{array}$$

and

$$\begin{array}{ccc} \mathbf{u}(t) \in \mathrm{SO}(n) & \xrightarrow{k_t^{t+\Delta t}} & \mathbf{u}(t+\Delta t) \in \mathrm{SO}(n) \\ \Big\downarrow{\scriptstyle \tau^{-1}} & & \Big\uparrow{\scriptstyle \tau} \\ \mathfrak{u}(t) \in \mathfrak{so}(n) & \xrightarrow{\mathfrak{k}_t^{t+\Delta t}} & \mathfrak{u}(t+\Delta t) \in (so)(n) \end{array}$$

The integration with numerical methods $\mathfrak{K}$ and $\mathfrak{k}$ on the Lie algebra has two benefits. First, the solution always remains on $\mathrm{SO}(n)$, which preserves orthogonality. Second, the dimension of equations on Lie algebra reduces to $\dim(\mathfrak{so}(n)) = \binom{n}{2}$, which is the number of plane rotations on any two pairs of an axis. This is in contrast to n^2 equations of the matrices. Hence, the composition of integration methods yields a significant reduction in ODEs to be solved. This fact is of most importance in using Lie algebra for our application.

The integrators $\mathfrak{K}$ and $\mathfrak{k}$ and the Lie algebra tensors $\mathfrak{U}$ and $\mathfrak{u}$ are not unique. Several numerical integration schemes have been developed based on various mappings (see e.g., Hairer, Lubich, and Wanner [2002] and references therein). For instance, a straightforward method is the *Cayley transformation*,

$$\mathbf{U} = (\mathbf{I} + \mathfrak{U})(\mathbf{I} - \mathfrak{U})^{-1}.$$

Such transformation has been used by Udwadia and von Bremen [2002] for computing Lyapunov exponents using QR decomposition. However, the Cayley transform becomes singular when any of the eigenvalues of the rotator $\mathbf{U}$ is equal to -1. In Udwadia and von Bremen [2002], this issue was resolved by re-starting the ODEs with new initial conditions. An alternative trivialization that is not singular is the *exponential map*, $\tau : \mathbf{U} \mapsto \exp(\mathfrak{U})$ that we will brief on the section that follows.

8.4 Trivialization with Exponential Map

The exponential map is a common trivialization of Lie groups. We motivate the application of the exponential map on the autonomous differential equation $\dot{U} = WU$ in 8.2.1 where we assume W is time-independent. The analytical solution can be immediately given by the exponentials $U(t) = \exp(Wt)U(t_0)$. However, in practice, the matrix W is time-dependent and an explicit exponential solution cannot be directly given for non-autonomous systems. Inspired by the autonomous system, the exponential solution can be extended to non-autonomous equations as follows.

Suppose the non-autonomous dynamical system

$$\dot{U}(t) = W(t)U(t) = W_t(U(t)), \tag{8.4.1}$$

is given, and assume $U(t) \in \mathrm{SO}(n)$. The angular velocity $W \in \Gamma(\mathfrak{so}(n))$ can be thought of as a vector field (a section) on the Lie algebra at the point U of the Lie group, and denoted by $W_t(U) \in \mathfrak{so}(n)$. The equation (8.4.1) is a differential equation on the Lie group $\mathrm{SO}(n)$. We wish to *lift* this equation to its Lie algebra using the trivialization map $\tau^{-1} = \exp^{-1} : \mathrm{SO}(n) \to \mathfrak{so}(n)$. Denote the corresponding lift of U as $\mathfrak{U}$, which is related to U by

$$U(t) = \exp_{U_0}(\mathfrak{U}(t)) = \exp(\mathfrak{U}(t))U_0, \tag{8.4.2}$$

In our notation, $\exp_{U_0}(\mathfrak{U})$ denotes the exponential map defined on the tangent space $T_{U_0}(\mathrm{SO}(n))$ at the point $U_0 = U(t_0)$, and projects the tangent vector $\mathfrak{U}(t) \in \mathfrak{so}(n)$ to the manifold $\mathrm{SO}(n)$. This is carried out by the matrix multiplication $\exp(\mathfrak{U}(t))U_0$. Take the time derivative of (8.4.2) by the chain rule as (see [Hairer, Lubich, and Wanner, 2002, §III.4, Lemma 4.1])

$$\dot{U}(t) = \left(d\exp_{U_0}\right)_{\mathfrak{U}(t)} \left(\dot{\mathfrak{U}}(t)\right) \exp_{U_0}(\mathfrak{U}(t)) .$$

where $(d\exp_{U_0})_{\mathfrak{U}(t)} : T_{\mathfrak{U}(t)}(\mathfrak{so}(n)) \to T_{U(t)}(\mathrm{SO}(n))$ is the derivative of the exponential map at the tangent vector $\mathfrak{U}(t)$. By comparing with (8.4.1), we obtain the Magnus theorem [Hairer, Lubich, and Wanner, 2002, §IV.7, Theorem 7.1]

$$W(t) = \left(d\exp\right)_{\mathfrak{U}(t)} \left(\dot{\mathfrak{U}}(t)\right),$$

By the inverse map, the differential equation on the Lie algebra is obtained as

$$\dot{\mathfrak{U}}(t) = \left(d\exp^{-1}\right)_{\mathfrak{U}(t)}(W(t)), \qquad \mathfrak{U}(t_0) = 0. \tag{8.4.3}$$

The operator $\left(d\exp_{U_0}^{-1}\right)_{\mathfrak{U}} : T_{U(t)}(\mathrm{SO}(n)) \to T_{\mathfrak{U}(t)}(\mathfrak{so}(n))$ is the inverse of $\left(d\exp_{U_0}\right)_{\mathfrak{U}(t)}$. The commutative diagram

$$\begin{array}{ccc} T_{\mathfrak{U}}(\mathfrak{so}(n)) & \xrightarrow{d\tau = d\exp} & T_U(\mathrm{SO}(n)) \\ \uparrow{\scriptstyle \dot{\mathfrak{U}}} & & \uparrow{\scriptstyle W} \\ \mathfrak{U} \in \mathfrak{so}(n) & \xrightarrow{\tau=\exp} & U \in \mathrm{SO}(n) \end{array}$$

summarizes the relations described above. The right side of the diagram represents the original differential equation (8.4.1) where U is related to its rate, $\dot{U}$ by W, and W is shown as a section. Similarly, the left side of the diagram represents the same differential equation, but on the Lie algebra through the trivialization, here being the exponential map.

The analytical solution to the equation (8.4.3) is given by the *Magnus expansion* after Magnus [1954], which applies the analytical representation of $d\exp$ by Baker-Campbell-Hausdorff formula

$$\left(d\exp^{-1}\right)_{\mathfrak{U}}(W) = \sum_{k=0}^{\infty} \frac{B_k}{k!} \mathrm{ad}_{\mathfrak{U}}^k(W). \tag{8.4.4}$$

where B_k are Bernoulli numbers. The adjoint action of the Lie algebra $\mathrm{ad}_{\mathfrak{U}} : \mathfrak{so}(n) \to \mathfrak{so}(n)$ is defined by the Lie bracket (matrix commutator)

$$\mathrm{ad}_{\mathfrak{U}}(W) = [\mathfrak{U}, W] = \mathfrak{U}W - W\mathfrak{U}.$$

The k-fold commutator $\mathrm{ad}_{\mathfrak{U}}^k$ is given by the recursion $[\mathfrak{U}, \mathrm{ad}_{\mathfrak{U}}^{k-1}]$.

An example of a numerical scheme that embeds the exponential map is *Munthe-Kaas* integration developed by Munthe–Kaas and Owren [1999]. This method approximates the $d\exp$ map by the first few terms of the Hausdorff formula and derives a numerical scheme similar to Runge-Kutta. This numerical scheme belongs to the general family of Lie integrators, where the integrated variables evolve naturally on their Lie group [Hairer, Lubich, and Wanner, 2002, §IV.8].

8.5 Representation with Quaternions

In three-dimensional space, the *unit quaternions* provide a well-suited representation for rotation. Numerical integration with quaternions has been used extensively in attitude dynamics and computer graphics and has several advantages, including ease of implementation, not

requiring transcendental functions, and not having singularities. All three-dimensional parameterizations (such as Euler angles, Euler-Rodrigues parameterizations, and Gibbs vectors using Cayley-Klein parameterizations) can become singular leading to *gimbal lock*. The main cost of using unit quaternions is the renormalization to maintain their unit norm. In the following, we describe the approach we have used to solve the equations (8.2.1) using unit quaternions in three-dimensional applications.

Define the referential and spatial quaternions,

$$\mathfrak{Q} = \begin{bmatrix} \mathfrak{Q}_s \\ \mathfrak{Q}_v \end{bmatrix}, \quad \text{and} \quad \mathfrak{q} = \begin{bmatrix} \mathfrak{q}_s \\ \mathfrak{q}_v \end{bmatrix}, \tag{8.5.1}$$

where, $\mathfrak{Q}_s$ and $\mathfrak{q}_s$ are the scalar (or real) component of the quaternions. Also, $\mathfrak{Q}_v$ and $\mathfrak{q}_v$ are the vector (or imaginary) part of the quaternions, represented by $\mathfrak{Q}_v = \mathfrak{Q}_v^1 i + \mathfrak{Q}_v^2 j + \mathfrak{Q}_v^3 k$ and $\mathfrak{q}_v = \mathfrak{q}_v^1 i + \mathfrak{q}_v^2 j + \mathfrak{q}_v^3 k$ where i, j and k are the fundamental quaternion units with the property $i^2 = j^2 = k^2 = ijk = -1$. The relation (8.5.1) is shown in matrix form, which can also be written as $\mathfrak{Q} = \mathfrak{Q}_s + \mathfrak{Q}_v$ and $\mathfrak{q} = \mathfrak{q}_s + \mathfrak{q}_v$. However, matrix notation is more useful in numerical implementation.

We assume $\mathfrak{Q}$ and $\mathfrak{q}$ are ***unit quaternions***. The unit quaternion implies the unit norms $\mathfrak{Q}^* \circ \mathfrak{Q} = 1$ and $\mathfrak{q}^* \circ \mathfrak{q} = 1$, where $\circ$ denotes the quaternionic product, and the quaternionic conjugates are $\mathfrak{Q}^* = \mathfrak{Q}_s - \mathfrak{Q}_v$ and $\mathfrak{q}^* = \mathfrak{q}_s - \mathfrak{q}_v$. Thus, the relations

$$\mathfrak{Q}_s^2 + \|\mathfrak{Q}_v\|^2 = 1, \quad \text{and} \quad \mathfrak{q}_s^2 + \|\mathfrak{q}_v\|^2 = 1,$$

constraint quaternions on the unit sphere $\mathbb{S}^3 \hookrightarrow \mathbb{R}^4$. Unit quaternions are homomorphic to the special unitary group $\mathrm{SU}(2)$, which itself is the covering group of the rotators $\mathbf{U}, \mathbf{u} \in \mathrm{SO}(3)$ (see e.g., [Altmann, 2005, §12.6]). For this reason, unit quaternions are referred to as ***versors*** that represent rotations in $\mathbb{R}^3$.

Also, define the referential and spatial ***pure quaternions***,

$$\mathfrak{W} = \begin{bmatrix} 0 \\ \vec{\boldsymbol{W}} \end{bmatrix}, \quad \text{and} \quad \mathfrak{w} = \begin{bmatrix} 0 \\ \vec{\boldsymbol{w}} \end{bmatrix}. \tag{8.5.2}$$

The scalar component of pure quaternions is zero. The imaginary part of quaternions are the pseudo-vectors of the referential and spatial inertial angular velocities $\vec{\boldsymbol{W}} := *\mathbf{W}^\flat$ and $\vec{\boldsymbol{w}} := *\mathbf{w}^\flat$ respectively, which we have defined in §8.2.

The attitude kinematics equations (8.2.1) can be reformulated in terms of quaternions as (see e.g., [Holm, 2011, §4.1.1])

$$\frac{D\mathfrak{Q}(t)}{dt} = \frac{1}{2}\mathfrak{W}(t) \circ \mathfrak{Q}(t), \qquad \mathfrak{Q}(t_0) = \begin{bmatrix} 1 \\ \mathbf{0} \end{bmatrix}, \tag{8.5.3a}$$

$$\frac{D\mathfrak{q}(t)}{dt} = \frac{1}{2}\mathfrak{w}(t) \circ \mathfrak{q}(t), \qquad \mathfrak{q}(t_0) = \begin{bmatrix} 1 \\ \mathbf{0} \end{bmatrix}. \tag{8.5.3b}$$

We can use the fact that the group of versors is homomorphic to the special unitary group SU(2) (see e.g., [Marsden and Ratiu, 1999, §9.2] or [Shuster, 1993, p. 477]) to represent the above equations with 2×2 complex matrices, or equivalently 4×4 real matrices as

$$\frac{D\mathfrak{Q}(t)}{dt} = \frac{1}{2}\mathbf{B}(\vec{\boldsymbol{W}}(t))\mathfrak{Q}(t), \qquad \mathfrak{Q}(t_0) = \begin{bmatrix}1\\ \mathbf{0}\end{bmatrix}, \tag{8.5.4a}$$

$$\frac{D\mathfrak{q}(t)}{dt} = \frac{1}{2}\boldsymbol{\beta}(\vec{\boldsymbol{w}}(t))\mathfrak{q}(t), \qquad \mathfrak{q}(t_0) = \begin{bmatrix}1\\ \mathbf{0}\end{bmatrix}, \tag{8.5.4b}$$

where the skew-symmetric matrices $\mathbf{B}$ and $\boldsymbol{\beta}$ are[3]

$$\mathbf{B}(\vec{\boldsymbol{W}}) = \begin{bmatrix}0 & -\vec{\boldsymbol{W}}^{\mathsf{T}}\\ \vec{\boldsymbol{W}} & \mathbf{W}^{\flat}\end{bmatrix}, \quad \text{and} \quad \boldsymbol{\beta}(\vec{\boldsymbol{w}}) = \begin{bmatrix}0 & -\vec{\boldsymbol{w}}^{\mathsf{T}}\\ \vec{\boldsymbol{w}} & \mathbf{w}^{\flat}\end{bmatrix}. \tag{8.5.5}$$

The set of ODEs in (8.5.4) are the evolution equations on the special unitary group SU(2). The Pauli spin matrices are a standard basis on SU(2). The group $\mathfrak{su}(2)$ is the Lie algebra of SU(2) and is isomorphic to $(\mathbb{R}^3,\times)$ with elements of pseudo-vectors $\vec{\boldsymbol{W}}$ or $\vec{\boldsymbol{w}}$. The advantage of (8.5.4) over (8.5.3) is that we now have *matrix* differential equations, which can be easily implemented for numerical computation.

For autonomous systems that $\vec{\boldsymbol{W}}$ and $\vec{\boldsymbol{w}}$ do not depend on time, the analytical solution can be obtained using the exponential map as

$$\mathfrak{Q}(t) = \exp\left(t\frac{1}{2}\mathbf{B}(\vec{\boldsymbol{W}})\right)\mathfrak{Q}(t_0), \tag{8.5.6a}$$

$$\mathfrak{q}(t) = \exp\left(t\frac{1}{2}\boldsymbol{\beta}(\vec{\boldsymbol{w}})\right)\mathfrak{q}(t_0). \tag{8.5.6b}$$

In contrast, for general time-dependent pseudo-vectors $\vec{\boldsymbol{W}}$ and $\vec{\boldsymbol{w}}$, the set of ODEs in (8.5.4) can be solved with a conventional integration scheme such as Runge-Kutta, provided that at each step the versors $\mathfrak{Q}$ and $\mathfrak{q}$ are normalized by projecting them onto $\mathbb{S}^3$. An alternative and more sophisticated numerical integration schemes are the geometric integrators given by Iserles, Munthe-Kaas, Nørsett, and Zanna [2000]. An example of such numerical schemes for integration of quaternions is the 3^{rd} order Crouch-Grossman integration method (see Andrle and Crassidis [2013]. A general discussion in this topic can be found in [Hairer, Lubich, and Wanner, 2002, §IV.8]).

Thus far in this chapter, we have presented the evolution equations for the rotator frames U and u of the Theorem 7.3.4. Recall that the differential equations of evolution are coupled.

[3] In standard literature such as Shuster [1993] or Crassidis and Junkins [2011], these matrices are denoted by Ω, however, we have reserved Ω for vorticity or symplectic form in Chapter 10. Moreover, the matrices $\mathbf{B}$ and $\boldsymbol{\beta}$ are essentially the same, but we distinguish them in notation to follow the upper case/lower case notation in this manuscript for referential and spatial variables.

This means to evolve other variables, like the position $\boldsymbol{x}$, or the eigenvalues Λ, the variables U and u in their matrix form should be known. If we use the quaternionic representation, in each numerical step, the versors $\mathfrak{Q}$ and $\mathfrak{q}$ should be converted back to the matrix rotations U and u to be used for other coupled equations, and vice-versa. To do so, the rotators U and u are related to versors $\mathfrak{Q}$ and $\mathfrak{q}$ by Euler-Rodrigues parameterization of the rotation matrix as

$$U(\mathfrak{Q}) = \Xi_+^\intercal(\mathfrak{Q})\Xi_-(\mathfrak{Q}), \quad \text{and} \quad u(\mathfrak{q}) = \xi_+^\intercal(\mathfrak{q})\xi_-(\mathfrak{q}), \tag{8.5.7}$$

where the matrices $\Xi_\pm$ and $\xi_\pm$ are defined as (see e.g., [Crassidis and Junkins, 2011, Appendix A.7] or [Shuster, 1993, p. 482])

$$\Xi_\pm(\mathfrak{Q}) \coloneqq \begin{bmatrix} \mathfrak{Q}_s I_{3\times 3} \pm [\mathfrak{Q}_v\times] \\ -\mathfrak{Q}_v^\intercal \end{bmatrix}, \quad \text{and} \quad \xi_\pm(\mathfrak{q}) \coloneqq \begin{bmatrix} \mathfrak{q}_s I_{3\times 3} \pm [\mathfrak{q}_v\times] \\ -\mathfrak{q}_v^\intercal \end{bmatrix}. \tag{8.5.8}$$

The skew-symmetric matrices $[\mathfrak{Q}_v\times]$ and $[\mathfrak{q}_v\times]$ are indeed the spinors of pseudo-vectors $\mathfrak{Q}_v$ and $\mathfrak{q}_v$. In other words, they are the Hodge dual of $\mathfrak{Q}_v$ and $\mathfrak{q}_v$ respectively. In matrix form, this means

$$[\mathfrak{Q}_v\times] \coloneqq *\mathfrak{Q}_v = \begin{bmatrix} 0 & -\mathfrak{Q}_v^3 & \mathfrak{Q}_v^2 \\ \mathfrak{Q}_v^3 & 0 & -\mathfrak{Q}_v^1 \\ -\mathfrak{Q}_v^2 & \mathfrak{Q}_v^1 & 0 \end{bmatrix}, \tag{8.5.9a}$$

and

$$[\mathfrak{q}_v\times] \coloneqq *\mathfrak{q}_v = \begin{bmatrix} 0 & -\mathfrak{q}_v^3 & \mathfrak{q}_v^2 \\ \mathfrak{q}_v^3 & 0 & -\mathfrak{q}_v^1 \\ -\mathfrak{q}_v^2 & \mathfrak{q}_v^1 & 0 \end{bmatrix}. \tag{8.5.9b}$$

In the above, the Hodge star operator is the isomorphism $* : \bigwedge^1(\mathscr{P}) \to \bigwedge^2(\mathscr{P})$ where $\mathscr{P}$ is either of $\mathscr{P}_{t_0}$ or $\mathscr{P}_t$ (also compare with the Hodge star operator in §8.2). The inverse transformation from rotators U and u to the versors $\mathfrak{Q}$ and $\mathfrak{q}$ is given by (see Kuipers [2002] or [Diebel, 2006])

$$4(\mathfrak{Q}_s)^2 = 1 + U^1{}_1 + U^2{}_2 + U^3{}_3, \qquad 4(\mathfrak{q}_s)^2 = 1 + u^1{}_1 + u^2{}_2 + u^3{}_3, \tag{8.5.10a}$$
$$4(\mathfrak{Q}_v^1)^2 = 1 + U^1{}_1 - U^2{}_2 - U^3{}_3, \qquad 4(\mathfrak{q}_v^1)^2 = 1 + u^1{}_1 - u^2{}_2 - u^3{}_3, \tag{8.5.10b}$$
$$4(\mathfrak{Q}_v^2)^2 = 1 - U^1{}_1 + U^2{}_2 - U^3{}_3, \qquad 4(\mathfrak{q}_v^2)^2 = 1 - u^1{}_1 + u^2{}_2 - u^3{}_3, \tag{8.5.10c}$$
$$4(\mathfrak{Q}_v^3)^2 = 1 - U^1{}_1 - U^2{}_2 + U^3{}_3, \qquad 4(\mathfrak{q}_v^3)^2 = 1 - u^1{}_1 - u^2{}_2 + u^3{}_3. \tag{8.5.10d}$$

Other alternative solutions to the quaternions exist. For instance, from the trace and also the off-diagonal elements of U in (8.5.7) along with the unit norm constraint $\mathfrak{Q}^* \circ \mathfrak{Q} =$

$(\mathfrak{Q}_s)^2 + (\mathfrak{Q}_v^1)^2 + (\mathfrak{Q}_v^2)^2 + (\mathfrak{Q}_v^3)^2 = 1$ we can obtain the *Grubin's solution* for the four components of $\mathfrak{Q}$, namely

$$\begin{aligned}\mathfrak{Q}_s &= \pm\frac{1}{2}\sqrt{1 + \operatorname{trace}(U)},\\ \mathfrak{Q}_v^i &= \frac{1}{4\mathfrak{Q}_s}\epsilon^{ijk}U_{jk}, \qquad i = 1,2,3.\end{aligned}$$

A similar relation can be expressed between $\mathfrak{q}$ and u. In above, ϵ is the Levi-Civita's permutation symbol. The twofold ambiguity in the sign of $\mathfrak{Q}$ represents the same rotation. For certain rotation matrices, the above method might be singular or might not have a real answer. To avoid such issues, stable and singularity-free methods were developed, such as *Shepperd's algorithm* by Shepperd [1978] and its modification by Markley [2008].

8.6 Representation with Euler Angles

The Euler parameterization is another trivialization map and relates the rotation matrix to Euler angles. Such parameterization can become singular for $n = 3$ and is not privileged over the other methods. However, in $n = 2$, the Euler parameterization is a smooth map from $\mathrm{SO}(2)$ to $\mathbb{S}^1$, and the Lie algebra can be represented by a single variable since $\dim(\mathfrak{so}(2)) = 1$. Here, we present the evolution equations of rotator frames by Euler angles.

Let the *pseudo-scalars* $\mathring{\Theta}, \mathring{\theta} \in \mathbb{S}^1$ denote the Euler rotation angles for Lie algebra of referential and spatial configurations.[4] Using the Hodge star operator, define

$$\Theta(t) \coloneqq *\mathring{\Theta}(t) = \begin{bmatrix} 0 & -\mathring{\Theta}(t) \\ \mathring{\Theta}(t) & 0 \end{bmatrix}, \qquad \theta(t) \coloneqq *\mathring{\theta}(t) = \begin{bmatrix} 0 & -\mathring{\theta}(t) \\ \mathring{\theta}(t) & 0 \end{bmatrix}. \tag{8.6.1}$$

By using the exponential map $\exp : \mathfrak{so}(2) \to \mathrm{SO}(2)$, the rotators (on Lie group $\mathrm{SO}(2)$) are expressed by the Euler angles (on Lie algebra $\mathfrak{so}(2)$) as

$$U = \exp(\Theta(t))U_0, \quad \text{and} \quad u = \exp(\theta(t))u_0.$$

by applying the chain rule to (8.2.1), the attitude kinematics can be written as

$$W = \frac{DU}{dt}U^{\mathsf{T}} = \frac{D\Theta(t)}{dt}, \tag{8.6.2a}$$

$$w = \frac{Du}{dt}u^{\mathsf{T}} = \frac{D\theta(t)}{dt}. \tag{8.6.2b}$$

[4] We denote pseudo-scalars with a circle above the variable.

The non-zero components of the above equations are

$$\frac{D\mathring{\Theta}(t)}{dt} = W^2{}_1(t), \qquad \mathring{\Theta}(t_0) = 0, \tag{8.6.3a}$$

$$\frac{D\mathring{\theta}(t)}{dt} = w^2{}_1(t), \qquad \mathring{\theta}(t_0) = 0. \tag{8.6.3b}$$

These relations represent the kinematics of rotation in two-dimensional Euclidean space. In the next chapter, we extend these equations to Riemannian 2-manifolds.

Chapter 9

Reduction on Two-Dimensional Manifolds

9.1 Introduction

In Chapter 8 we have seen that the presence of symmetry allows us to represent the evolution equations on the Lie algebras, leading to the dimensionality reduction of evolution equations. Of particular interests are 2-manifolds where rotation is represented by the Euler angles in $\mathrm{SO}(2)$. Contrary to Chapter 8, here, we present a non-Euclidean formulation on $\mathrm{SO}(2)$.

As we have seen in §8.6, the evolution equations of eigenvector frames consist of two groups of related variables, (a) the Euler angles θ and Θ (variables on Lie algebra), and (b) their rotator matrices u and U (variables on Lie group). The numerical computation of ODEs requires the conversion between these variables back and forth. In this chapter, we derive rate equations that are exclusively depended on the Euler angles θ and Θ without a need to convert them to rotator matrices. These equations reduce computational costs since they shortcut several matrix multiplications.

In our formulations, we also address the role of the Riemannian metric in the evolution equations and introduced the concept of *induced vorticity*. We will show that a non-isothermal metric induces a vorticity in addition to the vorticity due to the flow itself. The induced vorticity is interpreted by the skewness of a non-isothermal coordinate system.

Recall that the rate of deformation tensor $\mathbf{d}$ and vorticity ω depend on the connection. Throughout this chapter, it is assumed the connection on the vector bundle is trivial. Thus, the metric tensor is not necessarily a parallel section, and the rate of metric tensor appears in the evolution equations. By defining new variables that absorb the influence of metric tensor into the rate of deformation and vorticity, we have introduced the *Euclidean equivalence* of the rate of deformation and vorticity. When these new variables are employed, the evolution equations simplify as if they are written in Euclidean space.

9.2 Symmetry Reduction of Evolution Equations

Let $u, U \in \mathrm{GL}(2,\mathbb{R})$ denote 2×2 rotation matrices of the referential and spatial eigenvector frames. Recall from Proposition 7.3.2 that we defined the pullback metrics $\hat{G} = U^* G U$ and $\hat{g} = u^* g u$. Later in Theorem 7.3.4, we have identified them as $\hat{G} = \hat{I}$ and $\hat{g} = \hat{\imath}$ where $\hat{I}$ and $\hat{\imath}$ are referential and spatial identity matrices respectively. The relations $U^* G U = \hat{I}$ and $u^* g u = \hat{\imath}$ indicate that

$$G^{-\frac{1}{2}} U \in \mathrm{SO}(2), \quad \text{and} \quad g^{-\frac{1}{2}} u \in \mathrm{SO}(2).$$

In other words, using the exponential map $\exp\colon \mathfrak{so}(2) \to \mathrm{SO}(2)$,

$$U = G^{-\frac{1}{2}} e^{J\Theta}, \quad \text{and} \quad u = g^{-\frac{1}{2}} e^{J\theta}, \tag{9.2.1}$$

where the matrix $J \coloneqq \begin{bmatrix} 0 & 1 \\ -1 & 0 \end{bmatrix}$ is the standard complex structure[1] on tangent bundle $T\mathscr{P}_t$, and $e^{J\Theta}, e^{J\theta} \in \mathrm{SO}(2)$ are unitary matrices. Indeed, $\Theta, \theta \in \mathfrak{so}(2) \cong \mathbb{S}^1$ are the *Euler angles* for referential and spatial eigenvector frames on the Lie algebra. We aim to replace u and U in evolution equations of Theorem 7.3.4 with the Lie algebra variables Θ and θ.

We wish to take the time rate of (9.2.1) to derive their kinematics equations. To do so, we need to compute the derivative $Dg^{\frac{1}{2}}/dt$. To explicitly derive this quantity, one may attempt to take the derivative of $g^{\frac{1}{2}} g^{\frac{1}{2}} = g$ by

$$g^{\frac{1}{2}} \frac{Dg^{\frac{1}{2}}}{dt} + \frac{Dg^{\frac{1}{2}}}{dt} g^{\frac{1}{2}} = \frac{Dg}{dt}, \tag{9.2.2}$$

where $Dg^{\frac{1}{2}}/dt$ is the unknown variable and the other terms (i.e., $g^{\frac{1}{2}}$ and Dg/dt) are known. Equation (9.2.2) is the ***Sylvester's equation*** of type $AX + XA = B$ where $A = g^{\frac{1}{2}}$ and $B = Dg/dt$ and known matrices, and the algebraic equation is solved for the unknown $X = Dg^{\frac{1}{2}}/dt$. Usually, the Sylvester equation is solved by *vectorization* of the matrix equation (see for instance [Hogben, 2006, §57.4]). Unfortunately, such a component-wise approach is not desirable for our purpose since it does not provide us with an explicit solution for the unknown $Dg^{\frac{1}{2}}/dt$. To circumvent this issue, in the following Lemma we express the derivative of $g^{\frac{1}{2}}$ with a different approach and in terms of a useful variable, ζ, that will be interpreted later.

Lemma 9.2.1 (Decomposition of rate of square-root matrices). *Let $g = [g_{ij}] \in \mathrm{C}^1(\mathbb{R}^{2\times 2})$ for $i, j = 1, 2$ be any symmetric positive-definite matrix, therefore, its square root exists. The matrix $g^{\frac{1}{2}} \dfrac{Dg^{\frac{1}{2}}}{dt}$ is then decomposed into its symmetric and skew-symmetric parts by*

$$g^{\frac{1}{2}} \frac{Dg^{\frac{1}{2}}}{dt} = \frac{1}{2}\frac{Dg}{dt} + \zeta J, \tag{9.2.3}$$

[1] The symbol J in this chapter is exclusively used for the standard complex structure, and should not be confused with the Jacobian, J, given in §4.4.

where $J \coloneqq \begin{bmatrix} 0 & 1 \\ -1 & 0 \end{bmatrix}$ *is the standard complex structure and* $\zeta(g) \in \mathrm{C}^1(\mathbb{R})$ *is given by*

$$\zeta(g) \coloneqq \frac{1}{2\left(\mathrm{trace}(g) + 2\sqrt{\det(g)}\right)}\left(\left(g_{11} - g_{22}\right)\frac{Dg_{12}}{dt} - g_{12}\frac{D\left(g_{11} - g_{22}\right)}{dt}\right). \tag{9.2.4}$$

Proof. Since g is symmetric positive-definite, the spectral decomposition of g indicates that $g^{\frac{1}{2}}$ is also symmetric positive-definite. Taking the derivative of $g = g^{\frac{1}{2}}g^{\frac{1}{2}}$ gives

$$\begin{aligned}\frac{Dg}{dt} &= g^{\frac{1}{2}}\frac{Dg^{\frac{1}{2}}}{dt} + \frac{Dg^{\frac{1}{2}}}{dt}g^{\frac{1}{2}} \\ &= g^{\frac{1}{2}}\frac{Dg^{\frac{1}{2}}}{dt} + \left(g^{\frac{1}{2}}\frac{Dg^{\frac{1}{2}}}{dt}\right)^{*}.\end{aligned}$$

The star $(*)$ denotes the Hermitian adjoint, which here is simply the transpose of a matrix. From the relation (9.2.2) observe that $\frac{1}{2}\frac{Dg}{dt}$ is the symmetric part of equation (9.2.3). The skew-symmetric part of a 2×2 matrix can be represented with skew-symmetric matrix ζJ as

$$\begin{aligned}2\zeta J &= g^{\frac{1}{2}}\frac{Dg^{\frac{1}{2}}}{dt} - \left(g^{\frac{1}{2}}\frac{Dg^{\frac{1}{2}}}{dt}\right)^{*} \\ &= g^{\frac{1}{2}}\frac{Dg^{\frac{1}{2}}}{dt} - \frac{Dg^{\frac{1}{2}}}{dt}g^{\frac{1}{2}}.\end{aligned} \tag{9.2.5}$$

Denote the components of the symmetric matrix $g^{\frac{1}{2}}$ by $g^{\frac{1}{2}} = [\alpha_{ij}]$ where $\alpha_{12} = \alpha_{21}$. By construction, the non-zero component of equation (9.2.5) is given in terms of α_{ij} as

$$2\zeta = \left(\alpha_{11} - \alpha_{22}\right)\frac{D\alpha_{12}}{dt} - \alpha_{12}\frac{D(\alpha_{11} - \alpha_{22})}{dt}.$$

By an elementary trick, one can rewrite the right-hand side of the above equation in the following form,

$$2\zeta = \frac{1}{\left(\alpha_{11} + \alpha_{22}\right)^2}\left(\left(\alpha_{11}^2 - \alpha_{22}^2\right)\frac{D}{dt}\left(\alpha_{12}\left(\alpha_{11} + \alpha_{22}\right)\right) - \alpha_{12}\left(\alpha_{11} + \alpha_{22}\right)\frac{D}{dt}\left(\alpha_{11}^2 - \alpha_{22}^2\right)\right).$$

We avoid computing the square root of g directly, i.e., the components α_{ij}. Instead, it is preferable to represent the above equation in terms of the known matrix g_{ij}. By construction of matrices $g^{\frac{1}{2}}g^{\frac{1}{2}} = g$ in their components form, we obtain three relations,

$$\begin{aligned}\alpha_{11}^2 + \alpha_{12}^2 &= g_{11}, \\ \alpha_{12}^2 + \alpha_{22}^2 &= g_{22}, \\ \alpha_{12}\left(\alpha_{11} + \alpha_{22}\right) &= g_{12}.\end{aligned}$$

Subtracting the first two relations yield $\alpha_{11}^2 - \alpha_{22}^2 = g_{11} - g_{22}$. Moreover, $\alpha_{11} + \alpha_{22} = \operatorname{trace}(g^{\frac{1}{2}})$. Hence,

$$2\zeta = \frac{1}{\left(\operatorname{trace}(g^{\frac{1}{2}})\right)^2}\left(\left(g_{11} - g_{22}\right)\frac{Dg_{12}}{dt} - g_{12}\frac{D\left(g_{11} - g_{22}\right)}{dt}\right).$$

Now we relate the trace of $g^{\frac{1}{2}}$ with the invariants of g. Suppose α_1 and α_2 are eigenvalues of $g^{\frac{1}{2}}$ (note, α_{ij} indicates the components of the matrix $g^{\frac{1}{2}}$, while α_i denotes its eigenvalues). Therefor α_1^2 and α_2^2 are eigenvalues of g, also $\det(g) = \alpha_1^2\alpha_2^2$ and $\operatorname{trace}(g) = \alpha_1^2 + \alpha_2^2$. The elementary identity $(\alpha_1 + \alpha_2)^2 = \left(\alpha_1^2 + \alpha_2^2\right) + 2\alpha_1\alpha_2$ reads as

$$\left(\operatorname{trace}(g^{\frac{1}{2}})\right)^2 = \operatorname{trace}(g) + 2\sqrt{\det(g)},$$

and concludes the proof. ∎

Now we present Proposition 9.2.2 and Proposition 9.2.4 respectively for the evolution equation of u and U in terms of Euler angles θ and Θ.

Proposition 9.2.2 (Evolution of spatial eigenvectors frame on metric 2-manifolds). *Suppose on the two-dimensional configuration space the hypotheses of the Theorem 7.3.4 holds. Let $u \in \mathrm{GL}(2,\mathbb{R})$ denote the matrix of the left eigenvectors frame. Then, $u = g^{-\frac{1}{2}}e^{J\theta}$ where the evolution equation of the Euler angle $\theta(\boldsymbol{x}, t)$ is given by*

$$\frac{D\theta}{dt} = \frac{\omega_{12}^\flat + \zeta}{\sqrt{\det(g)}} + \left(\frac{\Lambda_2 + \Lambda_1}{\Lambda_2 - \Lambda_1}\right)\left[e^{-J\theta}g^{-\frac{1}{2}}\left(d^\flat + \frac{1}{2}\frac{Dg}{dt}\right)g^{-\frac{1}{2}}e^{J\theta}\right]_{12}, \qquad \theta(\boldsymbol{X}, t_0) = \theta_0. \quad (9.2.6)$$

In our notation above, $[\cdot]_{12}$ indicates the component $(1,2)$ of the matrix inside the bracket. The matrix

$$\omega^\flat = g\omega = \frac{1}{2}\left(l^\flat - l^{\flat *}\right),$$

is the associated spin, where $l^\flat = gl$ and $l = \dfrac{\partial v}{\partial \boldsymbol{x}}$. Also, $\theta_0 \in \mathbb{S}^1$ is the initial condition and $\dfrac{Dg}{dt} = \dfrac{\partial g}{\partial \boldsymbol{x}^k}v^k$ is the rate of the Riemannian metric.

Proof. From the equation (9.2.1) the Hermitian adjoint of u is $u^* = e^{-J\theta}g^{-\frac{1}{2}}$. Recall from our notation in Proposition 7.3.2 that $f^\flat := \dfrac{\partial g}{\partial \boldsymbol{x}^k}v^k = \dfrac{Dg}{dt}$. From Theorem 7.3.4 we calculate $\hat{f}$, $\hat{d}$,

and $\hat{\omega}$ by

$$\hat{f} = u^* \frac{Dg}{dt} u = \left(e^{-J\theta} g^{-\frac{1}{2}}\right) \frac{Dg}{dt} \left(g^{-\frac{1}{2}} e^{J\theta}\right), \tag{9.2.7a}$$

$$\hat{d} = u^* d^\flat u = \left(e^{-J\theta} g^{-\frac{1}{2}}\right) d^\flat \left(g^{-\frac{1}{2}} e^{J\theta}\right), \tag{9.2.7b}$$

$$\hat{\omega} = u^* \omega^\flat u = \left(e^{-J\theta} g^{-\frac{1}{2}}\right) \omega^\flat \left(g^{-\frac{1}{2}} e^{J\theta}\right) = \frac{\omega_{12}^\flat}{\sqrt{\det(g)}} J. \tag{9.2.7c}$$

It is straightforward to obtain (9.2.7a) and (9.2.7b). The relation (9.2.7c) is derived as follows. First, recall from Remark 7.3.8 that both $\omega^\flat$ and $\hat{\omega}$ are skew-symmetric. We express the skew-symmetric matrix $\omega^\flat = \omega_{12}^\flat J$, where $\omega_{12}^\flat$ is the non-zero component of the 2×2 matrix $\omega^\flat$. By matrix construction, we can show that[2]

$$g^{-\frac{1}{2}} J g^{-\frac{1}{2}} = \det(g^{-\frac{1}{2}}) J = \frac{1}{\sqrt{\det(g)}} J. \tag{9.2.8}$$

In addition, since $J = e^{J\frac{\pi}{2}}$, it holds

$$e^{-J\theta} J e^{J\theta} = e^{-J\theta} e^{J\frac{\pi}{2}} e^{J\theta} = e^{J\frac{\pi}{2}} = J. \tag{9.2.9}$$

Putting (9.2.8) and (9.2.9) together, we obtain $\hat{\omega} = \dfrac{\omega_{12}^\flat}{\sqrt{\det(g)}} J$ that is given in (9.2.7c).

Now, we obtain an expression for the angular velocity matrix $\hat{w}$. By its definition from equation (6.4.1d), we obtain

$$\begin{aligned} \hat{w} = u^{-1} \frac{Du}{dt} &= \left(e^{-J\theta} g^{\frac{1}{2}}\right) \left(\frac{D\left(g^{-\frac{1}{2}}\right)}{dt} e^{J\theta} + g^{-\frac{1}{2}} e^{J\theta} \frac{D\theta}{dt} J \right) \\ &= e^{-J\theta} g^{\frac{1}{2}} \frac{D\left(g^{-\frac{1}{2}}\right)}{dt} e^{J\theta} + \frac{D\theta}{dt} J. \end{aligned} \tag{9.2.10}$$

Taking the material time derivative of $g^{\frac{1}{2}} g^{-\frac{1}{2}} = \mathrm{id}$ yields

$$g^{\frac{1}{2}} \frac{D\left(g^{-\frac{1}{2}}\right)}{dt} = -\frac{Dg^{\frac{1}{2}}}{dt} g^{-\frac{1}{2}} = -g^{-\frac{1}{2}} \left(g^{\frac{1}{2}} \frac{Dg^{\frac{1}{2}}}{dt}\right) g^{-\frac{1}{2}}. \tag{9.2.11}$$

[2]For any 2×2 symmetric matrix A, it holds $AJA = \det(A) J$.

We substitute the relation (9.2.11) into (9.2.10). Also, from Lemma 9.2.1 we use the decomposition of $g^{\frac{1}{2}}\frac{Dg^{\frac{1}{2}}}{dt}$. All together gives

$$\begin{aligned}\hat{w} &= -e^{-J\theta}g^{-\frac{1}{2}}\left(g^{\frac{1}{2}}\frac{Dg^{\frac{1}{2}}}{dt}\right)g^{-\frac{1}{2}}e^{J\theta} + \frac{D\theta}{dt}J \\ &= -\frac{1}{2}e^{-J\theta}g^{-\frac{1}{2}}\frac{Dg}{dt}g^{-\frac{1}{2}}e^{J\theta} - \zeta e^{-J\theta}g^{-\frac{1}{2}}Jg^{-\frac{1}{2}}e^{J\theta} + \frac{D\theta}{dt}J \\ &= -\frac{1}{2}\hat{f} - \frac{\zeta}{\sqrt{\det(g)}}J + \frac{D\theta}{dt}J. \end{aligned} \tag{9.2.12}$$

In the second line above, the first term is replaced with $\hat{f}$ from equation (9.2.7a). Also in the second term of the second line above, we have substituted both relations (9.2.8), and (9.2.9). In components, equation (9.2.12) reads as

$$\hat{w} = \begin{bmatrix} -\frac{1}{2}\hat{f}^1_{\ 1} & -\frac{1}{2}\hat{f}^1_{\ 2} - \frac{\zeta}{\sqrt{\det(g)}} + \frac{D\theta}{dt} \\ -\frac{1}{2}\hat{f}^2_{\ 1} + \frac{\zeta}{\sqrt{\det(g)}} - \frac{D\theta}{dt} & -\frac{1}{2}\hat{f}^2_{\ 2} \end{bmatrix}. \tag{9.2.13}$$

We compare the $\hat{w}$ obtained in (9.2.13) with $\hat{w}$ in Theorem 7.3.4. From equation (7.3.11b) we have

$$\hat{w} = \begin{bmatrix} -\frac{1}{2}\hat{f}^1_{\ 1} & \hat{\omega}^1_{\ 2} + \left(\frac{\Lambda_2+\Lambda_1}{\Lambda_2-\Lambda_1}\right)\hat{d}^1_{\ 2} + \left(\frac{\Lambda_1}{\Lambda_2-\Lambda_1}\right)\hat{f}^1_{\ 2} \\ \hat{\omega}^2_{\ 1} + \left(\frac{\Lambda_1+\Lambda_2}{\Lambda_1-\Lambda_2}\right)\hat{d}^2_{\ 1} + \left(\frac{\Lambda_2}{\Lambda_2-\Lambda_2}\right)\hat{f}^2_{\ 1} & -\frac{1}{2}\hat{f}^2_{\ 2} \end{bmatrix}. \tag{9.2.14}$$

It can be seen that the diagonal components of $\hat{w}$ between equations (9.2.13) and (9.2.14) are the same. It suffices to only compare the off-diagonal component $\hat{w}^1_{\ 2}$ between the two relations (9.2.13) and (9.2.14). Substituting $\hat{f}^1_{\ 2}$, $\hat{d}^1_{\ 2}$, and $\hat{\omega}^1_{\ 2}$ from equations (9.2.7) and solving for $\frac{D\theta}{dt}$ yields

$$\begin{aligned}\frac{D\theta}{dt} &= \hat{\omega}^1_{\ 2} + \frac{\zeta}{\sqrt{\det(g)}} + \left(\frac{\Lambda_2+\Lambda_1}{\Lambda_2-\Lambda_2}\right)\hat{d}^1_{\ 2} + \left(\frac{\Lambda_1}{\Lambda_2-\Lambda_1}\right)\hat{f}^1_{\ 2} + \frac{1}{2}\hat{f}^1_{\ 2} \\ &= \frac{\omega^\flat_{12}+\zeta}{\sqrt{\det(g)}} + \left(\frac{\Lambda_2+\Lambda_1}{\Lambda_2-\Lambda_1}\right)\left[e^{-J\theta}g^{-\frac{1}{2}}\left(d^\flat + \frac{1}{2}\frac{Dg}{dt}\right)g^{-\frac{1}{2}}e^{J\theta}\right]_{12}. \end{aligned}$$

Note that comparing $\hat{w}^2_{\ 1}$ between equations (9.2.13) and (9.2.14) also leads to the same result. ■

Remark 9.2.3 (Vorticity on metric 2-manifolds). $\omega^\flat_{12}$ can be represented in terms of components of the metric g and the velocity gradient $\dfrac{\partial v}{\partial x}$ as

$$\omega^\flat_{12} = g_{11}\frac{\partial v^1}{\partial x^2} - g_{22}\frac{\partial v^2}{\partial x^1} + g_{12}\left(\frac{\partial v^2}{\partial x^2} - \frac{\partial v^1}{\partial x^1}\right).$$

In matrix form, we can write $\omega^\flat = \omega^\flat_{12} J$. As a tensor, $\boldsymbol{\omega}^\flat$ is given by the 2-form

$$\boldsymbol{\omega}^\flat = \omega^\flat_{12}\ \left(\mathrm{d}x^1 \wedge \mathrm{d}x^2\right) \in \Omega^2\left(\mathscr{P}_t\right),$$

and represents the skew-symmetric associated spin tensor $\boldsymbol{\omega}^\flat = \mathbf{g}\boldsymbol{\omega}$. Indeed, $\omega^\flat_{12}$ is the ***vorticity*** of the two-dimensional flow for the metric $\mathbf{g}$ and the trivial connection. ▲

Proposition 9.2.4 (Evolution of referential eigenvectors frame on metric 2-manifolds). *Suppose on the two-dimensional configuration space, the hypotheses of the Theorem 7.3.4 holds. Let $U \in \mathrm{GL}(2,\mathbb{R})$ denote the matrix of the right eigenvectors frame. Then, $U = G^{-\frac{1}{2}} e^{J\Theta}$ where the evolution of Euler angle $\Theta(\boldsymbol{X}, t)$ is given by*

$$\frac{D\Theta}{dt} = \left(\frac{2\sqrt{\Lambda_1\Lambda_2}}{\Lambda_2 - \Lambda_1}\right)\left[e^{-J\theta} g^{-\frac{1}{2}}\left(d^\flat + \frac{1}{2}\frac{Dg}{dt}\right) g^{-\frac{1}{2}} e^{J\theta}\right]_{12}, \qquad \Theta(\boldsymbol{X}, t_0) = \Theta_0, \tag{9.2.15}$$

In our notation above, $[\cdot]_{12}$ indicates the $(1,2)$ component of the matrix inside the bracket, and $\Theta_0 \in \mathbb{S}^1$ is an arbitrary initial condition.

Proof. From equation (9.2.1) we have $U^{-1} = e^{-J\Theta} G^{\frac{1}{2}}$. By the definition of $\hat{W}$ from equation (6.4.1c) and using the fact that $\dfrac{DG}{dt} = 0$ we obtain

$$\hat{W} = U^{-1}\frac{DU}{dt} = \left(e^{-J\Theta} G^{\frac{1}{2}}\right) G^{-\frac{1}{2}} e^{J\Theta}\frac{D\Theta}{dt} J = \frac{D\Theta}{dt} J. \tag{9.2.16}$$

On the other hand, $\hat{W}$ in equation 7.3.11a of the Theorem 7.3.4 is

$$\hat{W} = \begin{bmatrix} 0 & \left(\dfrac{\sqrt{\Lambda_1\Lambda_2}}{\Lambda_2 - \Lambda_1}\right)\left(2\hat{d}^1{}_2 + \hat{f}^1{}_2\right) \\ -\left(\dfrac{\sqrt{\Lambda_1\Lambda_2}}{\Lambda_2 - \Lambda_1}\right)\left(2\hat{d}^1{}_2 + \hat{f}^1{}_2\right) & 0 \end{bmatrix}. \tag{9.2.17}$$

Comparing the component $\hat{W}^1{}_2$ of equations (9.2.16) and 9.2.17 and substituting $\hat{d}^1{}_2$ and $\hat{f}^1{}_2$ from equations (9.2.7) in the proof of Proposition 9.2.2 solves for material rate of Θ by

$$\begin{aligned}\frac{D\Theta}{dt} &= \left(\frac{\sqrt{\Lambda_1\Lambda_2}}{\Lambda_2 - \Lambda_1}\right)\left(2\hat{d}^1{}_2 + \hat{f}^1{}_2\right) \\ &= \left(\frac{2\sqrt{\Lambda_1\Lambda_2}}{\Lambda_2 - \Lambda_1}\right)\left[e^{-J\theta} g^{-\frac{1}{2}}\left(d^\flat + \frac{1}{2}\frac{Dg}{dt}\right) g^{-\frac{1}{2}} e^{J\theta}\right]_{12}.\end{aligned}$$

■

9.3 Effect of Riemannian Metric on Deformation

In this section, we define quantities that allow us to interpret the effect of the Riemannian metric on the evolution of nonlinear deformation of the flow. In the end, we restate the previous derivations in terms of newer quantities in a theorem.

A Riemannian manifold is characterized by metric tensor $\mathbf{g}$. However, as we have seen in the previous section, in the evolution equations of deformation of flow on the manifold, the geometry of Riemannian manifolds is characterized by the role of matrix $g^{\frac{1}{2}}\frac{Dg^{\frac{1}{2}}}{dt}$ rather than only g. In this section, we will explore the role of matrix $g^{\frac{1}{2}}\frac{Dg^{\frac{1}{2}}}{dt}$ in more detail.

Definition 9.3.1. *We define the **metric velocity gradient** by*

$$l_g \coloneqq l + g^{-\frac{1}{2}}\frac{Dg^{\frac{1}{2}}}{dt}. \tag{9.3.1a}$$

Similar to Euler-Cauchy-Stokes decomposition in Definition 4.5.3, we define the symmetric and skew-symmetric parts of the above by

$$d_g \coloneqq \frac{1}{2}\left(l_g + l_g^\intercal\right) = d + \frac{1}{2}g^{-1}\frac{Dg}{dt}, \tag{9.3.1b}$$

$$\omega_g \coloneqq \frac{1}{2}\left(l_g - l_g^\intercal\right) = \omega + \zeta g^{-1}J. \tag{9.3.1c}$$

▲

Recall from Proposition 4.5.2 that in metric space the transposition is given by $l_g^\intercal = g^{-1}l_g^* g$. By using $l^\flat = gl$, the above definitions can be written as

$$l_g^\flat = g l_g = l^\flat + g^{\frac{1}{2}}\frac{Dg^{\frac{1}{2}}}{dt}, \tag{9.3.2a}$$

$$d_g^\flat = g d_g = d^\flat + \frac{1}{2}\frac{Dg}{dt}, \tag{9.3.2b}$$

$$\omega_g^\flat = g\omega_g = \omega^\flat + \zeta J = \left(\omega_{12}^\flat + \zeta\right)J. \tag{9.3.2c}$$

By applying the above definition into Proposition 9.2.2 and Proposition 9.2.4, we can observe that the symmetric and skew-symmetric parts of $g^{-\frac{1}{2}}\frac{Dg^{\frac{1}{2}}}{dt}$ respectively contribute to the rate of deformation and rotation (vorticity). Such an effect of the symmetric Riemannian metric g is hidden without deriving direct evolution equations for spectral information of the deformation tensors. Therefore, in the presence of metric g, the matrix $d_g^\flat$ acts as a replacement to $d^\flat$, similarly, $\omega_g^\flat$ acts as a replacement to $\omega^\flat$. In other words, the *effective vorticity* on the Riemannian manifold is $\omega_{12}^\flat + \zeta$.

Definition 9.3.2. *We define the* ***induced rate of deformation*** *by* $\frac{1}{2}\frac{Dg}{dt}$ *and* ***induced vorticity*** *by* ζ *due to the motion on a metric space.* ▲

The induced vorticity can be interpreted as follows. Observe from (9.2.4) that the induced vorticity ζ exists if and only if g is not an isothermal metric. We remind the reader that a metric tensor is isothermal if g is a scalar multiple of the identity metric. On a 2-manifold, it means $g_{11} = g_{22}$ and $g_{12} = g_{21} = 0$. In a non-isothermal coordinate system, the coordinates are *skewed* in the sense that lengths and angles between pairs of the basis vectors are not identical. When a flow is parameterized in such a coordinate system, the skewness of the coordinate system is perceived as if there exists the vorticity ζ. This effect is in addition to the vorticity $\omega^{\flat}_{12}$ due to the velocity vector field $\boldsymbol{v}$ itself.

From another perspective, the vorticity tensor $\boldsymbol{\omega}$ and the rate of deformation tensor $\mathbf{d}$ are not unique since they depend on the connection of the tangent bundle. We remind the reader that in this chapter we have assumed the connection is trivial. By this assumption, for instance, the matrix of the rate of deformation gradient is written as $l^a{}_b = v^a{}_{|b} = \partial v^a/\partial x^b$ without the Christoffel symbols. Also, for a trivial connection, the metric tensor is not necessarily a parallel section, i.e., $\nabla\mathbf{g}$ might not vanish. The non-vanishing $\nabla\mathbf{g}$ tensor appears in the evolution equations of deformation tensors that we have derived in Chapter 4. However, our formulations for the evolution equations of eigenvalues and eigenvectors in Chapter 7 and the subsequent chapters are intrinsic and independent of the connection. It means that even if we use a metric connection (such as Levi-Civita connection), the contribution of the metric tensor still appears as the induced vorticity ζ that we have encountered here.

9.4 Euclidean Equivalence of Deformation on 2-Manifolds

So far in this chapter, we have derived evolution equations for the eigenvectors (Euler angles) of a flow on a Riemannian 2-manifold. In our formulations, we assumed the connection is trivialized. The trivial connection is a natural choice when the manifold is a Euclidean space with the Cartesian coordinate system. On the other hand, if the metric g is an identity matrix representing the Euclidean space, then the evolution equations are in their simplest form. But, when g is nontrivial, it is desirable to reformulate the evolution equations so that they look like as they are equations in the Euclidean space. That is, here, we aim to define new variables so that they absorb the Riemannian metric. Specifically, we define the *Euclidean equivalence* of the velocity gradient, rate of deformation, and vorticity. When these new variables are employed instead, the evolution equations are simplified.

Definition 9.4.1. *We define the* ***Euclidean equivalence of velocity gradient*** *by*

$$l_E^\flat := g^{\frac{1}{2}} l_g g^{-\frac{1}{2}} = g^{-\frac{1}{2}} l_g^\flat g^{-\frac{1}{2}}. \tag{9.4.1a}$$

The ***Euclidean equivalence of the rate of deformation*** *and the* ***Euclidean equivalence of vorticity*** *follow by*

$$d_E^\flat := g^{\frac{1}{2}} d_g g^{-\frac{1}{2}} = g^{-\frac{1}{2}} d_g^\flat g^{-\frac{1}{2}} = g^{-\frac{1}{2}} \left(d^\flat + \frac{1}{2} \frac{Dg}{dt} \right) g^{-\frac{1}{2}}, \tag{9.4.2a}$$

$$\omega_E^\flat := g^{\frac{1}{2}} \omega_g g^{-\frac{1}{2}} = \left(\omega_{12}^\flat + \zeta \right) g^{-\frac{1}{2}} J g^{-\frac{1}{2}} = \frac{\omega_{12}^\flat + \zeta}{\sqrt{\det(g)}} J. \tag{9.4.2b}$$

▲

Now we summarize the Proposition 9.2.2, Proposition 9.2.4 and the above definitions in the following theorem.

Theorem 9.4.2 (Evolution on Riemannian 2-manifold). *Suppose the flow on the two-dimensional Riemannian manifold* $(\mathscr{P}_t, \mathbf{g})$ *satisfies the hypotheses of the Theorem 7.3.4 holds. Then, the complete set of differential equations describing the nonlinear spectral evolution of deformation of the flow are*

$$\frac{D\boldsymbol{x}}{dt} = \boldsymbol{v}, \qquad \boldsymbol{x}(\boldsymbol{X}, t_0) = \boldsymbol{X}, \tag{9.4.3a}$$

$$\frac{D\Theta}{dt} = \left(\frac{2\sqrt{\Lambda_1 \Lambda_2}}{\Lambda_2 - \Lambda_1} \right) \left(\hat{d}_E^\flat \right)_{12}, \qquad \Theta(\boldsymbol{X}, t_0) = \Theta_0, \tag{9.4.3b}$$

$$\frac{D\theta}{dt} = \left(\hat{\omega}_E^\flat \right)_{12} + \left(\frac{\Lambda_2 + \Lambda_1}{\Lambda_2 - \Lambda_1} \right) \left(\hat{d}_E^\flat \right)_{12}, \qquad \theta(\boldsymbol{X}, t_0) = \Theta_0, \tag{9.4.3c}$$

$$\frac{D\Lambda_i}{dt} = 2\Lambda_i \left(\hat{d}_E^\flat \right)_{ii}, \qquad \Lambda_i(\boldsymbol{X}, t_0) = 1, \tag{9.4.3d}$$

where

$$\hat{d}_E^\flat = e^{-J\theta} d_E^\flat e^{J\theta}, \quad \textit{and} \quad \left(\hat{\omega}_E^\flat \right)_{12} = \frac{\omega_{12}^\flat + \zeta}{\sqrt{\det(g)}}. \tag{9.4.4}$$

Proof. This is just the restatement of Proposition 9.2.2 and Proposition 9.2.4 applied to Theorem 7.3.4. ■

Remark 9.4.3. If $\mathscr{P}_t$ is the Euclidean space with the trivial metric, then $d_E^\flat = d$ and $\omega_E^\flat$ are the symmetric and skew-symmetric parts of $l = \dfrac{\partial v}{\partial x}$. Hence, we can interpret the equations in Theorem 9.4.2 as if they are evolving in Euclidean space with an equivalent rate of deformation $d_E^\flat$ and an equivalent vorticity $\omega_E^\flat$. ▲

Part II

Examples and Applications

Chapter 10

A Hamiltonian Flow on Symplectic Manifold

10.1 Introduction

In this chapter, we demonstrate the previous results, namely Theorem 7.3.4 and Corollary 7.4.1 by a numerical example of deformation for a symplectic flow on the Riemann sphere $\mathbb{S}^2$. The two-dimensional flow is generated by the set of ideal localized vortices on the surface of a sphere. The Hamiltonian function of this flow has been given in the literature, such as by Newton [2001]. We re-derive the complexified Hamiltonian function on the Kähler manifold, where we can leverage three compatible geometric structures together, namely the Riemannian, complex and symplectic structures. We present our local chart on the Riemann sphere through stereographic projection. A brief introduction to the Kählerian structures is presented to establish complex Hamiltonian of the flow. In complexified representations, the evolution equations of deformations are simplified.

We will show numerical results for the set of six different vortex configurations that are in equilibrium. A goal throughout our development is to identify the Lagrangian coherent structures (LCS) of the fluid flows. Most methods of identifying LCS depend on eigenvalues of deformation (see e.g., a review by Haller [2015] and references therein). To this end, we demonstrate the FTLE field of the deformation for these six examples and observe that the ridges of the FTLE field distinguish the basins of individual vortices.

Lastly, for the case of antipodal bipolar vortices, we present an exact solution to the evolution equations of the spectral decomposition of deformation. Namely, we derive analytical equations of fields for the eigenvalues and eigenvectors of deformation for the flow of two vortices at north and south poles of the sphere. Our analytical solution may be used as a benchmark example for varieties of LCS identification methods.

10.2 Riemann Sphere

Let $(\tilde{x}^1, \tilde{x}^2, \tilde{x}^3) \in \mathbb{R}^3$ denote the Euclidean coordinates of the ambient space with the flat metric $g_{ab} = \delta_{ab}$. In our setting the configuration space is the manifold $\mathscr{P}_t = \mathbb{CP}^1 \cong \mathbb{S}^2 = \mathbb{C} \cup \{\infty\}$, which is the complex projective line (or Riemann sphere). As shown in Figure 10.2.1 we project the flow onto the Riemann sphere by the stereographic projection $\pi^{-1}\colon \mathbb{CP}^1 \hookrightarrow \mathbb{R}^3$,

$$\pi^{-1}\colon z \mapsto \frac{1}{|z|^2+1}\left(2\,\mathrm{Re}(z), 2\,\mathrm{Im}(z), |z|^2 - 1\right), \tag{10.2.1}$$

where $z = x^1 + ix^2 \in \mathbb{CP}^1$ and $i^2 = -1$. Also, $|z|^2 = z\bar{z}$ and $\bar{z}$ is the complex conjugate of z. In practice, covering the atlas of the full sphere $\mathbb{S}^2$ requires at least two compatible charts since the above projection maps the north pole to infinity.

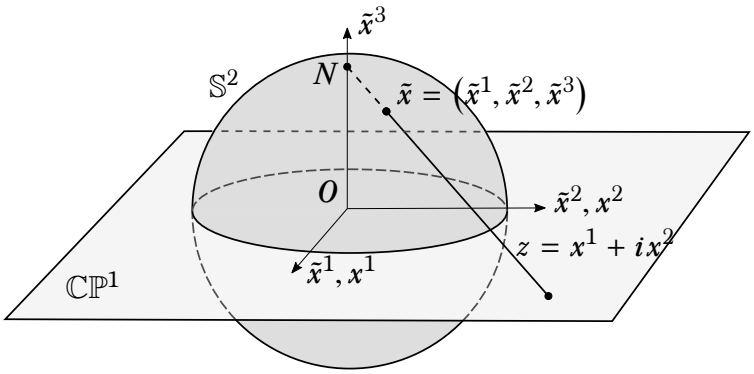

Figure 10.2.1: Stereographic projection $z = \pi(\tilde{x})$ of the Riemann sphere $\mathbb{CP}^1$, where $\tilde{x} = (\tilde{x}^1, \tilde{x}^2, \tilde{x}^3) \in \mathbb{R}^3\big|_{\mathbb{S}^2}$ and $z = x^1 + ix^2 \in \mathbb{CP}^1$. The north pole N is mapped to infinity.

The complexification of the tangent space consists of the composition

$$T\mathscr{P}_t \otimes_{\mathbb{R}} \mathbb{C} = T^{1,0}\mathscr{P}_t \oplus T^{0,1}\mathscr{P}_t = T\mathbb{CP}^1,$$

with the complexified local frames

$$\begin{aligned} \frac{\partial}{\partial z} &= \frac{1}{2}\left(\boldsymbol{e}_1 - i\boldsymbol{e}_2\right) \in T^{1,0}\mathscr{P}_t, \\ \frac{\partial}{\partial \bar{z}} &= \frac{1}{2}\left(\boldsymbol{e}_1 + i\boldsymbol{e}_2\right) \in T^{0,1}\mathscr{P}_t, \end{aligned} \tag{10.2.2}$$

where $\boldsymbol{e}_a = \dfrac{\partial}{\partial x^a} \in T\mathscr{P}_t$ are the covariant real local frames. The pullback of the basis $\{\partial/\partial z, \partial/\partial \bar{z}\}$ can be represented in terms of the Euclidean basis $\tilde{\boldsymbol{e}}_a := \partial/\partial \tilde{x}^a$, $a = 1, 2, 3$ by applying the

chain rule on the map (10.2.1) as

$$\begin{aligned}\frac{\partial}{\partial z} &= \frac{\partial \tilde{x}^a}{\partial z}\frac{\partial}{\partial \tilde{x}^a} = \frac{1}{\left(1+|z|^2\right)^2}\Big(\left(1-\bar{z}^2\right)\tilde{\boldsymbol{e}}_1 - \boldsymbol{i}\left(1+\bar{z}^2\right)\tilde{\boldsymbol{e}}_2 + 2\bar{z}\tilde{\boldsymbol{e}}_3\Big),\\ \frac{\partial}{\partial \bar{z}} &= \frac{\partial \tilde{x}^a}{\partial \bar{z}}\frac{\partial}{\partial \tilde{x}^a} = \frac{1}{\left(1+|z|^2\right)^2}\Big(\left(1-z^2\right)\tilde{\boldsymbol{e}}_1 + \boldsymbol{i}\left(1+z^2\right)\tilde{\boldsymbol{e}}_2 + 2z\tilde{\boldsymbol{e}}_3\Big).\end{aligned} \tag{10.2.3}$$

In the complex local frame (10.2.3), the Riemannian metric $\mathbf{g} \in \Gamma\left(T\mathbb{CP}^1 \odot T\mathbb{CP}^1\right)$ is expressed by

$$\mathbf{g} = \frac{1}{2}\left(\frac{2}{1+|z|^2}\right)^2 \mathrm{d}z \odot \mathrm{d}\bar{z}, \quad \text{or} \quad g_{ab} = \left(\frac{2}{1+|z|^2}\right)^2 \delta_{ab},$$

where, the symbol $\odot$ denotes the symmetric tensor product[1], i.e.,

$$\mathrm{d}z \odot \mathrm{d}\bar{z} \coloneqq \mathrm{d}z \otimes \mathrm{d}\bar{z} + \mathrm{d}\bar{z} \otimes \mathrm{d}z = 2\left(\mathrm{d}x^1 \otimes \mathrm{d}x^1 + \mathrm{d}x^2 \otimes \mathrm{d}x^2\right).$$

The tensor $\mathbf{g}$ defined above is the *Fubini-Study metric* on the complex projective line $\mathbb{CP}^1$.

The above metric is isothermal, meaning that the tensor coordinates of the bases $\mathrm{d}z \otimes \mathrm{d}z$ and $\mathrm{d}\bar{z} \otimes \mathrm{d}\bar{z}$ vanish. To verify this, observe in relations (10.2.3) that $\frac{\partial}{\partial z} \cdot \frac{\partial}{\partial z} = \frac{\partial}{\partial \bar{z}} \cdot \frac{\partial}{\partial \bar{z}} = 0$. The iso-thermal metric allows us further simplification of our formulation (see Remark 7.3.6). One can show that $\mathbf{g} = \left(\pi^{-1}\right)^* \mathbf{g}^{\mathrm{Eucl}}$ where $\mathbf{g}^{\mathrm{Eucl}}$ is the flat metric on Euclidean space [Lee, 1997, p. 37]. Hence, π^{-1} is a desirable Riemannian isometric immersion on $\mathbb{CP}^1$.

Remark 10.2.1 (Isothermal metric). In general, a symmetric metric tensor $\mathbf{g} = g_{ij}\boldsymbol{e}^{*i} \otimes \boldsymbol{e}^{*j}$ with $g_{12} = g_{21}$ can be written in the complex local frame as

$$\mathbf{g} = \frac{\rho}{2}\mathrm{d}w \odot \mathrm{d}\bar{w},$$

with $\mathrm{d}w \coloneqq \mathrm{d}z + \eta\mathrm{d}\bar{z}$, and the coefficients $\rho \in \mathbb{R}_+$ and $\eta \in \mathbb{C}$ are

$$\rho \coloneqq \frac{1}{4}\left(\mathrm{trace}(\mathbf{g}) + 2\sqrt{\det(\mathbf{g})}\right), \quad \text{and} \quad \eta \coloneqq \frac{1}{4\rho}\left(g_{11} - g_{22} + 2ig_{12}\right).$$

When the metric is isothermal, $g_{11} = g_{22}$ and $g_{12} = g_{21} = 0$, meaning that $\eta = 0$, and $\mathbf{g} = \frac{\rho}{2}\mathrm{d}z \odot \mathrm{d}\bar{z}$. The complex basis consists of $\mathrm{d}z = \boldsymbol{e}^{*1} + i\boldsymbol{e}^{*2}$ and $\mathrm{d}\bar{z} = \boldsymbol{e}^{*1} - i\boldsymbol{e}^{*2}$. For an arbitrary metric $\mathbf{g}$, if $\|\eta\|_\infty < 1$, it is always possible to find a coordinate transformation in which the metric becomes isothermal (see ***Beltrami equation*** in [McDuff and Salamon, 1998, p. 127]). ▲

[1] The symbol $\odot$ here should not be confused with the Hadamard matrix product used before.

10.3 Kähler Structure

On the Riemann 2-sphere, the Kähler structures provide a natural framework to present of Hamiltonian flows. Kähler manifolds are almost complex manifolds with a mutually compatible triple $(\mathbf{g}, \mathbf{\Omega}, \mathbf{J})$, namely the Riemannian metric $\mathbf{g}$, the symplectic structure $\mathbf{\Omega}$, and the complex structure $\mathbf{J}$. The compatible triple $(\mathbf{J}, \mathbf{g}, \mathbf{\Omega})$ is known as the ***Kählerian structure*** on the manifold $\mathscr{P}_t$, here $\mathbb{CP}^1$. We will brief each structure as follows.

The complex structure $\mathbf{J} \in \Gamma\left(\mathrm{End}(T\mathscr{P})\right)$ is a $\binom{1}{1}$ tensor satisfying

$$\mathbf{J}^2 = -\,\mathrm{id}_{T\mathscr{P}_t}\,.$$

A manifold $(\mathscr{P}_t, \mathbf{J})$ is called an ***almost complex manifold***. The complex structure $\mathbf{J}$ decomposes the complexified tangent bundle into its eigenspaces, i.e., $T_{\mathbb{C}}\mathscr{P}_t = T^{1,0}\mathscr{P}_t \oplus T^{0,1}\mathscr{P}_t$. We assume $\mathbf{J}$ is linear. In particular to our Riemann sphere, we set $\mathbf{J}$ to be the *standard complex structure* $\mathbf{J}_0 \in \Gamma\left(\mathrm{End}(T\mathbf{CP}^1)\right)$ defined by (see for instance [da Silva, 2001, §13]),

$$\mathbf{J}_0\left(\frac{\partial}{\partial z}\right) = i\frac{\partial}{\partial z}. \tag{10.3.1}$$

The second structure on a Kähler manifold is the symplectic form $\mathbf{\Omega} \in \Omega^2(\mathscr{P}_t)$, that is a non-degenerate closed 2-form. This means $\mathbf{\Omega}^n = \mathbf{\Omega} \wedge \cdots \wedge \mathbf{\Omega} \neq \mathbf{0}$ is a volume form, and $\mathrm{d}\mathbf{\Omega} = \mathbf{0}$. The manifold $(\mathscr{P}_t, \mathbf{\Omega})$ is called ***symplectic*** equipped with symplectic form $\mathbf{\Omega}$. On Kählerian manifolds, we can generate a symplectic structure $\mathbf{\Omega}$ by defining a ***Kähler potential*** $K \in C^\infty\left(\mathbb{CP}^1; \mathbb{R}\right)$. On our Riemann sphere, we set the Kähler potential to be

$$K(z, \bar{z}) = 4\ln\left(1 + |z|^2\right).$$

The ***symplectic canonical Kähler*** is the 2-form $\mathbf{\Omega} \in \Omega^2\left(\mathbb{CP}^1\right)$ induced by the Kähler potential with (see [da Silva, 2001, §16])

$$\mathbf{\Omega}(z, \bar{z}) \coloneqq \frac{i}{2}\partial_z\partial_{\bar{z}}K(z, \bar{z}) = \frac{i}{2}\left(\frac{2}{1 + |z|^2}\right)^2 \mathrm{d}z \wedge \mathrm{d}\bar{z} = \left(\frac{2}{1 + |z|^2}\right)^2 \mathrm{d}x \wedge \mathrm{d}y, \tag{10.3.2}$$

where ∂_z and $\partial_{\bar{z}}$ are *Dolbeault operators* and defined by

$$\begin{aligned} \partial_z &= \frac{\partial}{\partial z}\mathrm{d}z : \Omega^{p,q}(\mathscr{P}_t) \to \Omega^{p+1,q}(\mathscr{P}_t), \\ \partial_{\bar{z}} &= \frac{\partial}{\partial \bar{z}}\mathrm{d}\bar{z} : \Omega^{p,q}(\mathscr{P}_r) \to \Omega^{p,q+1}(\mathscr{P}_t), \end{aligned} \tag{10.3.3}$$

and $\Omega^{p,q}$ is the complexified space of (p, q)-forms. Also, $\mathrm{d}z \wedge \mathrm{d}\bar{z} = -2i\mathrm{d}x \wedge \mathrm{d}y$ is the area form on $\Omega^2(\mathbb{CP}^1)$.

The compatibility of the triples $(\mathbf{g}, \mathbf{\Omega}, \mathbf{J})$ on Kählerian manifolds is specified by a set of constraints on each structure. Namely, $\mathbf{J}$ is said to tame $\mathbf{\Omega}$ if

$$\mathbf{\Omega}\left(\boldsymbol{u}, \boldsymbol{J}\boldsymbol{u}\right) > 0, \quad \forall \boldsymbol{u} \in T\mathscr{P}_t.$$

The positive definiteness of the above form suggests a compatible metric $\mathbf{g}$ given by

$$\mathbf{g}(v, \boldsymbol{u}) = \mathbf{\Omega}\left(v, \mathbf{J}\boldsymbol{u}\right), \quad v, \boldsymbol{u} \in T\mathscr{P}_t.$$

It is straightforward to show that the standard complex structure in (10.3.1) and the symplectic Kähler form (10.3.2) are compatible with the Riemannian metric given in (10.2), which we refer to as *Kähler metric*. The corresponding ***Hermitian metric*** $\mathbf{h} \in \Gamma\left(T^*\mathbb{CP}^1 \otimes T^*\mathbb{CP}^1\right)$ is

$$\mathbf{h} = \mathbf{g} - i\mathbf{\Omega} = \left(\frac{2}{1+|z|^2}\right)^2 \mathrm{d}z \otimes \mathrm{d}\bar{z}. \tag{10.3.4}$$

10.4 Hamiltonian System

We generate a flow on the Riemann sphere by setting N ideal vortices of strength $\Gamma_i \in \mathbb{R}$ lying on the surface of the Riemann sphere at locations $z_i(t) \in \mathbb{CP}^1$ where $i = 1, \cdots, N$. In addition to the point vortices, we may also add background vorticity of strength Ω_0 that resembles the Coriolis effect due to the rotation of the sphere. Figure 10.4.1 shows the schematic configuration of three-point vortices and the background vorticity of the system.

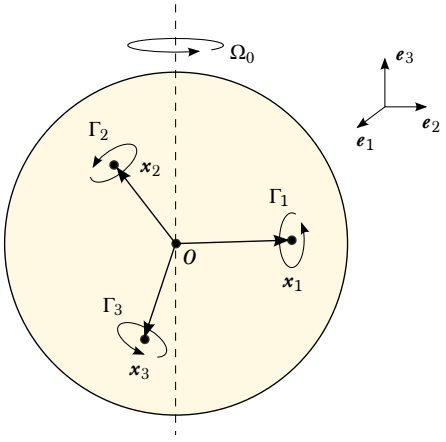

Figure 10.4.1: Point vortices at locations $\boldsymbol{x}_j$ and strength Γ_j, for $j = 1, \cdots, N$, and the background vorticity Ω_0.

The Hamiltonian and velocity field of this flow is derived in [Newton, 2001, p.141] and Newton and Shokraneh [2006]. Here we obtain the same Hamiltonian and velocity of the flow

in the complex setting of the Kähler manifold as follows. A fluid particle can be thought of like a vortex with zero strength. By Helmholtz's assumption [Helmholtz, 1858], the motion of a fluid particle is the superposition of the flow generated by the other point vortices. Such a velocity field can be derived from the superposition of the potential energies of the group of vortices. The potential energy of a point vortex z_i at the location z is a function of the chordal (Euclidean) distance of the two points given by (see e.g., [Ahlfors, 1966, p. 20])

$$d(z, z_i) = \frac{2|z - z_i|}{\sqrt{\left(1 + |z|^2\right)\left(1 + |z_i|^2\right)}}.$$

Following Newton [2001, p. 174], we define the Hamiltonian function H by

$$H(z, \bar{z}) = \frac{1}{4\pi} \sum_{i=1}^{N} \Gamma_i \ln\left(d(z, z_i)\right), \tag{10.4.1}$$

which is the superposition of the potential energy of each vortex z_i at the location z. Without loss of generality, we have set the background vorticity Ω_0 to zero since our results later are invariant under a solid rotation (i.e., isometric isomorphism).

Integral curves of the Hamiltonian vector field contour the Hamiltonian *symplectomorphism* $\boldsymbol{\phi}_t \in \mathrm{Symp}\left(\mathbb{CP}^1, \boldsymbol{\Omega}\right)$ where $z_t = \boldsymbol{\phi}_t(z_0)$. The symplectomorphism $\boldsymbol{\phi}$ satisfies

$$\pounds_{\boldsymbol{\phi}} \boldsymbol{\Omega} = \mathbf{0}. \tag{10.4.2}$$

On 2-manifolds, such as our Riemann sphere, the symplectic structure $\boldsymbol{\Omega}$ is also an area-form. Hence, the relation (10.4.2) implies the symplectomorphism $\boldsymbol{\phi}$ is area-preserving, i.e., isochoric (see also §4.4).

The evolution equation of the flow can be derived from the exterior derivative of the Hamiltonian $\mathrm{d}H$. The exterior derivative d can be expressed by the Dolbeault operators in (10.3.3) as $\mathrm{d} = \partial_z + \partial_{\bar{z}}$. A simple derivation yields the *Hamiltonian system*

$$\iota_v \boldsymbol{\Omega} = \mathrm{d}H. \tag{10.4.3}$$

From the Cartan's magic formula we have $\pounds_{\boldsymbol{\phi}} \boldsymbol{\Omega} = \mathrm{d}\left(\iota_v \boldsymbol{\Omega}\right) + \iota_v\left(\mathrm{d}\boldsymbol{\Omega}\right) = \mathrm{d}^2 H = \mathbf{0}$ which justifies (10.4.2).

We express the velocity v in the complex local frame by

$$\boldsymbol{v} = \dot{z}\frac{\partial}{\partial z} + \dot{\bar{z}}\frac{\partial}{\partial \bar{z}}. \tag{10.4.4}$$

The components of the Hamiltonian system (10.4.3) in the complex cotangent local frame $\mathrm{d}z$ and $\mathrm{d}\bar{z}$ is (see Zhang [2006] for derivation)

$$\dot{z} = -2i\bar{\mathbf{h}}^{-1}\frac{\partial H(z, \bar{z})}{\partial \bar{z}}, \qquad \text{and} \qquad \dot{\bar{z}} = 2i\mathbf{h}^{-1}\frac{\partial H(z, \bar{z})}{\partial z}.$$

By substituting the Hamiltonian H in the equation (10.4.1) and the Hermitian metric $\mathbf{h}$ in the relation (10.3.4), the evolution equation becomes

$$\dot{\bar{z}} = i\frac{(1+|z|^2)^2}{16\pi}\left(\left(\sum_{i=1}^{N}\frac{\Gamma_i}{z-z_i}\right) - \frac{\sigma\bar{z}}{1+|z|^2}\right), \tag{10.4.5}$$

where $\sigma := \sum_{i=1}^{N}\Gamma_i$ is the total vorticity in the field.

The velocity vector can also be given in the real local chart with the basis $\boldsymbol{e}_1$ and $\boldsymbol{e}_2$. To do so, we substitute $\dot{z} = \dot{x}^1 + i\dot{x}^2$, $\dot{\bar{z}} = \dot{x}^1 - i\dot{x}^2$, and the two relations in (10.2.2) in (10.4.4), which yield the velocity $\boldsymbol{v} = v^1\boldsymbol{e}_1 + v^2\boldsymbol{e}_2$ by the components

$$\begin{aligned} v^1 &= \frac{(1+r^2)^2}{16\pi}\sum_{i=1}^{N}\Gamma_i\frac{x^2-x_i^2}{(x^1-x_i^1)^2+(x^2-x_i^2)^2} - \frac{\sigma}{1+r^2}, \\ v^2 &= \frac{(1+r^2)^2}{16\pi}\sum_{i=1}^{N}\Gamma_i\frac{-(x^1-x_i^1)}{(x^1-x_i^1)^2+(x^2-x_i^2)^2} + \frac{\sigma}{1+r^2}. \end{aligned} \tag{10.4.6}$$

where $(x_i^1, x_i^2) \in \mathbb{CP}^1$ are the locations of the point vortices. Newton [2001, p.3] derived the velocity vector field (10.4.6) by the discrete Biot-Savart law.

10.5 Steady Flow of Vortices at Equilibrium

The flow generated by the group of vortices influences the movement of vortices themselves. It is possible to arrange an equilibrium configuration of vortices so that none of the vortices move. In such a case, the resulted flow is autonomous.

In our examples, we use a few stable configurations of the vortices which have been studied by Meleshko, Newton, and Ostrovs'kyi [2010] and Jamaloodeen and Newton [2006]. If we assume all vortices have equal strengths, there exist three nonlinearly stable configurations [Meleshko, Newton, and Ostrovs'kyi, 2010, Theroem 2], which are (a) the 4 vortices on a tetrahedron, (b) 6 vortices on an octahedron and (c) 12 vortices on an icosahedron. With non-uniform vortex strengths, other nonlinearly stable equilibrium configurations exist, for instance, when the antipodal vortices have opposite strength [Newton and Ostrovskyi, 2012, Theorem 3.1].

We use six equilibrium configurations of vortices that are located at the vertices of polyhedrons embedded in the unit sphere as shown in Figure 10.5.1. All vortices have equal strength $\Gamma = +1$. In the figure, the configurations (a), (b) and (c) are nonlinearly stable equilibrium with respectively $N = 4$, 6 and 12 vortices. Whereas, the configurations (d), (e) and (f) are

nonlinearly unstable equilibrium with respectively $N = 12$, 20 and 30 vortices. The coordinates of vertices in each of these six cases are presented in Table 10.1. In the table, $\alpha := 1/\sqrt{2}$, $\beta := 1/\sqrt{3}$, $\rho := \left(1+\sqrt{5}\right)/2$ is the golden ratio, and $\eta := 1/\sqrt{1+\rho^2}$. All vertices lie on the surface of the unit sphere.

Table 10.1: Coordinates of vertices of Polyhedrons embedded in the unit sphere.

Polyhedron in $\mathbb{S}^2$	N	Coordinates of vertices		
Tetrahedron	4	$(0,0,1)$,	$(0,\frac{2\sqrt{2}}{3},-\frac{1}{3})$,	$(\pm\sqrt{\frac{2}{3}},-\frac{\sqrt{2}}{3},-\frac{1}{3})$
Octahedron	6	$(0,0,\pm1)$,	$\alpha(\pm1,\pm1,0)$,	
Icosahedron	12	$\eta(\pm\rho,0,\pm1)$,	$\eta(0,\pm1,\pm\rho)$,	$\eta(\pm1,\pm\rho,0)$
Cuboctahedron	12	$\alpha(\pm1,\pm1,0)$,	$\alpha(\pm1,0,\pm1)$,	$\alpha(0,\pm1,\pm1)$
Dodecahedron	20	$\beta(0,\pm\rho^{-1},\pm\rho)$, $\beta(\pm1,\pm1,\pm1)$	$\beta(\pm\rho^{-1},\pm\rho,0)$,	$\beta(\pm\rho,0,\pm\rho^{-1})$
Icosidodecahedron	30	$(0,0,\pm1)$, $\frac{1}{2}(\pm\rho^{-1},\pm1,\pm\rho)$,	$(\pm1,0,0)$, $\frac{1}{2}(\pm1,\pm\rho,\pm\rho^{-1})$,	$(0,\pm1,0)$ $\frac{1}{2}(\pm\rho,\pm\rho^{-1},\pm1)$

The Hamiltonian functions H for each of the six configurations of the Figure 10.5.1 are shown in the Figure 10.5.2. In that figure, the solid curves are contours of the Hamiltonian, which also represent the streamlines of the steady flow. Adjacent to a vortex, the Hamiltonian is dominated by the strong potential energy of the vortex. Hence, the streamlines resemble the flow of an almost ideal vortex with closed circular orbits.

We are interested to uncover the qualitative patterns generated by the flow. One approach to identify structures of autonomous flow is to trace the *heteroclinic orbits* of the flow, which joins the heteroclinic connections (or separatrix). These orbits act as barriers that separate the basin of vortices. The heteroclinic connections can be found by the saddle points of the equilibriums of the Hamiltonian. Saddle points are the locations with negative Gauss curvature K of the Hessian of H evaluated at equilibrium points. The Gauss curvature is the product of the eigenvalues of the Hessian and obtained by its determinant as

$$K = \det(\mathrm{Hess}(H)) = \frac{\partial^2 H}{\partial x^2}\frac{\partial^2 H}{\partial y^2} - \frac{\partial^2 H}{\partial x \partial y} = 4\left(\frac{\partial^2 H}{\partial z \partial \bar{z}} - \frac{\partial^2 H}{\partial z^2}\frac{\partial^2 H}{\partial \bar{z}^2}\right).$$

A straightforward calculation on the Hamiltonian (10.4.1) yields

$$\det(\mathrm{Hess}(H)) = \frac{1}{\pi^2}\left(\left(\frac{\sigma}{\left(1+|z|^2\right)}\right)^2 - \left|\sum_{i=1}^{N}\frac{\Gamma_i}{|z-z_i|^2} - \frac{\sigma z^2}{\left(1+|z|^2\right)^2}\right|^2\right).$$

As shown in Figure 10.5.2 the saddle points are the intersection of the orbits, and they can be found between the midpoint of each two vortices. Also, Figure 10.5.3 illustrates the

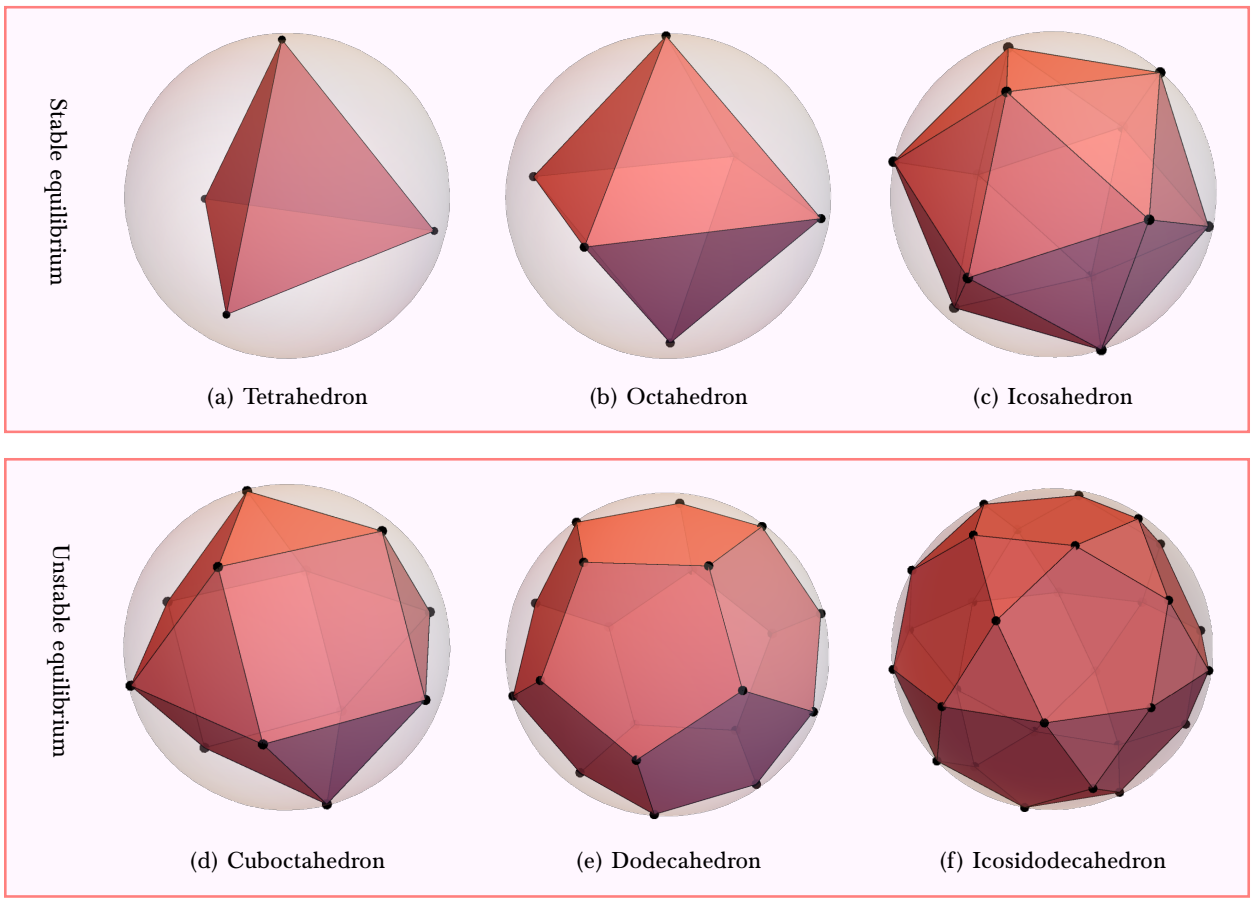

Figure 10.5.1: (a) Tetrahedron, (b) Octahedron, (c) Icosahedron, (d) Cuboctahedron, (e) Dodecahedron and (f) Icosidodecahedron embedded in the unit sphere.

Hamiltonian function projected onto the complex plane using the stereographic projection for the configuration (c) of Figure 10.5.2 (Icosahedron with $N = 12$). The bright spots are the vortices and the solid black curves are the heteroclinic orbits of the flow, separating the basin of each vortex.

10.6 Lagrangian Coherent Structures

Heteroclinic orbits are an effective tool to reveal the structure of an autonomous flow, however, they are less useful for non-autonomous flows. The ***Lagrangian coherent structures*** (LCS) are a more commonly accepted concept to identify structures of aperiodic flows. LCS is often identified by the ***finite-time Lyapunov exponents*** (FTLE) and defined for instance in Shadden, Lekien, and Marsden [2005] and Lekien, Shadden, and Marsden [2007]. FTLEs are $t^{-1} \ln \sqrt{\Lambda_a}$

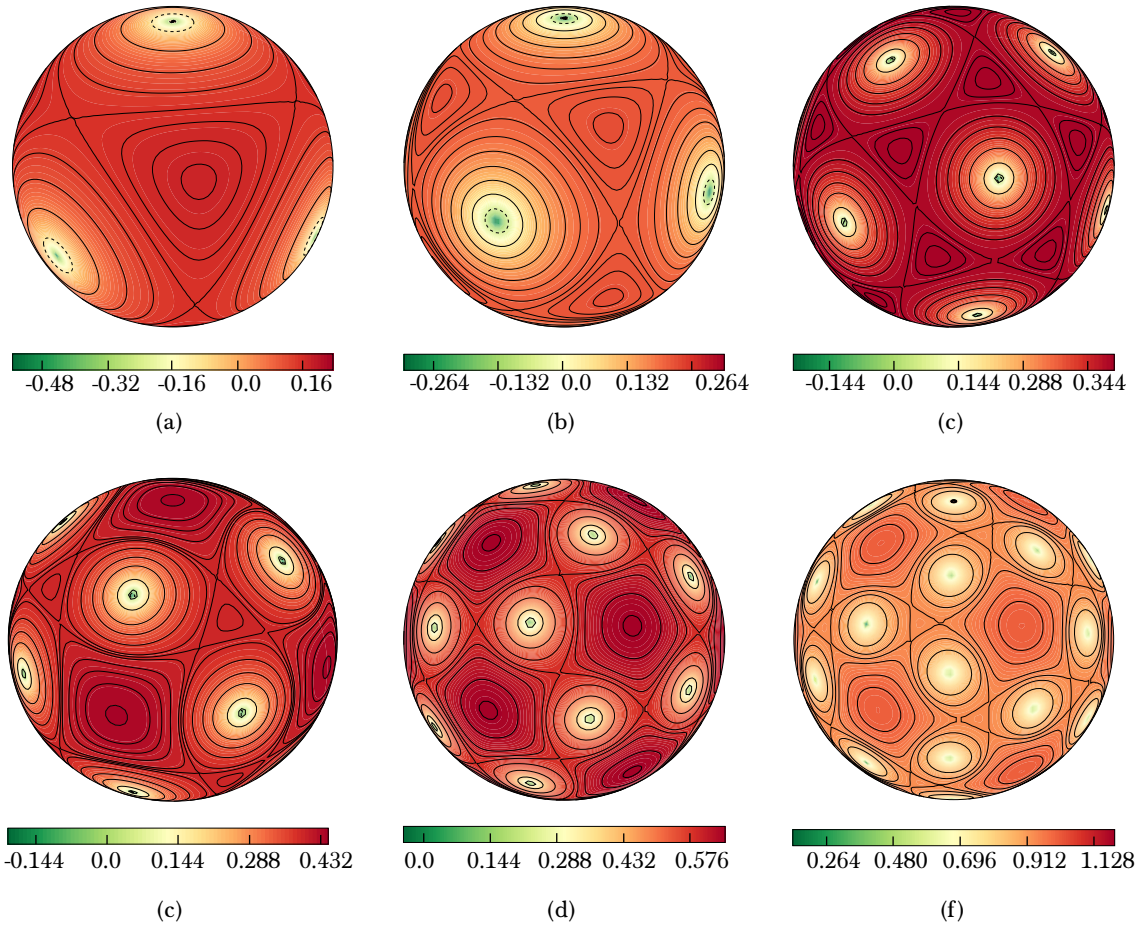

Figure 10.5.2: Hamiltonian H corresponding to the six vortex configurations of Figure 10.5.1.

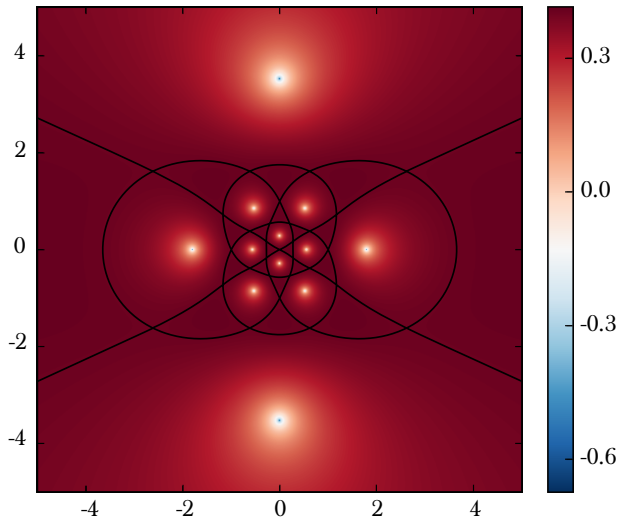

Figure 10.5.3: Hamiltonian for the configuration (c) of Figure 10.5.2 projected on the complex plane.

where Λ_a are the eigenvalues of the Cauchy-Green deformation tensor. Recall from §7.4 that $\mu_a = \frac{1}{2}\ln\Lambda_a$. Thus, FTLEs are the eigenvalues of $t^{-1}\mathbf{H}$ where $\mathbf{H}$ is the *Hencky strain tensor* (see §7.1), and t is the advection time. FTLEs measure the exponential growth-rate of deformation along the principal directions of deformation tensor. In literature, it is common to only consider the largest FTLE known as ***forward FTLE*** which corresponds to the largest eigenvalue of $\mathbf{H}$. Also, the ***backward FTLE*** is the largest FTLE for the reversed flow, i.e., when the direction of time is reversed. Forward and backward FTLEs respectively represent the repulsion and attraction exponential rates of deformation.

Despite the example given earlier is an autonomous flow, here we explore the structure of that flow by the FTLE field. In particular, we aim to find the eigenvalues Λ_1 and Λ_2 of the nonlinear deformation. Recall that the evolution of eigenvalues is given in Theorem 7.3.4, and is coupled with evolution equations for the left and right eigenvector frames. Figure 10.6.1 demonstrates a schematic evolution of eigenvector frames on the Riemann sphere $\mathbb{S}^2$. In the figure, the right eigenvector $\mathbf{U} = [\boldsymbol{U}_1, \boldsymbol{U}_2]$ and left eigenvectors $\mathbf{u} = [\boldsymbol{u}_1, \boldsymbol{u}_2]$ are shown on the tangent planes $T_{\boldsymbol{X}}\mathbb{S}^2$ and $T_{\boldsymbol{x}}\mathbb{S}^2$ respectively. To evolve eigenvector frames on the 2-manifold we use the simplified evolution equations of Proposition 9.2.2 and Proposition 9.2.4 in which Euler angles represent the frames.

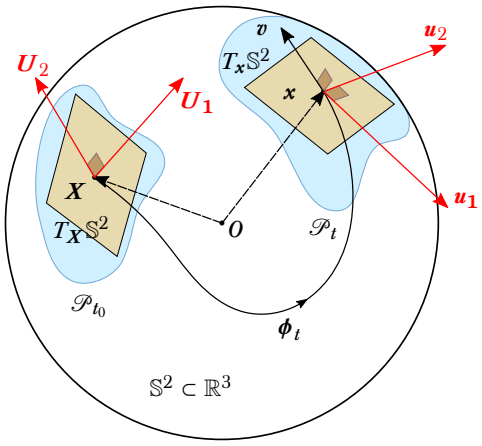

Figure 10.6.1: Schematic evolution of eigenvectors frame on the Riemann sphere $\mathbb{S}^2$.

Figure 10.6.2 shows the backward FTLE field for the Hamiltonian flows corresponding to the six vortex configurations of Figure 10.5.2. The integration time for all examples are $t = 20$. The field is computed on a *geodesic dome* grid consists of 450000 triangular elements and 225002 points. We note that since these flows are steady and isochoric, the forward and backward FTLE fields are identical by the Liouville theorem. Also, it can be seen from the figure that the ridges of the FTLE field trace out the distinct regions of each vortex, which is in an agreement with the heteroclinic orbits shown in Figure 10.5.2. However, the advantage of the FTLE is understood in aperiodic flows which we will present in Chapter 11.

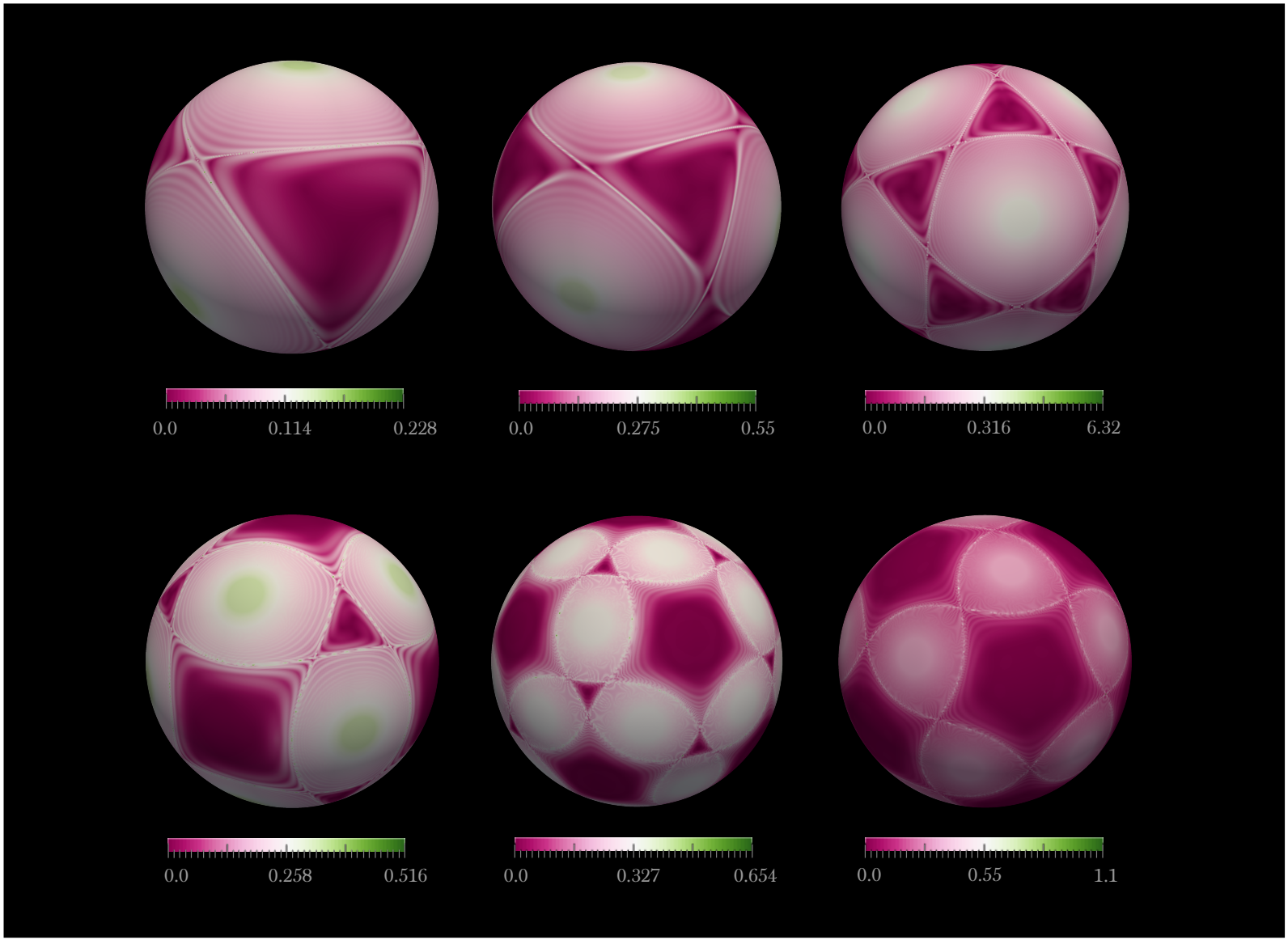

Figure 10.6.2: The backward finite-time Lyapunov exponent field for the Hamiltonian flows of the Figure 10.5.2

10.7 An Exact Solution for Eigenvalues of Deformation

We present an analytical solution of the evolution equations of eigenvalues and eigenvectors for the case of two antipodal vortices. Our motivation to seek an exact solution is twofold. First, it enables us to validate the numerical solution of equations by a benchmark solution. Second, we can use the exact solutions in the neighborhoods of vortices where the velocity is almost singular.

We parameterize the Riemann sphere with the spherical coordinate (θ, ϕ), given by the local chart

$$\begin{aligned} x^1 &= \sin(\theta)\cos(\phi), \\ x^2 &= \sin(\theta)\sin(\phi), \\ x^3 &= \cos(\phi), \end{aligned}$$

where $\theta \in [0, \pi]$ is the polar angle measured from the north pole and $\phi \in [0, 2\pi)$ is the azimuthal angle. We choose an orthogonal local frame on the tangent space $T_{\boldsymbol{x}}\mathscr{P}_t$ at the location $\boldsymbol{x} = (\theta, \phi)$ by

$$\begin{aligned} \boldsymbol{e}_\theta &= \frac{\partial}{\partial\theta} = \cos(\theta)\cos(\phi)\tilde{\boldsymbol{e}}_1 + \cos(\theta)\sin(\phi)\tilde{\boldsymbol{e}}_2 - \sin(\theta)\tilde{\boldsymbol{e}}_3, \\ \boldsymbol{e}_\phi &= \frac{\partial}{\partial\phi} = -\sin(\phi)\sin(\phi)\tilde{\boldsymbol{e}}_1 + \sin(\theta)\cos(\phi)\tilde{\boldsymbol{e}}_2. \end{aligned}$$

In the above, $(x^1, x^2, x^3) \in \mathbb{R}^3$ is a Cartesian point and $(\tilde{\boldsymbol{e}}_1, \tilde{\boldsymbol{e}}_2, \tilde{\boldsymbol{e}}_3) = \left(\frac{\partial}{\partial x^1}, \frac{\partial}{\partial x^2}, \frac{\partial}{\partial x^3}\right)$ is the usual orthonormal covariant basis in the Cartesian coordinates. We note that $(\boldsymbol{e}_\theta, \boldsymbol{e}_\phi)$ is the *covariant* basis, not the *physical basis*; that is, the base vectors are not unit vectors and their length is not normalized.

The components of the metric tensor $\mathbf{g}$ are given by $g_{ij} = \boldsymbol{e}_i \cdot \boldsymbol{e}_j$ for indices $(i, j) = (\theta, \phi)$ with the usual inner product in the Euclidean space. We have

$$\mathbf{g}(\boldsymbol{x}) = \boldsymbol{e}^{*\theta} \otimes \boldsymbol{e}^{*\theta} + \sin^2(\theta)\boldsymbol{e}^{*\phi} \otimes \boldsymbol{e}^{*\phi},$$

where $\boldsymbol{e}^{*\theta} = \mathrm{d}\theta$ and $\boldsymbol{e}^{*\phi} = \mathrm{d}\phi$ are the basis on the cotangent bundle. Similar to the above, we can define the covariant basis $\boldsymbol{E}_\Theta$ and $\boldsymbol{E}_\Phi$ on the referential tangent space $T_{\boldsymbol{X}\mathscr{P}_{t_0}}$. The referential metric tensor $\mathbf{G}$ at the point $\boldsymbol{X} = (\Theta, \Phi)$ is

$$\mathbf{G}(\boldsymbol{X}) = \boldsymbol{E}^{*\Theta} \otimes \boldsymbol{E}^{*\Theta} + \sin^2(\Theta)\boldsymbol{E}^{*\Phi} \otimes \boldsymbol{E}^{*\Phi},$$

where $\boldsymbol{E}^{*\Theta} = \mathrm{d}\Theta$ and $\boldsymbol{E}^{*\Phi} = \mathrm{d}\Phi$. The norm of covariant bases are $\|\boldsymbol{e}_\theta\|^2 = \mathbf{g}(\boldsymbol{e}_\theta, \boldsymbol{e}_\theta) = g_{\theta\theta} = 1$ and $\|\boldsymbol{e}_\phi\|^2 = \mathbf{g}(\boldsymbol{e}_\phi, \boldsymbol{e}_\phi = g_{\phi\phi} = \sin^2(\theta))$. Hence, one can normalize the covariant basis to get

the physical unit basis $(\tilde{\boldsymbol{e}}_\theta, \tilde{\boldsymbol{e}}_\phi)$[2],

$$\begin{aligned}\tilde{\boldsymbol{e}}_\theta &= \frac{1}{\sqrt{g_{\theta\theta}}}\boldsymbol{e}_\theta = \boldsymbol{e}_\theta,\\ \tilde{\boldsymbol{e}}_\phi &= \frac{1}{\sqrt{g_{\phi\phi}}}\boldsymbol{e}_\phi = \csc(\theta)\boldsymbol{e}_\phi.\end{aligned}$$

The physical velocity vector field $\boldsymbol{v} = \tilde{v}^\theta\tilde{\boldsymbol{e}}_\theta + \tilde{v}^\phi\tilde{\boldsymbol{e}}_\phi$ of the set of N vortices can be represented in spherical coordinate by (see Kidambi and Newton [1998])

$$\begin{aligned}\tilde{v}^\theta &= \dot{\theta} = -\frac{1}{4\pi}\sum_{i=1}^{N}\frac{\Gamma_i \sin(\theta_i)\sin(\phi-\phi_i)}{1-\cos(\kappa_i)},\\ \tilde{v}^\phi &= \sin(\theta)\dot{\phi} = \frac{1}{4\pi}\sum_{i=1}^{N}\frac{\Gamma_i\left(\sin(\theta)\cos(\theta_i) - \cos(\theta)\sin(\theta_i)\cos(\phi-\phi_i)\right)}{1-\cos(\kappa_i)} + \Omega_0,\end{aligned}$$

where Ω_0 is the background vorticity, κ_i is the arc angle on sphere between the point at (θ, ϕ) and the j-th vortex at (θ_i, ϕ_i). Using the cosine rule on the sphere, i.e., $\cos(\kappa_i) = \cos(\theta)\cos(\theta_i) + \sin(\theta)\sin(\theta_i)\cos(\phi-\phi_i)$.

In contrast to the above physical vector field, we use the velocity vector field $\boldsymbol{v} = v^\theta\boldsymbol{e}_\theta + v^\phi\boldsymbol{e}_\phi$[3] in the covariant basis, which is simply $v^\theta = \dot{\theta}$ and $v^\phi = \dot{\phi}$. We consider two antipodal vortices that are located at the north and south poles at $\theta_N = 0$ and $\theta_S = \pi$ and respectively with the strengths Γ_N and Γ_S. The velocity vector field of this configuration is

$$v^\theta = \dot{\theta} = 0, \qquad \theta(t_0) = \Theta, \tag{10.7.1a}$$

$$v^\phi = \dot{\phi} = \frac{1}{4\pi}\left(\frac{\Gamma_N}{1-\cos(\theta)} - \frac{\Gamma_S}{1+\cos(\theta)}\right) + \Omega_0, \qquad \phi(t_0) = \Phi. \tag{10.7.1b}$$

With the initial condition (Θ, Φ), the solution of above differential equations is

$$\theta(t) = \Theta, \tag{10.7.2a}$$

$$\phi(t) = \left(\frac{1}{4\pi}\left(\frac{\Gamma_N}{1-\cos(\Theta)} - \frac{\Gamma_S}{1+\cos(\Theta)}\right)\Omega_0\right)(t-t_0) + \Phi. \tag{10.7.2b}$$

Recall from Proposition 4.3.1 that regardless of the coordinate system and the connection ∇ on the vector bundle, the evolution of the matrix F of the deformation gradient tensor $\mathbf{F}$

[2]We use tilde symbol $\tilde{\cdot}$ for physical quantities such as basis vectors and vector coordinates.

[3]In contrast to variables on a physical basis, the corresponding covariant basis and the contravariant vector coordinates are represented without the tilde symbol $\tilde{\cdot}$.

is $\dot{F} = lF$ (see (4.3.4)). The matrix l of the rate of the deformation gradient tensor for the velocity field (10.7.1) is computed as

$$l = \begin{bmatrix} \dfrac{\partial v^\theta}{\partial \theta} & \dfrac{\partial v^\theta}{\partial \phi} \\ \dfrac{\partial v^\phi}{\partial \theta} & \dfrac{\partial v^\phi}{\partial \phi} \end{bmatrix} = \begin{bmatrix} 0 & 0 \\ \beta(\theta) & 0 \end{bmatrix},$$

where $\beta(\theta) := \partial\dot{\phi}/\partial\theta$ and given in terms of the tangent half-angle formula as

$$\beta(\theta) = -\frac{\csc(\theta)}{4\pi}\left(\Gamma_N \cot^2\left(\frac{\theta}{2}\right) + \Gamma_S \tan^2\left(\frac{\theta}{2}\right)\right). \tag{10.7.3}$$

From the fact that $\theta(t) = \Theta$ is constant in (10.7.1a), the differential equation for the components of the matrix F can be solved with the initial condition $\mathbf{F}(\Theta, t_0) = \mathbf{I}$ to yield

$$F(\Theta, t) = \begin{bmatrix} 1 & 0 \\ \beta(\Theta)t & 1 \end{bmatrix}. \tag{10.7.4}$$

Now we form the deformation tensors $\mathbf{C}$ and $\mathbf{b}$. Recall from (2.4.2) that the transposition of the tensor $\mathbf{F}$ is given by $\mathbf{F}^\intercal = \mathbf{G}^{-1}\mathbf{F}^*\mathbf{g}$ where $\mathbf{F}^*$ is the adjoint of $\mathbf{F}$ and is the same as the usual transposition of the matrix representation of $\mathbf{F}$. Also, the matrices of the metric tensors are

$$g(\theta, \phi) = \begin{bmatrix} 1 & 0 \\ 0 & \sin^2(\theta) \end{bmatrix}, \quad \text{and} \quad G(\Theta, \Phi) = \begin{bmatrix} 1 & 0 \\ 0 & \sin^2(\Theta) \end{bmatrix}.$$

According to (10.7.1a), on pathlines $\theta(t) = \Theta$, we have $G(\Theta, \Phi) = g(\theta, \phi)$, hence, the matrices C and b of the tensors $\mathbf{C}$ and $\mathbf{b}$ become

$$C(\Theta, t) = \begin{bmatrix} 1 + \beta^2(\Theta)t^2 \sin^2(\Theta) & \beta(\Theta)t \sin^2(\Theta) \\ \beta(\Theta)t & 1 \end{bmatrix}, \tag{10.7.5a}$$

and

$$b(\Theta, t) = \begin{bmatrix} 1 & \beta(\Theta)t \sin^2(\Theta) \\ \beta(\Theta)t & 1 + \beta(\Theta)^2 t^2 \sin^2(\Theta) \end{bmatrix}. \tag{10.7.5b}$$

The eigenvalues of the tensors $\mathbf{C}$ and $\mathbf{b}$ can be easily found by

$$\Lambda_{1,2}(\Theta, t) = \left(1 + \frac{1}{2}\left(\beta(\Theta)t \sin(\Theta)\right)^2\right) \pm \sqrt{\left(1 + \frac{1}{2}\left(\beta(\Theta)t \sin(\Theta)\right)^2\right)^2 - 1}. \tag{10.7.6}$$

We note that $\Lambda_1\Lambda_2 = 1$, which was expected for the isochoric flow of vortices. The right eigenvectors $\boldsymbol{U}_1$ and $\boldsymbol{U}_2$ and the left eigenvectors $\boldsymbol{u}_1$ and $\boldsymbol{u}_2$ are respectively,

$$\begin{aligned} \boldsymbol{U}_{1,2} &= \left(\Lambda_{1,2} - 1\right)\boldsymbol{E}_\theta + \beta(\Theta)t\boldsymbol{E}_\phi, \\ \boldsymbol{u}_{1,2} &= \left(\Lambda_{2,1} - 1\right)\boldsymbol{e}_\theta - \beta(\Theta)t\boldsymbol{e}_\phi. \end{aligned}$$

Remark 10.7.1 (Orthogonality of eigenvectors). At first, it seems that the above eigenvectors are not orthogonal, while, the eigenvectors of deformation tensors are expected to form an orthogonal basis. This misleading result comes from the fact that the above eigenvectors are represented in the covariant basis. By using the proper inner product with metric tensors, we have $\mathbf{G}(\boldsymbol{U}_i, \boldsymbol{U}_j) = \delta_{ij}$ and $\mathbf{g}(\boldsymbol{u}_i, \boldsymbol{u}_j) = \delta_{ij}$ with i and j being θ and ϕ directions. ▲

By scaling the components of eigenvectors with $\sqrt{g_{\theta\theta}} = 1$ and $\sqrt{g_{\phi\phi}} = \sin(\Theta)$ the eigenvectors can be represented in the physical basis as

$$\begin{aligned}\boldsymbol{U}_{1,2} &= \left(\Lambda_{1,2} - 1\right)\tilde{\boldsymbol{E}}_\theta + \beta(\Theta)t\sin(\Theta)\tilde{\boldsymbol{E}}_\phi,\\ \boldsymbol{u}_{1,2} &= \left(\Lambda_{2,1} - 1\right)\tilde{\boldsymbol{e}}_\theta - \beta(\Theta)t\sin(\Theta)\tilde{\boldsymbol{e}}_\phi.\end{aligned}$$

By substituting the physical basis vectors in terms of Cartesian basis $(\tilde{\boldsymbol{e}}_1, \tilde{\boldsymbol{e}}_2, \tilde{\boldsymbol{e}}_3)$, we can obtain the matrices of rotators U and u. However, instead of the rotator matrices we obtain the corresponding Euler angles Ξ and ξ of the rotators, which are

$$\Xi_{1,2} = \tan^{-1}\left(\frac{\beta(\Theta)t\sin(\Theta)}{\Lambda_{1,2} - 1}\right) = \pm\frac{1}{2}\tan^{-1}\left(\frac{1}{2}\beta(\Theta)t\sin(\Theta)\right)^{\mp 1},$$

and

$$\xi_{1,2} = -\tan^{-1}\left(\frac{\beta(\Theta)t\sin(\Theta)}{\Lambda_{2,1} - 1}\right) = \mp\frac{1}{2}\tan^{-1}\left(\frac{1}{2}\beta(\Theta)t\sin(\Theta)\right)^{\pm 1}.$$

On the right-hand side of the above relations, we have substituted $\Lambda_{1,2}$ and $\beta(\Theta)$ and simplified the expression.[4] It can be seen that $\Xi_{1,2} = -\xi_{2,1}$ and $\Xi_1 - \Xi_2 = \xi_1 - \xi_2 = \dfrac{\pi}{2}$, indicating an orthogonal set of eigenvectors.

Lastly, observe that when $\Gamma_N\Gamma_S < 0$, on the stagnation locus at $\Theta = \tan^{-1}\left(\sqrt[4]{-\Gamma_N/\Gamma_S}\right)$ where velocity vanishes, we have degenerate eigenvalues $\Lambda_1 = \Lambda_2 = 1$, indicating no deformation and rotation. This circle on the sphere draws a barrier between two opposite shear flows in the north and south regions.

In Figure 10.7.1(a) the analytical solutions for the eigenvalues of equation (10.7.6) are plotted for the two antipodal dipole vortices at north and south poles with strengths $\Gamma_N = +1$ and $\Gamma_S = -1$. The blue curves are $\ln(\Lambda_1)$ and the orange curves are $\ln(\Lambda_2)$. Figure 10.7.1(b) shows the Euler angle Ξ_2 versus the position Θ. On both figures (a) and (b), the cascade of curves from inner to outer denote the times $t = 10^{-2}, 10^{-1}, \cdots, 10^3$.

In close neighborhoods of vortices, the velocity vector field is mainly influenced by only one vortex. The streamlines of this flow are circular, provided that the vortices themselves

[4] The inverse trigonometric identity $\tan^{-1}(x) = 2\tan^{-1}\left(\dfrac{x}{1+\sqrt{1+x^2}}\right)$ is used.

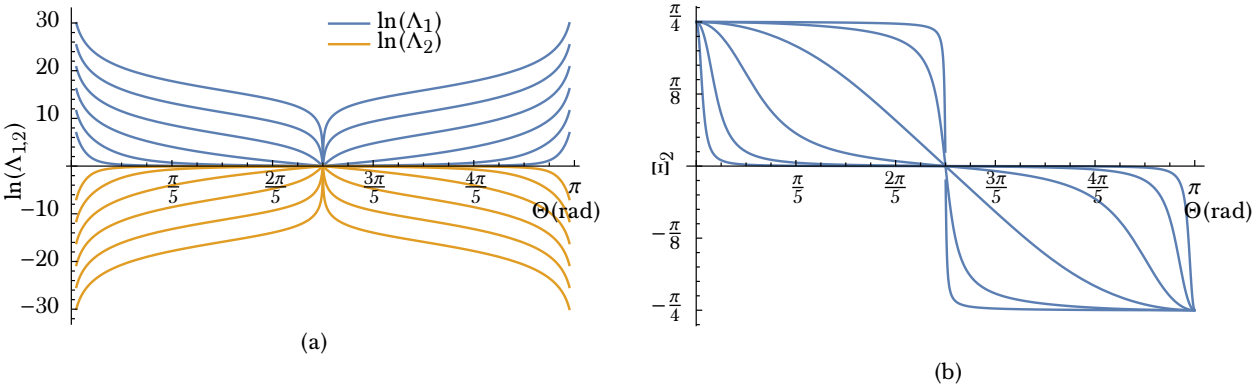

Figure 10.7.1: A plot of the exact solution of (a) eigenvalues Λ_1 and Λ_2 and (b) Euler angle Ξ versus the position Θ at for antipodal dipole vortices of opposite strength.

are stationary. In such case by ignoring the effect of other vortices, the exact solution for eigenvalues are

$$\Lambda_{1,2}(\Theta,t) = 1 + \frac{1}{2}\left(\frac{\Gamma}{4\pi}\cot^2\left(\frac{\Theta}{2}\right)t\right)^2 \pm \sqrt{\left(1+\frac{1}{2}\left(\frac{\Gamma}{4\pi}\cot^2\left(\frac{\Theta}{2}\right)t\right)^2\right)^2 - 1}. \tag{10.7.7}$$

and one of the Euler angles is

$$\Xi_2(\Theta,t) = -\frac{1}{2}\tan^{-1}\left(\frac{\Gamma t}{8\pi}\cot^2\left(\frac{\Theta}{2}\right)\right). \tag{10.7.8}$$

The other Euler angles can be obtained from above. In the neighborhood of a vortex when $\Theta \ll 1$, the above answer is approximated by

$$\Lambda_{1,2}(\Theta,t) = \left(\frac{\Gamma t}{\pi\Theta^2}\right)^{\pm 2} + \mathcal{O}\left(\Theta^{2\mp 4}\right). \tag{10.7.9}$$

and the Euler angle simplifies to

$$\Xi_2(\Theta,t) = \frac{\pi}{4} - \frac{\Theta^2\pi}{\Gamma t} + \mathcal{O}\left(\Theta^4\right). \tag{10.7.10}$$

Figure 10.7.2 shows the plot of $\Lambda_{1,2}$ versus Θ for only one vortex of strength $\Gamma = 1$ at the north pole. The cascades of curves from inner to outer correspond to the times $t = 10^{-2}, 10^{-1}, \cdots, 10^{3}$. It can be seen from the linear portion of the curves in the logarithmic plot that the exact solution in (10.7.7) is well agreement with the approximated solutions in (10.7.9) for small angles.

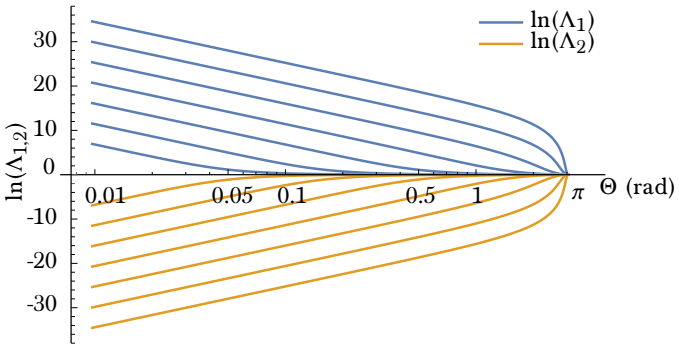

Figure 10.7.2: A plot of the exact solution of $\Lambda_{1,2}$ versus Θ for a monopole vortex configuration.

We note that to use the exact solutions in the neighborhood of a vortex, the angle Θ in the above relations should be measured with respect to the vortex. That is, around the i-th vortex the angle Θ in the above solution is $\Theta = \cos^{-1}(\boldsymbol{x} \cdot \boldsymbol{x}_i)$.

In Figure 10.7.3 we have compared the exact solution and the numerical solution of Λ_1 at the time $t = 20$ (second) with 1000 angle points in the interval $0 \leq \Theta \leq \pi$ (radian). Here, the same vortex configuration of Figure 10.7.1 is used, namely $\Gamma_N = 1$ and $\Gamma_S = -1$. In the figure, for almost all locations the exact and numerical solution agrees up to the integrator's tolerance 10^{-5}. However, in neighborhoods close to north and south poles (i.e., $\Theta < 5^\circ$ and $\Theta > 175^\circ$) the relative error shows a spike up to 4 orders of magnitude. We also observe a spike in the relative error at $\Theta = \pi/2$. At the latter angle, the velocity vector field is zero and the deformation gradient is degenerate with identical eigenvalues, which cause a singularity on evolution differential equations.

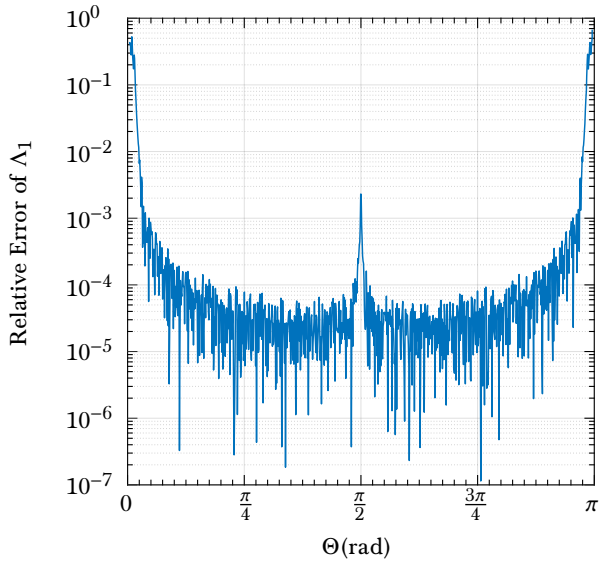

Figure 10.7.3: The relative error of comparing the exact solution and the numerical solution for Λ_1.

Chapter 11

Examples in Euclidean Space

11.1 Introduction

In this chapter, we provide numerical examples for the theory presented earlier. In particular, we compute the finite-time Lyapunov exponent for simple flows. Recall that Λ_i are the eigenvalues of the deformation tensor $\mathbf{C}$. The eigenvalues in the logarithmic scale, i.e., $\mu_a = \ln \sqrt{\Lambda_a}$, are the eigenvalues of the Hencky strain tensor. We remind the reader that FTLE is the eigenvalues of Hencky strain tensor that is normalized by the time, $t^{-1}\mu_i$. The FTLE field shows the exponential growth of the deformation along the principal (eigenvector) directions.

The first three examples are the two-dimensional double-gyre model, the three-dimensional Arnold-Beltrami-Childress flow and the three-dimensional stretch-twist-fold flow. All these flows are presented in Euclidean space with the trivial metric, and the analytical equation for their velocity vector field is known. Accordingly, the rate of deformation gradient tensor $\mathbf{l}$ can be calculated readily. Thus, these flows can be used as a benchmark to test the accuracy of calculations. We leverage the incompressibility (isochoric) property of these flows to test the volume preservation in our theoretical formulations. Recall from the Liouville theorem that the sum of eigenvalues μ_i for an isochoric flow should vanish. We will verify how well this quantity is close to zero. Also, we repeat the calculations with existing methods of computing nonlinear deformation and compare our results. We will demonstrate that our method is significantly more accurate by orders of magnitude.

For the final example in this chapter, we use the turbulence dataset that an analytical equation of the flow is no longer known. These data are obtained by an extensive direct numerical simulation (DNS) at Los Alamos National Laboratory and available for the public. We postpone the practical applications of our framework till Chapter 12 where we present numerical computations on large scale geophysical currents.

11.2 Double-Gyre Model

The double-gyre is a two-dimensional periodic velocity flow that was introduced by Shadden, Lekien, and Marsden [2005, §6, Example 1]. With a slight generalization to the original equations of the authors, the stream-function for this flow is[1]

$$\psi(\boldsymbol{x}, t) = A \sin(\pi k_1(\boldsymbol{x}, t)) \sin(\pi k_2(\boldsymbol{x}, t)),$$

and defined in the domain $\boldsymbol{x} = (x_1, x_2) \in \mathscr{D} := [-1, 1] \times [0, 1]$. The spatial pattern of the flow is determined by the kernel functions k_1 and k_2 where $k_1(\pm 1, x_2, t) = \pm 1$, $k_2(x_1, 0, t) = 0$, and $k_2(x_1, 1, t) = 1$. The simplest form of these functions is the quadratic polynomials,

$$\begin{aligned} k_1(\boldsymbol{x}, t) &= x_1 + p_1(\boldsymbol{x})(x_1^2 - 1)\epsilon_1(t), \\ k_2(\boldsymbol{x}, t) &= x_2 + p_2(\boldsymbol{x}) x_2 (x_2 - 1)\epsilon_2(t). \end{aligned}$$

where p_1 and p_2 are arbitrary functions. The oscillatory functions ϵ_1 and ϵ_2 introduce perturbations to the flow, and given by

$$\epsilon_i(t) = \bar{\epsilon}_i \sin(\omega_i t + \varphi_i), \quad i = 1, 2, \quad 0 \le \bar{\epsilon}_i \le \frac{1}{2},$$

where $\bar{\epsilon}_i$ and ω_i are amplitude and frequency of the oscillations. At all times t, the stream-function on the boundary of $\mathscr{D}$ vanishes, meaning that the flow is always confined in the rectangular domain. Also, this flow is volume presenting. Double-gyre is not physically realistic flow as it does not satisfy the Navier-Stokes equation. However, it is a suitable model to study the mixing and chaotic flows in large deformations.

The components of the spatial velocity (v_1, v_2) are obtained from the stream-function by

$$\begin{aligned} v_1(\boldsymbol{x}, t) &= A\pi \left(\frac{\partial k_1}{\partial x_2} \cos(\pi k_1) \sin(\pi k_2) + \frac{\partial k_2}{\partial x_2} \sin(\pi k_1) \cos(\pi k_2) \right), \\ v_2(\boldsymbol{x}, t) &= -A\pi \left(\frac{\partial k_1}{\partial x_1} \cos(\pi k_1) \sin(\pi k_2) + \frac{\partial k_2}{\partial x_1} \sin(\pi k_1) \cos(\pi k_2) \right). \end{aligned}$$

The velocity vector field of the double-gyre flow is shown in Figure 11.2.1, where we set the parameters $p_1(\boldsymbol{x}) = p_2(\boldsymbol{x}) = 1$, $\omega_1 = \frac{\pi}{5}$, $\omega_2 = 0$, $\varphi_1 = \varphi_2 = 0$, $\epsilon_1 = \frac{1}{4}$, $\omega_2 = 0$, and $A = 0.1$. The figure shows the velocity at time $t = T$, where $T = 2\pi/\omega_1 = 10$ (seconds) is the period of oscillation. The center of the two *gyre* vortices oscillates horizontally, which moves the borderline between the two basins of vortices. However, the pathlines of this flow are aperiodic and chaotic.

[1] Unlike our previous notations for contravariant variables, here we use lower indices for vectors, such as (x_1, x_2) for the components of position, and (v_1, v_2) for the components of velocity.

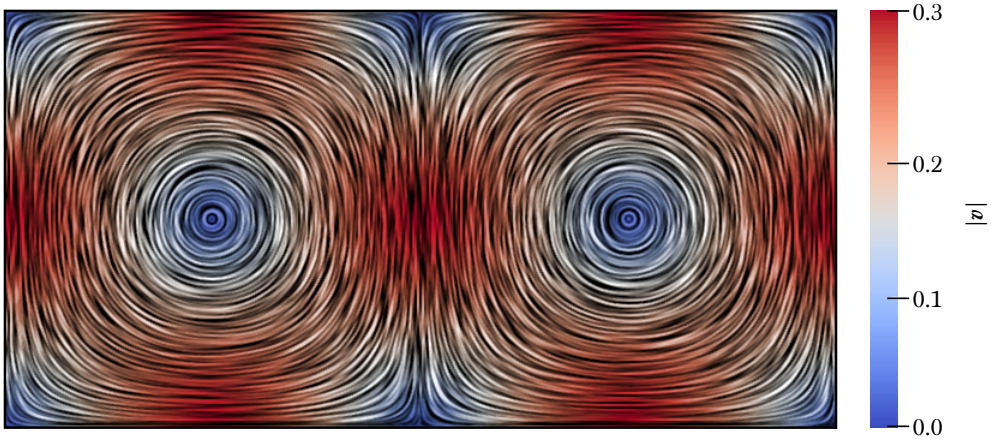

Figure 11.2.1: The streamlines and magnitude of the velocity field for the double-gyre flow in the domain $[-1,1]\times[0,1]$.

To compute the FTLE field for this flow, we have integrated the evolution equations, namely, we used Proposition 9.2.2 and Proposition 9.2.4 to integrate the Euler angles of eigenvector frames, and we used Theorem 7.3.4 to evolve the eigenvalues of deformation. These quantities are computed on a Cartesian grid of 2001×1001 points and the evolution equations are integrated for one oscillation cycle, i.e., $t = T = 10$ seconds for the reversed flow. The set of differential equations was solved by the adaptive Runge-Kutta scheme of order 4-5 with the numerical integration tolerance 10^{-8} and the initial time step $\Delta t = 10^{-3}$. The FTLE field for this flow is shown in Figure 11.2.2. Recall that $\Lambda_{1,2}$ are the eigenvalues of deformation tensor, and the logarithms $\mu_{1,2} = \ln\sqrt{\Lambda_{1,2}}$ are the eigenvalue of the Hencky strain tensor. The backward FTLE is $t^{-1}\mu_1$ when the flow is reversed, i.e., time direction is reversed. In Figure 11.2.2, the main ridge of the backward FTLE field is the red curve in the middle of the domain and acts as an almost material barrier that separates the two gyres.

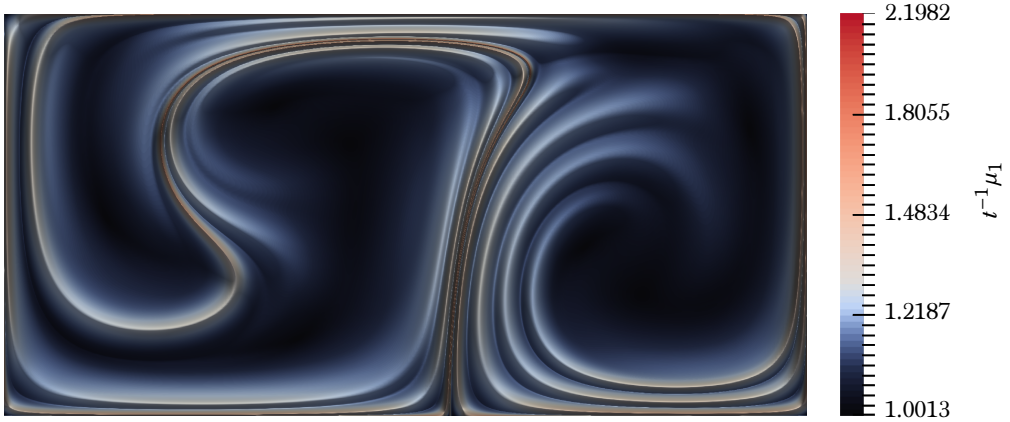

Figure 11.2.2: The backward FTLE field of the double-gyre flow.

Recall from the Liouville theorem in Corollary 7.4.1 that the sum $\mu_1 + \mu_2$ should vanish for isochoric flows. This quantity can be used as a measure to test the numerical accuracy of the integration method. Figure 11.2.3 shows the sum $t^{-1}(\mu_1 + \mu_2)$ for the double-gyre flow. Except for the ridges of the FTLE field, the sum is considerably close to the error tolerance of the integrator scheme, $\mathcal{O}(10^{-8})$. The chaotic nature of the flow is more significant on the ridge of the FTLE field where any small perturbation of the initial point on the ridge may switch the trajectory from one to the other gyre domain. For this reason, the numerical integration produces higher errors on the ridge.

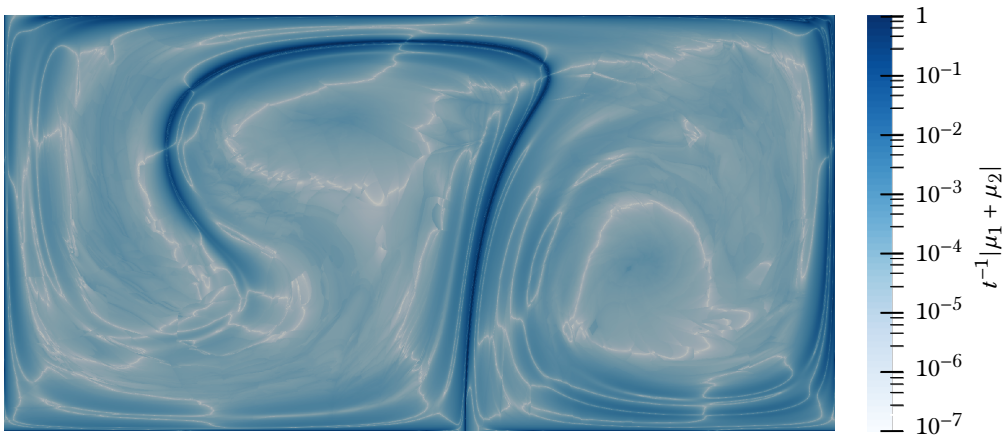

Figure 11.2.3: Sum of first and second backward FTLE fields of the double-gyre flow.

We note our method produces significantly lower error compared to the conventional methods of computing FTLE. For the comparison, we have also computed the FTLE field with the finite-difference method. In this method the deformation tensor is directly computed by advecting a grid of flow particles, then with finite-difference, the deformation gradient tensor is estimated. The eigenvalues are calculated from the singular value decomposition of the deformation gradient. Figure 11.2.4 compares the error of the two methods method by showing the histogram of the sum of FTLE over points of the domain. The error of the presented method is in order of $\mathcal{O}(10^{-11})$, which is less than the tolerance error of our numerical integration scheme. On the contrary, if we use the finite-difference method to compute the deformation tensor and calculate its eigenvalues, the error is on the order $\mathcal{O}(10^{-4})$.

11.3 Arnold-Beltrami-Childress Flow

The Arnold-Beltrami-Childress (ABC) flow is a three-dimensional steady-state inviscid flow model that satisfies the steady incompressible Euler equation,

$$\boldsymbol{v} \cdot \nabla \boldsymbol{v} + \nabla p = \mathbf{0},$$

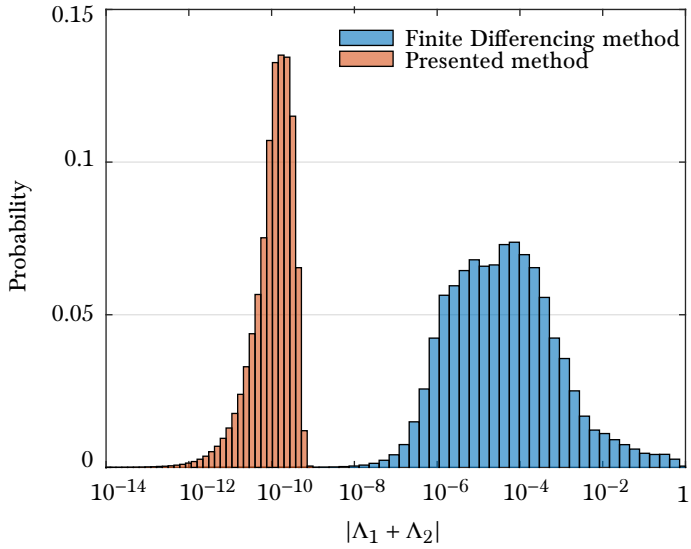

Figure 11.2.4: Comparison of the sum of FTLE values as a histogram over domain points for the presented method versus other methods.

where p is the pressure field. The autonomous spatial velocity vector field $\boldsymbol{v}(\boldsymbol{x}) = v_a(\boldsymbol{x})\boldsymbol{e}_a$ for $a = 1, 2, 3$ has a simple analytical representation given by

$$\begin{aligned} v_1(x_1, x_2, x_3) &= A\sin(x_3) + C\cos(x_2), \\ v_2(x_1, x_2, x_3) &= B\sin(x_1) + A\cos(x_3), \\ v_3(x_1, x_2, x_3) &= C\sin(x_2) + B\cos(x_1), \end{aligned}$$

which is spatially periodic by tiling the domain $(x_1, x_2, x_3) \in [-\pi, \pi]^3$. The streamlines of ABC flow have been introduced in Arnold [1965]. Numerical experiments by Henon [1966] for the choice of constants $A = \sqrt{3}$, $B = \sqrt{2}$ and $C = 1$ has shown that the flow possesses a chaotic behavior. The chaotic behavior means that the infinitesimally close initial fluid particles diverge exponentially in time. The chaotic behavior of the flow is further studied by Dombre, Frisch, Henon, Greene, and Soward [1986]. Additionally, the ABC flow has the Beltrami property, in which the vorticity and velocity are co-linear, i.e., $\boldsymbol{v} \wedge (\nabla \wedge \boldsymbol{v}) = \boldsymbol{0}$. Beltrami flows are believed to play a significant role in describing turbulent flows Pelz, Yakhot, Orszag, Shtilman, and Levich [1985]. From the dynamical system point of view, the Beltrami property violates Arnold's condition of existence of invariant tori [Arnold, 1966, p. 346], hence, this flow carries interesting chaotic properties. The velocity field of the ABC flow is shown in Figure 11.3.1 for the set of parameters mentioned above.

The three backward FTLE fields corresponding to the eigenvalues $\mu_1 > \mu_2 > \mu_3$ of the Hencky strain tensor are shown in Figure 11.3.2. In the first row of the figure, the deformation tensor is computed by the finite-difference method and then their eigenvalues are evaluated.

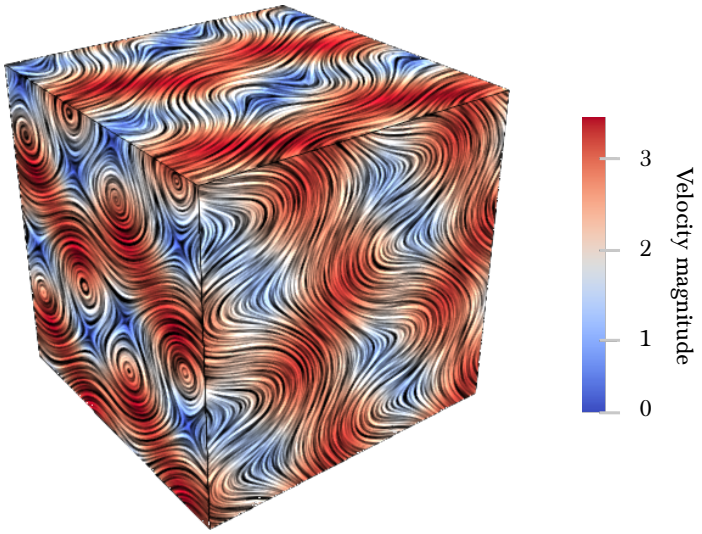

Figure 11.3.1: Velocity streamlines and magnitude of ABC flow in the cube $[-\pi, \pi]^3$.

In the second row of the figure, we have computed the eigenvalues with our method, in which we have used the quaternionic evolution equations given in §8.5 to evolve the left and right eigenvector frames of deformation, together with Theorem 7.3.4 for the eigenvalues of deformation. The set of differential equations is integrated by the adaptive Runge-Kutta scheme of order 4-5, with the error tolerance 10^{-8} and the initial integration time step $\Delta t = 10^{-3}$, and the integration duration $t = 10$ (seconds) on a Cartesian grid of 201^3 points. The FTLE fields with our method are more resolved, especially near the ridges of the fields.

The ABC flow is isochoric, meaning that $\nabla \cdot \boldsymbol{v} = 0$. Thus, by the Liouville theorem, the sum $\mu_1 + \mu_2 + \mu_3$ should vanish. To test the accuracy of our method, we have shown this sum in Figure 11.3.3. The left of the figure is computed by the finite-difference method and shows errors of order $\mathcal{O}(1)$. In contrast, the right side of the figure is computed by our method and the error range is on the order $\mathcal{O}(10^{-6})$. The accuracy of the finite-difference method depends on the grid size and the integration method. Whereas, in our method, the error is independent of the grid size and only depends on the numerical error of the integration scheme.

11.4 Stretch-Twist-Fold Flow

The stretch-twisting-fold (STF) is a class of chaotic viscous flows inside the unit ball $\mathbb{B} = \{r \mid |r| < 1\}$ that the velocity field is quadratic in coordinates. These flows are introduced by Bajer, Moffatt, and Nex [1990] and have been generalized by Bajer and Moffatt [1990]. The flow is steady-state and satisfies Stokes (creeping) flow with the momentum equation

$$\nabla^2 \boldsymbol{v} = \nabla p.$$

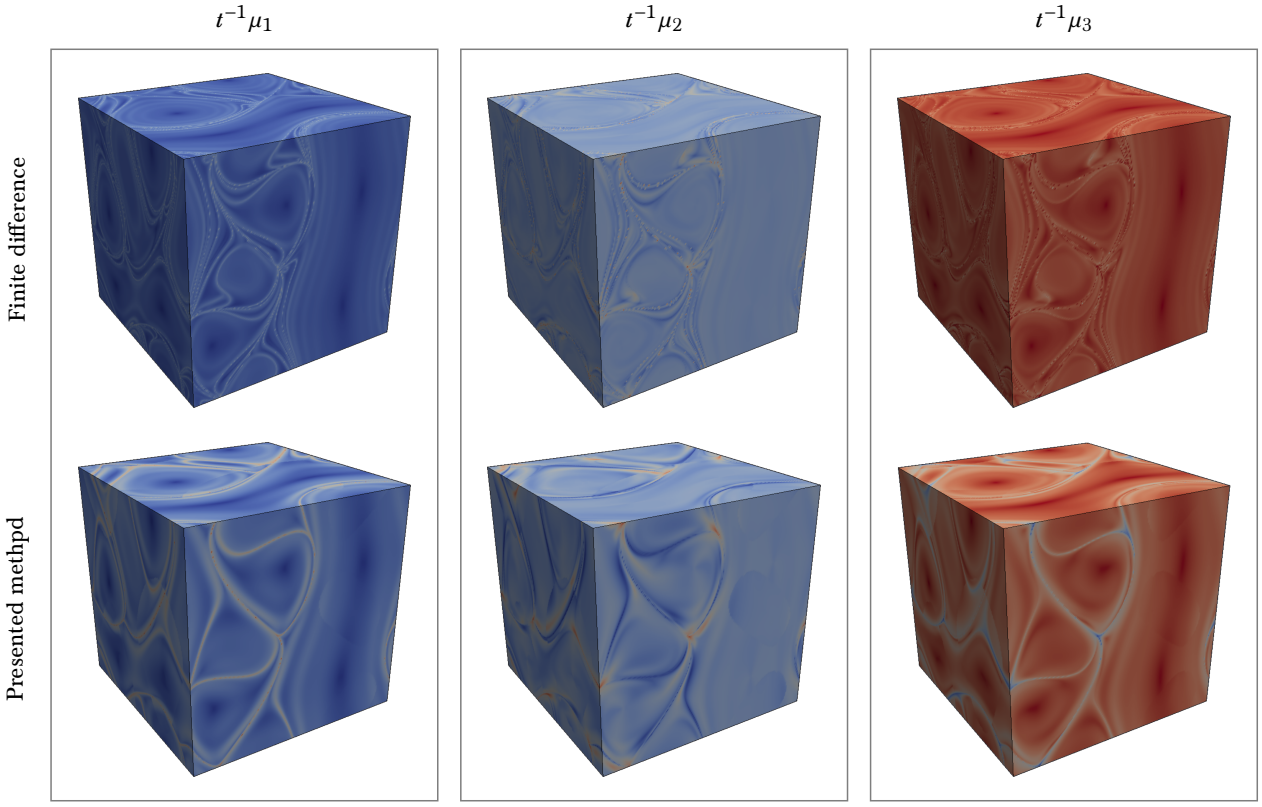

Figure 11.3.2: The three FTLE fields for eigenvalues $\mu_1 > \mu_2 > \mu_3$. The first row is computed by finite difference and the second row is computed by the presented method.

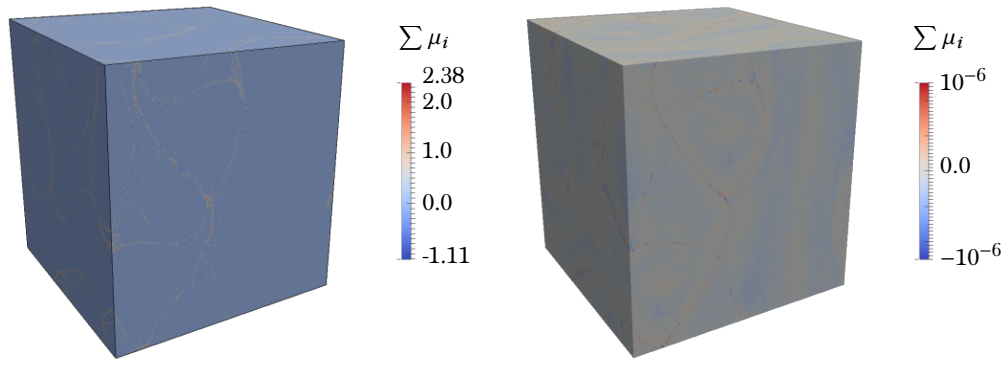

(a) Finite difference method (b) Presented method

Figure 11.3.3: Sum of FTLE fields. Left: finite-difference method. Right: the presented method.

Alternatively, $\nabla^2\boldsymbol{\omega} = \mathbf{0}$, where $\boldsymbol{\omega}$ is the vorticity. This flow has a zero flux on the spherical boundary of the ball, i.e., $\boldsymbol{v}\cdot\boldsymbol{n} = 0$ where $\boldsymbol{n}$ is the unit normal vector on the sphere. It has been shown that this flow can be decomposed into the sum of three flows, (a) a poloidal flow of the Hill's vortex structure, (b) a quasi-rigid rotation and (c) a twisted flow. The two-parameter model of the STF flow is given by the velocity field

$$\begin{aligned} v_1 &= \alpha x_3 - 8x_1x_2, \\ v_2 &= 11x_1^2 + 3x_2^2 + x_3^2 + \beta x_1x_3 - 3, \\ v_3 &= -\alpha x_1 + 2x_2x_3 - \beta x_1x_2. \end{aligned} \tag{11.4.1}$$

The STF flow has two heteroclinic stagnation points at $\boldsymbol{x} = (0, \pm 1, 0)$. Except for the heteroclinic orbits, most streamlines of this flow are closed. Additionally, for $\alpha \ll 1$, the STF flow is a weakly perturbed integrable flow and has closed streamlines. We set the parameters of (11.4.1) to the default values $\alpha = -1$ and $\beta = \frac{1}{4}$ as suggested by the authors.

The velocity field in the equation (11.4.1) has been generalized to accept more parameters, and given by

$$\boldsymbol{v} = \left(1 - 2|\boldsymbol{x}|^2\right)\boldsymbol{a} + (\boldsymbol{a}\cdot\boldsymbol{x})\,\boldsymbol{x} + \boldsymbol{\Omega}\wedge\boldsymbol{x} - \boldsymbol{x}\wedge\nabla\boldsymbol{\tau},$$

where $\boldsymbol{x} = (x_1, x_2, x_3)$ is the position in the unit ball, and $\boldsymbol{a} = (a_1, a_2, a_3)$ is a vector parameter. The first two terms on the right-hand side of the above velocity field are the contribution of the *poloidal field* and introduce stretching. The third term is a rigid rotation around the vector $\boldsymbol{\Omega} = (\Omega_1, \Omega_2, \Omega_3)$. The fifth term is the *toroidal field* that is characterized by the vector parameter $\boldsymbol{\tau} = (\tau_1, \tau_2, \tau_3)$ and introduces twisting to the flow. The parameter $\boldsymbol{\tau}$ is often set by $\boldsymbol{\gamma} = (\gamma_1, \gamma_2, \gamma_3)$ with $\gamma_1 := 2(\tau_2 - \tau_3)$, $\gamma_2 := 2(\tau_3 - \tau_1)$ and $\gamma_3 = 2(\tau_1 - \tau_2)$. The parameters γ_i are the principal rates of the twist. If we set $\boldsymbol{\gamma} = (0, \beta, -\beta)$ and $\boldsymbol{\Omega} = (0, \alpha, 0)$, the set of equations (11.4.1) are retrieved.

The FTLE field for this flow is computed based on the velocity field of equation (11.4.1) by the quaternionic evolution equations presented in §8.5 for the eigenvector frames, together with Theorem 7.3.4 for the eigenvalues. The set of differential equations is integrated by the adaptive Runge-Kutta scheme of order $4 - 5$ with the error tolerance 10^{-8} and the initial integration time step $\Delta t = 10^{-3}$. The computational domain is a grid of 1000^2 points in the spherical coordinate on the surface of the sphere. The results are shown in Figure 11.3.2. The first and second rows of the figure correspond to the backward integration times $t = 5$ and $t = 10$ seconds, respectively. The left, middle and right columns of the figure are the backward FTLE fields corresponding to the eigenvalues μ_1, μ_2 and μ_3 where $\mu_1 > \mu_2 > \mu_3$. Since this flow is isochoric, it is expected that $\mu_1 + \mu_2 + \mu_3 = 0$. With our method, the sum of μ_a vanish independent of the grid size, hence, the volume is preserved precisely.

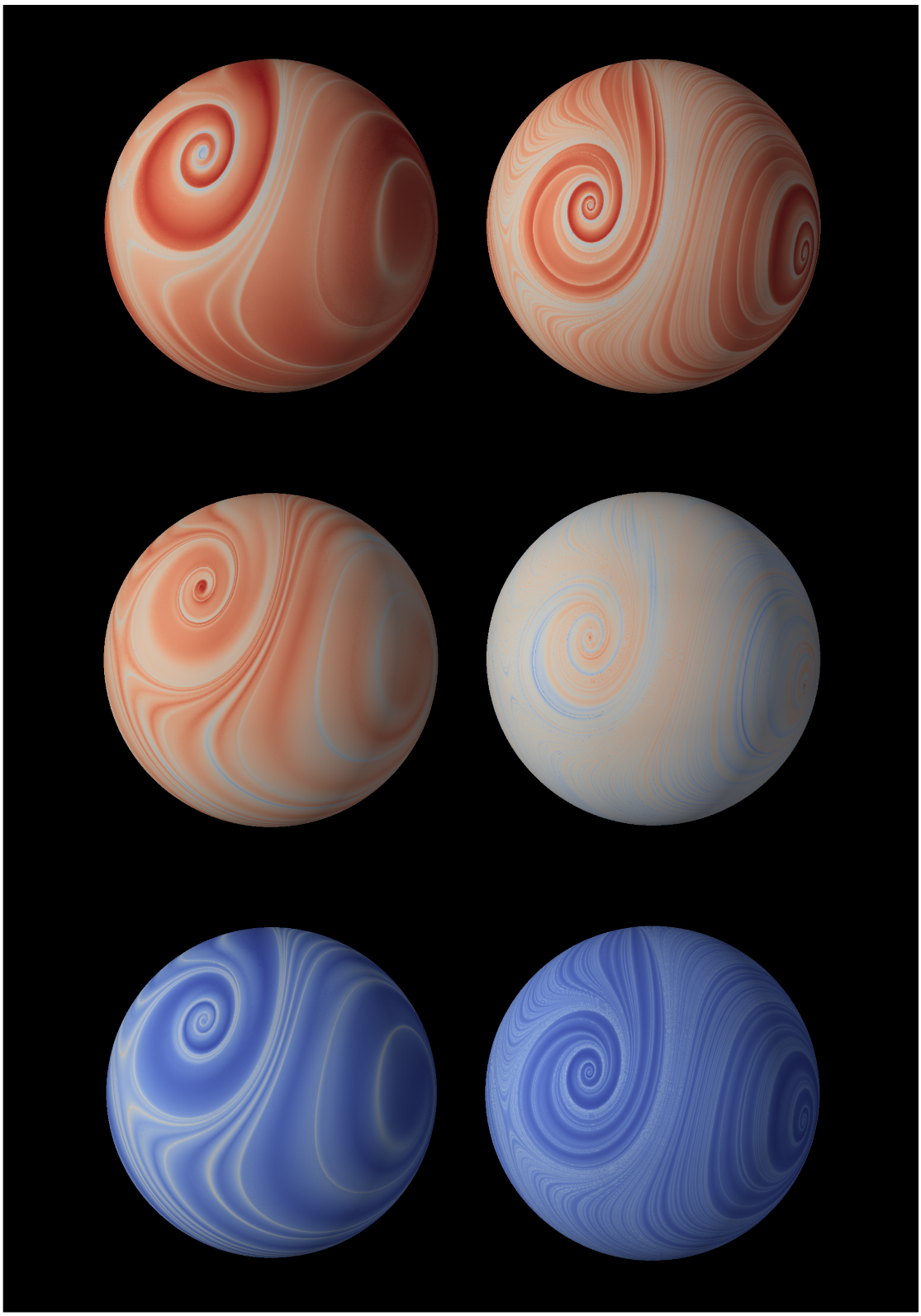

Figure 11.4.1: The backward FTLE fields of the STF flow. Left to right correspond to three eigenvalues $\mu_1 > \mu_2 > \mu_3$. Top and bottom rows correspond to the integration durations $t = 5$ and $t = 10$ seconds.

11.5 Mixing Turbulence

The mixing flow is homogeneous buoyancy-driven turbulence by the provenance of Livescu, Canada, Kanov, Burns, staff, and Pulido [2014] at the Los Alamos National Laboratory[2]. The data are computed by direct numerical simulation (DNS) with the full Navier-Stokes equation on 1024^3 grid points Livescu and Ristorcelli [2007, 2008]; Livescu [2013]. In this flow, two fluids with close densities are initialized at random bubbles and start at rest under constant gravitational force, then move in opposite directions due to the buoyancy forces.

In Figure 11.5.1(a), we have shown the velocity field after $t = 9$ seconds from rest when the Reynolds turbulent kinetic energy of mixing is at its highest. After this time, the mixing cascades to smaller length scales, till the two fluids completely mix.

We have calculated the FTLE field on the Cartesian grid of 256^3 points. To estimate the rate of deformation tensor $\mathbf{I}$ from the velocity field, we have used quadratic interpolation on finite-element basis functions in a rectangular grid. The quaternionic evolution equations in §8.5 are used to evolve the eigenvector frames together with Theorem 7.3.4 for the eigenvalues. The set of differential equations is integrated by the adaptive Runge-Kutta scheme of order 4-5 for $t = 9$ (seconds). The results of the FTLE field are shown in Figure 11.5.1(b). The ridges of the FTLE field unveil the structures of the flow from the Lagrangian perspective. These Lagrangian structures cannot be inferred from the Eulerian information such as the velocity field.

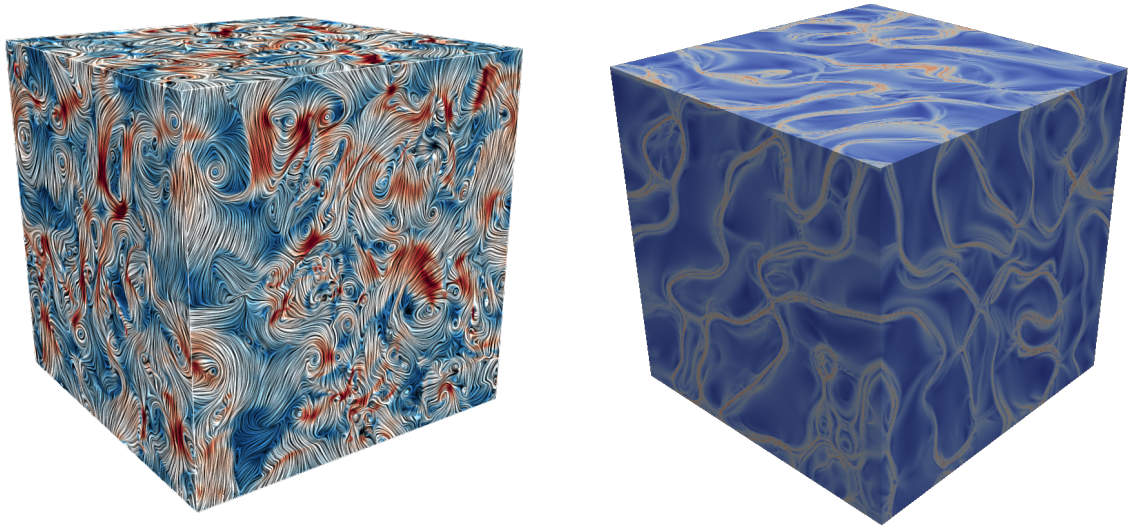

(a) Velocity field (b) FTLE field

Figure 11.5.1: Mixing turbulence flow at $t = 9$ seconds. (a) Velocity field, (b) backward FTLE field.

[2]The turbulence dataset that we have used are publicly available online at the *John Hopkins Turbulence Database* at `http://turbulence.pha.jhu.edu/`.

Chapter 12

Software Development

"Science is what we understand well enough to explain to a computer. Art is everything else we do."

— Donald Knuth, $A = B$

12.1 TRACE: A Web-Based High-Performance Computing Gateway

Computing the FTLE field has become a standard tool to identify coherent structures and analysis of advective transport in unsteady flows. In practical applications, obtaining the FTLE field can be computationally intensive. We have developed a comprehensive computing platform for the Lagrangian analysis of practical oceanographic applications, which addresses the computational challenges and convenience of use for end-users. Our tool, *Trajectory Reconstruction and Analysis for Coherent Structure Evaluation* (*TRACE*) is a web-based computational gateway and available online as a community resource at

http://transport.me.berkeley.edu/trace.

The gateway features the ability to access remote datasets, is object-oriented, employs parallel processing to efficiently handle larger scale computation of trajectories and enables high-quality geospatial visualization. TRACE is capable of processing up to billion-point grids and has been employed in real-time ocean field experiments and search and rescue sea exercises. A short demo video of using TRACE can be found at

https://vimeo.com/sameli/trace-demo.

TRACE has a *server-client architecture* with multiple components communicating remotely, as shown in Figure 12.1.1. The client-side is a program that loads on the user's browser, renders the webpage and interacts with the user's requests. The server-side program, on the other hand, operates on a computing cluster, which communicates with a database server to stream input/output datasets and performs parallel numerical computations.

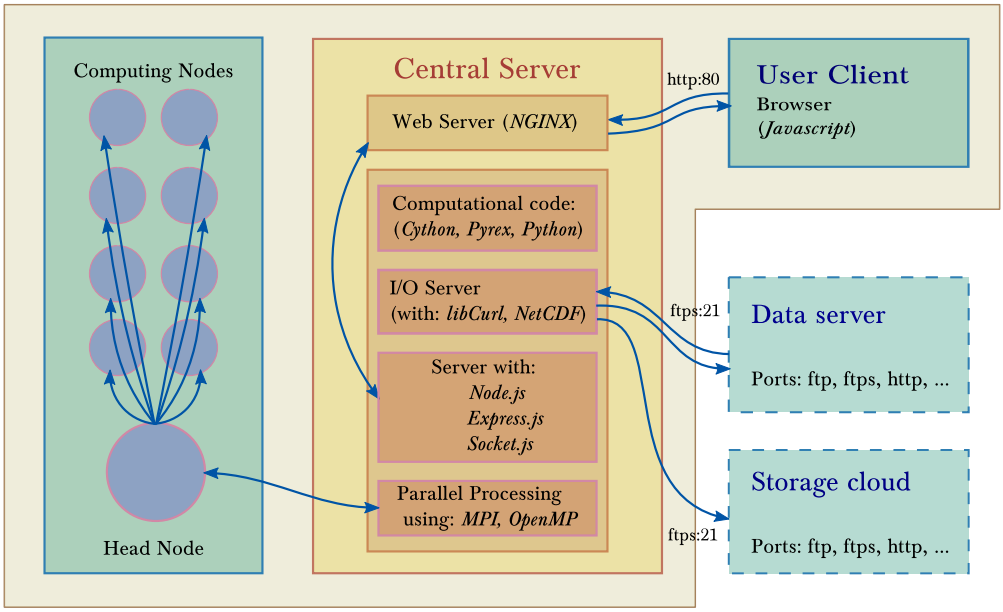

Figure 12.1.1: The server-client architecture of TRACE.

12.2 RESTORE: A Web-Based Data Pre-Processing Gateway

Measurements of oceanographic variables, such as the ocean surface velocity field, often do not have complete coverage. A few or isolated missing points in the data might be acceptable for an Eulerian analysis that is spatially and temporally localized. However, for applications that leverage Lagrangian analysis, complete coverage of the vector field is required. We have developed RESTORE, a computing platform to address this issue by the method of Ameli and Shadden [2019]. RESTORE is a web-based computational gateway and available online as a community resource at

`http://transport.me.berkeley.edu/restore`,

The gateway has a similar server-client architecture as TRACE that is shown in Figure 12.1.1. A short demo video of using RESTORE can be found at

`https://vimeo.com/sameli/restore-demo`.

Figure 12.2.1 shows an example of restoring missing velocity data at two sites, (a) Northern California and (b) at Martha's Vineyard Island, MA. The velocity field shown on the first row is measured remotely by an array of land-based high-frequency (HF) radars. The second row is the restored velocity data using RESTORE. This tool is an essential pre-processing step before any Lagrangian analysis is performed on the data.

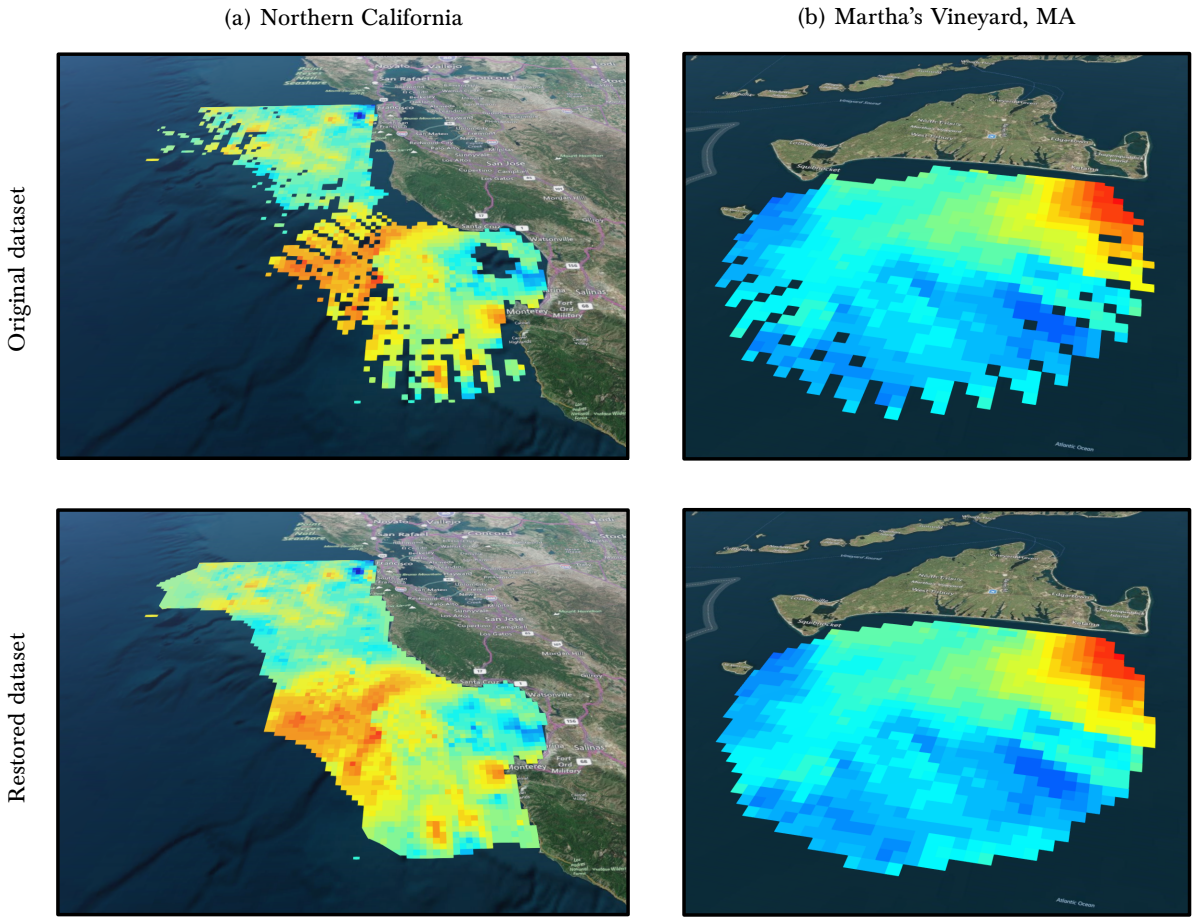

Figure 12.2.1: The magnitude of ocean surface velocity is shown in (a) Northern California and (b) Martha's Vineyard, MA. The first row is obtained by HF radar measurements, and the second row is the processed data using RESTORE.

12.3 Gallery

We present numerical computations of flow transport on oceanographic datasets by TRACE. In particular, we compute the *backward* FTLE field. The backward field is obtained when the time direction is reversed, hence the FTLE represent the exponential shrink rate (instead of growth rate) of deformation along the principal (eigenvector) directions. The oceanographic flows are three-dimensional and incompressible. However, we only use the two-dimensional components of the ocean's surface flows, because the third component of velocity (upwelling and downwelling) is insignificant in large-scale ocean flows.

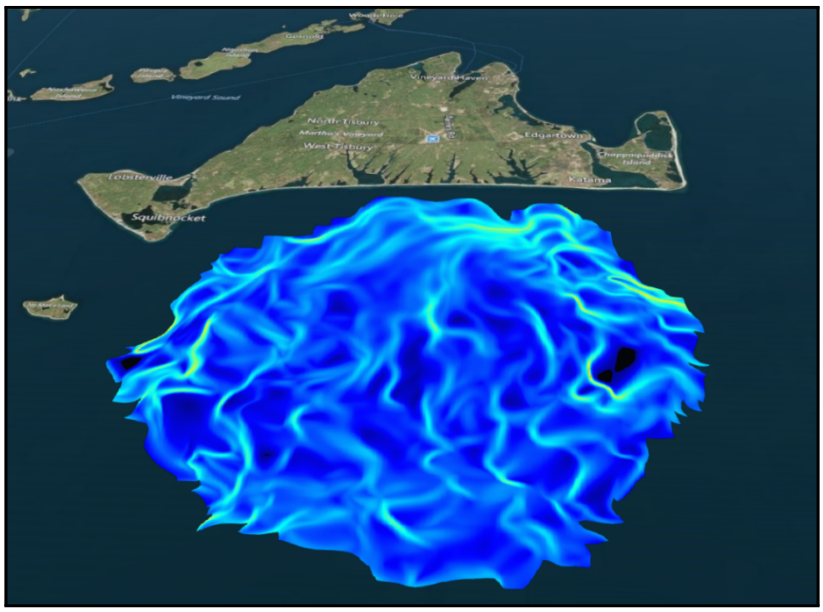

Figure 12.3.1: Backward FTLE computed on ocean surface velocity measured by HF radar. South of Martha's Vineyard Island, Massachusetts, August 2018. The ocean surface velocity data are the courtesy of the Woods Hole Oceanographic Institute (see Footnote 1 for credits).

Sub-mesoscale Ocean Currents

The sub-mesoscale oceanography studies ocean circulations that extend a few kilometers. On these scales, we ignore the Earth curvature and assume the velocity data are in the two-dimensional Euclidean (flat) space. We present three examples as follows.

In Figure 12.3.1 the backward FTLE is shown in the south of Martha's Vineyard Island, Massachusetts during our field experiment in August 2018. Details of the measurements can be found in Kirincich, de Paolo, and Terrill [2012] and Kirincich [2016][1]. To restore the incomplete coverage of the data we have employed the RESTORE tool (see §12.2). The backward FTLE is computed for the integration time $t = 6$ hours, which is half the duration of a tidal cycle. The computational domain is a Cartesian grid with 1000^2 points on the Euclidean space.

Figure 12.3.2 shows the backward FTLE at the similar time and location mentioned for Figure 12.3.1, with the difference that the velocity data are obtained from ocean model forecasts[2]. The FTLE is calculated for the integration duration of half the tidal cycle, $t = 6$

[1]The HF radar data are publicly available at `https://cordc.ucsd.edu//projects/mapping/global`. The data of the Martha's Vineyard Island are the courtesy of the Woods Hole Oceanographic Institute, Massachusetts. In particular, I am thankful to A. Kirincich for providing me the real-time data during our collaboration in the field experiments of August 2017 and 2018.

[2]I am grateful to Prof. P. Lermusiaux, P. Haley and the MSEAS group at MIT for providing me their

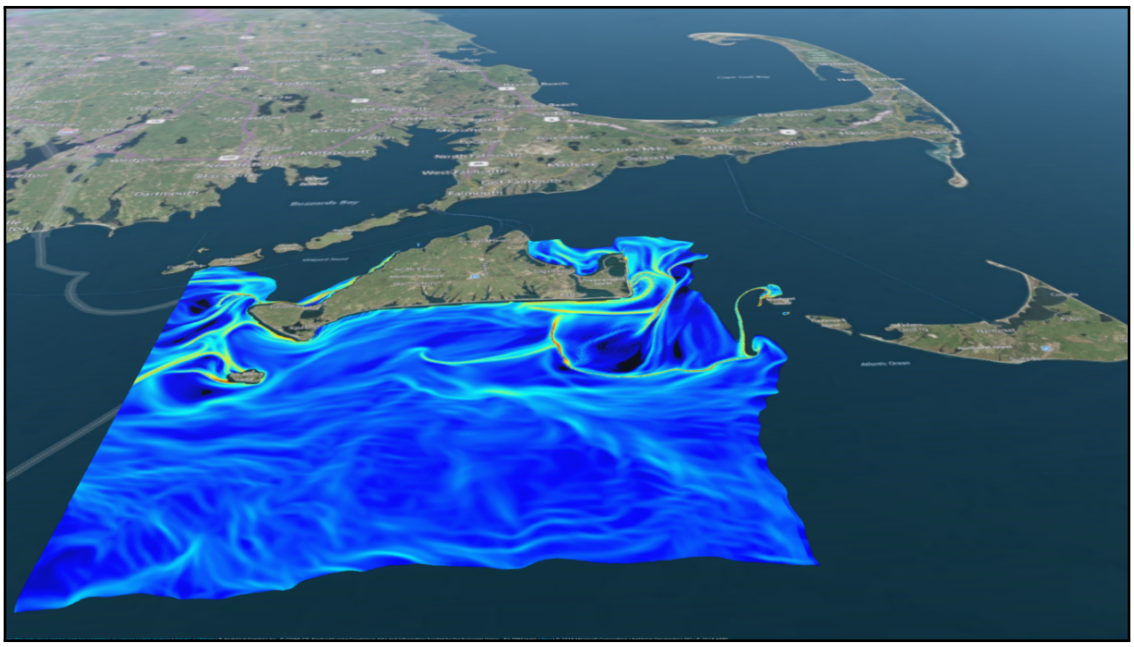

Figure 12.3.2: Backward FTLE calculated on ocean model data. South of Martha's Vineyard Island, Massachusetts, August 2017. The ocean model velocity data are the courtesy of MSEAS at MIT (see Footnote 2 for credits).

hours. The computational domain is a Cartesian grid with 3000^2 points.

Figure 12.3.3 displays the backward FTLE field computed in the south of Taiwan[3], which is a mesoscale domain. The computational domain is a Cartesian grid with 3000^2 points with quadratic element basis functions and the integration duration of $t = 7$ hours. In this domain, the effect of Earth's curvature begins to be sensible, particularly when the fluid particle trajectories are compared with and without assuming the Riemannian metric of the sphere. However, the structure of the FTLE field is not significantly affected.

Large-scale Ocean Currents

We present a global scale computation of FTLE covering all oceans. On such a scale, it is necessary to take into account the Earth curvature using Riemannian metric tensor on the Riemann sphere (see formulations in Chapter 7 and Chapter 10). The domain of velocity data (the *Eulerian* information) covers $-180°$ to $+180°$ longitudes and $-80°$ to $+80°$ latitudes on a grid of approximately 1440×720 points.

extensive ocean model forecast data during our collaboration on the field experiment of August 2017 and 2018. Further description of their data is available at http://mseas.mit.edu/Sea_exercises/NSF_ALPHA/2017.

[3]The ocean model velocity data are the courtesy of M. H. Chang at the Institute of Oceanography, National Taiwan University, and D. Ko at the United States Naval Research Laboratory.

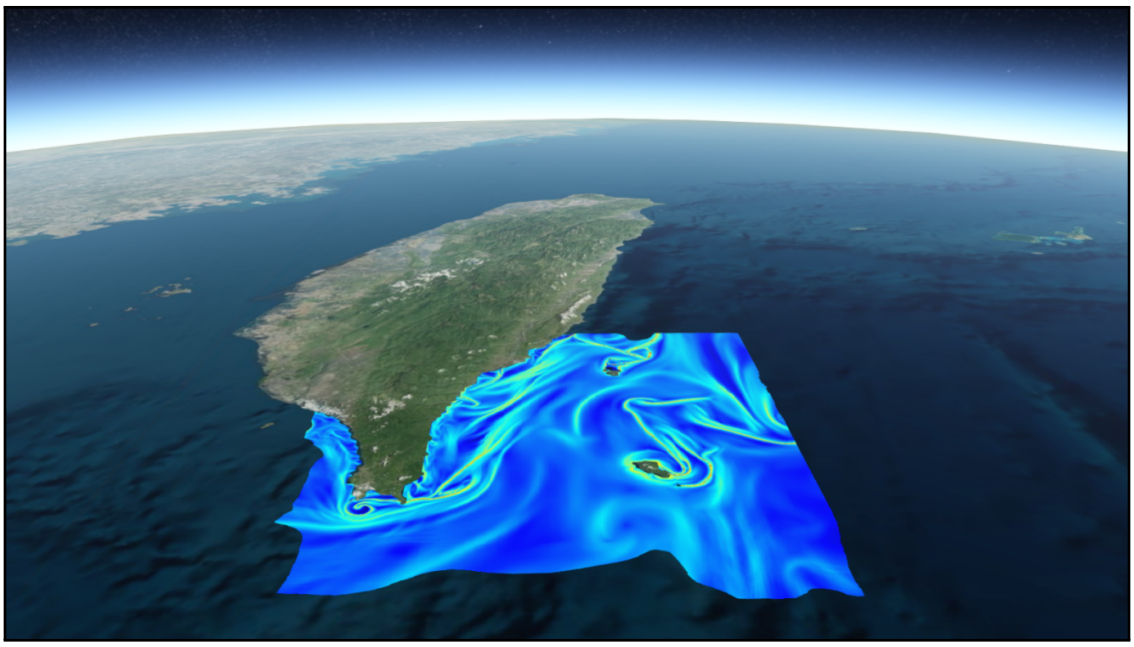

Figure 12.3.3: Backward FTLE field, south of Taiwan. Ocean model velocity data are the courtesy of the Institute of Oceanography at National Taiwan University (see Footnote 3 for credits).

In all FTLE computations presented below, the integration time t is 45 days using the adaptive Runge-Kutta-Verner integration scheme of order 6-7 with relative tolerance accuracy of 10^{-6}. Quadratic element basis functions are used to estimate velocity and velocity gradients form the discrete datasets at each numerical step. The computational grid of the FTLE field (to compute *Lagrangian* data) covers the longitude range of $-180°$ to $+180°$ and the latitudes range of $-90°$ to $+80°$. In contrast to the grid of Eulerian data (velocity), we compute the Lagrangian data (FTLE) on the very dense grid of 576 million points. We found that the Lagrangian information (i.e., FTLE) cannot be resolved sufficiently unless such a massive computational grid is employed.

For such an extensive grid the efficiency of the computation is not only important but a requirement. In our considerations in developing TRACE software was to address such massive computations, such as leveraging the reduced-order equations developed in Chapter 8 and Chapter 9, implementing parallelized computational platform, utilizing techniques for efficient data management data stream between servers, and visualization of large data. Without these considerations, computations on such large-scale data are impractical.

The global scale FTLE fields that we present are computed based on two sources of ocean velocity data at NASA and NOAA that we describe as follows. In Figures 12.3.4, 12.3.5, 12.3.8 and 12.3.11, the original velocity field is obtained from OSCAR ocean model by Bonjean

and Lagerloef [2002] and produced by JPL, NASA ESR. [2009][4]. The regions shown in the figures respectively are the Indian ocean in Figure 12.3.4, the Pacific Ocean in Figure 12.3.5, the Atlantic Ocean in Figure 12.3.8, and the Southern Ocean in Figure 12.3.11. In all these figures, the backward FTLE field is calculated for October 22, 2018.

In the Figure 12.3.13, we used the realistic ocean velocity data obtained from Jason-3 satellite provided by the Laboratory for Satellite Altimetry, NOAA[5]. This figure shows the Atlantic Ocean where the FTLE is calculated for May 05, 2019.

The coherent structures of the ocean flow can be visualized by the backward FTLE. To our surprise, we have observed that on the *ocean currents*, the ridge structures of the FTLE field are in agreement with the visual patterns of sea surface temperature (SST) and chlorophyll concentration. This is because the flows on the ocean's currents are advection dominant and the scalar fields such as SST laid out the flow structures. The three Figures 12.3.5, 12.3.8 and 12.3.11 respectively show Japan's *Kuroshio current*, the *Gulf stream*, and the *Agulhas current*. Accompanied by these figures, we have shown the SST and chlorophyll concentration at the same time and location for comparison with the FTLE fields. Namely, corresponding to each of the Figures 12.3.5, 12.3.8 and 12.3.11, we have shown the sea surface temperature, respectively in Figures 12.3.6, 12.3.9 and 12.3.12. The SST fields by Chao, Li, Farrara, and Huang [2009] are from the Group for High-Resolution Sea Surface Temperature (GHRSST) and obtained by the aggregation of eight satellite data with 0.01 grid resolution and publicly available at JPL OurOcean Project [2010]. The SST field in the figures is monthly averaged and ranges from 273 Kelvin (in purple) to 305 Kelvin (in red).

Also the chlorophyll concentration in Figures 12.3.7 and 12.3.10 is shown corresponding to the FTLE in the Figures 12.3.5 and 12.3.8. The chlorophyll data by Hu, Lee, and Franz [2012] are obtained by the Moderate Resolution Imaging Spectroradiometer Satellite (MODIS) and available at NASA Goddard Space Flight Center, Ocean Ecology Laboratory, Ocean Biology Processing Group [2018]. The chlorophyll concentrations are shown on a logarithmic scale ranging from 6.5×10^{-3} mg/m^3 (in purple) to 6.0 mg/m^3 (in red).

All our results in the FTLE calculations together with an overlay of SST fields in the Figures 12.3.4 to 12.3.11 can be accessed through an interactive visualization webpage at

`https://trace.page.link/earth`,

and a demo video of these fields can be found at

`https://vimeo.com/sameli/earth`.

[4]OSCAR ocean model data is publicly available at PO.DAAC service, JPL, NASA at `http://podaac.jpl.nasa.gov/dataset/OSCAR_L4_OC_third-deg`.

[5]I acknowledge S. Baker-Yeboah and E. Leuliette at NESDIS, NOAA, for proving me the satellite altimetry data. NESDIS NOAA is the National Environmental Satellite, Data, and Information Service at the National Oceanic and Atmospheric Administration.

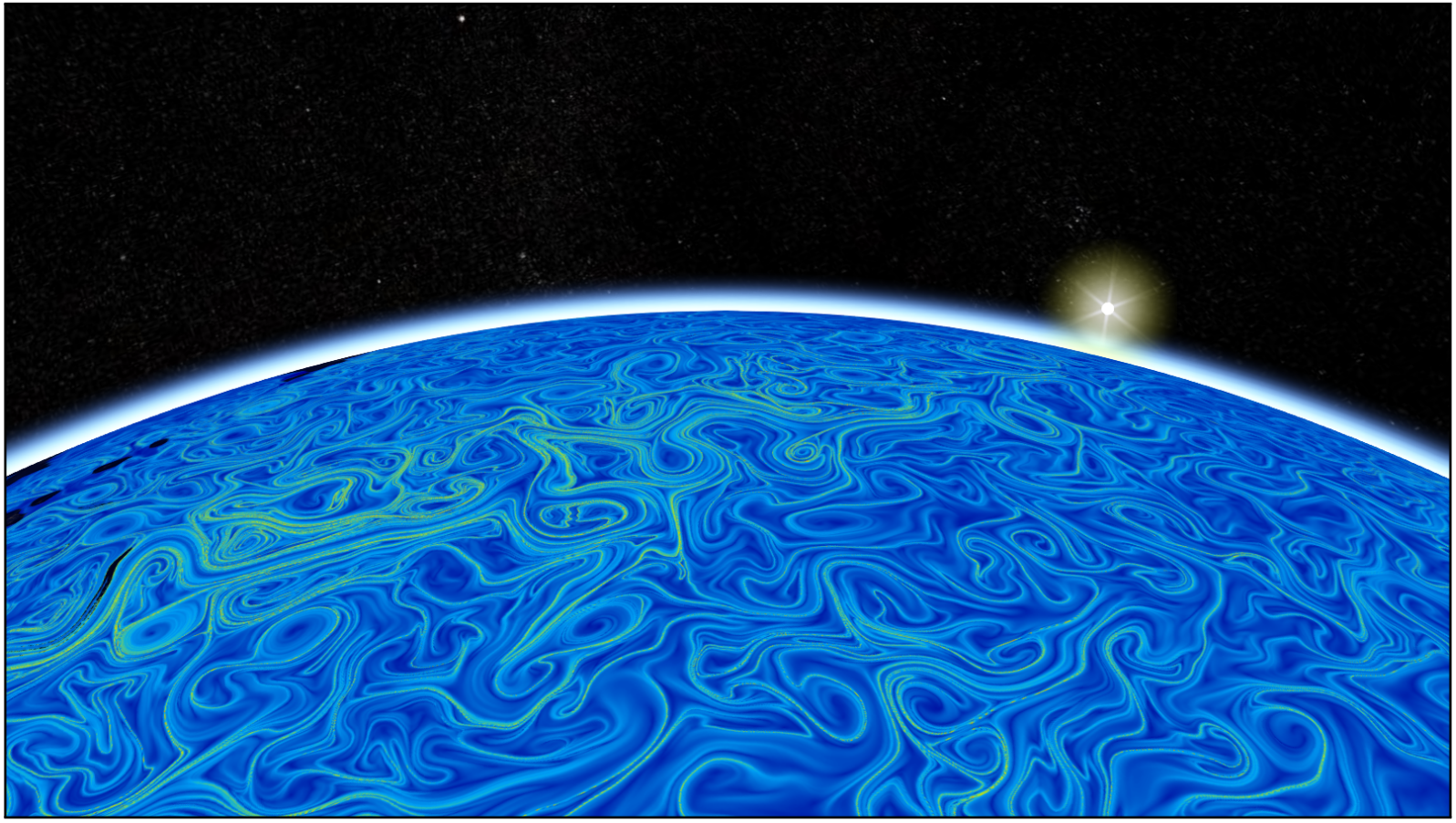

Figure 12.3.4: The backward FTLE field is computed on the surface grid of 576 million points over the globe for October 22, 2018. The image view shows the *Indian ocean*. The velocity data are obtained from the OSCAR ocean model [Bonjean and Lagerloef, 2002], and available at PO.DAAC database, JPL, NASA ESR. [2009].

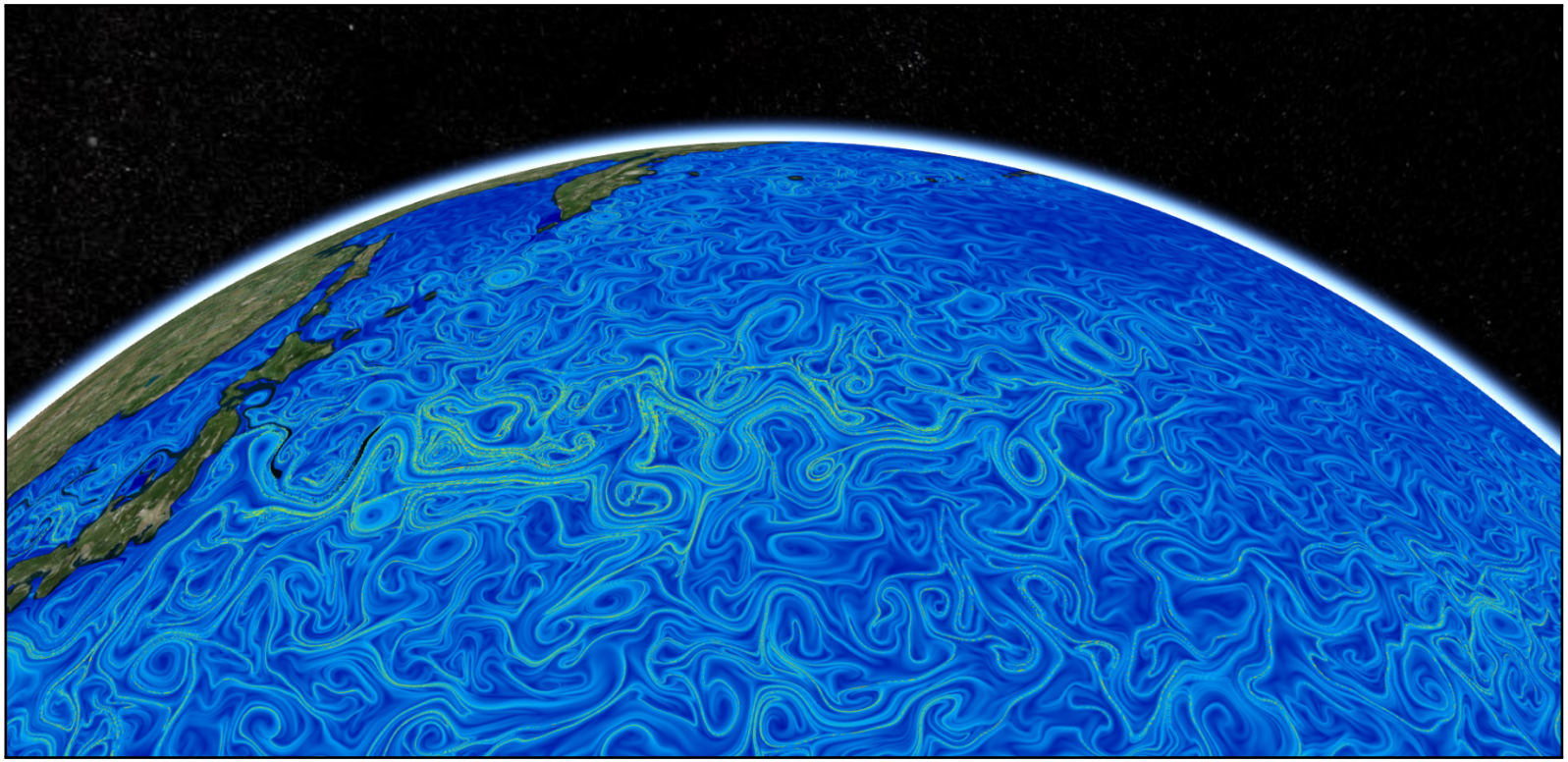

Figure 12.3.5: The backward FTLE is shown for the same data that is given in Figure 12.3.4. The image view shows the *Pacific Ocean* with Japan on the left. The *Kuroshio current* can be seen from the structures on the FTLE field spanning eastward of Japan. See also Figures 12.3.6 and 12.3.7 for comparison with the sea surface temperature and chlorophyll concentration.

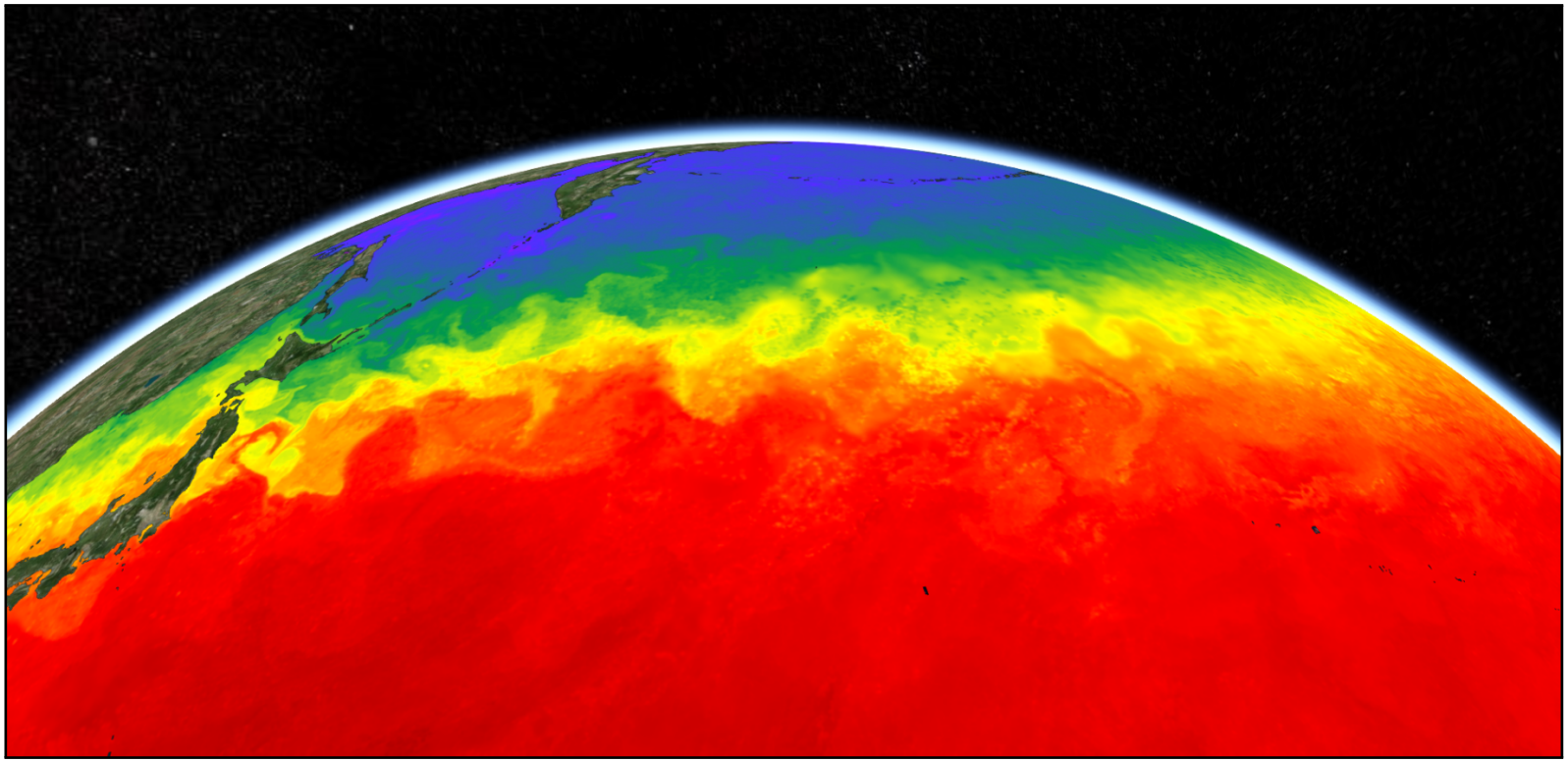

Figure 12.3.6: The sea surface temperature (SST) by Chao, Li, Farrara, and Huang [2009] and available at JPL OurOcean Project [2010]. SST is shown at the same time and location of the Figure 12.3.5 for comparison. The *Kuroshio current* can be seen spanning eastward of Japan. The data range from 273 Kelvin (in purple) to 305 Kelvin (in red).

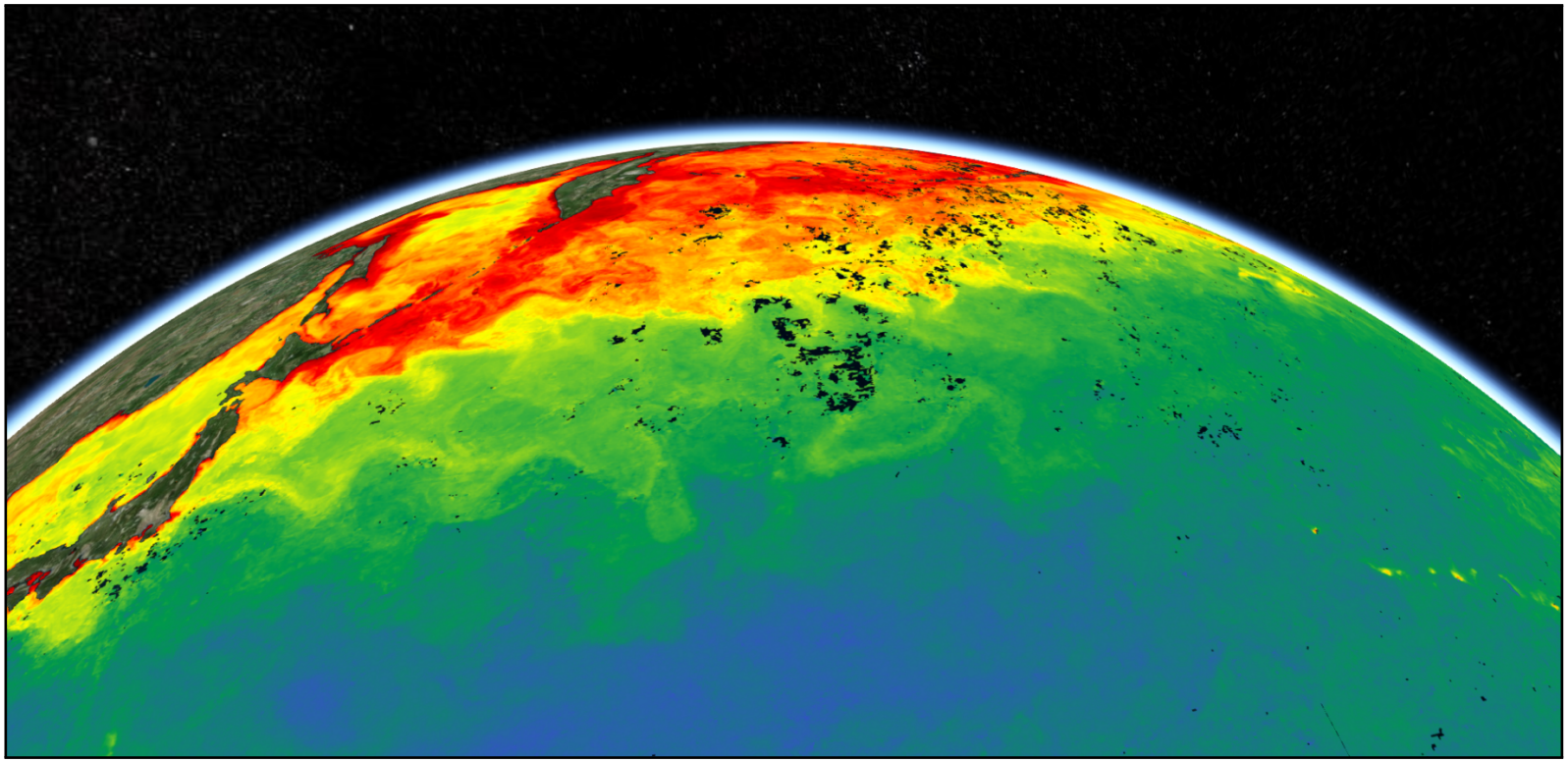

Figure 12.3.7: The chlorophyll concentration is shown to compare with FTLE in Figure 12.3.5 on the *Kuroshio current*. The data are the credit of Hu, Lee, and Franz [2012] and available at NASA Goddard Space Flight Center, Ocean Ecology Laboratory, Ocean Biology Processing Group [2018]. Data is on a logarithmic scale from 6.5×10^{-3} mg/m^3 (purple) to 6.0 mg/m^3 (red).

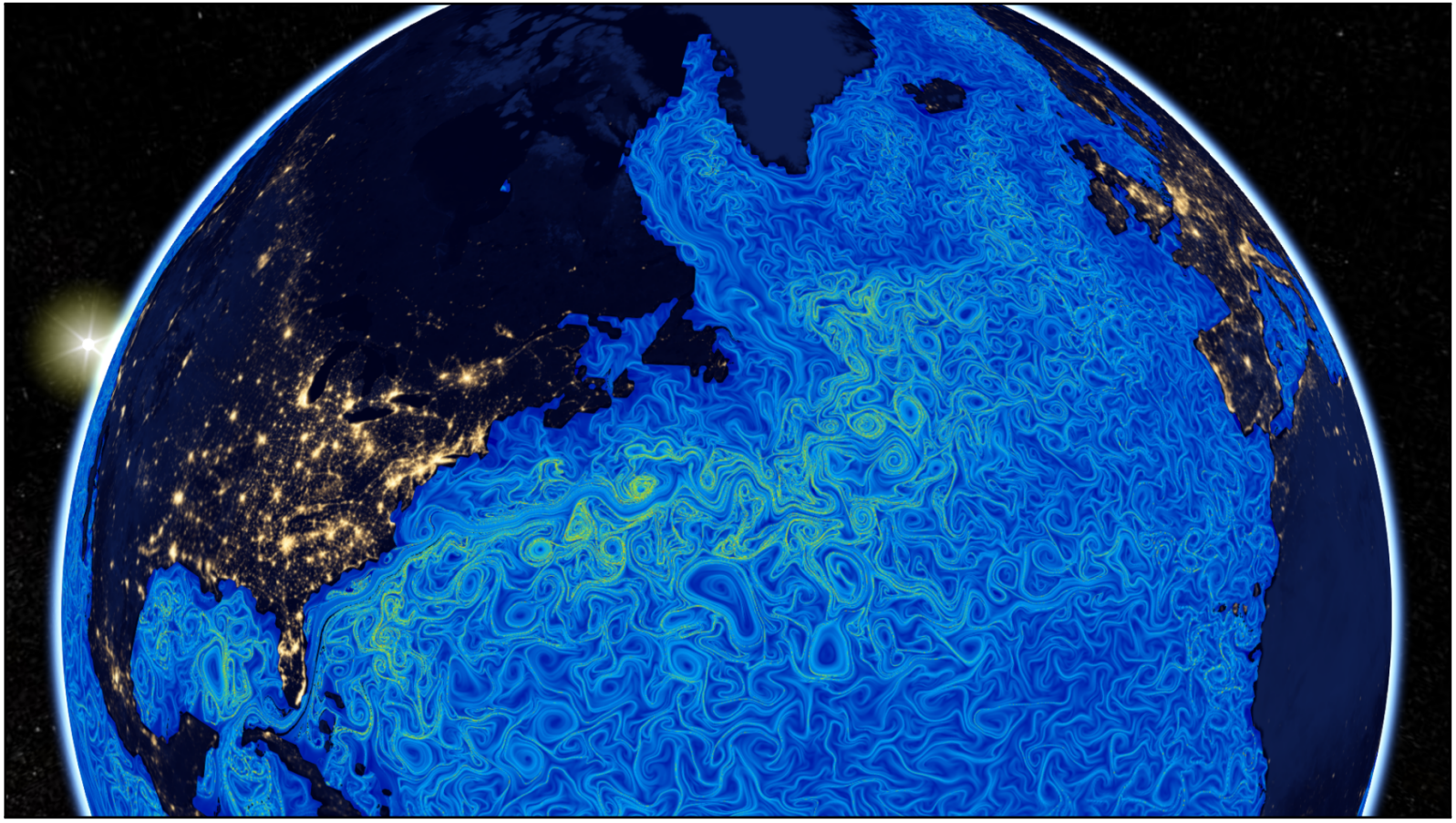

Figure 12.3.8: The backward FTLE field is shown with the same specifications given in Figure 12.3.4. The image view shows the *Atlantic Ocean*. The *Gulf stream* can be seen from the structures on the FTLE field stretching from eastward of the United States. See also Figures 12.3.9 and 12.3.10 for comparison with the sea surface temperature and the chlorophyll concentration.

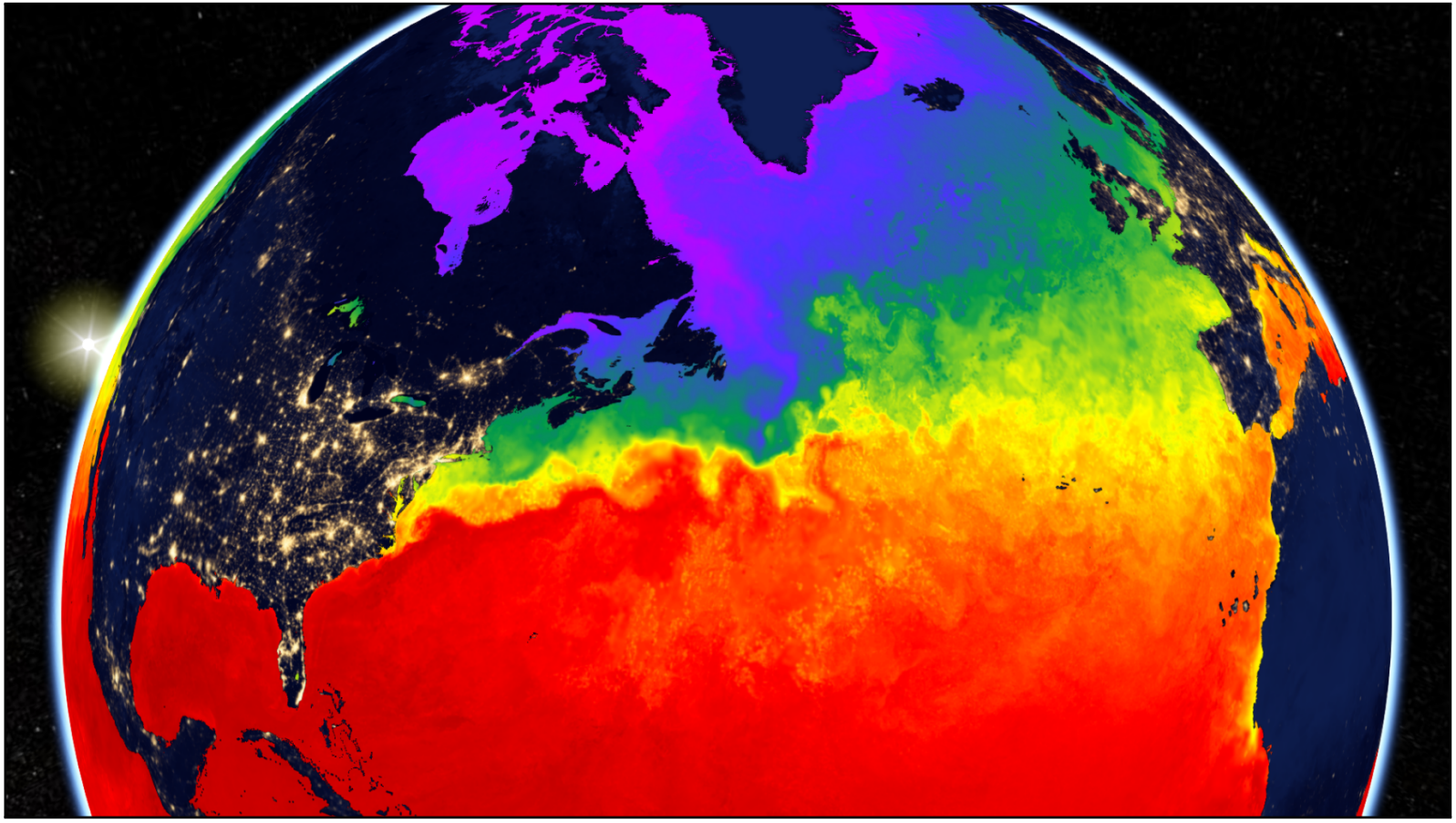

Figure 12.3.9: The sea surface temperature by Chao, Li, Farrara, and Huang [2009] is shown. The data are available at JPL OurOcean Project [2010]. SST is shown at the same time and location of the Figure 12.3.8 for comparison. The *Gulf stream* can be seen originating from eastward of the United States. The data range from 273 Kelvin (in purple) to 305 Kelvin (in red).

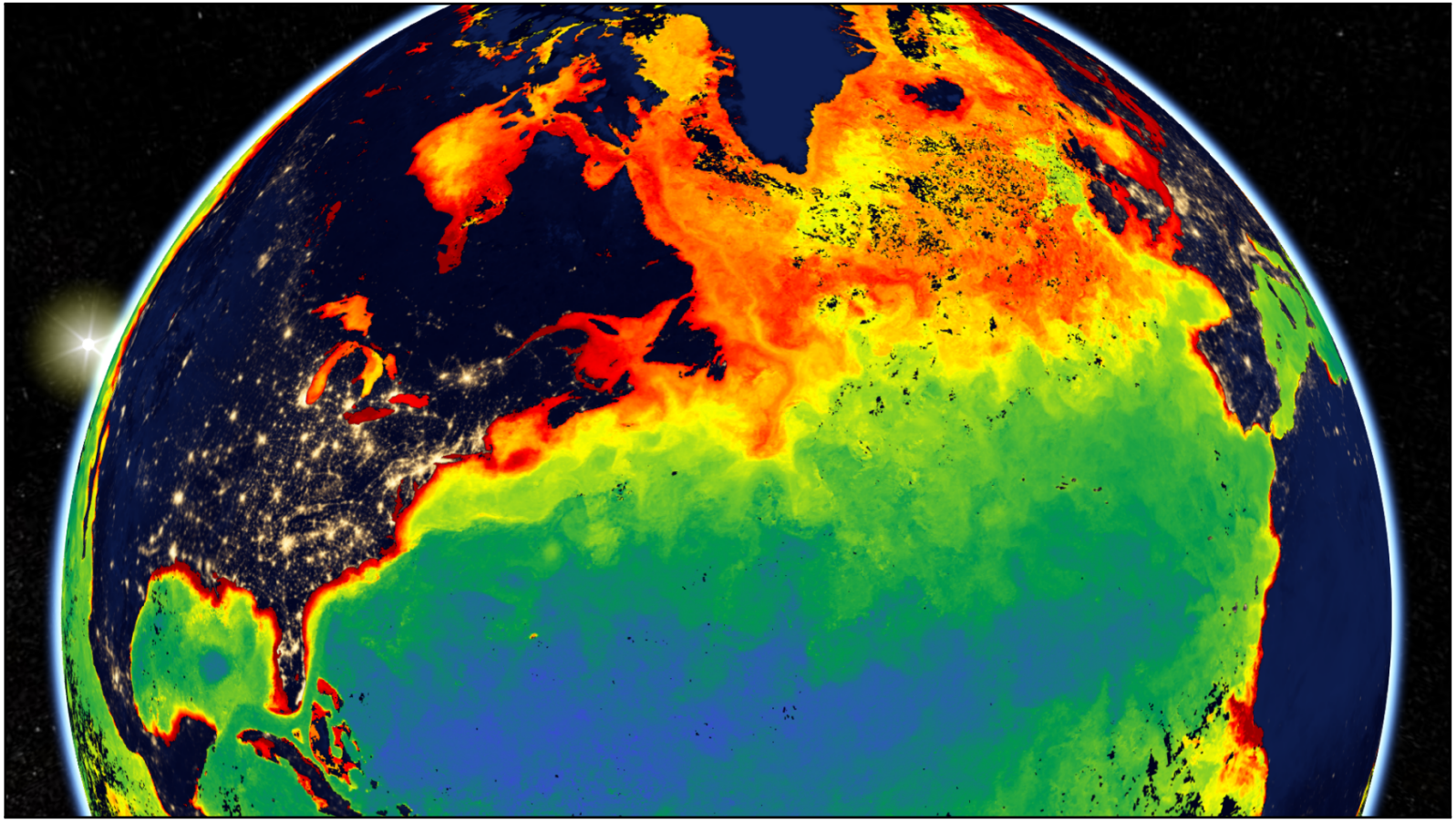

Figure 12.3.10: The chlorophyll concentration is shown to compare with FTLE in Figure 12.3.8 on the *Gulf stream*. The data are the credits of Hu, Lee, and Franz [2012] and available at NASA Goddard Space Flight Center, Ocean Ecology Laboratory, Ocean Biology Processing Group [2018]. Data is on a logarithmic scale from 6.5×10^{-3} mg/m^3 (purple) to 6.0 mg/m^3 (red).

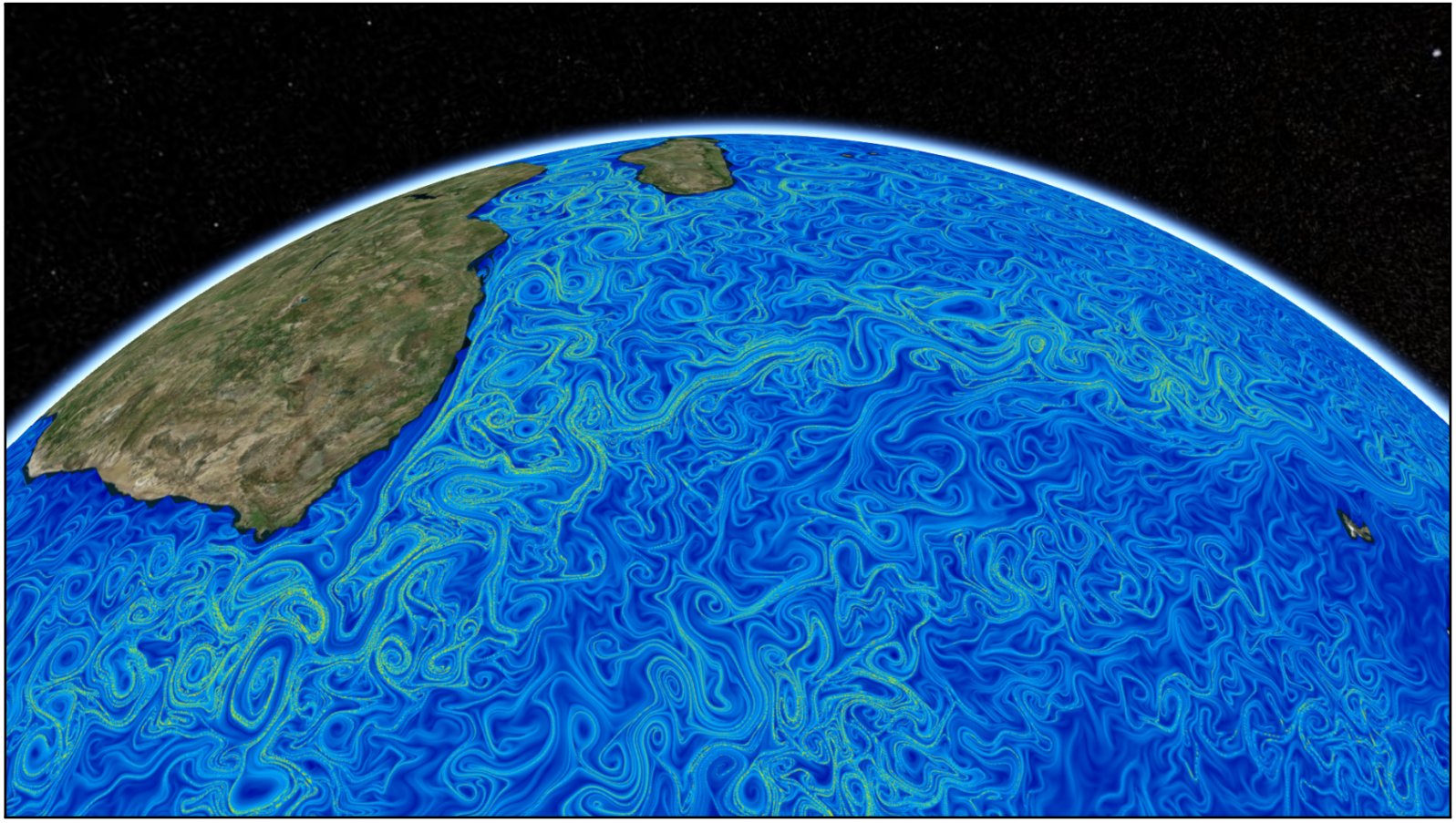

Figure 12.3.11: The backward FTLE is shown with the same specifications given in fig. 12.3.4. The image view shows the *Southern Ocean*. The *Agulhas current* can be seen from the structures on the FTLE field across the east of South Africa. See also Figure 12.3.12 for comparison with the sea surface temperature.

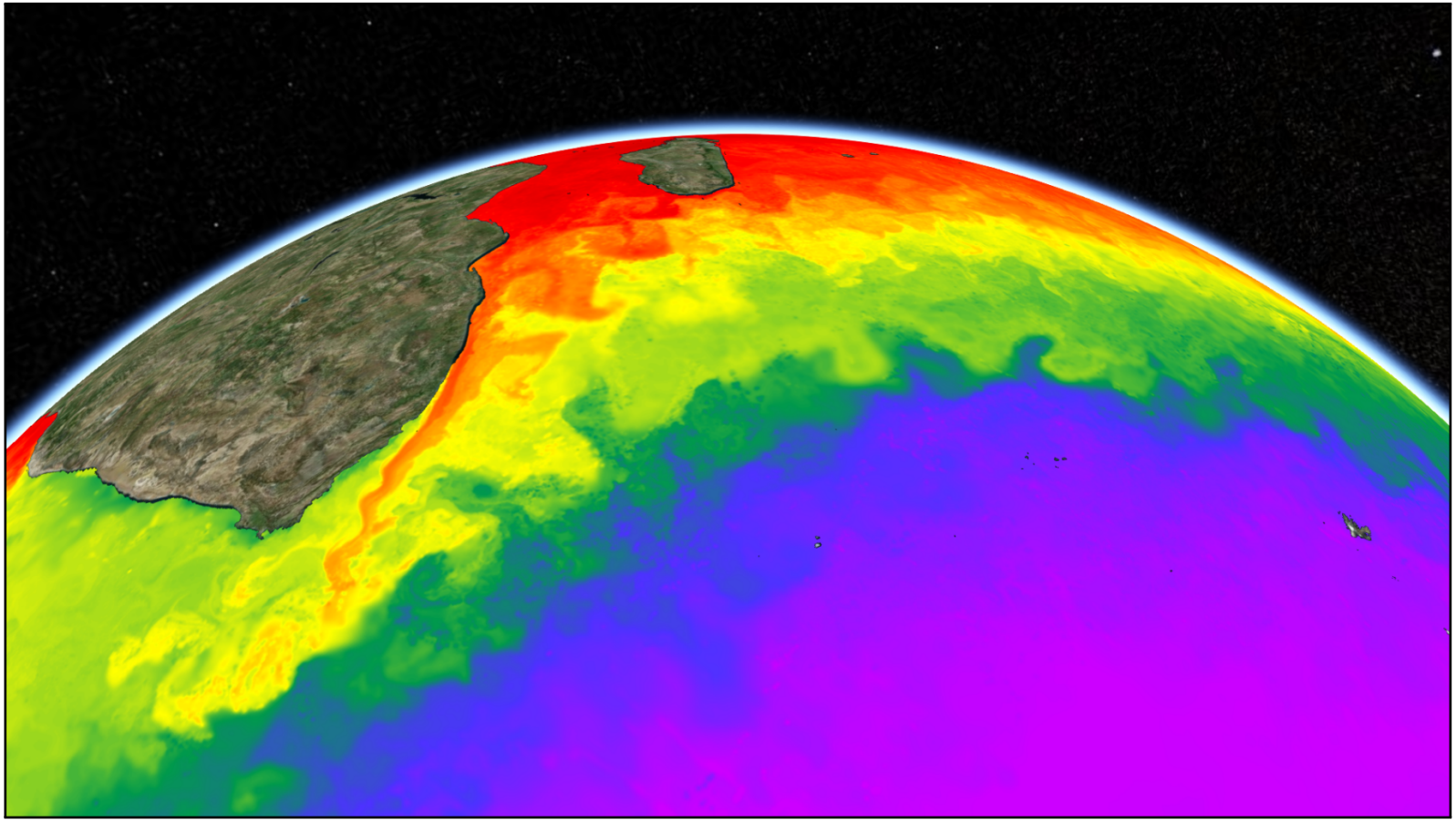

Figure 12.3.12: The sea surface temperature (SST) by Chao, Li, Farrara, and Huang [2009] is shown and available at JPL OurOcean Project [2010]. SST is shown at the same time and location of the Figure 12.3.11 for comparison. The *Agulhas current* can be seen across the east of South Africa. The data range from 273 Kelvin (in purple) to 305 Kelvin (in red).

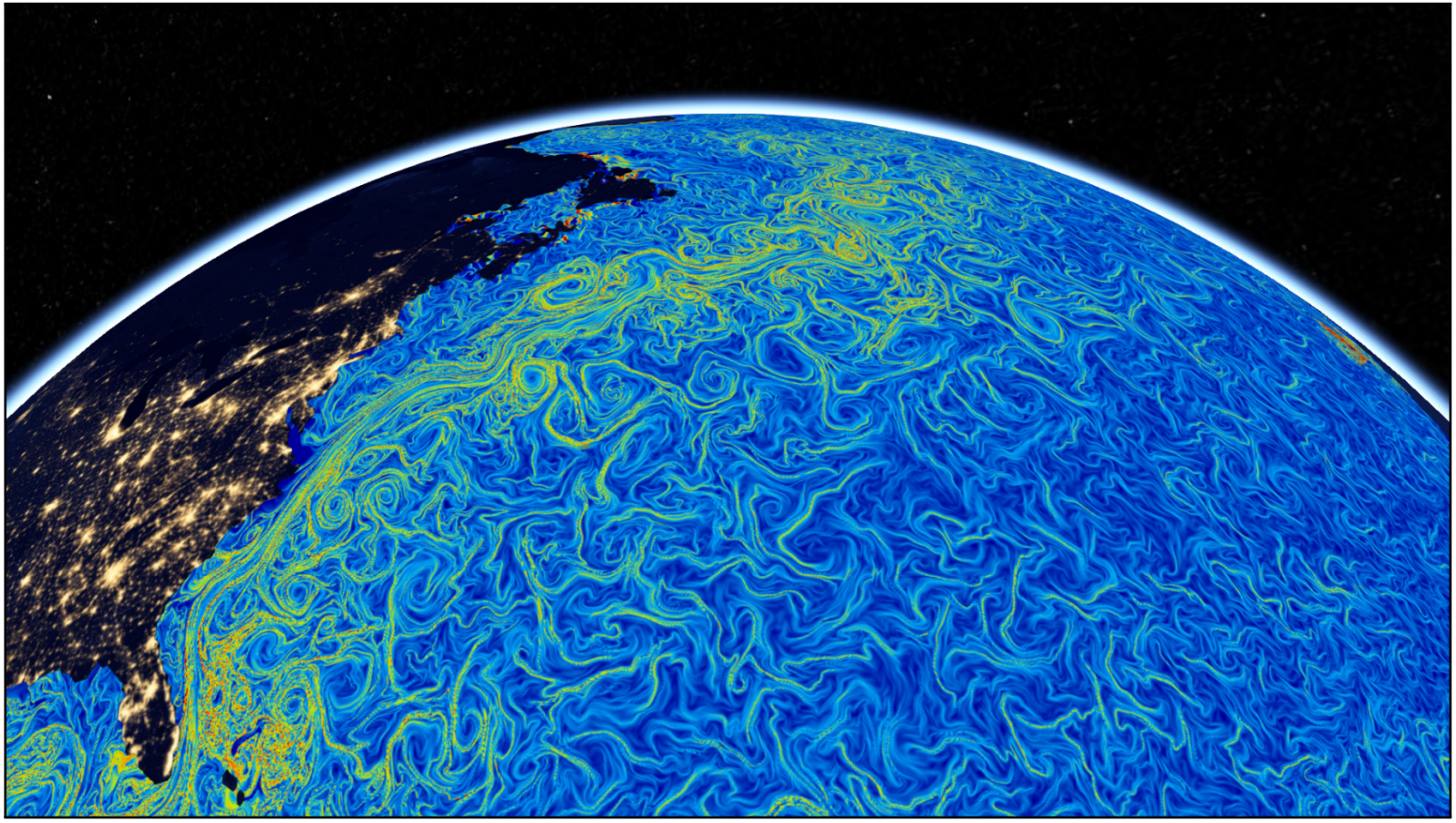

Figure 12.3.13: The backward FTLE field is computed on the surface grid of 576 million points over the globe for May 05, 2019. The image view shows the *Pacific Ocean*. The velocity field is obtained by altimetry data from satellite Jason-3, courtesy of The Laboratory for Satellite Altimetry, NOAA (see Footnote 4 for credits).

Chapter 13

Conclusion

In this dissertation, we used the geometric approach to study the kinematics of continua in a general manifold setting. Our particular interest is to derive the set of evolution equations for the spectral decomposition of finite (nonlinear) deformation tensors, namely, their eigenvalues and eigenvectors. To this end, we contributed to two topics as follows.

First, in Chapter 3, we have defined the eigenvalues for the deformation gradient tensor on Riemannian manifolds. The spectral representation is often studied for the maps from a space to itself. However, the deformation gradient is a two-point tensor that maps a space to another space. Using the Courant-Fischer-Weyl theorem, we have extended the definition of eigenvalues of the deformation gradient tensor to a Riemannian manifold. Besides spectral decomposition, we proposed a definition for the singular value decomposition of the deformation gradient tensor on a Riemannian manifold.

Second, in Chapter 4, we have derived the material time rates of the deformation gradient tensor and the left and right deformation tensors using an arbitrary connection on the tangent bundle. The arbitrary connection may include torsion. These formulations necessitate the redefinition of a few tensors to include the torsion, namely the spatial rate of deformation gradient tensor, the spatial rate of deformation tensor, and the spin tensor.

Combining the two previous developments, we derived novel evolution equations of the eigenvalues and eigenvectors of deformation on Riemannian manifolds. This process involves two steps. First, in Chapter 6, we transformed the referential and spatial configuration spaces by arbitrary time-dependent isometric isomorphisms. These transformations are characterized by rotator tensors and spinors representing a rate for rotators. On the transformed manifolds, we represent the material rates of tensors that we have derived earlier. Second, in Chapter 7, we have determined these transformations so that the matrix of deformation tensor is diagonalized in a coordinate system. The diagonal elements of the diagonalized matrix are the singular values of the deformation gradient tensor and have been defined in Chapter 3. The set of evolution equations for the singular values are coupled with the evolution equations for

the eigenvector frames of deformation tensors. Our novel set of equations represents the continuous singular value decomposition of deformation on a Riemannian manifold. In Euclidean space, our formulation for moving frames of the eigenvectors is analogous to the attitude kinematics.

To efficiently solve the differential equations, we used the geometric approach. Specifically, the eigenvector frames are evolved on the special orthogonal Lie group, in which their orthogonality property is preserved. By representing the matrices of eigenvectors on the corresponding Lie algebra, an optimal set of evolution equations for these matrices are obtained, which minimizes the cost of computations. In Chapter 8, we represented the eigenvector frames by unit quaternions, which leads to quaternionic evolution differential equations on the special unitary group. This is an efficient method for solving the attitude kinematics equations in three-dimensional Euclidean space.

In two-dimensional Euclidean space, the Lie algebra of orthogonal eigenvector frames is represented by Euler angles. In Chapter 9, we extended such representation to the Riemannian 2-manifolds and derived an optimal set of evolution equations. Further, in that chapter, we explained how the Riemannian metric influences the evolution equations. In particular, we found that a non-isothermal metric induces vorticity besides the vorticity due to the flow itself. By absorbing the metric into a few variables, we defined the Euclidean equivalence of the rate of deformation and vorticity. When the evolution equations are reformulated by the new variables, the equations look like as if they are written in Euclidean space.

Recall that in Chapter 4 we have derived the first-order material rates of deformation tensors. We deviated the flow of the dissertation in Chapter 5 to explore the second-order material rates of deformation expressed by an arbitrary connection on the tangent bundle. These formulations depend on the spatial acceleration of the flow and the Riemannian curvature of the manifold. These novel formulations are closely related to Einstein's field equations in the vacuum. We interpreted the second-order rates by assuming the flow is geodesic, and we found that a tangent vector field along a geodesic flow is a Jacobi field.

Also, in Chapter 5, we have explored the compatibility conditions of continua. The compatibility conditions in literature are given for deformation in the Euclidean space. We have extended these conditions to Einstein manifolds, which are more general than Euclidean space. Special cases of Einstein manifolds are the model spaces of constant sectional curvature. Besides the theoretical interest to study these manifolds, they have a practical use, for instance, the deformation on the surface of a sphere, which is an elliptic space of constant sectional curvature. We found that the compatibility conditions in three-dimensional Euclidean space can be directly derived by the Ricci curvature instead of the Riemannian curvature, and they lead to a compact set of equations.

We have supported our theoretical formulations in Part I with several analytical and numerical examples in Part II of the dissertation, which consists of Chapters 10 to 12. In Chapter 10, we have given an example of a symplectic flow on the Riemann sphere. This

flow is generated by a group of ideal vortices on the sphere. The Hamiltonian function and the velocity vector field of this flow are known. However, we have re-derived its Hamiltonian function by a new approach using geometric representations, namely by a Kähler structure on the Riemann sphere. These representations are complexified and given in the complex projective line.

A goal of this dissertation is to employ the eigenvalues of deformation to identify topological features of the flow using Lagrangian coherent structure (LCS). Often, LCS is identified by the finite-time Lyapunov exponents (FTLEs), which are related to the eigenvalues of the nonlinear deformation. As for the flow of ideal vortices on the sphere, we have computed the FTLE and compared them with the heteroclinic connections of the flow. Additionally, for a simple case of antipodal bipolar vortices, we have found an analytical solution of the evolution equations of deformation, namely the eigenvalues and eigenvectors of deformation. Our analytical solution can be used as a benchmark for the methods of identifying LCS that rely on the eigenvalues of deformation.

In Chapter 11, we have provided examples in Euclidean space for both the flows that their velocity field is analytically known and the flows given by velocity dataset. For all these examples, we have employed our quaternionic formulations of Chapter 8 to numerically integrate the evolution equations. We have shown that for the isochoric flows, the numerical solutions of eigenvalues with our evolution equations preserve the volume of the flow significantly better than other methods. The error produced by the numerical integration is less than other methods by orders of magnitude.

FTLE is one of the common methods that are used to characterize the topology of fluid flows. However, depending on the application, their calculations might be computationally expensive. Additionally, their computations by the existing direct methods, such as the finite-difference method, might not be accurate. Our theoretical formulations are comprehensive answers to these issues and further extend to other manifolds, such as flows on a sphere that has direct applications in geophysics.

In Chapter 12, we introduced a two comprehensive computational framework that we have developed to address several computational challenges, accessibility of the method, and convenience of using the tools for end-users. These computational tools are available to the public as online gateways where the users can leverage high-performance computations on remote servers and interactively visualize the results in place. The RESTORE tool preprocesses the ocean surface velocity field data obtained by incomplete measurements. Also, the TRACE computational platform performs Lagrangian analysis of geophysical data, such as computing the flow map, the eigenvalues and eigenvectors of nonlinear deformation, and forward/backward FTLE fields. TRACE leverages our novel Riemannian framework on the sphere. TRACE is capable of processing up to billion-point grid sizes. Such a computational scale is made possible by the efficient numerical implementation of our method.

Bibliography

Abraham, R., J. Marsden, and T. Raţiu (1988): *Manifolds, Tensor Analysis, and Applications*, no. v. 75 in Applied Mathematical Sciences. Springer New York. 27, 31, 34, 35, 92

Abraham, R., and J. E. Marsden (2008): *Foundations of Mechanics*, AMS Chelsea publishing. AMS Chelsea Pub./American Mathematical Society. 31

Ahlfors, L. V. (1966): *Complex analysis.* McGraw-Hill Book Co., New York, second edn. 117

Allshouse, M., and T. Peacock (2015): "Refining finite-time Lyapunov exponent ridges and the challenges of classifying them," *Chaos*, 25(087410). 2

Altmann, S. L. (2005): *Rotations, Quaternions, and Double Groups*, Dover books on mathematics. Dover Publications. 96

Ameli, S., and S. C. Shadden (2019): "A Transport Method for Restoring Incomplete Ocean Current Measurements," *Journal of Geophysical Research: Oceans*, 124(1), 227–242. 141

Andrle, M. S., and J. L. Crassidis (2013): "Geometric Integration of Quaternions," *Journal of Guidance, Control, and Dynamics*, 36(6), 1762–1767. 97

Arnold, V. I. (1965): "Sur une propriété topologique des applications globalement canoniques de la mécanique classique," *C. R. Acad. Sci. Paris*, 261, 3719–3722. 134

Arnold, V. I. (1966): "Sur la géométrie différentielle des groupes de Lie de dimension infinie et ses applications à l'hydrodynamique des fluides parfaits," *Annales de l'institut Fourier*, 16(1), 319–361. 134

Bajer, K., and H. K. Moffatt (1990): "On a class of steady confined Stokes flows with chaotic streamlines," *Journal of Fluid Mechanics*, 212, 337–363. 135

Bajer, K., H. K. Moffatt, and F. Nex (1990): "Steady confined Stokes flows with chaotic streamlines," *Topological Fluid Mechanics*, pp. 459–466. 135

Béda, G., I. Kozák, and J. Verhás (1996): *Continuum Mechanics*. Műzaki Könyvkiadó, Budapest. 48, 72

Besse, A. L. (1987): *Einstein Manifolds*, Classics in mathematics. London. 46

Bonjean, F., and G. S. E. Lagerloef (2002): "Diagnostic Model and Analysis of the Surface Currents in the Tropical Pacific Ocean," *Journal of Physical Oceanography*, 32(10), 2938–2954. vi, 145, 147

Bunse-Gerstner, A., R. Byers, V. Mehrmann, and N. K. Nichols (1991a): "Numerical computation of an analytic singular value decomposition of a matrix valued function," *Numerische Mathematik*, 60, 1–40. 2, 75

Bunse-Gerstner, A., R. Byers, V. Mehrmann, and N. K. Nichols (1991b): "Numerical computation of an analytic singular value decomposition of a matrix valued function," *Numerische Mathematik*, 60(1), 1–39. 72

Chandrasekhar, S. (1969): *Ellipsoidal Figures of Equilibrium*, Mrs. Hepsa Ely Silliman Memorial Lectures. Yale University Press. 90

Chao, Y., Z. Li, J. D. Farrara, and P. Huang (2009): "Blended sea surface temperatures from multiple satellites and in-situ observations for coastal oceans," *Journal of Atmospheric and Oceanic Technology*, 26, 1435–1446. vii, 146, 149, 152, 155

Chern, S. S., W. Chen, and K. S. Lam (1999): *Lectures on Differential Geometry*, Series on university mathematics. World Scientific. 45

Chow, B., P. Lu, and L. Ni (2006): *Hamilton's Ricci Flow*, Graduate studies in mathematics. American Mathematical Soc. 46, 49

Cohen, H., and R. Muncaster (1988): *The Theory of Pseudo-rigid Bodies*, Springer Tracts In Natural Philosophy. Springer-Verlag. 90

Conway, J. (1994): *A Course in Functional Analysis*, Graduate Texts in Mathematics. Springer New York. 19

Crassidis, J. L., and J. L. Junkins (2011): *Optimal Estimation of Dynamic Systems*, Chapman & Hall/CRC Applied Mathematics & Nonlinear Science. Taylor & Francis. 97, 98

da Silva, A. C. (2001): *Lectures on Symplectic Geometry*, vol. 1764 of *Lecture Notes in Mathematics*. Springer Berlin Heidelberg, Berlin, Heidelberg. 115

Diebel, J. (2006): "Representing Attitude: Euler Angles, Unit Quaternions, and Rotation Vectors," . 98

Dieci, L., and T. Eirola (1999): "On Smooth Decompositions of Matrices," *SIAM Journal on Matrix Analysis and Applications*, 20(3), 800–819. 3, 72

Dieci, L., and C. Elia (2006): "The singular value decomposition to approximate spectra of dynamical systems. Theoretical aspects," *Journal of Differential Equations*, 230(2), 502 – 531. 3, 73

——— (2008): "SVD algorithms to approximate spectra of dynamical systems," *Mathematics and Computers in Simulation*, 79(4), 1235 – 1254. 73

Dieci, L., M. S. Jolly, and E. S. Van Vleck (2010): "Numerical Techniques for Approximating Lyapunov Exponents and Their Implementation," *Journal of Computational and Nonlinear Dynamics*, 6(1), 011003. 73

Dieci, L., and E. S. V. Vleck (2003): "Lyapunov Spectral Intervals: Theory and Computation," *SIAM Journal on Numerical Analysis*, 40(2), 516–542. 73

Diele, F., and I. Sgura (1999): "Isospectral flows and the inverse eigenvalue problem for Toeplitz matrices," *Journal of Computational and Applied Mathematics*, 110(1), 25 – 43. 88

Dimitrienko, Y. I. (2002): *Tensor Analysis and Nonlinear Tensor Functions*. Springer Netherlands. 47

——— (2011): *Nonlinear Continuum Mechanics and Large Inelastic Deformations*, vol. 174 of *Solid Mechanics and Its Applications*. Springer Netherlands, Dordrecht. 32, 72

do Carmo, M. P. (1992): *Riemannian Geometry*, Mathematics (Boston, Mass.). Birkhäuser. 13, 39, 44, 49, 58, 59

Dombre, T., U. Frisch, M. Henon, J. M. Greene, and A. M. Soward (1986): "Chaotic streamlines in the ABC flows," *Journal of Fluid Mechanics*, 167, 353–391. 134

Einstein, A. (1915): "Die Feldgleichungen der Gravitation," *Sitzungsberichte der Königlich Preußischen Akademie der Wissenschaften (Berlin)*, pp. 844–847. 59

Epstein, M. (2010): *The Geometrical Language of Continuum Mechanics*. Cambridge University Press, New York, NY. 3, 26, 34

ESR. (2009): "OSCAR third degree resolution ocean surface currents," Ver. 1. PO.DAAC, CA, USA. vi, 146, 147

Flaschka, H. (1974): "The Toda lattice. II. Existence of integrals," *Phys. Rev. B*, 9, 1924–1925. 88

Gallot, S., D. Hulin, and J. Lafontaine (2004): *Riemannian Geometry*, Universitext. Springer Berlin Heidelberg. 46, 49

Geist, K., U. Parlitz, and W. Lauterborn (1990): "Comparison of Different Methods for Computing Lyapunov Exponents," *Progress of Theoretical Physics*, 83(5), 875–893. 72

Goldhirsch, I., P.-L. Sulem, and S. A. Orszag (1987): "Stability and Lyapunov stability of dynamical systems: A differential approach and a numerical method," *Physica D Nonlinear Phenomena*, 27, 311–337. 3

Golub, G., and C. Van Loan (1996): *Matrix Computations*, Johns Hopkins Studies in the Mathematical Sciences. Johns Hopkins University Press. 2, 24

Greene, J. M., and J.-S. Kim (1987): "The calculation of Lyapunov spectra," *Physica D Nonlinear Phenomena*, 24, 213–225. 3, 72

Gurtin, M. E., E. Fried, and L. Anand (2010): *The Mechanics and Thermodynamics of Continua*. Cambridge University Press. 33, 37, 52

Gurtin, M. E., and K. Spear (1983): "On the relationship between the logarithmic strain rate and the stretching tensor," *International Journal of Solids and Structures*, 19(5), 437 – 444. 84

Hairer, E. (2001): "Geometric Integration of Ordinary Differential Equations on Manifolds," *BIT Numerical Mathematics*, 41(5), 996–1007. 89

Hairer, E., C. Lubich, and G. Wanner (2002): *Geometric Numerical Integration: Structure-Preserving Algorithms for Ordinary Differential Equations*, Springer series in computational mathematics. Springer. 83, 86, 88, 93, 94, 95, 97

Haller, G. (2011): "A variational theory of hyperbolic Lagrangian coherent structures," *Physica D*, 240(7), 574–598. 2

Haller, G. (2015): "Lagrangian Coherent Structures," *Annual Review of Fluid Mechanics*, 47(1), 137–162. 112

Helmholtz, H. (1858): *On Integrals of the Hydrodynamical Equations, Which Express Vortex-motion*, vol. XXXIII, fourth series. Philosophical Magazine. 117

Henon, M. (1966): "Sur la topologie des lignes de courant dans un cas particular," *C. R. Acad. Sci. Paris A*, 262, 312,314. 134

Hestenes, D., and G. Sobczyk (1984): *Clifford algebra to geometric calculus : a unified language for mathematics and physics*. D. Reidel ; Distributed in the U.S.A. and Canada by Kluwer Academic Publishers, Dordrecht; Boston; Hingham, MA, U.S.A. 89

Hogben, L. (2006): *Handbook of Linear Algebra*, Discrete Mathematics and Its Applications. CRC Press. 102

Holm, D. (2011): *Geometric Mechanics, Part II: Rotating, Translating and Rolling*, no. pt. 2 in Geometric Mechanics. Imperial College Press. 96

Holm, D. D., T. Schmah, and C. Stoica (2009): *Geometric Mechanics and Symmetry: From Finite to Infinite Dimensions*, Oxford Texts in Applied and Engineering Mathematics. Oxford University Press, Oxford. 3, 90, 91

Holzapfel, G. A. (2000): *Nonlinear Solid Mechanics: A Continuum Approach for Engineering*. John Wiley & Sons, Ltd. 37, 84

Hu, C., Z. Lee, and B. Franz (2012): "Chlorophyll aalgorithms for oligotrophic oceans: A novel approach based on three-band reflectance difference," *Journal of Geophysical Research: Oceans*, 117(C1). vii, 146, 150, 153

Hughes, T. J. R., and J. E. Marsden (1977): "Some applications of geometry is continuum mechanics," *Reports on Mathematical Physics*, 12(1), 35 – 44. 3

Iserles, A., H. Z. Munthe-Kaas, S. Nørsett, and A. Zanna (2000): "Lie-group methods," *Acta Numerica 2000*, 9, 215–365. 97

Jamaloodeen, M. I., and P. K. Newton (2006): "The N-vortex problem on a rotating sphere. II. Heterogeneous Platonic solid equilibria," *Proceedings of the Royal Society A: Mathematical, Physical and Engineering Sciences*, 462(2075), 3277–3299. 118

Jost, J. (2011): *Riemannian Geometry and Geometric Analysis*, Universitext. Springer Berlin Heidelberg. 88

JPL OurOcean Project (2010): "GHRSST Level 4 G1SST Global Foundation Sea Surface Temperature Analysis. Ver. 1," . vii, 146, 149, 152, 155

Kanso, E., M. Arroyo, Y. Tong, A. Yavari, J. E. Marsden, and D. Desbrun (2007): "On the geometric character of stress in continuum mechanics," *Zeitschrift für angewandte Mathematik und Physik*, 58, 843–856. 3

Kasten, J., C. Petz, I. Hotz, B. R. Noack, and H. C. Hege (2009): "Localized finite-time Lyapunov exponent for unsteady flow analysis," in *Vision, Modeling and Visualization*, ed. by M. Magnor, B. Rosenhahn, and H. Theisel, pp. 265–274. 2

KATO, T. (1995): *Perturbation Theory for Linear Operators*, Classics in Mathematics. Springer-Verlag. 2, 20, 75

KIDAMBI, R., AND P. K. NEWTON (1998): "Motion of three point vortices on a sphere," *Physica D: Nonlinear Phenomena*, 116(1), 143 – 175. 125

KIRINCICH, A. (2016): "Remote Sensing of the Surface Wind Field over the Coastal Ocean via Direct Calibration of HF Radar Backscatter Power," *Journal of Atmospheric and Oceanic Technology*, 33(7), 1377–1392. 143

KIRINCICH, A. R., T. DE PAOLO, AND E. TERRILL (2012): "Improving HF Radar Estimates of Surface Currents Using Signal Quality Metrics, with Application to the MVCO High-Resolution Radar System," *Journal of Atmospheric and Oceanic Technology*, 29(9), 1377–1390. 143

KOBAYASHI, S., AND K. NOMIZU (1963): *Foundations of differential geometry*, vol. I of *Interscience tracts in pure and applied mathematics*. Interscience Publishers. 27, 40, 67

KUIPERS, J. B. (2002): *Quaternions and Rotation Sequences: A Primer with Applications to Orbits, Aerospace, and Virtual Reality*, Princeton paperbacks. Princeton University Press. 98

LAX, P. (1968): "Integrals of nonlinear evolution equations and solitary waves," *Communications on Pure and Applied Mathematics*, 21(5), 467–490. 88

LAX, P. D. (2007): *Linear Algebra and Its Applications*, Pure and Applied Mathematics: A Wiley Series of Texts, Monographs and Tracts. Wiley. 83

LEE, J. M. (1997): *Riemannian manifolds: an introduction to curvature*, no. 176 in Graduate texts in mathematics. Springer, New York. 31, 44, 51, 114

LEKIEN, F., S. C. SHADDEN, AND J. E. MARSDEN (2007): "Lagrangian coherent structures in n-dimensional systems," *Journal of Mathematical Physics*, 48(6), 065404. 120

LIVESCU, D. (2013): "Numerical simulations of two-fluid turbulent mixing at large density ratios and applications to the Rayleigh–Taylor instability," *Philosophical Transactions of the Royal Society A: Mathematical, Physical and Engineering Sciences*, 371(2003), 20120185. 139

LIVESCU, D., C. CANADA, K. KANOV, R. BURNS, I. STAFF, AND J. PULIDO (2014): "Homogeneous Buoyancy driven turbulence data set," . 139

LIVESCU, D., AND J. R. RISTORCELLI (2007): "Buoyancy-driven variable-density turbulence," *Journal of Fluid Mechanics*, 591, 43–71. 139

——— (2008): "Variable-density mixing in buoyancy-driven turbulence," *Journal of Fluid Mechanics*, 605, 145–180. 139

Magnus, W. (1954): "On the exponential solution of differential equations for a linear operator," *Comm. Pure Appl. Math.*, 7, 649–673. 95

Markley, F. L. (2008): "Unit Quaternion from Rotation Matrix," *Journal of Guidance, Control, and Dynamics*, 31(2), 440–442. 99

Marsden, J. E., and T. J. R. Hughes (1983): *Mathematical Foundations of Elasticity*, Prentice-Hall civil engineering and engineering mechanics series. Prentice-Hall, Englewood Cliffs N.J. 3, 9, 11, 13, 15, 19, 32, 33, 34, 37, 41, 47, 85, 87

Marsden, J. E., and T. Ratiu (1999): *Introduction to Mechanics and Symmetry: A Basic Exposition of Classical Mechanical Systems*, Texts in Applied Mathematics. Springer. 18, 30, 97

McDuff, D., and D. Salamon (1998): *Introduction to Symplectic Topology*, Oxford mathematical monographs. Clarendon Press. 114

McLachlan, R. I., and G. R. W. Quispel (2006): "Geometric integrators for ODEs," *jpa*, 39(19), 5251–5285. 89

Meleshko, V. V., P. K. Newton, and V. V. Ostrovs'kyi (2010): "Stability of the configurations of point vortices on a sphere," *Journal of Mathematical Sciences*, 171(5), 603–619. 118

Moser, J., and E. Zehnder (2005): *Notes on Dynamical Systems*, Courant lecture notes in mathematics. American Mathematical Soc. 88

Munthe–Kaas, H., and B. Owren (1999): "Computations in a free Lie algebra," *Philosophical Transactions of the Royal Society of London A: Mathematical, Physical and Engineering Sciences*, 357(1754), 957–981. 95

Myers, S. B., and N. E. Steenrod (1939): "The Group of Isometries of a Riemannian Manifold," *Annals of Mathematics*, 40(2), 400–416. 62

NASA Goddard Space Flight Center, Ocean Ecology Laboratory, Ocean Biology Processing Group (2018): "Moderate-resolution Imaging Spectroradiometer (MODIS) Aqua Chlorophyll Data; 2018 Reprocessing," . vii, 146, 150, 153

Neff, P., B. Eidel, and R. J. Martin (2016): "Geometry of Logarithmic Strain Measures in Solid Mechanics," *Archive for Rational Mechanics and Analysis*, 222(2), 507–572. 84

Newton, P. K. (2001): *The N-Vortex Problem*, vol. 145 of *Applied Mathematical Sciences*. Springer New York, New York, NY. 112, 116, 117, 118

Newton, P. K., and V. Ostrovskyi (2012): "Energy-Momentum Stability of Icosahedral Configurations of Point Vortices on a Sphere," *Journal of Nonlinear Science*, 22(4), 499–515. 118

Newton, P. K., and H. Shokraneh (2006): "The N-vortex problem on a rotating sphere. I Multi-frequency configurations," *Proceedings of the Royal Society A: Mathematical, Physical and Engineering Sciences*, 462(2065), 149–169. 116

Oettinger, D., D. Blazevski, and G. Haller (2016): "Global variational approach to elliptic transport barriers in three dimensions," *Chaos*, 26(033114). 2

Ogden, R. W. (1997): *Non-linear Elastic Deformations*, Dover Civil and Mechanical Engineering. Dover Publications. 72

Pelz, R. B., V. Yakhot, S. A. Orszag, L. Shtilman, and E. Levich (1985): "Velocity-Vorticity Patterns in Turbulent Flow," *Phys. Rev. Lett.*, 54, 2505–2508. 134

Petersen, P. (2006): *Riemannian Geometry*, Graduate Texts in Mathematics. Springer New York. 44, 48, 53, 58, 88

Rellich, F. (1969): *Perturbation Theory of Eigenvalue Problems*, New York University. Institute of Mathematical Sciences. Gordon and Breach. 2

Romano, G. (2014): *Geometry & Continuum Mechanics*. CreateSpace Independent Publishing Platform. 33

Romano, G., R. Barretta, and M. Diaco (2014): "Geometric continuum mechanics," *Meccanica*, 49(1), 111–133. 33

Sadik, S., and A. Yavari (2015): "On the origins of the idea of the multiplicative decomposition of the deformation gradient," *Mathematics and Mechanics of Solids*. 3

Sedov, L. I. (1966): *Foundations of the non-linear mechanics of continua*, International series of monographs in interdisciplinary and advanced topics in science and engineering. Pergamon Press. 48

Shadden, S. C., F. Lekien, and J. E. Marsden (2005): "Definition and properties of Lagrangian coherent structures from finite-time Lyapunov exponents in two-dimensional aperiodic flows," *Physica D: Nonlinear Phenomena*, 212(3), 271–304. 2, 84, 120, 131

Shepperd, S. W. (1978): "Quaternion from rotation matrix," *Journal of Spacecraft and Rockets*, 1, 223–224. 99

Shuster, M. D. (1993): "Survey of attitude representations," *Journal of the Astronautical Sciences*, 41, 439–517. 97, 98

Simo, J., and J. E. Marsden (1984a): "On the rotated stress tensor and the material version of the Doyle-Ericksen formula," *Archive for Rational Mechanics and Analysis*, 86(3), 213–231. 3

——— (1984b): "Stress tensors, Riemannian metrics and the alternative descriptions in elasticity," *Springer Lecture Notes in Physics*, 195, 369–383. 3

Sokolnikoff, I. (1951): *Tensor analysis: theory and applications to Geometry and Mechanics of Continua*, Applied mathematics series. Wiley. 39, 44, 45, 48, 85

Sowerby, R., and E. Chu (1984): "Rotations, stress rates and strain measures in homogeneous deformation processes," *International Journal of Solids and Structures*, 20(11), 1037 – 1048. 72

Spivak, M. (1999): *A Comprehensive Introduction to Differential Geometry*, vol. 2. Publish or Perish, inc., third edn. 13, 26

Tabor, M., and I. Klapper (1994): "Stretching and alignment in chaotic and turbulent flows," *Chaos, Solitons & Fractals*, 4, 1031–1055. 2

Talpaert, Y. (2002): *Tensor Analysis and Continuum Mechanics*. Springer Netherlands. 48

Truesdell, C. A. (1992): *A First Course in Rational Continuum Mechanics*, no. v. 1 in Pure and Applied Mathematics. Elsevier Science. 32, 57, 68

Truesdell, C. A., and W. Noll (2004): *The Non-Linear Field Theories of Mechanics*. Springer-Verlag Berlin Heidelberg, 3 edn. 1, 57

Udwadia, F. E., and H. F. von Bremen (2002): "Computation of Lyapunov characteristic exponents for continuous dynamical systems," *Z. Angew. Math. Phys.*, 53(1), 123–146. 94

von Neumann, J., and E. P. Wigner (1929): *Über das Verhalten von Eigenwerten bei adiabatischen Prozessen*vol. 30, pp. 467–470. 83

Wright, K. (1992): "Differential equations for the analytic singular value decomposition of a matrix," *Numerische Mathematik*, 63(1), 283–295. 3, 72

Xiao, H., O. T. Bruhns, and A. Meyers (1997): "Logarithmic strain, logarithmic spin and logarithmic rate," *Acta Mechanica*, 124(1), 89–105. 84

Zener, C. (1932): "Non-Adiabatic Crossing of Energy Levels," *Proceedings of the Royal Society of London. Series A, Containing Papers of a Mathematical and Physical Character*, 137(833), 696–702. 83

Zhang, R.-y. (2006): "Hamiltonian mechanics on Kähler manifolds," *Applied Mathematics and Mechanics*, 27, 353–362. 117

Index

Symbols

A

B

C